The role of microglia in spinal cord injury: Identification, importance and therapeutic implications

Thèse

Victor Bellver Landete

Doctorat en médecine moléculaire
Philosophiæ doctor (Ph. D.)

Québec, Canada

The role of microglia in spinal cord injury
Identification, importance and therapeutic implications

Thèse

Victor Bellver Landete

Sous la direction de :

Steve Lacroix

RÉSUMÉ

Une lésion à la moelle épinière entraine fréquemment un handicap permanent. À ce jour, il n'y a pas de traitement efficace. La connaissance et l'implication de la microglie au sein de la pathologie sont peu étudiées. L'un des obstacles principaux à l'étude de la microglie se trouve dans son phénotype identique à celui des macrophages dérivés des monocytes (MDMs) sanguins. Dans cette thèse, nous rapportons pour la toute première fois la distribution, la prolifération et l'importance de la microglie suite à une lésion de la moelle épinière (LME). Afin d'accomplir nos objectifs, nous avons publié deux articles présentés ci-dessous. Au chapitre deux, nous décrivons les fonctions de la microglie, grâce à l'utilisation de modèles de souris transgéniques. Les analyses spatio-temporelles des réponses microgliales montrent que ces cellules sont très dynamiques et prolifèrent abondamment durant la première semaine, avec comme point culminant une accumulation maximale autour de la lésion au temps deux semaines post-LME. À ce temps, les microglies réactives se placent à la jonction entre les MDMs et les astrocytes réactifs. L'élimination des microglies chez la souris lésée par le biais d'un antagoniste du récepteur CSF1R, PLX5622, retarde la formation de la cicatrice gliale, entrainant du même coup la migration de cellules immunitaires innées hors de la zone lésée, une réduction du nombre d'oligodendrocytes et de neurones et une réduction de la motricité. Fait intéressant, ces réponses furent associées à une réduction de la relâche du facteur de croissance similaire à l'insuline (IGF-1). Par contraste, une surprolifération microgliale, induite localement durant la première semaine post-SCI par une relâche de MCSF incorporé dans de l'hydrogel, a abouti à une meilleure récupération des fonctions locomotrices. Au chapitre trois, nous identifions que l'interleukine-1 alpha (IL-1α), une cytokine libérée par la microglie, favorise la réaction inflammatoire suite à une LME. L'invalidation du gène codant pour la cytokine dans des modèles transgéniques murins a pour effet de protéger les oligodendrocytes, cellules normalement vulnérables aux LME, par l'entremise du facteur de survie TOX3. Parallèlement, l'administration centrale d'anakinra, un antagoniste du récepteur de type 1 de l'IL-1 (IL1R1), améliore la récupération fonctionnelle suite à une LME. Nos résultats définissent donc la microglie comme une cellule régulatrice clef dans un contexte de LME. Dans cette thèse, nous avons donc ouvert la voie à deux traitements distincts pour améliorer la guérison d'une LME par le biais des microglies.

ABSTRACT

Spinal cord injury (SCI) is often associated with permanent disabilities. To date, there are no specific therapies available. Further, the knowledge and implication of microglia in the disordered physiological processes associated with SCI have been poorly studied. One of the major difficulties in studying microglia relies on its morphologic and phenotypic similarities with monocyte-derived macrophages (MDMs) recruited from the blood. During my thesis, we revealed the distribution and importance of microglia during SCI. These advancements were the object of two published articles that we present herein. In Chapter two, we define the functions of microglia in SCI using novel transgenic mouse models and depletion strategies that allow the specific targeting of microglia. Spatiotemporal analysis of the microglial response revealed that these cells are highly dynamic and proliferate extensively during the first week, with a maximum accumulation around the lesion site at two weeks post-SCI. There, activated microglia position themselves at the interface between leukocytes that infiltrate the lesion core and reactive astrocytes. Depletion of microglia using the CSF1R antagonist PLX5622 confirmed that microglia are critical regulators of glial scar formation. Accordingly, microglia depletion in the context of SCI resulted in disruption of glial scar formation, migration of innate immune cells away from the injured site, reduced oligodendrocyte and neuronal survival, as well as impaired locomotor recovery which was associated to a lack of insulin growth factor 1. In contrast, increased microglial proliferation induced by local delivery of MCSF in hydrogel during the first week post-SCI resulted in enhanced functional recovery. In Chapter 3, we identified interleukin-1 alpha (IL-1α) as a cytokine specifically released by microglia, and which induces the inflammatory response. The ablation of this cytokine in knockout mice reduced inflammation and protected these animals from SCI, inducing expression of the survival factor TOX3 in oligodendrocytes. Importantly, central administration of anakinra, an antagonist for the IL-1 receptor type 1 (IL-1R1), enhanced functional recovery after SCI. Altogether, our results identify microglia as a key cellular regulator of outcomes in SCI. Thus, my PhD thesis work identified two different therapeutic avenues implicating microglia to enhance recovery after SCI.

Table of content

Lists

List of tables

List of figures

List of abbreviations

AKT:	Serine/threonine protein kinase
ALS:	Amyotrophic lateral sclerosis
AP-1:	Activator protein-1
BAMs:	Border-associated macrophages
BBB:	Blood-brain barrier
BDNF:	Brain-derived growth factor
bFGF:	Basic fibroblast growth factor
BM:	Bone marrow
BMC:	Bone marrow chimeras
CCR2:	C-C chemokine receptor type 2
CD206:	Mannose receptor
CNS:	Central nervous system
CREB:	cAMP responsive element binding protein
CSF:	Cerebrospinal fluid
CSF-1:	Colony stimulation factor-1
CSF-1R:	Colony stimulation factor-1 receptor
CSPGs:	Chondroitin sulfate proteoglycans
DAM:	Disease-associated microglia
DAMPs:	Damage-associated molecular pattern
DD:	Death domain
DT:	Diphtheria toxin
DTA:	DT subunit A
DTR:	Diphtheria toxin receptor
E:	Embryonic day
EAE:	Experimental autoimmune encephalomyelitis
ECM:	Extracellular matrix
ECs:	Endothelial cells
ERK:	Extracellular signal-regulated kinase
FOXO:	Fork head transcription factor
GFAP:	Glial fibrillary acid protein

GFP:	Green fluorescent protein
HMGB1:	High mobility group box 1
HSC:	Hematopoietic stem cells
IGF-1:	Insulin growth factor 1
IGF-1R:	Insulin growth factor 1 receptor
IGFBP:	Insulin growth factor binding protein
IKK-β:	Kinase inhibitor of nuclear factor kappa-B kinase subunit beta
IL-1Ra:	IL-1R1 antagonist
IL-1α:	Interleukin-1 alpha
IL-1β	Interleukin-1 beta
IP:	Intraperitoneal
IRAK:	IL-1 receptor-associated kinase
IRF:	Interferon regulatory factor
IκBα:	Nuclear factor of kappa light polypeptide gene enhancer in B-cells inhibitor alpha
IRS:	Insulin receptor substrates
KO:	Knockout
LME:	Lésion de la moelle épinière
LPS:	Lipopolysaccharide
LysM:	Lysozyme M
MAPK:	Mitogen-activated protein kinase
MAPKK6:	MAP kinase kinase 6
MDMs:	Monocyte-derived macrophages
MHCII:	Major histocompatibility complex class II
mSOD:	Mutant superoxide dismutase
mTOR:	Mammalian target of rapamycin
MyD88:	Myeloid differentiation primary response protein 88
NF-κB:	Nuclear factor-kappaB
NGF:	Nerve growth factor
NT3	Neurotrophin-3
OPCs:	Oligodendrocyte precursor cell
P:	Postnatal day
p53:	p53 tumor suppressor

PAMPs:	Pathogen-associated molecular pattern molecules
PDK:	Phosphoinositide-dependent protein kinase
PI3K:	Phosphatidylinositol 3-kinase
PNI:	Peripheral nerve injury
PTP-ζ:	Protein tyrosine phosphatase-ζ receptor
SCI:	Spinal cord injury
TAB1:	TAK1 binding protein 1
TACE:	TNF-alpha converting enzyme
TAK1:	TGF-β-associated kinase 1
TBI:	Traumatic brain injury
TGF-β1:	Tumor growth factor beta-1
TIR:	Toll/IL-1 receptor
TIRAP:	TIR domain containing adaptor protein
TLR4:	Toll-like receptor 4
TNFR1	TNF receptor type 1
TNF-α	Tumor necrosis factor alpha
TOX3:	TOX high mobility group box family member 3
TRAF6:	TNF receptor-associated factor 6
TRAM:	TRIF-related adaptor molecule
TRIF:	TIR domain-containing adaptor inducing IFN-β
WD:	Wallerian degeneration

To my family: Irene, Pilar and Sofia

“Trata de no dejar huella por donde caminas y, las que queden, que sean bellas.”

“Try not to change the way you walk through, but if you do so, make it beautiful”

Arturo Piegrande

Acknowledgments

The success achieved during my PhD thesis is directly related to the many people I have met and worked with over the past years in Quebec City and at the CHUL. The entire experience, which meant for my family and I to immigrate in Quebec, happily concludes with this thesis. In my opinion, the overall experience not only achieved academic excellence, but also a personal growth which extents to my all aspects of my personal life. Because of that, I want to thank all the people who crossed my way during these years, even those who are not specifically named in this section.

First and foremost, I want to thank my PhD thesis supervisor, Steve Lacroix. Thanks for the opportunity to join your lab without really knowing me. You have always been a great scientific mentor, with your example and dedication you inspire all your lab members. On a personal view point, you have always been extremely empathetic with me, understanding the difficulties of moving to a different country and offering me several personal and scientific solutions, and for that thanks. Tanks for the research freedom you gave me, which encouraged me to develop creative projects that resulted in great publications in my opinion.

I want to thank all my teammates. Especially the 3 great research assistants with whom I had the opportunity to work with, Nadia, Martine and Nico. Nadia, thank you for the enormous work at the animal research facility, always ready to perform fancy new experiments, with an enormous success. It was a great pleasure to share time at the surgery room, chatting and laughing about different aspects of life. Nico, the lab manager on the floor, thanks for the great scientific and technical discussions we had over the past years. It was a pleasure to work with you on several projects and discuss which antibodies we should purchase or not. Martine, thanks for all your personal and professional support. I had never met such a meticulous person; your level of details made your protocols the best over the CHUL. Your perseverance helped me in the success of many experiments. Thanks for your cooking recipes, in particular “la tourtière”, which we will certainly share with our friends in the future. In addition, I want to thank all the students I met in the lab, all of you helped me with brilliant scientific discussions and personal advices: Dominic, Sébastien, Alex, Benoit, Jorge, Marie and Floriane.

I want to tank all of my collaborators who helped in the development of my projects, Marie-Eve Janelle, Nathalie Vernoux, Marie-Ève Tremblay, Tobias Fuehrmann and Molly Shoichet. Also, I want to thank Parmveer Singh and Andrey Rymar from Plexxikon Inc. for the PLX drugs support. Thanks to all the teams at the CHUL, who helped in different experiments, Serge Rivest, Denis Soulet, Francesca Cicchetti, Frédéric Calon, Manu Rangachari, Luc Vallières and Ayman ElAli. Finally, I want to thank Dr David Gosselin and Ayman ElAli from the CHUL, as well Dr Jason Plemel from the Alberta University to accept to be on my thesis committee.

I want to thank my parents, Jose Vicente and Ana, for your continuous support from across the sea and when I was in Spain. Thanks for your kind words that often encouraged me to face and solve problems with positivity.

Lastly but not least, I want to thank my wife Irene, who never doubt to cross the sea to allow me to fulfil my dreams. Only you and me know the many difficulties that we had to overcome to finish my thesis and make Quebec City our home. Thanks for all your support during the past years. Also, you gave me the best present in the whole world, our daughters Pilar and Sofia. Thanks for taking care of them when I had to work at the lab and during my thesis writing. Without your support, all this would have been impossible.

Avant-propos

During the last 5 years, I have been working mainly on SCI projects. The core of my thesis includes 2 peer-reviewed research articles. In **Chapter 2**, Bellver-Landete *et al.* published in *Nature Communication*, we reveal the beneficial implication of microglia in the SCI context. More specifically, we uncovered that proliferating microglia beneficially influence astrocytes by releasing growth factors such as IGF-1. I conceived the study, designed and performed most of the experiments, analyzed the data, prepared the figures and drafted the manuscript. In **Chapter 3**, Bastien *et al.* published in *The Journal of Neuroscience*, where I am the second author, we reveal the implication of interleukin (IL)-1α in SCI. We identified microglia as the main source of the early IL-1α production following SCI. In that study, I performed experiments that involved blocking IL-1α using the IL-1 receptor type 1 (IL-1R1) antagonist, anakinra, resulting in an amelioration of the locomotor behavior in SCI mice. Also, I performed *in vitro* studies that demonstrated the importance of TOX3 for oligodendrocyte survival.

During my PhD thesis at Université Laval, I also had the opportunity to participate in projects related to multiple sclerosis, which were performed in the lab of in my thesis director, Dr Steve Lacroix. The findings resulting from these experiments were published in the *Journal of Experimental Medicine* in *2016*, paper on which I am the fourth author. As well, I established a collaboration with the pharmaceutical company Plexxicon to test some of their drugs in different CNS disorders, including SCI, peripheral nerve injury and multiple sclerosis.

During the course of my thesis, I also published results from my master's thesis project, where we studied the implication of the glutamatergic system in progenitor cells from the subventricular zone in response to stroke. Finally, I was a collaborator and coauthor on some articles that analyzed the implication of Cxcr4 and Cxcr7 in progenitor cell migration from the subventricular zone.

To summarize, below is a list of my publications during my PhD thesis at Université Laval:

Bellver-Landete V, Bretheau F, Mailhot B, Vallières N, Lessard M, Janelle ME, Vernoux N, Tremblay MÈ, Fuehrmann T, Shoichet MS, Lacroix S. Microglia are an essential component of the neuroprotective scar that forms after spinal cord injury. Nat Commun. 2019 Jan 31;10(1):518. doi: 10.1038/s41467-019-08446-0.

Sánchez-Mendoza EH, **Bellver-Landete V**, Arce C, Doeppner TR, Hermann DM, Oset-Gasque MJ. Vesicular glutamate transporters play a role in neuronal differentiation of cultured SVZ-derived neural precursor cells. PLoS One. 2017 May 11;12(5):e0177069. doi: 10.1371/journal.pone.0177069. eCollection 2017.

Lévesque SA, Paré A, Mailhot B, **Bellver-Landete V**, Kébir H, Lécuyer MA, Alvarez JI, Prat A, de Rivero Vaccari JP, Keane RW, Lacroix S. Myeloid cell transmigration across the CNS vasculature triggers IL-1β-driven neuroinflammation during autoimmune encephalomyelitis in mice. J Exp Med. 2016 May 30;213(6):929-49. doi: 10.1084/jem.20151437. Epub 2016 May 2.

Bastien D, **Bellver Landete V**, Lessard M, Vallières N, Champagne M, Takashima A, Tremblay MÈ, Doyon Y, Lacroix S. IL-1α Gene Deletion Protects Oligodendrocytes after Spinal Cord Injury through Upregulation of the Survival Factor Tox3. J Neurosci. 2015 Jul 29;35(30):10715-30. doi: 10.1523/JNEUROSCI.0498-15.2015.

Merino JJ, **Bellver-Landete V**, Oset-Gasque MJ, Cubelos B. CXCR4/CXCR7 molecular involvement in neuronal and neural progenitor migration: focus in CNS repair. J Cell Physiol. 2015 Jan;230(1):27-42. doi: 10.1002/jcp.24695. Review.

To conclude, I was enrolled in several projects that soon will be all published, including one focusing on the implication of nerve growth factor in peripheral nerve injury and another on the implication of neutrophils in the context of SCI.

Thesis doctoral

Introduction

1.1. The spinal cord

The spinal cord connects to the brain via the brain stem. Altogether, they form the central nervous system (CNS). The overall function of the spinal cord is to transmit and process the sensory information from peripheral sensor and to conduct motor response from the cortex to the muscles.

1.1.1. External anatomy

The human spinal cord measures about 43-cm long and is 2-cm width. It is protected by the vertebral column that can be subdivided into cervical, thoracic, lumbar, sacral and coccygeal regions. The spinal cord extends from the brain stem to the L1 lumbar region, where it splits into the *cauda equina* and *filum terminal*.

The spinal cord is surrounded by several layers that confer support and protection. The first layer is the pia mater, followed by the subarachnoid space, where flows the cerebrospinal fluid (CSF), the arachnoid mater and the dura mater, which contacts through a lipid layer the vertebral column held together by tendons, ligaments and muscles. These layers confer the spinal cord protection from most external damage.

In humans, 31 nerve pairs expand from the dorsal and ventral roots, connecting the spinal cord with the periphery. Eight pairs of nerves exit the spinal cord at the level of the cervical region (C1-C8), 12 pair from the thoracic (T1-T12), 5 pairs from the lumbar (L1-L5) and sacral (S1-S5) regions and 1 pair from the coccygeal region.

Motor stimuli exit the spinal cord by efferent tracts traveling through the ventral roots and controlling voluntary movement and function of internal organs. Sensory information from

the organs or the external environment enters the spinal cord by afferent tracts at the dorsal root level.

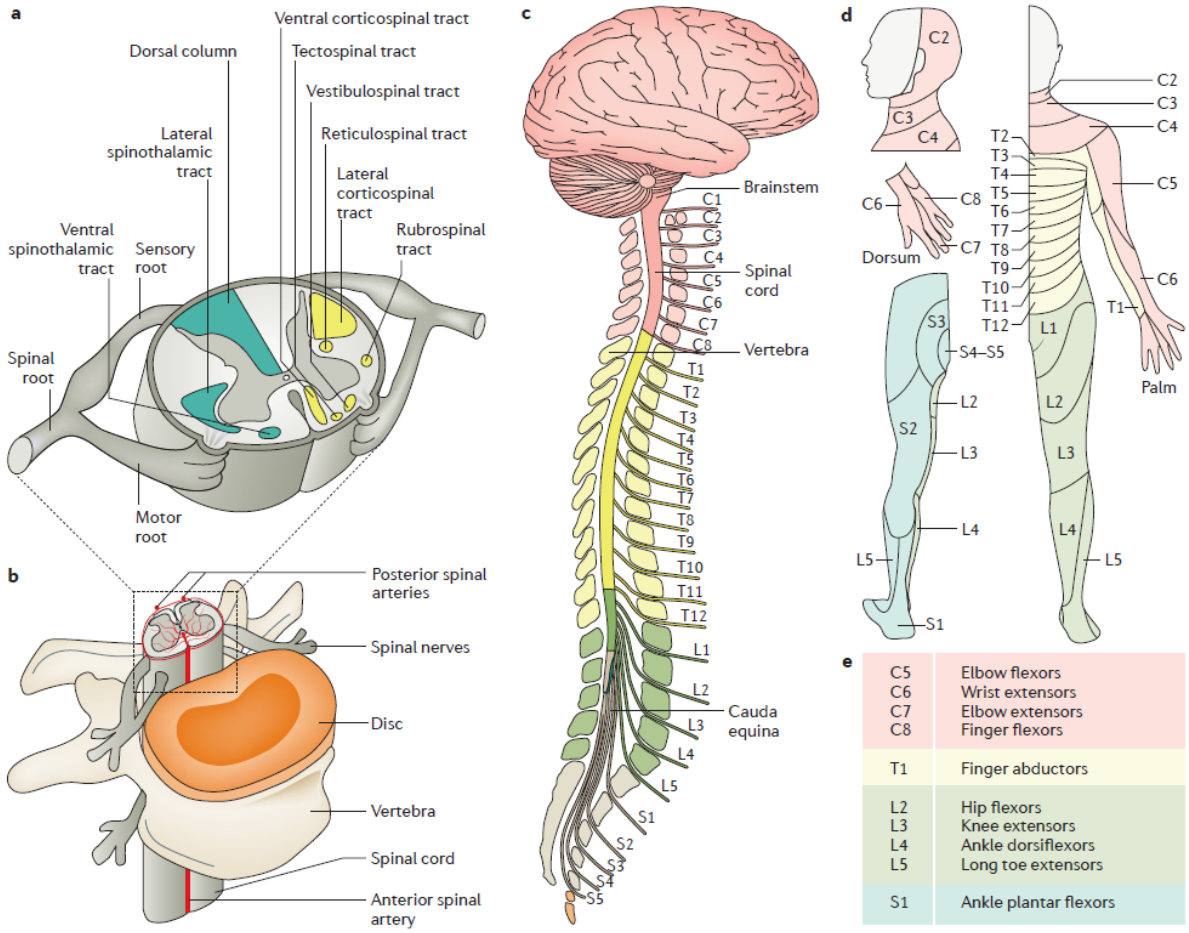

Figure 1.1. Anatomy of the spinal column.

Parts a–c are adapted with permission from REF[1], Macmillan Publishers Limited. Part d and part e are adapted with permission from the American Spinal Injury Association: International Standards for Neurological Classification of Spinal Cord Injury, revised 2011; Atlanta, GA, Revised 2011, Updated 2015. Obtained from REF [2].

1.1.2. Internal anatomy

In the spinal cord, there are two major regions, white and gray matter. The white matter surrounds the gray matter and traces a butterfly shape within the tissue. At the center, there is the central canal, a structure in contact with the CSF. The blood irrigation is performed by the anterior and the two posterolateral spinal arteries, which derive from the vertebral artery,

cervical radicular artery, thoracic radicular artery, radicularis magna and infrarenal radicular artery, depending on the spinal cord level.

The white matter is mainly composed of myelinated axons and glial cells. Human myelin is composed of 70% cholesterol and 30% proteins (in dry mass)[3], which confers its white color. Myelin favors action potential propagation from ascending (sensory) and descending (motor) tracts. The white matter can be divided in 3 regions: the ventral, lateral and dorsal funiculi. In humans, the ventral and lateral funiculi share ascending and descending tracts, whereas the dorsal funiculus is composed of ascending tracts only. The gray matter is composed of neuronal cell bodies, glial cells and non-myelinated axons. The gray matter can be divided in 4 main regions, the dorsal horn implicated in receiving somatosensory information, the ventral horn containing motor neurons that innervate the skeletal muscles, the intermediate column and the lateral horn that innervates the visceral and pelvic organs. The gray matter can be subdivided into a more detailed structure and function according to Redex's laminae I to X. Laminae I to IV are implicated in exteroceptive sensation, laminae V and VI in proprioceptive sensation, lamina VII contains neurons connecting to the autonomous system and motor visceral innervations, laminae VIII and IX modulate and innervate skeletal muscles, and lamina X surrounds the central canal and decussates axons from one side of the spinal cord to the other.

1.2. The glial cells during homeostasis

The concept of neuro-glia (neuro-gum) was first introduced in 1856 by Rudolf Virchow[4,5]. He considered neuroglia as supportive/connective tissue that binds to cellular elements of the nervous system. Since 1856, this concept has greatly evolved. Nowadays, glial cells are divided into 2 groups with 3 main cell types, the microglia and macroglia, the latter of which includes astrocytes and oligodendrocytes. In addition to their historical role, recent detailed studies highlighted new specific roles for each of these cell types, including a nutritional function. In this section, we will discuss the major roles of glial cells during CNS homeostasis, while in following sections we will analyze their role in CNS disorders such as SCI.

1.2.1. Microglia

Microglia was fully described by del Río-Hortega in 1919, the second most prominent member of the Spanish School of Histology and Histopathology, after Ramon y Cajal (nobel prize in 1906). Using its own impregnation method, based on Ramon y Cajal's method, del Rio-Hortega described microglia as a separate group of cells of mesodermal origin, and therefore distinct from neurons and glial cells (e.g. oligodendrocytes, astrocytes)[6–8]. Del Rio-Hortega suggested that microglia enter the brain in the early days during the developmental period and colonize the brain through blood vessels using white matter tracts as scaffolds. Microglia then transform from an amoeboid to a ramified morphology during the adult period and can be found throughout the entire CNS. Finally, he found that microglia switch back to an amoeboid morphology with phagocytic, migrating and proliferative capacities under pathological conditions[9]. For a more historic detailed study on microglia origin, please read Chapter 2 of the 'Microglia in Health and Disease' 2014 edited book[10].

A century later, we now understand that microglia originate from primitive erythro-myeloid progenitors from the yolk-sac, and that they colonize the CNS at embryonic day 8.5 in mice[11–13]. Within the CNS, according to their gene signatures, early progenitors undergo at least three temporal stages of development before becoming mature microglia[14]. Early microglia can be found from embryonic day (E) 10.5 to E14, pre-microglia from E14 to post-natal day (P) 9, and adult microglia starting at 4 weeks after birth in mice. During this development process, microglia rely on key transcription factors, such as PU.1 and IRF8, as well as cytokines (e.g. CSFs), adaptor proteins (e.g. DAP12) and receptors (e.g. CSF1R, CX3CR1) to ensure their correct development and migration to and within the CNS[11,15–18]. As del Rio-Horterga described, early and pre-microglia that colonize the CNS have an amoeboid morphology, in contrast with adult microglia which are highly ramified[6]. In the adult CNS, under physiological conditions, microglia are widely distributed and survey a defined area. Their number is relative stable although it varies depending on the CNS area and, accordingly, microglia tend to have a reduced turnover rate[6,19–21]. Each microglia is continuously screening its proximity, detecting any changes in their environment and participating in the process of synaptic pruning by engulfing synaptic buttons that are inactive, which earned them the name of surveyors of the CNS[22–25]. When an insult occurs

within the CNS, microglia are among the first cells to react, initiating an inflammatory response that results in a reduction of branching and amoeboid morphogenesis[26,27].

1.2.2. Astrocytes

The astrocyte concept was gathered over the 19th century by different researchers. Heinrich Müller first described in 1851 the radial-like glial retinal cells. One year later, Kölliker gave these cells the name they still have today, i.e. Müller cells, and Max Schulze studied them in more detail[28]. In 1856, Virchow introduced the "nervenkitt" (neuroglia) concept[5]. In 1857, Karl Bergmann observed astrocytes and their processes in the cerebellum and gave them the name of Bergmann glial cells[29]. In 1865, Otto Deiters first drew star like cells that resembled to astrocytes[30]. During the 1870s, Camillo Golgi, using his silver-chromate impregnation technique, was able to define neuroglia as round-shaped cells that project their fine processes in all direction, especially towards blood vessels. He described astrocyte endfeet and proposed that neuroglia transfer substances from the blood towards the parenchyma, which became the first indication of what we now today as the blood-brain barrier (BBB)[31]. In 1895, the term astrocyte was proposed by Michael von Lenhossék. By then, the two types of astrocytes had been identified as protoplasmic or grey matter astrocytes and the fibrous or white matter astrocytes. During the 20th century appeared the great figure of Santiago Ramon y Cajal, who with his impregnation mercury and gold chloride-sublime techniques based on Golgi's work, labeled both fibrous and protoplasmic astrocytes, thus revealing the enormous variety in shape (and function) of astrocytes. These researchers and many others in the coming years experimented and theorized enormously about astrocyte functions, coming up with many concepts that are still valid today.

Astrocytes are generated from radial glial that differentiate to glial intermediate progenitors during CNS development, which again differentiate into immature or mature astrocytes that retain proliferation capacities and, in some specific cases, can differentiate from NG2-positive glial cells. In the spinal cord, radial glia switch towards the gliogenic route at E12.5 under the effect of the transcription nuclear factor I-A and SOX9, downstream of Notch signaling[32,33]. These changes implicate the JAK/STAT signaling pathway as phosphorylated STAT3 with the co-activator complex p300/CBP bind to the promoter of several astroglial

genes, including the *glial fibrillary acid protein* (*Gfap*) gene[34]. Astrocytes are very heterogeneous, and their different shapes and functions depend on local signals within the CNS. For example, ventral astrocytes in the spinal cord are regulated by bHLH factor (scl/tal1) during embryogenesis[35]. Astrocyte's functions include the maintenance of homeostasis by recycling ions and protons, removing and releasing neurotransmitters, the control of entrance of any metabolite to the CNS from the periphery, the formation of the BBB, and support of neuronal functions. Their presence is a *sine qua non* condition for life in mammals, as the absence of SOX9 in radial glial cells impaired the differentiation of astrocytes during embryogenesis, resulting in a non-viable progeny[32,33].

1.2.3. Oligodendrocytes

CNS myelination depends on oligodendrocytes. The oligodendroglia was first comprehensively studied and defined by del Rio-Hortega in 1921[36,37]. Del Rio Hortega predicted that oligodendrocytes had a neuroepithelium origin and shared phylogeny with astrocyte progenitors. He proposed that they are the last cells to develop during CNS formation, as evidenced by their reduced number after birth, which is in contrast to their large accumulation in white matter tracts in adult CNS tissue. Additionally, Del Rio Hortega suggested that 'young' oligodendrocytes migrate using axons as scaffolds, following one or many axons, and once myelin is formed, remain immobile. Based on his observations, 4 different types of myelinated oligodendrocytes were identified[38].

During spinal cord development, oligodendrocytes rely on the transcription factors SOX8, SOX9, and SOX10 for their differentiation from radial glial cells[39–41]. OLIG2 promotes the expression of SOX10 in oligodendrocyte precursor cells (OPCs) and oligodendrocytes, which in turn maintains *Olig2* expression[42]. Although SOX9 is downregulated upon OPC differentiation, SOX8 and SOX10 are continuously expressed and therefore key transcription factors implicated in myelin formation[41,43]. As del Rio Hortega suggested, oligodendrocytes are one of the last cells to be formed during CNS development, and OPCs migrate using the vasculature as a scaffold during CNS development[36,44]. Single-cell RNA-seq transcriptomic analysis recently revealed the presence of at least 12 populations of oligodendrocyte cell lineages distributed over the CNS[45]. Starting with OPCs followed by differentiation-

committed oligodendrocytes, newly-formed oligodendrocytes (at least 2 subsets), myelin-forming oligodendrocytes, and up to 6 subsets of mature oligodendrocytes. The main function of oligodendrocytes is the formation of myelin. Myelination is an important regulator of motor learning[46]. When myelinating oligodendrocytes are killed during adulthood, mice motor capacities are highly reduced. Interestingly, deficiency in myelin formation by newly generated oligodendrocytes results in impairment in new motor learning process upon training[46]. Oligodendrocytes rapidly die after CNS injury, but their myelin stays within the CNS for several weeks afterward[47]. It has been demonstrated on several occasions that myelin accumulation after injury in the adult CNS reduced axonal plasticity and is one of the leading causes of axonal regeneration failure[48–52].

1.3. Spinal cord injury

Spinal cord injury (SCI) currently affects more than 86,000 individuals in Canada, with 3,675 new cases each year[53,54]. The estimated cost exceeds $3 million per individual throughout their lifetime[53,54]. SCI can be divided into traumatic SCI and non-traumatic SCI[53]. Traumatic SCI occurs when an external impact causes a mechanical compression or damage to the spinal cord. The most important causes of SCI are traffic accidents, falls, sports accidents, and violence. Most traumatic SCI cases affect men between 16-34 years. On the other hand, women above 40 years of age have an increased prevalence of non-traumatic SCI resulting from complications of spondylosis, tumor or infections.

The consequences of SCI vary depending on the severity and the level of the injury. From the severity standpoint, a complete SCI will affect all spinal cord segments, often resulting in a complete loss of motor and sensory functions. Incomplete SCI will affect specific regions of the spinal cord and, depending on the damaged area, lead to a loss of motor and/or sensation functions. A lesion at the cervical level (C1-C8) will lead to tetraplegia or an incapacity to move the arms and/or legs. In contrast, lesions below the cervical level (i.e. T1-L5) will affect different trunk muscles depending on the level of injury, and thus be associated with paraplegia or impairment in leg movement. Lesions at the sacral level (S1-S5), which are very rare, will affect hips and legs but patients will most likely be able to walk. Other

complications associated to SCI are immune depression, and issues with the urinary, respiratory and sexual systems.

The cellular and molecular consequences of SCI can be divided into at least 3 different categories: the primary damage, the secondary damage and the chronic injury/regeneration phase. Overall, the primary damage phase, or primary cell death phase, ranges from seconds to days after SCI. The secondary damage phase, or inflammation phase, which results in the expansion of the primary lesion to surrounding tissue, can last from hours to weeks after SCI. Inflammation also induces the proliferation of resident cells, which contributes to partial tissue replacement. Finally, the chronic injury phase, or regeneration/tissue remodeling phase, is characterized by the neuronal plasticity events that occur during weeks to months after SCI. The exact timing of these phases may vary depending on several circumstances and can often overlap during SCI.

1.3.1. Primary damage

After traumatic SCI in humans, often the broken bone impacts the spinal cord leading to prolonged pressure and damage. The impact causes death of spinal cord-resident cells including neurons, glia and cells forming the blood vessels, which results in a necrotic area[55,56]. The breakdown of the vasculature also causes intense hemorrhages in the spinal cord parenchyma[57]. In addition to the cellular debris, platelets, leukocytes and red blood cells can therefore accumulate in the spinal cord parenchyma.

The primary damage determines the severity and outcome of SCI in patients. It is therefore important to avoid additional damage to the spinal cord by moving the injured person and to get professional help as soon as possible. Studies suggest that treatment within the first 4 hours has an increased chance to ameliorate the outcome of SCI patients[58–67]. Importantly, surgical decompression, which consists in removing the pressure of the bone that crushes the spinal cord by surgery, is the only standardized procedure that showed an increased benefit in SCI patients. Surgical decompression was found to be effective, as shown by meta-analysis of preclinical studies, when performed early after SCI[68].

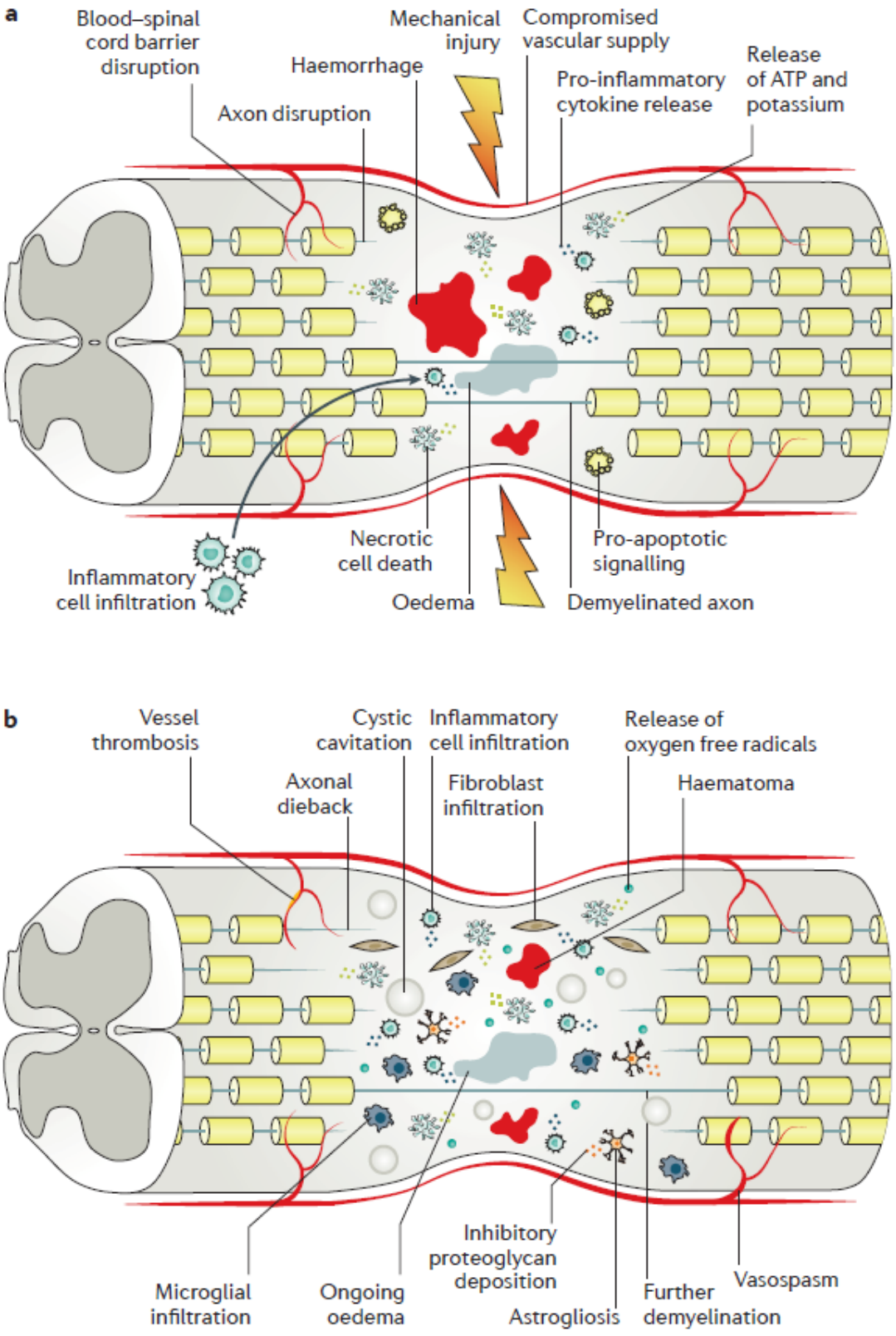

Figure 1.2. Early physiopathology following SCI.

a Primary damage events, between 0 to 48 hours following SCI. **b** Secondary damage events, between 2 to 4 days following SCI. From REF[2].

1.3.2. Secondary damage and tissue replacement

After SCI, necrotic cells release their cellular content within the extracellular milieu. Alarmins, glutamate and reactive oxygen species, among others, thus become detectable in the spinal cord parenchyma. These molecules can diffuse in the surrounding tissue and cause further damage, a process that has been referred to as secondary tissue damage. For example, free glutamate may bind to its receptors at the surface of challenged neurons, increasing excitatory currents and intracellular calcium waves that can cause cellular death in a process known as excitotoxicity[69]. Also, alarmins or damage-associated molecular patterns (DAMPs), such as interleukin-1 alpha (IL-1α), S100 proteins, high mobility group box protein 1 (HMGB1), heat shock proteins, and nucleotides, are released by dead or dying cells[70–72]. Alarmins must bind their specific receptor(s) to initiate inflammation. Then, proinflammatory cytokines produced by neurons and glial cells, such as interleukin-1 beta (IL-1β) and tumor necrosis factor alpha (TNF-α), amplify the inflammatory response and increase myeloid cell recruitment[70,73–77]. Recruited neutrophils and monocytes release a plethora of cytokines that regulate inflammation in the injured spinal cord. As well, myeloid cells produce high amounts of free radicals (e.g. nitric oxide) that interact with biomolecules and promote irreversible oxidation, thus causing apoptosis of CNS-resident cells[78–84]. In summary, the enormous inflammatory response that occurs in the spinal cord can promote the death of challenged cells in the surrounding tissue, expanding the original damage.

But not all inflammatory events are negative. The inflammatory response activates CNS-resident cells and triggers mechanism of wound healing. Proliferation is one of the first cellular responses that occurs during this phase, starting around 2-3 days post-injury and lasting approximately 10 days in SCI rodents[85–89]. The newly generated cells try to replace dead cells and promote recovery. However, cell replacement within the CNS cannot be fully completed for unknown reasons, thus leading to permanent deficits in mammals.

The BBB is a complex structure composed of up to 6 types of endothelial cells (ECs), 3 types of mural cells, pericytes, perivascular macrophages, and up to 2 types of fibroblasts, all that

surrounded by astrocyte endfeet[90]. Its break down at 24h post-SCI allows the rapid entry of blood-derived immune cells and molecules[85]. During the secondary damage phase, the BBB starts to recover with significantly less penetration of Evans Blue, a dye widely used to analyze BBB leakage, from day 5 post-SCI in mice[85]. Interestingly, recovery of the BBB function parallels EC proliferation, which also peaks at 5 days post-SCI with ~15% of blood vessel-associated ECs expressing the cell proliferation marker Ki67[91]. In parallel, the maximum accumulation of monocyte-derived macrophages in the injured spinal cord is also at 7 days post-SCI[91]. Recently, Liu and collaborators, using intravital microscopy in a zebrafish model, showed that macrophages can promote brain vascular repair by direct interaction with ECs[92]. Monocyte-derived macrophages produce several growth factors, (i.e. VEGF, basic fibroblast growth factor (bFGF) and angiopoietin-1) which may also influence the behavior and function of ECs[93–97]. Interestingly, Greenhalgh and collaborators demonstrated that blocking the infiltration of monocytes into the injured spinal cord using C-C chemokine receptor type 2 knock out mice *(Ccr2-KO*) exacerbated damage[98]. Thus, the protection of vasculature disruption and promotion of EC proliferation, through exogenous delivery of pro-angiogenic factors such as VEGF, angiopoietin-1 and bFGF produced by MDMs are promising therapies for human SCI based on the work done in rodent models[99].

Glial cells such as astrocytes, oligodendrocytes and microglia also proliferate extensively during the first week after SCI. Astrocyte proliferation is a key step in the formation of the glial scar[89,100]. Transgenic mouse models in which the activation of astrocytes was inhibited or impaired showed poor recovery from SCI[86,87,101–104]. The glial scar is a compact barrier that restricts the migration of blood-derived myeloid cells and separates the fibrotic tissue from neuronal elements, thus reducing the possibility of secondary tissue damage that may be caused by inflammation. However, a bystander negative effect of the glial and fibrotic scars is the inhibition of axonal regeneration and plasticity (please see section 1.3.3.1, The glial scar)[86,87,101–104].

Mature oligodendrocytes may die because of secondary damage following SCI, probably owing to their high specialization and the enormous energy requirements for their cellular functions. The loss of mature oligodendrocytes is compensated by the proliferation of OPCs during the first week after SCI[88]. Although the proliferation of OPCs was initially thought to

be beneficial for functional recovery, Duncan et al. elegantly demonstrated that blocking the proliferation of OPCs does not affect spontaneous recovery in SCI mice[105]. Instead, the preservation of mature oligodendrocytes is determinant since the death of these cells promotes the release of myelin, which has been shown to impair axonal plasticity[48–52], for further details please refer to section 1.3.3.3.

Perivascular cells also proliferate during the first week post-SCI. Type B pericytes were initially described as one of the main cell types that proliferate and invade the core of the lesion, forming what is now known as the fibrotic scar, based on expression of markers such as PDGFR-A, PDGFR-B and CD13[106,107]. However, a detailed analysis of these markers in adult CNS perivascular cells using single cell RNA-seq technology revealed that type 1 fibroblasts are the cells that coexpress *Pdgfra*, *Pdgfrb* and *Anpep*[90]. In contrast, pericytes only coexpress *Pdgfrb* and *Anpep*, but not *Pdgfra*. This led to an intense competition to identify the cells at the origin of the fibrotic scar after CNS injury. Still, while pericytes and fibroblasts invade the core of the lesion, they release extracellular matrix (ECM) molecules[106,107]. This ECM, composed among other things of collagen, can inhibit axonal growth and functional recovery after SCI. It starts at day 3 post-SCI, is completed at 14 days and lasts for months in mice. In a recent study, Dias and collaborators demonstrated that full inhibition of pericyte/fibroblast proliferation increased tissue loss and reduced functional recovery after SCI[107]. In contrast, partial inhibition of pericyte/fibroblast proliferation was associated with reduced expression of collagen-1 and other ECM molecules, which resulted in enhanced axonal plasticity and locomotor recovery[106,107]. Thus, an attenuation of the fibrotic scar might be an interesting way to promote axonal plasticity after SCI. This will be further discussed in section 1.3.3.1.

In sum, inflammatory events could promote either detrimental or beneficial effects after SCI. An adequate balance of inflammation, i.e. reducing the detrimental effects and promoting of the beneficial ones, should be targeted to promote recovery after SCI.

1.3.3. Chronic injury/regeneration phase

The beginning of the chronic injury phase follows the early acute and subacute phases and is associated with the establishment of the glial scar, which occurs between 2-4 weeks after SCI

in mice. The core of the lesion is mainly composed of non-neuronal cells such as pericytes/fibroblasts, microglia, ECs and blood-derived immune cells. These cells contribute to the release of ECM proteins, such as collagen-1, that interact with N-cadherins at the membrane surface of proliferating reactive, scar-forming astrocytes located at the edge of the lesion core and potentially inhibiting axonal regeneration[108]. In humans, the lesion core is sometimes filled with interstitial fluids rather than cells, as illustrated by the presence of cavities surrounded by astrocyte endfeet. The glial scar, whose primary role is to protect neuronal elements that survived the primary mechanical impact, is strategically located at the interface between the lesion core and penumbral CNS tissue. As for microglia, astrocytes are activated in a distance-dependent manner from the core. Although spinal cord-resident cells tend to return to a homeostatic state, they nevertheless remain somewhat activated for months in mice and years in humans[109].

Axonal regeneration is reduced in the adult CNS. In contrast, during CNS development, axons can travel long distances with the support of the appropriate growth factors. Upon SCI, neurons subjected to axonal injury undergo a series of pathophysiologic changes, starting with acute retrograde axonal degeneration ("dying back") of the proximal axon segment and Wallerian degeneration (WD) of the distal axon segment. WD occurs in the axon segment disconnected from the neuronal cell body because of the lack of appropriate growth support, thus causing the axonal cytoskeleton to breakdown. The acute axonal degeneration consists in the retraction of axons that remain connected to the neuronal body, which eventually could account for plasticity events.

1.3.3.1. The glial scar

The glial scar separates fibrotic non-neuronal tissue from reactive spinal cord-resident cells. A number of studies have established that the formation of the glial scar is a critical step that prevents further damage to the injured spinal cord tissue. First, the interruption of astrocyte cell division in transgenic mice expressing the suicide gene *Thymidine kinase* (TK) specifically in *Gfap*-expressing cells (i.e. *Gfap-TK* mice) was not only associated with a disrupted glial scar, but also resulted in increased BBB permeability, more widespread inflammation, increased neuronal and oligodendrocyte death, and reduced locomotor recovery[87]. Second, Okada and collaborators demonstrated that reduced reactivity in

proliferating astrocytes, through the blockade of STAT3 signaling in *Nestin*-expressing cells, disrupted glial scar formation, thus showing results similar to those obtained in *Gfap-TK* mice[86]. Third, deletion of the intermediate filaments GFAP and vimentin using double KO mice, abolished astrocyte reactivity, impaired glial scar formation, and was associated with an increased lesion area in a mouse stroke model[110–112]. Fourth, inducing astrocyte reactivity after SCI in mice with conditional deletion of the *Socs3* gene specifically in astrocytes led to an upregulation of STAT3 expression, favored glial scar formation, and improved locomotor recovery after SCI[86]. Finally, another study revealed that astrocytes supported (by direct contact) axonal regeneration in the spinal cord parenchyma, and that the absence of astrocyte reactivity increased the lesion volume and reduced the number of axons[102]. Altogether, these studies demonstrate that an adequate astrocyte response following CNS trauma is beneficial.

In addition to the astrocytic scar, some pericytes/fibroblast colonize the core of the lesion, thus creating the fibrotic scar[90,106]. Fibrotic cells associated with vessels, proliferate and accumulate at the lesion core and, in addition to infiltrating blood-derived immune cells and microglia, form the fibrotic scar[89,106]. The fibrotic tissue produces collagen 1 that interacts with N-cadherins in reactive scarring astrocytes located at the edge of the core, but also inhibits severed axons from growing inside the lesion core[108]. Indeed, the attenuation of these interactions with an antibody was shown to support axon regenerating across the fibrotic scar[108]. The attenuation of the fibrotic scar was also found to favor regeneration of cortico-motor and somato-sensory axons following SCI[107]. However, the complete inhibition of the fibrotic scar led to the formation of enormous cysts within the spinal cord, resembling those typically observed in rats and humans[107].

Regenerating axons rarely penetrate the fibrotic scar after SCI. Rather, they prefer to grow through reactive CNS tissue. Regenerating axons compensate the neuronal loss by creating new networks and synapses with the support of reactive astrocytes[102]. Evidence demonstrated that, for example, cortical serotoninergic motor neurons create new synapses with motor neurons in healthy tissue above the lesion in rodents that suffered a lateral hemisection, allowing rats to compensate the motor deficiency created by the hemisection[113,114]. Events of axonal outgrowth and plasticity require, however, the presence of appropriate neurotrophic factors combined with a reduction in expressions of inhibitory molecules.

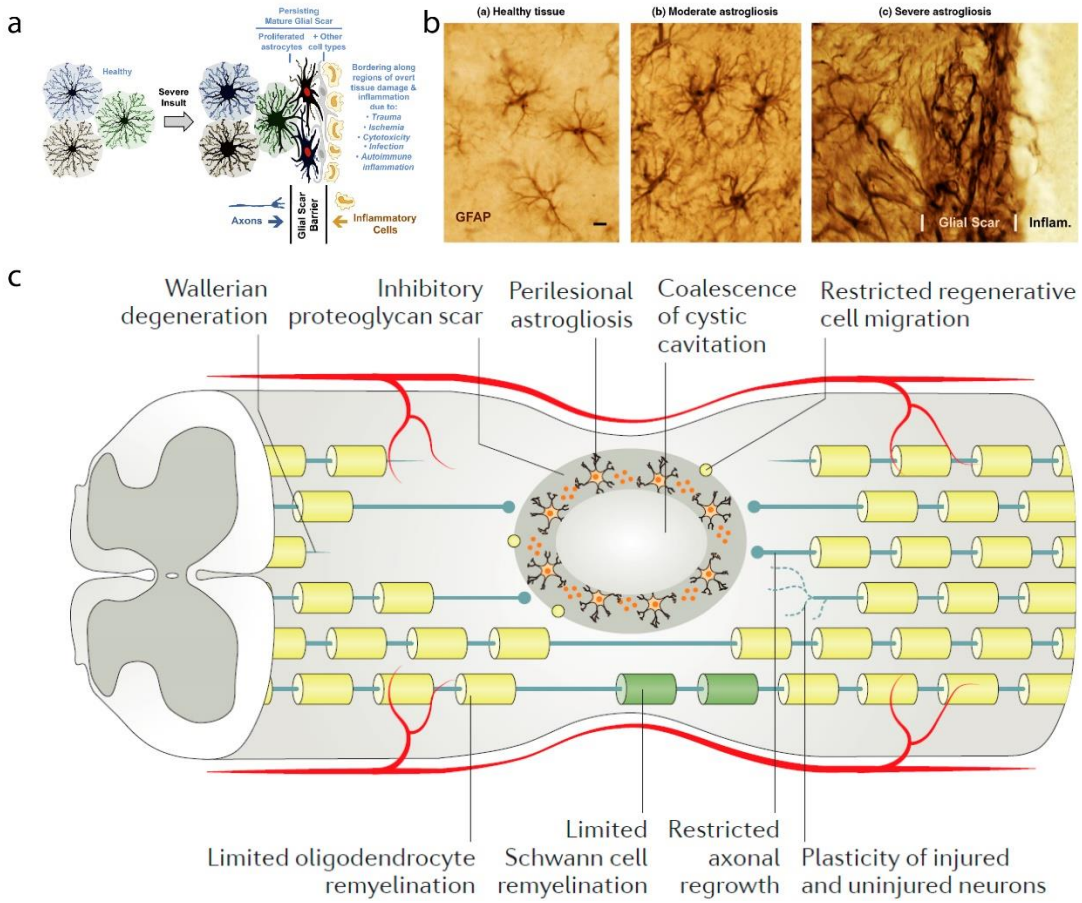

Figure 1.3. Glial scar formation, chronic phase.

a and **b** show the proliferation and activation of astrocytes during glial scar formation, from REF[115]. **c** schematic representation of chronic phase events, between 7 days to months following SCI, from REF[2].

1.3.3.2. Enhanced axonal regrowth: Neurotrophic factors

Early in the 20th century, Cajal described that transected CNS axons invade peripheral nerve grafts, but when cells in the grafts are killed upon chloroform treatment no regeneration is possible. The chemical extraction of molecules within the grafts and their loading onto a cellulose matrix also supported axonal regeneration[116]. This was elegantly validated by Albert Aguayo's group at the end of the century[117,118]. They further confirmed the need for proliferating cells in the peripheral nerve grafts to promote axonal outgrowth[119,120]. Although, originally, axonal regeneration in the injured peripheral nerve was solely associated with Schwann cells, Barrette and collaborators elegantly demonstrated that myeloid cells share the responsibility for axonal outgrowth, as demonstrated by the fact that *Cd11b-TK* mice, in

which myeloid cells can be depleted upon ganciclovir administration, failed to regenerate axons after peripheral nerve injury (PNI) and in peripheral nerve grafts placed at the site of SCI[121]. During peripheral nerve regeneration, macrophages are implicated in cellular and myelin debris clearance and helping in the formation of new vasculature by the release of diverse factors and/or by physical mechanical traction[92]. Accordingly, ganciclovir-treated *Cd11b-TK* mice showed impaired vasculature[121]. Interestingly, Schwann cells have been shown to migrate using nerve vasculature as a scaffold to promote their axon growth promoting effects after PNI[122]. Recently, Anderson and collaborators demonstrated that axonal regrowth events after SCI require contact with astrocytes, which they used as scaffold[102]. This once again confirms the capacity of CNS axons to regenerate pending the right conditions.

As previously mentioned, the regeneration capacity of the CNS is dramatically reduced after SCI and axonal plasticity does not seem to be able to compensate for all of the consequences of the injury. Importantly, during the process of axonal guidance and plasticity events, CNS-resident cells release a variety of neurotrophic factors that enhance axonal growth, such as nerve growth factor (NGF), brain-derived growth factor (BDNF), insulin growth factor-1 (IGF-1), and neurothrophin-3 (NT3)[123]. Accordingly, the exogenous administration of these molecules was found to promote axonal regrowth "in vivo" following SCI[102,124,125]. Axonal regrowth events will be briefly discussed below, but are largely reviewed by O'Shea and colleagues[126].

1.3.3.3. Axonal regeneration inhibitory factors

Many lessons regarding the role of neurotrophic factors were learned from studies dealing with peripheral nerve injury, where spontaneous axonal regeneration occurs. As previously discussed, axonal regeneration is limited in the injured spinal cord, thus causing permanent disabilities. The impaired plasticity is believed to be caused by the lack of neurotrophic factors and the presence of growth-inhibitory molecules.

During the process of WD, myelin is released in the extracellular milieu and inhibits axonal regrowth through several growth cone inhibitory molecules, including: Myelin associated glycoprotein (MAG), oligodendrocyte myelin glycoprotein (OMGP), Nogo-A, Ephrins and

Semaphorins[48–52,127]. After peripheral nerve injury, myelin debris are rapidly eliminated within 14 days post-injury. However, myelin debris clearance takes several months or years following SCI[47]. The myelin inhibitory molecules MAG, OMGP and Nogo-A all interact with a common receptor, namely the Nogo receptor type 1 (NGR1), found on the membrane surface of neurons. NGR1 recruits Lingo-1, $p75^{NTR}$ or Troy to form a transmembrane complex that inhibits axonal growth[48,128]. The blockade of the Nogo-A signaling pathway via the injection of an anti-Nogo-A antibody was reported to promote recovery after SCI in various animal models[129–142]. Of note, the injection of anti-Nogo-A antibodies in SCI primates improved their hands and arms dexterity compared to control animals[143]. For an extensive review on myelin inhibitory molecules, please see[144].

ECM production has also been associated with axonal growth inhibition. For example, pericytes/fibroblasts that accumulate at the lesion core produce Chondroitin Sulfate Proteoglycans (CSPGs) and Collagen-1 that showed axonal growth inhibitory properties both in vitro and in vivo[145,146]. Interestingly, intrathecal administration of Chondroitinase ABC, an enzyme that hydrolyzes CSPGs, induced robust regrowth of descending serotoninergic axons and ascending sensory tract axons after SCI, an effect that was associated with improved locomotor recovery[147].

As discussed before, astrocytes can either promote or inhibit axonal regeneration after SCI. This may depend on the type of astrocytes being involved. At least two subsets of astrocytes have been described following SCI, i.e. reactive and scarring astrocytes. Reactive astrocytes are often associated with the beneficial effects of astrocytes after SCI, which include cell proliferation and enhance axonal regrowth. However, reactive astrocytes eventually differentiate into scarring astrocytes at ~14 days post-SCI in mice, leading to the formation of a mature glial scar. This interaction reduces axonal plasticity and/or regrowth. However, the administration of antibodies directed against the β1 Integrin disrupted this interaction, thus allowing axonal plasticity and locomotor recovery after SCI[108].

At least two conditions are therefore needed to ensure axonal regrowth and/or CNS plasticity: 1) the presence of axon growth promoting signals (e.g. growth factors) and 2) the absence axon growth inhibitory signals (e.g. Myelin-associated Inhibitory Molecules, N-Cadherins-Collagen-1).

1.4. The microglial response following SCI

Microglia are believed to be among the first responders following SCI. In this section, I will discuss their roles during the different phases of SCI. A special attention will be paid to the differences between microglia and monocyte-derived macrophages, and how new research tools allow us to distinguish between the two cell types and their respective effects in the context of SCI. As well, we will discuss the different pathways associated with their beneficial and detrimental effects.

1.4.1. The early microglial response following SCI

Following an impact, resident cells within the spinal cord die as a consequence of the primary insult. It is generally believed that microglia rapidly migrate towards the site of SCI, as they do following a laser-induced CNS lesion during which microglia rapidly send their ramifications towards nucleotides (e.g. ATP) being released from dying and dead cells[27,148]. However, the kinetics of the microglial response following SCI and their exact role remain unknown.

Microglia are believed to initiate the inflammatory response through the release of DAMPs and proinflammatory cytokines. Recent work from the late Ben Barres has identified some of the key signals produced by microglia, which include IL-1α, TNF-α and C1q[149]. The study revealed that microglia-derived IL-1α, TNF-α and C1q act synergistically to activate astrocytes, leading to the generation of A1 astrocytes. Notably, A1 astrocytes were associated with a neurotoxic phenotype and found to be deleterious in various animal models of CNS insult and diseases. We previously demonstrated that microglia produce IL-1α as early as 4 hours post-SCI[70]. IL-1α was found to promote myeloid cell recruitment at the site of injury. The recruitment of myeloid cells, in particular neutrophils and proinflammatory (M1) monocytes, has been historically associated with an increased lesion volume[150,151]. Accordingly, *IL-1α-KO* mice exhibit improved locomotor recovery compared to wild-type mice after SCI[70]. But this effect cannot be solely associated with a reduced myeloid cell recruitment, because *IL-1β-KO* mice have similar deficits in terms of myeloid cell infiltration, despite showing a reduced locomotor recovery compared with *IL-1α-KO* mice[70].

This highlights the influence that IL-1α may have on other cell types, such as astrocytes and oligodendrocytes[70,149].

Tnfa mRNA expression peaks at 1 hour post-SCI and all CNS-resident cells contribute to its production in both rats and mice, including microglia[76,152,153]. The two receptors of TNF-α, i.e. *Tnfr1* and *Tnfr2*, are highly expressed by microglia. *Tnfr1* is also expressed by astrocytes, oligodendrocytes, and endothelial cells in the CNS under steady state conditions, highlighting the ability of basically all CNS cell types to respond to inflammation after SCI[154]. The elimination of the TNF-α response using *Tnfa-KO* mice protects these animals from SCI-induced inflammation, favoring the differentiation of microglia/macrophages towards an M2 phenotyope and reducing at the same time the number of apoptotic cell bodies[155]. Similar results were obtained using *Tnfr1-KO* mice after SCI, i.e. reduced inflammation, apoptosis and tissue damage correlated with enhanced locomotor recovery compared to their wild-type littermates[156]. Interestingly, the blockade of TNF-α with either etanercept, a TNF inhibitor functioning as a decoy receptor that binds to TNF-α, or infliximab, an antibody directed against TNF-α, also protected mice from SCI[156,157]. Once again, the neutralization of TNF-α led to reduced inflammation, reduced apoptosis, increased myelination, and enhanced locomotor recovery. These studies suggest that blocking TNF-α signaling is a promising therapeutic avenue for SCI in the years to come.

The complement cascade is rapidly activated in a variety of infections and stressful situations[158–162]. Microglia, which are the main cellular source of C1q within the CNS and express the complement receptor 3 (CR3), rapidly respond to basically any changes from the normal homeostatic condition[149,163,164]. Following an insult such as SCI, there is a rapid upregulation of C1q in both mice and humans[165,166]. Deletion of the *C1qa* gene in an immunocompetent mouse line resulted in an improved locomotor recovery at early time points post-SCI[167]. In a subsequent study, the same authors revealed that the complement C1q also favors axonal sprouting and/or regeneration after SCI, thus suggesting a dual role for this molecule[168]. The late effect seen on axonal sprouting/regeneration could depend on microglia, because these cells express complement receptor which respond to C1q and accumulate at the site of SCI at later time points[86,87,89,169]. Regarding the deleterious early response, it is true that other CNS cell types may respond to the complement cascade and

that infiltrating innate immune cells may do so as well following SCI[149]. Thus, further studies will need to be conducted to identify the major actors on this response. One way to answer the role of microglia, might be to study mice with conditional deletion of the *C1qa* gene specifically in microglia.

Altogether, these studies indicate that microglia are crucial cells initiating the immune response after SCI. Overall, the cytokines described above appear to be associated with a poor outcome and are promising therapeutic targets for SCI.

1.4.2. The late microglial response following SCI

From day 2 to weeks after SCI, microglia gradually adapt to the damaged environment. They lose their ramified morphology and acquire an ameboid shape, making them even more difficult to discriminate from MDMs that have infiltrated the lesion core and which remain present throughout the chronic phase[7,27,169]. Those similarities, along with a similar protein expression profile, make it very difficult to assign an individual function to each one of these cell populations. For this reason, they are often described in the SCI literature as microglia/macrophages.

Since most foamy cells within the injured spinal cord present myelin debris load, myelin phagocytosis has been associated to both microglia and MDMs[170–173]. In experimental autoimmune encephalomyelitis (EAE), a mouse model of multiple sclerosis, MDMs seem to initiate demyelination by attacking myelin at the Ranvier Nodes, allowing microglia to access and clear myelin debris[174]. Therefore is not surprising that both cell types present the necessary machinery to undergo myelin debris clearance following SCI (for review[175–178]). However, the effect of myelin debris clearance on macrophage polarization is still controversial, with different reports suggesting that myelin phagocytosis polarizes macrophages towards the M1, M2 or both phenotypes in vivo[155,179–188]. In vitro experiments showed, as well, confusing results in terms of microglia and MDM polarization upon myelin phagocytosis[155,182,183,186,189–192]. These contradictory results may be explained, at least partially, by the use of cell lines instead of primary cultures. For example, microglia cell lines and primary cultures of microglia respond differently to stimulation with MCSF, GM-CSF+INF-γ+LPS, MCSF+IL-4 or MCSF+TGF-β[193]. Also, the culture conditions need to be

carefully monitored, as a recent *in vitro* study demonstrated that myelin phagocytic capacities of microglia are impaired in defined medium conditions. In contrast, the addition of fetal bovine serum to the serum was sufficient to induce myelin phagocytosis by microglia[194]. Myelin pre- or post-incubation following cytokine stimulation may also affect the macrophage response[179,181,182]. Therefore, additional well-controlled experiments will be required to fully understand the individual contribution of microglia and MDMs, as well as the mechanisms involved in myelin debris phagocytosis in the injured CNS.

Microglia and macrophages have both been associated with sprouting and synaptic plasticity events occurring following SCI (for review[126]). During the developmental period, microglia assure the correct migration of axons and the wiring of neuronal networks through the regulation of synaptic pruning[18,23–25,195–202]. Interestingly, microglia and MDMs release a plethora of growth factors, including IGF-1 and BDNF, that may favor axonal plasticity under various circumstances[89,203–207]. However, the relative importance of each cell type for CNS plasticity and regeneration is unclear and will need to be carefully addressed since prior reports found that axonal length is reduced when axons are in contact with macrophages[208,209]. Thus, it is possible that one of these two cell populations, or even a subclass of these cells, may be associated to CNS damage[204,207,210], whereas the other may be responsible for CNS plasticity events.

In the next section, I will discuss in more detail the knowledge we have on each one of these two cell populations. I will introduce and discuss the new tools that were recently developed to distinguish microglia from MDMs, and vice-versa. Finally, I will talk about models of microglia depletion that can be used to understand the function of these cells in the context of SCI.

1.4.3. Solving the unknown: Microglia vs monocyte-derived macrophages

1.4.3.1. Origin

During early stages of embryonic development, hematopoiesis occurs in the yolk sac and the fetal liver. In the yolk sac, primitive erythro-myeloid progenitors produce primitive macrophages which colonize different embryonic tissues, including the CNS. Primitive

macrophages are unique in the sense that they do not differentiate from monocytic intermediates, as it occurs during adulthood. At E10.5-E11.5, a new wave of hematopoietic progenitors is generated in the para-aortic splanchnopleura region and then in the aorta, gonads, and mesonephros (AGM) region[211,212]. Hematopoietic stem cells generated within the AGM will eventually lead to the establishment of definitive hematopoiesis[213]. From now on, hematopoietic progenitors from the yolk sac and AGM region will invade the fetal liver[214]. The liver will then become the major hematopoietic source during embryonic development and give rise to cells of all hematopoietic lineages, including monocytes[215]. Few days before birth, the hematopoietic progenitors will migrate towards the bone marrow (BM), establishing adult hematopoiesis, and becoming the major source of all the different blood cells for the entire life span. For an extensive review, please see[216].

1.4.3.2. Differences

As described above, a major difference between microglia and MDMs is their origin. When they colonize the CNS, primitive macrophages proliferate and expand to all CNS regions. These primitive macrophages are retained within the CNS by pericytes, which settle on the parenchymal (abluminal) side of the CNS endothelium, thus starting to create a physical barrier between the blood circulation and CNS. Soon after birth, astrocytes will shield the CNS vasculature, conferring to the brain and spinal cord the status of immune-privileged organs. At the end of this period, microglia are confined within the CNS, where they autoregulate their own destiny by self-renewal[217–220]. In contrast, monocytes originate from hematopoietic stem cells (HSCs) and progenitor cells in the bone marrow (BM)[221]. Monocytes can travel to all organs via the blood circulation and differentiate into specialized macrophages[12,222,223]. Depending on the organ and conditions, tissue-resident macrophages derived from the yolk sac or liver during embryonic hematopoiesis can be replaced at a different rate after birth by MDMs [12,224,225].

The turnover rate varies widely between microglia and MDMs. Monocytes have a rapid turnover and renew virtually every week from BM progenitor cells [226,227]. On the contrary, microglia self-renew locally in the CNS, with a turnover rate estimated at 96 days in rodents[89,218,228]. In humans, 28% of the microglial population is renewed every single year. Microglia depletion experiments have confirmed that these cells divide exclusively from a

local progenitor pool residing inside the brain and spinal cord after birth, being able to repopulate the almost entire population within a week[17,89,219,229]. During the repopulation process, virtually all microglia were found to divide, as demonstrated by their expression of the proliferation marker Ki67[17,89,219,229]. Repopulating microglia express Nestin, an intermediate filament associated with precursor cells.

Under normal (naïve) conditions, microglia are ramified with long, thin, highly branched processes[6]. In contrast, monocytes and MDMs have a round or ameboid shape. Interestingly, the star-like morphology of surveilling microglia is typically associated with strong expression of the purinergic receptor P2Y12, now recognized as a signature gene for homeostatic microglia[27,148,193]. The P2Y12 purinergic receptor was associated with the chemotaxis of microglia in response to ATP released following a cortical laser-induced lesion[27].

Butovsky and collaborators have elegantly demonstrated that microglia are unique when compared to other types of tissue-resident macrophages and immune cells under naïve conditions, not only on a morphological standpoint but also in terms of their gene expression profile[193]. Analysis of the microglial transcriptome in the naïve adult brain identified a total 239 genes uniquely expressed by these cells. Notably, many of these genes are downstream of the transforming growth factor-beta (TGF-β) signaling pathway. Deletion of the *Tgfbr2* gene specifically in microglia reduced their ramification levels, which is normally considered as a sign of activation, and enhanced their proliferation and production of proinflammatory cytokines[193,230]. This suggests that TGF-β is important for the maintenance of microglia in a resting state of activation. Within the adult mouse CNS, microglia are the main source of *Tgfb1*, but astrocytes produce significant amounts of *Tgfb2* mRNA[154]. As both cytokines can bind TGFβR2, expressed preferentially at the surface of microglia, microglia may be regulated by themselves, each other or neighboring glia, such as astrocytes. Deletion of the *Tgfb1* gene in all cell types but T-cells, to bypass postnatal lethality normally seen in full knockout mice, led to reduced expression of signature genes previously attributed to surveillant microglia, including *P2y12*, *Sall1*, *Gpr34* and *Mertk*, as well as the upregulation of disease-associated microglia (DAM) genes such as *Axl* and *Apoe*, thus suggesting that microglia maybe regulated in autocrine manner to maintain their surveillance

phenotype[193,231]. However, further studies will be required to confirm the autocrine function of TGF-β1 and the influence of astrocyte-derived TGF-β2 on the microglial function.

Nonetheless, only few transcription factors are differently expressed (or regulated) in adult microglia compared to other types of myeloid cells[193]. The comparison of microglia with peritoneal macrophages identified *Smad* as an enhancer of the myeloid lineage-determining transcription factor PU.1 specifically in microglia[232]. SMAD, which is an enhancer downstream of TGF-β signaling, may therefore link TGF-β and the microglia-specific gene signature through the recruitment of the transcription factor PU.1 to bind DNA[232,233]. *Sall1* has also been identified as a transcription factor highly regulated specifically in microglia[14,193,210,230,232]. Deletion of the *Sall1* gene in microglia caused major alterations, such as the acquisition of an ameboid morphology, increased phagocytic capacities, and expression of proinflammatory genes[230]. Further, deletion of *Sall1* impaired neuroblast survival in the subgranular zone of the neurogenic niche in the hippocampus, highlighting the importance of microglia in brain homeostasis[230]. Another transcription factor associated with homeostasis of microglia is *Mafb*[193]. This transcription factor is expressed early during microglia development and its expression increases in adult microglia[14]. Deletion of the *Mafb* gene in *Csf1r* expressing cells caused profound alterations in microglia gene expression during development and adulthood[14]. Interestingly, many of the upregulated genes are associated with the type 1 interferon JAK/STAT signaling pathway, a response normally associated with the immune response against viruses[14]. In support of this, many of these genes were also found to be upregulated in microglia following olfactory bulb infection with the mouse hepatitis virus[234]. Thus, MAFB maintains microglia under homeostatic conditions and regulates the virus-mediated immune response.

Many of the differences observed between microglia and the rest of the other myeloid cells appear to help the former to maintain an immune-privileged status in the normal resting CNS, consisting in the surveillance of their immediate environment and synaptic pruning[18,23–25,148,195–202,235,236]. However, microglia remain very plastic at all times, which means that a subtle change in their tissue environment will affect the expression of transcription factors that may, in return, affect CNS functions.

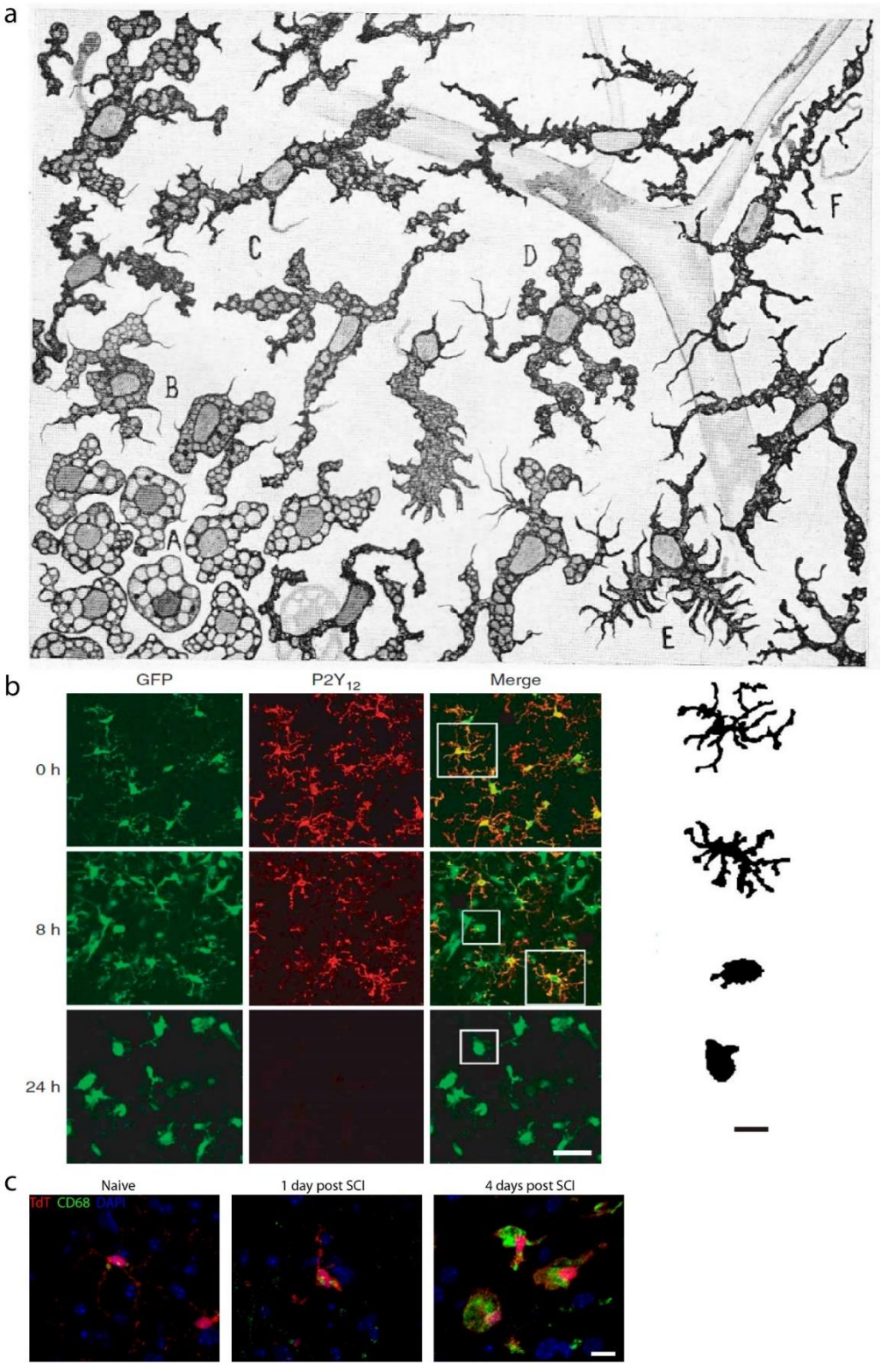

Figure 1.4. The different morphologies of microglia in the normal and pathological CNS.

a Represents postnatal microglia, gaining ramifications during CNS colonization in a 4-days-old rabbit, from REF[9]. **b** Microglia activation in slice culture conditions, results in reduced ramifications and loss of P2y12 receptor expression, from REF[27] **c** Microglia activation following SCI results in reduction of ramification levels and gain in CD68 protein expression, from REF[89] .

1.4.3.3. Similarities

A big effort has been made during the past decade to elucidate the differences between naïve microglia and other myeloid cells. Under pathological CNS conditions, such as after SCI, major changes occur in microglia. As will be discussed in more detail below, those changes will render microglia and MDMs almost indistinguishable from each other using the classical research tools, mainly because infiltrating blood-derived monocytes differentiate once within the CNS environment, and because microglia adopt an activated phenotype soon after the injury. In the context of the SCI, the recruitment of myeloid cells was initially described by electron microscopy and largely associated with the progression of the injury in the presence of hemorrhage. The intravenous injection of ^{3}H-thymidine, a radioactive nucleoside analog that cells incorporate during the DNA synthesis phase, allowed researchers to confirm the entry of peripheral blood monocytes at the site of stab wound injury or SCI and their differentiation into MDMs[237,238]. Most of these authors assumed that macrophage/microglia-like cells found at the site of injury had a monocytic origin, because the vast majority of them incorporated ^{3}H-thymidine[239,240], thus underestimating the capacity of the dye to cross the BBB and label proliferating microglia. However, Roessmann and Friede, and later on Imamoto and Leblond, demonstrated the coexistence of MDMs and ameboid microglia at the site of lesion by experiments in which they extracted BM cells, cultured them *in vitro* with ^{3}H-thymidine and then performed injections in rats prior to injury[241,242]. At that time, however, their hypothesis was that recruited MDMs are the main source for microglia[243–246]. As a reason of this, many groups are still to this day referring to microglia/macrophages as a whole. The use of this terminology is widely used, even though these cells show major differences under naïve conditions, as previously described, as well as different functions after CNS injury[21].

Microglia, which typically have a star-like morphology in the intact CNS, rapidly transform when an insult occurs. Microglia retract their processes over time, in a distance-dependent

manner, acquire an amoeboid shape and migrate towards the insult[7]. The adoption of an amoeboid shape correlates with the dedifferentiation of highly-specialized microglia into macrophage-like cells, as evidenced by their loss of P2Y12, a hallmark of homeostatic microglia[27,89]. Ameboid microglia participate in the engulfment of cell and myelin debris, by upregulating their expression of phagocytosis receptors such as CD68 and AXL, which are also shared by MDMs[89,218,234,247]. On the contrary, infiltrated monocytes differentiate into MDMs and upregulate expression of markers such as IBA1, which has been widely used to define microglia and other tissue-resident macrophages both *in vitro* and *in vivo*[248–250]. Thus, morphological analysis and classical markers cannot be used to discriminate between these two cell populations.

Microglia and MDMs also share many signaling pathways and transcription factors in the context of inflammation, adding more complexity to the challenge of deciphering cell-specific responses after SCI. For example, activation of the Toll-like receptor 4 (TLR4) by its natural agonist lipopolysaccharide (LPS) stimulates identical signals in both microglia and MDMs. When LPS binds to TLR4, it promotes the recruitment of Toll/IL-1 receptor (TIR) domain containing adaptor protein (TIRAP) and TRIF-related adaptor molecule (TRAM) that, in return, recruits the myeloid differentiation primary response protein 88 (MyD88) and TIR domain-containing adaptor inducing IFN-β (TRIF)[251–253]. The stimulation of TLR4 activates MyD88, which eventually recruits IL-1 receptor associated kinase 4 (IRAK4) and then activates both IRAK1 and IRAK2[254–256]. The IRAK complex interacts with the TNF receptor-associated factor 6 (TRAF6)[257–259], leading to activation via ubiquitination of the complex formed by TGF-β-associated kinase 1 (TAK1), TAK1 binding protein 1 (TAB1), TAB2, and TAB3[260]. This in return phosphorylates the kinase inhibitor of nuclear factor kappa-B kinase subunit beta (IKK-β) and the MAP kinase 6 (MAPKK6), which form a complex with the nuclear factor-kappaB essential modulator (NEMO). The complex then phosphorylates the nuclear factor of kappa light polypeptide gene enhancer in B-cells inhibitor alpha (IκBα), allowing the translocation of NF-κB to the nucleus to activate the expression of proinflammatory genes, including IL-1β and TNF-α[261,262]. Other transcription factors shared include the activator protein-1 family (AP-1), interferon regulatory factor family (IRF), p53 tumor suppressor (p53) and the STAT family, all reviewed elsewhere[263]

1.4.3.4.Models to identify the two populations

1.4.3.4.1. Bone marrow chimeras.

The debate about the origin of microglia started during the 1980s, based on data generated using bone marrow chimeras (BMC). This experimental model consisted in substituting the BM hematopoietic stem pool, using lethal irradiation followed by transplantation of hematopoietic stem cells coming from a different mouse line, typically expressing a fluorescent reporter or characteristic protein[264,265]. These early studies evidenced that transplanted BM cells could only differentiate into perivascular macrophages, but not microglia, in the adult brain[264,265]. Surprisingly, some groups found that transplanted BM cells could cross the BBB and differentiate into microglia, and even sometimes in astrocytes[243]. A separate group found that BM cells expressing the green fluorescent protein (GFP) entered the CNS at 4 weeks post-irradiation, and that their number increased over time[266]. The study further revealed that GFP-positive microglia-like cells have a ramified morphology, but discarded the possibility of astrocyte trans-differentiation. That was followed by a long list of studies, with some approving and some disproving the conclusion that microglia are of BM origin, thus raising the possibility that the infiltration of BM cells inside the CNS are an artifact of the irradiation procedures.

Several side effects have been associated to irradiation of humans and rodents. First, endothelial cells are sensitive to radiation, which can cause a disruption of blood-CNS barriers throughout the CNS vasculature[267–270]. Leakage of the blood-CNS barriers could therefore allow BM progenitors and monocytes to enter the CNS, where they could differentiate into microglia-like cells. Following radiation, highly-proliferating HSCs die, which causes immunodeficiency. Opportunistic pathogens may therefore benefit from that situation, which could cause death. To avoid opportunistic diseases, mice receive antibiotics during the radiation protocol. Antibiotics, in addition to the gastrointestinal dysfunction caused by the death of rapidly-dividing cells in the gastrointestinal tract, may alter the microbiota and allow the entry of pathogen-associated molecular pattern molecules (PAMPs) into the bloodsteam[271]. Acute and chronic PAMP exposure have been associated with changes in the microglial response, raising once again questions about the validity of using models of BMC when it comes to distinguishing microglia from MDMs, or vice-versa[272,273].

Finally but not least, about 10^7 BM cells collected from donor mice are intravenously injected into the circulatory system of recipient mice in the hours of the irradiation procedure to restore the HSC pool. The endothelium being activated by the irradiation, it leads to the adherence and migration of HSC and progenitor cells into the CNS and other organs/tissues of recipient mice[267,268,274–276]. Altogether, this suggests that results obtained using radiation BMC need to be interpreted with care.

To circumvent these artifacts, scientists have used various adaptations of the technique originally used to create BMC, such as shielding the skull to protect the brain during the radiation procedure or using chemotherapeutic agents to avoid breaking down the BBB[277–281]. Alternatively, parabiotic mice have been used to avoid the exogenous injection of BM cells into the bloodstream[282,283]. Thus, depending on the question being asked, alternative approaches exist to create the ideal type of BMC (for an extensive review, we refer to[284]).

1.4.3.4.2. Parabiosis

Parabiosis consists in the connection of the circulatory system of two (or more) mice. This technique was first described during the mid-19th century[285]. The first experiment in which parabiosis was used to distinguish microglia from MDMs after a CNS insult in rats generated confusing results, mainly because parabionts were exposed to ionizing-radiation and were injected with the nucleoside analog ^{3}H-thymidine, which we now know crosses the BBB. The authors nevertheless conclude that monocytes invade the CNS following herpes virus infection and that microglia can self-renew[286]. In 1998, Kurz and Christ, using chick parabiotic embryos, proposed that microglia do not originate from blood progenitors/monocytes, as these cells are not capable of penetrating the BBB[287]. Ajami and collaborators later demonstrated using parabiosis that self-renewing microglia, but not recruited MDMs, were the main cellular source that populates the CNS following facial nerve axotomy and in transgenic mice overexpressing mutant superoxide dismutase (mSOD), an animal model of amyotrophic lateral sclerosis (ALS)[21]. The same group later discovered that monocytes enter the CNS following EAE[283]. However, MDMs did not contribute to the microglia pool and could not differentiate into microglia-like cells during the recovery phase. Using a model of photothrombotic stroke and parabiosis between *Cx3cr1*-eGFP and WT mice, Li et al. demonstrated that microglia are the main cell type that rapidly proliferate and

accumulate at the site of damage[288]. Another study found that microglia are the main cells that accumulate in the dorsal horn in a model of peripheral nerve injury (PNI) associated with chronic pain[289,290]. Thus, parabiosis experiments demonstrated the importance of the microglial response in the context of a CNS insult highlighting the differences between both cell populations.

Thus, the information obtained using parabiosis has proven to be very useful when trying to understand the role of microglia versus MDMs. However, a few limitations need to be considered. First, parabiosis is associated with, at best, 50% of chimerism in total blood monocytes, which can lead to an underestimation of the importance of blood-derived macrophages compared to microglia. To avoid this problem, several studies have preferred BMC, but as discussed in the previous section ionizing radiation has important secondary effects (see also[21]). Second, parabionts often show retarded growth compared to mice of the same age. Third, important ethical issues come with the use of this surgical model.

1.4.3.4.3. Cell injection

This procedure consists in injecting cells obtained from a donor source into a recipient animal. The major benefit of this technique relies on its simplicity: an injection of labeled cells into a tissue of interest. Obviously, the donor cells may harbor a mutation or be treated *in vitro* before transplantation. The use of fluorescently-labeled cells allows to track them easily over time. The main limitation consists in the total number of cells that you inject versus the tissue-resident population and their clearance over time[291]. Some groups perform several injections to counteract this phenomenon.

The injection of cells has been largely used in the context of SCI. One of the first SCI studies that used this strategy to effectively distinguish microglia from MDMs reported that MDMs infiltrate from blood and have a different origin than microglia[241,242]. Other studies, which will be discussed in more detail in section 1.5.2., suggested that the injection of monocytes could be an interesting strategy to promote SCI repair[203,206,292,293]. Overall, cell injection is a rapid and easy approach to answer specific questions about MDMs.

1.4.3.4.4. Genetic models

The use of transgenic mice changed the way we make science. Regarding microglia, the use *Cx3cr1-eGFP* mice has become a must. *Cx3cr1-eGFP* mice express GFP under the control of the fractalkine receptor, *Cx3cr1*, which is highly expressed in microglia and in circulating monocytes[294]. Davalos and collaborators were among the first to take advantage of *Cx3cr1-eGFP* mice, showing that microglia are a highly dynamic cell population that continuously screens its environment using two-photon intravital microscopy in the normal mouse brain[148]. This was in drastic opposition to the ancient view that microglia are inactivate under naïve conditions, thus earning them the name of surveying microglia. Several following studies used *Cx3cr1-eGFP* mice to understand the functions of surveying microglia[18,23–25,148,195–202,235,236]. However, these studies were flawed by the fact that both microglia and infiltrating monocytes express *Cx3cr1* (and GFP), which reduced the interest of using this mouse line in models of CNS trauma and inflammation because it would now on require to be complemented by approaches such as irradiation, BMC transplantation, parabiosis, and/or cell injection to be able distinguish the two cell populations[291].

The CCR2 found on blood monocytes aid in their recruitment inside the CNS under inflammatory conditions and their differentiation in situ[295]. Accordingly, *Ccr2-KO* mice exhibit impaired monocyte recruitment and proinflammatory cytokine production at sites of inflammation[172,295]. In light of these results, mice expressing RFP fluorescence under the control of the *Ccr2* promoter were created, thus allowing the tracking of monocytes and natural killer (NK) lymphocytes in vivo[296]. The crossing of *Ccr2-RFP* mice with *Cx3cr1-eGFP* mice helped even more in the identification of both cell types[296,297]. The double transgenic mice were particularly useful in EAE, the most widely used animal model of MS, as they allowed for first time to perform comparative transcriptomic analysis between microglia and blood-derived macrophages in CNS inflammatory conditions[298].

Another useful transgenic fluorescent reporter model is the *LysM-eGFP* mouse line, which allows GFP expression under the lysozyme M (*LysM*) promoter and the visualization of cells of the granulomyelomonocytic lineage [299]. *LysM-eGFP* mice were particularly useful in the context of SCI, confirming the presence of both MDMs and microglia at the site of injury. Mawhinney and collaborators showed that recruited GFP^+ MDMs are typically surrounded

by GFP^- microglia[169]. The same group further analyzed the dynamics of monocytes to reveal that classical M1-monocytes, identified as GFP^+ $CD45^+$ $F4/80^{lo}$ $Ly6C/G^{hi}$ cells, outnumber M2-monocytes (i.e. GFP^+ $CD45^+$ $F4/80^{hi}$ $Ly6C/G^{lo/-}$ cells) during the acute phase of SCI, and that M2-monocytes accumulate later on during the subacute phase (i.e. days 7-14 post-SCI). Intriguingly, M1-monocytes were found to reappear during the chronic phase of SCI (day 42)[91]. Other groups successfully used the same *LysM-eGFP* mice to identify monocytes in models of glioblastoma, EAE, stroke and CNS infection[155,300–303]. However, a recent study revealed that damage-associated microglia (DAM) upregulate the expression of *LysM* during Alzheimer's disease, raising some concerns about the specificity of the *LysM-eGFP* mouse line[231].

The use of knockin mice expressing fluorescent proteins under the control of cell-specific gene promoters has been very helpful. However, one has to keep in mind that cell dynamics and maturation (differentiation) might regulate the expression of those same promoters, resulting in a loss or gain of fluorescence expression. In Alzheimer's disease, DAM downregulate their expression of *Cx3cr1* and *Tmem119* and upregulate their expression of *Lyz2* and *Tyrobp*[231]. For this reason, many scientists prefer to use inducible transgenic mouse models, which allows the conditional expression of genes (e.g. fluorescent reporters) in specific cells and tissues at specific times. The most commonly used methods to control gene expression in mice are based on the tet-operon/repressor bi-transgenic system and the estrogen receptor (ER) ligand-binding domain[304]. The ER is most commonly fused with a Cre recombinase, which is translocated into the cell nucleus after binding between the drug tamoxifen and ER receptor. The translocation of the Cre recombinase into the nucleus results in the excision of the floxed gene[304].

The creation of mice expressing tamoxifen-inducible Cre recombinase under the control of the *Cx3cr1* promoter (*Cx3cr1-creER^{T2}* mice) has been a revolution in the world of microglia biology[291]. Because monocytes have a high turnover compared to microglia, it becomes possible to treat *Cx3cr1-creER^{T2}* mice with tamoxifen and wait for a few weeks until short-lived cells are replaced. After such treatment regimen, recombination should have occurred in virtually all microglia, whereas monocytes should not be affected[25,89,291,297,305]. The use of these mice was particularly useful to distinguish microglia from infiltrating monocytes. For

example, we now know that PNI and facial nerve injury cause microgliosis in the dorsal horn and facial nucleus, respectively[218,297]. We also know that monocytes that infiltrate the substantia nigra in the MPTP model participate in the death of dopaminergic neurons[306]. In our lab, we created a new triple transgenic mouse line, *Cx3cr1-CreER^{T2}::Rosa26-TdT::LysM-eGFP*, that allowed to differentiate microglia from blood-derived myeloid cells and visualize them in vivo. Using these triple transgenic mice, we demonstrated that infiltrating monocytes release IL-1β, thus favoring EAE progression[307]. As for any other model, the *Cx3cr1-creER^{T2}* mouse line has some limitations, however, as it recombines CNS border-associated macrophages (BAMs), including perivascular macrophages, meningeal macrophages and choroid plexus macrophages[307]. BAMs have been defined based on expression of the macrophage mannose receptor (CD206) and major histocompatibility complex class II (MHCII)[308,309]. Thus, immunofluorescence labeling using antibodies directed against microglia-specific markers (e.g. P2Y12) and BAM-specific marker (e.g. CD206 or MCHII) may be required to truly validate cell origin[27,89]. Another approach could be to use *Sall1-CreER^{T2}* transgenic mice[230]. Until proven otherwise, *Sall1* is a transcription factor exclusively expressed by microglia, but not by BAMs or any other immune cell type in peripheral tissues[193].

1.4.4. Microglia depletion strategies

During the past years, several strategies have been developed to unequivocally deplete microglia and understand their role in response to CNS insult. Some of these strategies include both pharmacological and transgenic approaches. In the next section, I will describe these approaches and their limitations. For further information about microglia depletion strategies, the following two reviews may be consulted[310,311].

1.4.4.1.CSF1R antagonists

The colony stimulating factor-1 receptor (CSF1R) is a tyrosine kinase class III receptor that gets activated by its glycoprotein agonists, colony stimulating factor-1 (CSF1) and IL-34, through the formation of a homodimer[312,313]. As far as we know, CSF1 only interacts with CSF-1R, whereas IL-34 interacts with CSF1 and another receptor, the protein tyrosine phosphatase-ζ receptor (PTP-ζ)[314–316]. The expression of both glycoproteins varies in location

and time[316], suggesting both cytokines may have different roles. In support of this idea, KO mice targeting the individual receptors or cytokines showed different phenotypes. For example, *Csf1r-KO* mice are not viable and die in utero during embryonic development[317]. *Csf1-KO* mice exhibit reduced survival associated with impaired cognition and reduced brain size[317,318]. In contrast, *Il-34-KO* mice have a normal brain and survival rate[319,320]. This suggests a distinct and non-redundant role for both cytokines.

Among its principal functions, CSF1R regulates macrophage development and the homeostasis of tissue macrophages[318,321–326]. With regard to the CNS, *Csf1r* expression has been detected on neural progenitor cells, radial glia, immature cortical neurons and microglia[16,317,327]. It was suggested that the CNS deficits observed in *Csf1r-KO* mice could be related to the absence of microglia typically observed in these animals[18,199,328–330]. However, some authors consider that the CNS deficits rather depend on CSF1R signaling in neurons, based on the fact that *Nestin-cre*$^{+/-}$*::Csf1r*$^{flox/flox}$ mice exhibited some of the defects seen in *Csf1r-KO* mice, such as a decreased brain size and increased lethality[317]. Although all neural progenitor cells express *Nestin*, is important to note that microglial progenitor cells also express *Nestin* during their proliferative phase, such as when they colonize the CNS during embryogenesis or after pharmacological depletion[14,17,331]. Since the authors did not investigate whether microglia are absent or functionally impaired in the brain of *Nestin-cre*$^{+/-}$*::Csf1r*$^{flox/flox}$ mice, it is still possible that both cell types may be responsible for the CNS development defects[317]. For more detailed information, we refer to[332].

In the adult CNS, CSF1R is expressed by all microglia, while its expression on neurons is maintained in only few cortical and hippocampal neurons[333]. However, additional neurons may upregulate *Csf1r* mRNA expression after CNS injury[327]. Microglia, similarly to yolk sac embryonic progenitors, rely on CSF1R signaling for their maintenance and survival[11,16,17]. Accordingly, deficiency in CSF1R compromised the presence of microglia in the embryonic CNS[11]. Some studies suggest that the main ligand for microglial CSF1R in the adult brain would be IL-34, which is in contrast to the situation in other body tissues, where *Csf1* levels are higher than *Il-34* levels[316]. Interestingly, *Il-34-KO* mice exhibited a 70% reduction in total microglia compared to 30% in *Csf1-KO* mice that survived postnatally[316,319,320]. CSF1R not only controls the survival of microglia, but also their proliferation and response to damage.

In vitro, microglia depend on CSF1 or IL-34 for their long-term survival and proliferation[194]. In vivo, studies have shown that the number of CNS microglia can be boosted by the administration of CSF1 given either centrally or peripherally[89,334,335]. Interestingly, dorsal root ganglion (DRG) sensory neurons, which project axons through the ventral and dorsal columns of the spinal cord, release CSF1 after PNI, thus promoting microglia proliferation and reactivity causing pain[336].

Over the past few years, small inhibitors that cross the BBB and target CSF1R in the brain and spinal cord have been developed. These inhibitors, which include PLX5366 and PLX3397, block the microglial receptor, thus causing microglial cell death probably through apoptosis[17]. Exposure to CSF1R inhibitors was shown to cause the rapid loss of microglia, resulting in a 60% depletion by 3 days and nearly complete depletion by 7 days post-treatment[17,89,219,234,337–343]. Importantly, the elimination of microglia for up to 8 weeks using PLX compounds did not affect the total number of oligodendrocytes, neurons and astrocytes, nor mice showed deficits in motor and memory functions[17,89]. Mice however showed an enhanced astrocyte reactivity, as evidenced by the increased GFAP expression[17]. Microglia depletion was also associated with reduced synaptic pruning and synaptic formation[337]. Thus, PLX compounds can be used to better understand the role of microglia during homeostasis and after an insult in the adult CNS[17,89,219,234,337–343].

As for all drugs, some precautions need to be considered when using PLX compounds for research purposes. As previously mentioned, CSF1R may be expressed by cells other than microglia within the CNS. Although the late stage of monocyte maturation appears to depend on CSF1R, recent studies have been conflicting on the potential requirement of CSF1R signaling for their survival under normal and inflammatory conditions[344]. To discard the possible effects of CSF1R inhibitors on peripheral monocytes, a novel inhibitor that does not cross the BBB can be used as control, i.e. PLX73086[89]. Using the PLX73086 compound, we demonstrated that peripheral CSF1R antagonism had little effect on monocytes under both normal and SCI conditions[89]. As each CNS disease has its own etiology, we believe that including PLX73086 as a control in the experimental design would provide valuable information.

1.4.4.2.*Cx3cr1*-CreER^{T2}::*Rosa26*-iDTR and *Cx3cr1*-CreER^{T2}:: *Rosa26*-iDTA mice

Primates express the diphtheria toxin receptor (DTR), coded by the heparin-binding EGF-like growth factor (*Hbegf*) gene, and rapidly die after exposure to diphtheria toxin (DTx)[345–350]. The DTx has two subunits, and the B subunit binds to DTR and allows the complex to be internalized inside the cytoplasm[348,351,352]. Upon entry into the cytoplasm, the A subunit of DTx (DTA) may now bind to the elongation factor 2, inhibiting protein synthesis and causing cell death[348,351–353]. The presence of only one active DTA molecule is sufficient to kill an eukaryotic cell[348]. Interestingly, the DTR is not expressed in rodents, making rodent cells highly resistant to DT exposure compared to primate cells.

The creation of transgenic mice in which were incorporated the full *Hbegf* gene (*iDTR* mice) or the DNA sequence coding for the DTA subunit (*iDTA* mice), both preceded by a loxp-STOP-loxp sequence, has made possible to experimentally deplete specific cell types in mice[349,354]. In the case of *iDTR* mice, specific rodent cells will express DTR in a cre-dependent manner and external administration of the DTx will be required to induce cell death, allowing researchers to control the exact time of cell death[349]. In *DTA* mice, the cell type of interest will be constantly depleted upon expression of the Cre recombinase[355].

The crossing of *Cx3cr1-CreER^{T2}* and *iDTR* mice, with the appropriate regimen of tamoxifen and DTx administration, is promising strategy to target microglia[25]. Parkhurst and collaborators demonstrated that tamoxifen administration 2 weeks prior to DT exposure was ideal to kill more that 90% of microglia within the CNS, with very little effect on blood monocytes[25]. Importantly, these results have been replicated by several groups including ours[331,356]. However, the use of this mouse model has a few limitations that need to be kept in mind when planning an experiment. The first limitation is that the elimination of microglia using the DTx-based system causes cell necrosis[331]. Consequently, microglia release a plethora of proinflammatory cytokines, resulting in a cytokine storm that drastically changes tissue homeostasis, causing widespread astrocyte activation[331]. As well, the DTx injection may cause toxicity, despite the fact that mice have a reduced response to the toxin compared to humans. In our hands, treatment with 500ng of the A subunit of DTx for 3 consecutive days efficiently eliminated more than 80% of microglia in the spinal cord, with no sign of toxicity for at least 14 days post-administration of DT in the absence of injury. However, the

same regimen of DT administration starting 3 days prior to SCI induced lethality in 50% of *Cx3cr1-CreER^{T2}::Rosa26-iDTR* and WT mice. A time course study further revealed that DTx treatment caused death when given during the week before or during the first 2 weeks after SCI. Therfore, the DTx-based system may be useful for microglia depletion but only under certain conditions.

1.4.4.3.CD11b-TK mice

The herpes simplex virus thymidine kinase (HSV-TK) is not by itself harmful to mammal cells. However, the HSV-TK is capable of phosphorylating different nucleoside analogues, such as ganciclovir and acyclovir, and convert them into nucleoside monophosphates[357,358]. Nucleoside analogue monophosphates can be converted into nucleoside triphosphates under the action of kinases, and then incorporated into DNA during the DNA synthesis phase, thus causing death of proliferating cells[358,359]. The incorporation of HSV-TK in the mouse genome under the control of the *Cd11b* promoter can thus impede the proliferation of microglia and myeloid cells, ultimately causing their death, upon systemic administration of ganciclovir[360,361]. The *Cd11b* promoter is active in all myeloid cells, including neutrophils, MDMs and microglia. Thus, to target exclusively microglia in *CD11b-TK* mice, BMC must be generated using WT donor cells. In the past few years, some studies used central administration of ganciclovir to avoid the effect on peripheral myeloid cells[361–364]. However, continuous central administration may not be ideal when behavioral testing is performed.

In keeping with models of CNS injury, in particular stroke, microglia depletion was found to exacerbate the infarct area and increase neuronal death, suggesting a beneficial role for microglia[365]. However, this issue has never been addressed in SCI models. In our laboratory, we generated BMC using the *CD11b-TK* mouse model, but these mice showed high lethality following ganciclovir administration.

1.4.4.4.Clodronate

Clodronate-loaded liposomes have been largely used in the scientific literature to deplete peripheral monocytes and macrophages[366–368]. Clodronate is, by itself, not toxic because it does not penetrate cellular membranes. However, macrophages will ingest the drug through phagocytosis of the liposomes, thus releasing clodronate into the cytoplasm. Once inside the

cell, the free clodronate will affect the ATP proton pumps, thus causing apoptosis[366]. To kill peripheral monocytes and macrophages, clodronate liposomes must be injected directly into the bloodstream, which will minimally affect microglia since liposomes cannot cross the BBB[151,208,368,369]. The injection of clodronate liposomes directly into the CSF, by means of an intracerebral ventricular injection, can bypass the BBB and deplete CNS microglia[340,370,371]. The use of this method, although successful in some cases, requires a major brain surgery and is not ideal for subsequent behavioral testing.

1.4.4.5.Antibodies

Antibodies have also been used to eliminate different subsets of myeloid cells in peripheral tissues. In the context of SCI, the administration of anti-CD11b, anti-LY6G, anti-GR1 and anti-LY6C antibodies has been used to deplete myeloid cells such as neutrophils and monocytes, with variable results depending on the antibody clone and treatment regimen (see next section for more information)[150,151,372,373]. However, antibodies show low penetrance across the BBB. Thus, microglia are somehow protected from antibody exposure under normal conditions. To bypass this limitation, Yao and collaborators injected in the cisterna magna Mac-1-saporin, an anti-CD11b antibody conjugated to the saporin immunotoxin, which resulted in depletion of approximately 50% of microglia in the spinal cord 1 day after the injection[335]. The use of this delivery method is very interesting because it avoids the substantial brain damage normally associated with an intracerebral ventricular injection. However, similar to the situation seen in *Cx3cr1-CreER^{T2}::Rosa26-iDTR*, the use of the immunotoxin causes rapid cell necrosis and is associated with a cytokine storm[335].

1.5. The role of infiltrating blood-derived cells in SCI

The BBB disruption and local proinflammatory response that develops after SCI orchestrate the infiltration of blood-derived leukocytes, a phenomenon shared by all living mammals, including rodents, primates and humans[109,374,375]. The first cells to arrive at sites of SCI are the neutrophils, immediately followed by M1 monocytes[109,372,374–376]. Over time, neutrophils disappear and M1 MDMs are replaced or change their activation status, becoming M2 MDMs[91,207,377]. As previously mentioned, infiltrating myeloid cells remain within the SC

tissue for long periods of time, sequestrated in the core of the lesion[89,169,378]. Regarding lymphocytes, B cells are rapidly detected in the SC parenchyma, but their presence decrease over time. The T cell infiltration follows the one of MDMs[376,379–381].

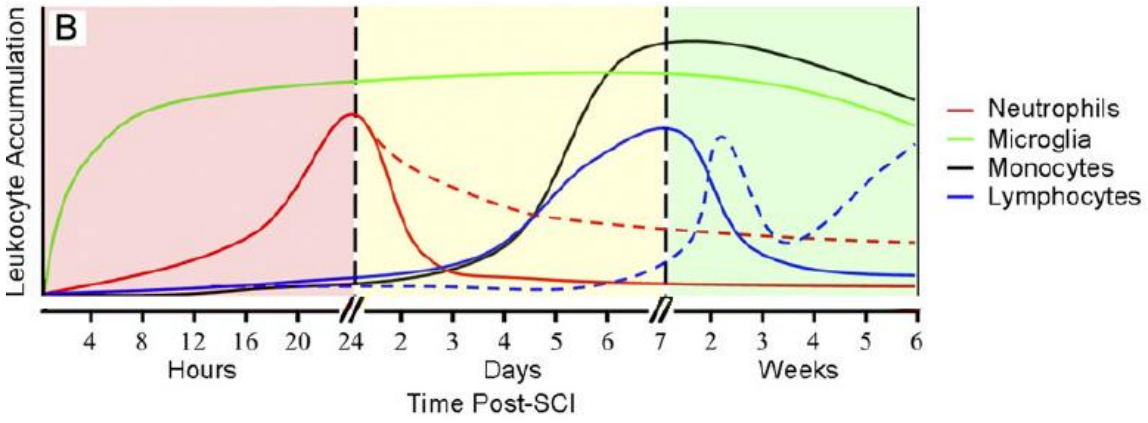

Figure 1.5. Leukocytes dynamic following SCI.

Graph represents the cellular load of leukocytes found in the spinal cord following SCI, modified from REF[382].

1.5.1. Neutrophils

Neutrophils are considered the first line defense in innate immunity. These cells were originally described as specialized bactericide cells implicated in host defense against bacterial infection. However, new studies have revealed that neutrophils are active participants in the sterile inflammatory response (for review, see[383]). Neutrophils are short living cells with a half-life of around 5 days in blood[384]. In healthy individuals, they are replenished at rhythm of about 2 x 10^{11} cells per day from BM-derived HSCs and neutrophil progenitors, through a highly-regulated system implicating the circadian clock and the G-CSF cytokine[385–387]. The final differentiation step of neutrophil progenitors into mature neutrophils depends on C-EBPε, as *Cebpe-KO* mice are characterized by neutropenia and low life expectancy caused by opportunistic infections[388,389]. Nowadays, treatment with G-CSF is widely used to counteract neutropenia and opportunistic infections in human patients subjected to chemotherapy[390].

In the context of SCI, neutrophils are the first cells to be recruited at the site of injury[109,374,375]. Their presence starts at around 6 hours post-SCI and peaks at 24 hours in rodents[109,374,375]. They show a very transient accumulation as they are almost all gone by day 4 post-SCI. However, some groups including ours have suggested that there could be a second wave of neutrophil infiltration occurring between 14 and 35 days post-SCI, whose role is sill unclear[374,375]. Neutrophils not only colonize the site of SCI, but extensively accumulate in the meninges and CSF[391]. In the blood, the neutrophil presence is remarkedly augmented at 24 hours post-SCI[70,89,375].

The function of neutrophils is highly controversial after SCI. Some studies blocked neutrophil recruitment, using anti-ICAM1 or anti-P-Selectin antibodies, which both target neutrophil-binding proteins on the surface of activated CNS endothelial cells. Both antibodies were found to reduce neutrophil recruitment after SCI, as evidenced by a reduction on myeloperoxidase activity, an enzyme highly expressed by neutrophils, which led to an improved locomotor recovery and reduced hemorrhage[372,373]. On the contrary, more recent studies revealed that mice treated with an anti-GR1 antibody prior to SCI exhibited a 90% reduction in blood neutrophil and M1 monocyte numbers at 12 hours post-SCI, and that this response was associated with an increased lesion volume, more axonal damage and a poorer recovery of locomotion, suggesting a protective role for these cells[150]. Since the anti-GR1 antibody also reacted with the LY6C antigen found at the surface of monocytes[392], in addition to the LY6G epitope expressed by neutrophils, a more specific antibody depletion approach was used in subsequent studies by others. Using an anti-LY6G antibody, Lee and collaborators showed that a full depletion of neutrophils has no effect on functional recovery after SCI[91,151]. However, a depletion of blood neutrophils does not warrant an effect at the site of injury. In support of this, we found that PLX73086 treatment caused a 50% reduction in blood neutrophils at 24 hours post-SCI, but the neutrophil load within the injured SC was left unchanged, highlighting the capacity of the remaining neutrophils to respond to the cues released at the site of lesion[89].

Using the opposite approach, a few groups stimulated the neutrophil response by injecting G-CSF[393–395]. The treatment of rodents with G-CSF following SCI, either immediately or 1 week post-SCI, resulted in enhanced locomotor recovery[393–395]. The injection of G-CSF

attenuated the production of IL-1β and TNF-α, an effect correlated with a reduction in apoptosis of neurons and oligodendrocytes[393–395]. Similar results were obtained in stroke models when G-CSF was injected[396,397]. Although these studies might indicate that the promotion of neutrophil activity is beneficial, none of them presented a total neutrophil count and evaluated the activation state of the cells at the site of SCI, thus raising the possibility that G-CSF has an effect on cells other than neutrophils. The neutrophil response therefore remains a subject of controversy that requires more investigation using appropriate transgenic mouse models to deplete neutrophils specifically and completely.

1.5.2. Monocytes / MDMs

Monocytes follow neutrophils in the order of the steps of the innate immune response. Monocytes represent approximately 5-10% of total blood leukocytes[221]. As previously described, they originate from HSCs[398]. Monocytes are the principal source of macrophages and replace them at different rates in many healthy tissues of the body[12]. The rodent monocyte subset can be identified based on expression of CD45, CD11b and CD115. In human monocytes, the CD14 marker is also used. Villani and collaborators recently identified at least 4 subtypes of monocytes in humans, recognizing M1 and M2 monocytes as the larger and better studied subsets[399]. The "proinflammatory" or "classic" M1 monocytes represent about 89% of all monocytes and like neutrophils are short-lived and rapidly recruited under inflammatory conditions[400]. M1 monocytes can be identified in mice based on expression of $LY6C^{hi}$ and $CXCR3^{lo}$, and in humans based on expression of $CCR2^{+}$ and $CD16^{+}$[401–405]. In contrast, the "patrolling" or "non-classical" M2 monocytes represent about 10% of the total monocyte population, have an increased lifespan and often appear during the resolution phase of inflammation[226,400,406]. M2 monocytes can be identified based on expression of $LY6C^{lo/-}$ and $CXCR3^{hi}$ or $CCR2^{-}$ in mice, and based on expression of $CD16^{+}$ in humans[226]. Interestingly, M2 monocytes rely on the transcription factor *Nr4a1* for their maturation from M1 monocytes[407].

After SCI, the recruitment of M1 monocytes follows the one of neutrophils, entering the site of injury at 24 hours and peaking in number at 48 hours[91,109,372,374–376]. Once inside the CNS tissue, M1 monocytes differentiate into MDMs with a proinflammatory phenotype (iNOS,

CD32, CD86) and release cytokines such as IL-1β[70,207]. Interestingly, the M1 MDM population gradually disappears and is substituted by the M2 MDM population, which peaks between 7 and 14 days post-SCI[91,207,377]. M2 MDMs present an anti-inflammatory phenotype (Arg1, CD14, CD206) and release cytokines such as IL-10[155,205]. The switch from one to another is still under debate. During sterile inflammation, M1 MDMs seem to transform into M2 MDMs during inflammation resolution phase. However, it cannot be excluded that M2 MDMs are recruited from blood and/or CSF via the choroid plexus[391]. Dal-Secco and collaborators demonstrated using intravital microscopy in double-transgenic mice that infiltrated *Ccr2-RFP* M1 monocytes switch into M2 monocytes, with gain of *Cx3cr1-eGFP* expression, favored under the effect of IL-10 and IL-4 during the resolution phase of hepatic sterile inflammation[408]. Importantly, both of these cytokines were shown to favor recovery after SCI[205,409]. Shichita and collaborators demonstrated that M1 monocytes respond to alarmins using Msr1 and Marco receptors, whose expression relies on the *Mafb* transcription factor, causing MDMs to switch from the M1 to the M2 phenotype[410]. They further demonstrated that following stroke, the absence of the *Msr1*, *Marco* or *Mafb* gene on monocytes, using *LysM*^{cre} mice as a driver for gene deletion, led these cells to fail to switch from the M1 to the M2 phenotype, thus resulting in an exacerbated inflammatory response and increased neuronal injury[410]. However, further experiments are required to validate these findings.

The function of monocytes and MDMs is still today controversial. MDMs have mainly been associated with a supportive role after SCI[203,206,293,411]. Rapalino and collaborators reported a beneficial effect of MDM transplantation after SCI, as shown by an improved locomotor function[411]. The beneficial effect of macrophage transplantation was confirmed and even augmented when MDMs were pre-stimulated by exposure to the injured sciatic nerve environment[293]. This suggests that the axon-growth supporting effect of MDMs may vary depending on the tissue conditions. Depletion of monocytes and neutrophils with the anti-GR1 antibody caused an increased lesion size and worsened locomotor recovery[150]. A recent study showed that inhibition of monocyte recruitment in *Ccr2-KO* mice prevented microglia from adopting an anti-inflammatory response, an effect correlated with increased tissue damage and reduced locomotor recovery[98]. On the other hand, many studies demonstrated that impairment in functions of monocytes/MDMs or their elimination is beneficial for

recovery after SCI[209,368,412–414]. In particular, depletion of monocytes prior to SCI using clodronate was associated with enhanced locomotor recovery and reduced fibrotic scar formation in rats and mice[209,368]. The combination of clodronate and anti-Ly6G antibody injection to deplete both M1 monocytes and neutrophils resulted in improved locomotor recovery[151]. Interestingly, splenectomy in mice following SCI caused a reduction in the number of peripheral monocytes, an effect correlated with enhanced functional recovery[415]. At roughly the same time, another group demonstrated that the beneficial effect of MDMs depends on Cx3cr1 signaling[416]. It is important to note, however, that many of the studies that reported a detrimental effect of monocytes/macrophages performed cell depletion at the time of the injury, thus probably reducing secondary damage associated with inflammatory events. London and collaborators demonstrated that MDMs exhibit different phenotypes depending on their location with regard to the lesion itself, with some of them releasing anti-inflammatory cytokines, such as IL-10, favoring functional recovery[205]. As highlighted above, the functions of monocytes and MDMs are complex and will require more studies to be elucidated.

1.5.3. The adaptive immune system: T and B cells

T and B cells belong to the adaptive immune system. B cells entrance occurs following week 1 while increasing their accumulation during the following weeks at the core of the lesion[417]. In contrast, the accumulation of T cells occurs in two distinct waves. The first peak of accumulation in SCI rodents is at 7-14 days, whereas the second one is at 42 days[380,381]. The function of the adaptive immune system in the context of SCI is not yet well defined and requires further investigation, but I will discuss below what is known to date.

The overall inhibition of the adaptive system appears to be protective following SCI. The use of nude rats, in which T cells are not present, showed enhanced locomotor recovery[418]. Nude rats showed reduced microglia/macrophage activation correlated with reduced secondary damage[418]. Pharmacological inhibition of T cells with either FTY720, a sphingosine receptor modulator that impairs T cell migration, or both cyclosporin A and FK506, immunosuppressive agents that abolish T cell proliferation, enhanced functional recovery after SCI[419–427]. Along the same line, RAG2-knockout mice, a gene implicated in lymphocyte

maturation and whose deletion results in animals devoid of B and T cells, showed improved locomotor recovery, reduced tissue damage, and increased axonal counts[428,429]. Using a B cell-specific KO mouse line, Ankeny and collaborators reported a reduction in IgG levels within the injured spinal cord, an effect associated with an increased locomotor recovery[430]. B cell-KO mice also presented with reduced microglia/MDM activation, most likely a consequence of the reduction in CR3 activation via the IgGs released from B cells[430]. Although the specific molecular mechanisms remain obscure, absence of B cells impaired the production of all types of antibodies which exacerbates the inflammatory response increasing the tissue damage. The use of FTY720 has been particularly studied to reduce T cell activity following SCI, highlighting the importance of T cells in exacerbating the inflammatory responses, BBB leakage and tissue damage following SCI.

Yet, certain aspects of the adaptive immune response could improve functional recovery after SCI. T helper (Th) cells are subdivided into Th1, Th2, Th9, Th17 and Tregs, among others. The first series of investigations on the role of T cells in SCI was very promising. Several studies from Michal Schwartz's laboratory reported an increased in locomotor recovery with an enhanced BBB integrity following injection of T cells directed against the MBP peptide (T_{MBP})[431–435]. However, this finding could not be replicated by work from Phil Popovich's laboratorty[436]. In the ischemic brain, the stimulation of Tregs showed to produce anti-inflammatory cytokines, such as IL-10 and TGF-β, which improved the overall outcome of this disease[437–443]. However, the molecular mechanisms that could explain the beneficial effects of T cells in SCI remain nebulous for the most part[444,445].

The adaptive immune response also generates antibodies that may have beneficial effects following SCI. For example, some groups have tried to neutralize myelin-associated inhibitory molecules by developing antibodies directed against as Nogo-A, MAG or OMgp [143,446,447]. The administration of these antibodies was shown to promote axonal regrowth and plasticity, favoring functional recovery in SCI rodents and primates[143,446,447]. Importantly, some antibodies directed against myelin-associated inhibitory molecules are currently being tested in clinical trials.

1.6. Microglia-related cytokines in SCI

Microglia rapidly respond to changes following SCI. One of their major functions is to initiate and control the immune response through the release of cytokines. Recently, some microglia-derived cytokines were identified, including IL-1α, TNF and TGF-β1, and described as key regulators of astrocytic and immune responses during CNS pathologies[149]. In the following section, I will describe some of these cytokines and their modulation of outcomes after SCI.

1.6.1. The IL-1 superfamily

The IL-1 superfamily of cytokines has been linked to inflammation and innate immunity since its early discovery back in 1940s. As the name implies, the first cytokine that was discovered is IL-1 for its role in fever and T cell proliferation[448]. Since this discovery, the family has grown tremendously and can be classified based on the length of the pro-segment of the protein. Members of the IL-1 subfamily (IL-1α, IL-1β and IL-33) encode precursor molecules of 269-271 amino acids (aa). Members of the IL-18 subfamily, IL-18 and IL-37, have between 192-193 aa, while those of the IL-36 subfamily (IL-36Ra, IL-36α, IL-36β, IL-36γ and IL-38) have between 155-158 aa (for review[449]).

1.6.1.1. IL-1α

Despite the low protein homology between IL-1α and IL-1β, they share a similar three-dimensional structure and bind to the same receptor, the IL-1 receptor type 1 (IL-1R1). For these reasons, IL-1α and IL-1β were originally thought to share similar functions. However, recent evidence showed that in the context of inflammation, the precursor form of IL-1α (pro-IL-1α) acts as an alarmin, while IL-1β acts as an inducer of inflammation[450]. The maturation and release of IL-1α requires Ca^{2+} intracellular influx to activate proteases, such as calpain, or the activation of the Nlrp3 inflammasome during necroptosis. Yet, both pro-IL-1α and mature IL-1α are able to bind IL-1R1. Pro-IL-1α detected in the supernatant of necrotic melanoma B16 cells can induce immune cell recruitment and inflammation[72]. Accordingly, pro-IL-1α released by dying cells during hypoxia is able to induce sterile inflammation and neutrophil recruitment[71]. In contrast, apoptotic B16 cells sequestrate pro-IL-1α into the

chromatin, thus impeding its release into the milieu and the induction of inflammation[72]. Pro-IL-1α is widely expressed by different cell types in the body, including keratinocytes, epithelial cells and endothelial cells. The pro-IL-1α contains a nuclear location signal (NLS) that allows its translocation towards the nucleus where it interacts with histone acetyltransferases and acts as a DNA damage sensor[451]. However, the specific genes regulated by pro-IL-1α remain unknown.

In the CNS, pro-IL-1α can bind to either IL-1R1, IL-1R2 or IL-1R3. The IL-1α/IL-1R1 complex recruits the IL-1 receptor accessory protein (IL-1RacP), which promotes the recruitment of MyD88 and activates downstream signaling via NF-κB, a transcription factor responsible for the expression of several proinflammatory genes. Despite the fact that the IL-1α/IL-1R2 complex also recruits IL-1RacP, IL-1R2 lacks an intracellular domain, impeding downstream signaling. It is believe that IL-1R2 acts as negative regulator of inflammation (for review[452]). IL-1R3 is a truncated splice variant of IL-1R1 that is highly expressed in neural tissue. The N-terminal Ig-like domain of IL-1R3 is significantly reduced compared to the one of IL-1R1. The IL-1α/IL-1R3 complex recruits IL-1RacPb, a splice variant of IL-1RacP, and activates the AKT kinase[453]. IL-1R1 is expressed in certain types of neurons, in epithelial cells of the choroid plexus, and in the adventia wall of endothelial cells in post-capillary venules of the BBB[90,307,454]. IL-1R1 signaling may also be implicated in microglial cell proliferation, following binding to IL-1α[331]. IL-1R3 is expressed by some types of neurons, but its function remains unexplored[453].

After CNS injury, IL-1α is rapidly released by dead and dying cells. Its release precedes the expression of IL-1β, making it an alarmin whose role is to initiate sterile inflammation[70,71,455]. IL-1α is released by dead and dying microglia located in the penumbra after ischemic stroke or at the lesion epicenter in SCI[70,455]. As indicated above, we recently demonstrated that post-capillary venules in the CNS express IL-1R1, which favors myeloid cell recruitment in an animal model of multiple sclerosis[307]. IL-1α-knockout (KO) and IL-1β-KO mice both exhibited important deficits in myeloid cell infiltration compared to wild-type (WT) mice at 24 hours post-SCI[70], highlighting the importance of IL-1R signaling in immune cell recruitment. Interestingly, only IL-1α-KO mice showed a prolonged recovery of locomotion and a reduced lesion volume at 35 days after SCI[70]. The better outcome observed in the IL-

1α-KO group after SCI was correlated to an increase in the number of CC1+ oligodendrocytes expressing the nuclear factor Tox3. We speculate that the release of IL-1α from dead/dying microglia may bind to astrocytic IL-1R1, thus generating a neurotoxic astrocyte response that could influence oligodendrocyte survival[149]. Regarding Tox3, a high-mobility group box protein that regulates calcium-dependent transcripts via the cAMP-response-element-binding protein (CREB) or Cited1, *in vitro* studies have shown that its overexpression in neurons and oligodendrocytes is protective in ischemic conditions[70,456]. The upregulation of Tox3 in oligodendrocytes of naïve IL-1α-KO mice therefore suggests an interaction between microglia and oligodendrocytes during development. Indeed, we counted significantly more $Tox3^+$ $CC1^+$ oligodendrocytes in the spinal cord of IL-1α-KO mice than control mice at postnatal day 10, as well as after SCI. How Tox3 mediates OL survival remains, however, a mystery[70].

1.6.1.2.IL-1β

IL-1β is synthesized as a 31-kDa pro-form, but only the mature form (17 kDa) of IL-1β is capable of binding to IL-1R1[450,457]. For its production, maturation and release, cells require at least two inflammatory stimuli. The first one involves the activation of Toll-like receptors (TLRs) by PAMPs or DAMPs, which results in the activation of NF-kB and the expression of proinflammatory genes, including the one coding for pro-IL-1β[252,458,459]. However, pro-IL-1β cannot be released from the cytoplasm and requires a second signal, consisting in the activation of NOD-like receptors or purinergic P2X receptors by nucleotides such as ATP and AMP. Activation of these receptors results in a K^+ efflux that promotes the formation/activation of an inflammasome complex, whose role is to cleave pro-IL-1β into IL-1β via caspase-1[460–462]. Interestingly, the TWIK-related Halothane-Inhibited K^+ channel has recently been identified as a key K^+ regulator that favors the microglial release of IL-1β after LPS stimulation[463]. The release of IL-1β guarantees a sustained inflammatory response. In the case of sterile inflammation, IL-1β is produced by infiltrated monocytes as a consequence of the release of IL-1α[70]. In CNS pathologies, IL-1β regulates the entry of myeloid cells inside the CNS by activating IL-1R1 at the surface of cerebral blood vessels[90,307]. Recruited myeloid cells subsequently produce more IL-1β, thus amplifying the inflammatory response[70,307,464]. Accordingly, IL-1β-KO mice have impaired myeloid cell

infiltration during experimental autoimmune encephalomyelitis and SCI[70,307,464]. IL-1β also induces astrocyte proliferation and reactivity and promotes the release of molecules with potentially detrimental effects, such as glutamate, reactive species (e.g. ROS) and proinflammatory cytokines[465]. Recent *in vitro* studies suggested that stimulation of astrocytes with either IL-1α or IL-1β may promote different effects[72,466]. Indeed, stimulation of astrocytes by IL-1α caused gliosis, creating a harmful phenotype which caused neuronal death. The activation of astrocytes by IL-1β also caused gliosis, but did not induce the neurotoxic phenotype[149]. The effects of IL-1β on astrocytes will require, however, further investigation.

Microglia also express IL-1R1[154,331], and few studies highlighted the role of IL-1R1 signaling in microglia proliferation[331]. Deletion of the *Il1r1* gene from microglia resulted in reduced microglia counts in several regions of the CNS[331]. Although the study implicated IL-1α as the major cytokine involved in microglia proliferation, the potential effect of IL-1β was not explored[331]. In support of this possibility, deficiency in IL-1β in the context of SCI caused a drop in total microglia/macrophage counts in the spinal cord[467]. Reduction in the number of microglia/macrophages in IL-1β-KO mice caused a reduction in the expression of several proinflammatory cytokines, which was correlated with enhanced locomotor recovery after SCI[468]. Thus, IL-1β is implicated in microglia proliferation and activation and the release of proinflammatory molecules following SCI.

1.6.1.3.The IL-1R1 antagonist (anakinra)

Since the discovery that IL-1 signaling initiates inflammation, the use of antagonists was largely explored during the end of 20th century. IL-1RA is an endogenous protein that acts as a competitive inhibitor of IL-1R1[469]. Anakinra, a recombinant form of the naturally occurring IL-1RA, has a low toxicity and short half-life. It was approved for the treatment of autoimmune and inflammatory diseases such as rheumatoid arthritis, gout, type 2 diabetes, and familial Mediterranean fever[452,469]. However, its use for the treatment of CNS pathologies remains to be demonstrated.

Over the recent years, we and others have demonstrated the capacity of anakinra to ameliorate the outcome of several CNS disorders. Following middle cerebral artery occlusion, a single

injection of anakinra reduced by 33% the infarct volume in rats[470,471]. Similar results were obtained when the IL-1R antagonist was administrated during the reperfusion phase, leading to a significant reduction in inflammation[472]. In SCI, acute or chronic delivery of anakinra, starting during the first few hours after SCI, reduced apoptosis in rats and enhanced locomotor recovery in mice[70,473]. The incorporation of anakinra into a gelatin sponge that promotes sustained release was associated with enhanced locomotor recovery in rats[474]. In sum, the use of anakinra for the treatment of CNS disorders was found to be effective in experimental models of stroke and SCI, opening the way for clinical trials.

1.6.2. TNF

The role of TNF, as for IL-1, is to initiate the inflammatory response. TNF has two active forms. The first one is a transmembrane form and the second one is a soluble form which may act as autocrine or paracrine regulator of inflammation[475]. TNF is synthesized as a 26-kDa membrane-bound precursor (mTNF) which may be cleaved into a 17-kD mature form by the TNF-converting enzyme (TACE or ADAM17)[476]. TNF may then bind to TNF receptor type 1 (TNFR1) or TNFR2. Both receptors are part of the TNFR superfamily and, like IL-1R1, signal through transcription factors such as NF-kB, JNK, ERK-1/2 and p38 MAPK, albeit through a different set of adaptor molecules[477]. The soluble form of TNF has a greater affinity for TNFR1, which possesses a death domain (DD) that can activate two opposite downstream signaling pathways. The first pathway is linked to the TNFR1 signaling complex and involves TNFR-associated death domain (TRADD), which prevents cell death with the production of anti-apoptotic proteins. The second pathway is linked to TNFR2 and involves both TRADD and FAS-associated death domain (FADD), causing cell death by necroptosis and initiating inflammation[478]. In contrast, mTNF prefers TNFR2 that lacks DD and signals through TNFR-associated factors (TRAFs), activating inflammation through transcription factors NF-kB and AP-1 and acting as a negative regulator of apoptosis[477,479].

TNF mRNA expression peaks at 1 hour post-SCI before vanishing at 2 days[76,152,153]. A second wave of TNF expression has also been described during the chronic phase of SCI, starting at 14 days post-SCI and increasing up to day 28, suggesting multiple effects of the cytokine during the course of SCI[76]. In mice and rats, all CNS cell types are able to produce it. TNFR1

and TNFR2, on the other hand, are highly expressed by microglia, highlighting their ability to produce but also respond to inflammatory cytokines in their function of CNS sentinel[154]. TNFR1 is also expressed by astrocytes, oligodendrocytes and CNS endothelial cells under steady state conditions. The global elimination of TNF using KO mice was previously shown to be protective in the context of SCI, resulting in reduced inflammation and the differentiation of macrophages towards a M2 repair phenotype[155]. In line with this observation, deletion of the *Tnfr1* gene in mice reduced inflammation, apoptosis and tissue damage, as well as enhanced functional recovery after SCI [156]. Furthermore, the blockade of TNF with etanercept, a TNF inhibitor functioning as a decoy receptor that can bind TNF, or infliximab, a function blocking antibody that recognizes TNF, protected mice from SCI, showing reduced inflammation and apoptosis, increased myelination, and enhanced locomotor recovery[156,157]. Although the SCI literature seems convincing about the benefit of interfering with the TNF pathway, some studies suggested otherwise. In cerebral ischemia, deletion of the *Tnf* gene in mice resulted in an exacerbated infarct area associated with more neuronal death and behavioral deficits[480,481]. One of two groups reported that TNF acted on microglia via TNFR1, exerting a neuroprotective role during stroke[481]. Supporting this view is a SCI study that showed an augmented expression of TNF in rats, an effect correlated with an increase in apoptotic cell death, astrocyte migration and reactivity, as well as a reduced tissue loss[482].

1.6.3. TGF-β

TGF-β is a cytokine implicated in a plethora of physiological and pathological processes, including inflammation, wound healing, ECM production, angiogenesis and proliferation[483–485]. There are 3 isoforms of TGF-β, namely TGF-β1, TGF-β2 and TGF-β3. Among them, TGF-β1 is the best described. TGF-β1 binds to TGF-βRII, forming a complex that recruits ALK5 (also known as TGF-βRI) and the accessory protein endoglin (CD105 or TGF-βRIII) and leads to phosphorylation of SMAD 2/3[389,486–489]. SMAD 2/3 then forms a homodimer or heterodimer that binds to SMAD4, allowing its translocation into the nucleus where it regulates target genes in cooperation with other transcription factors[490].

Tgfb1-KO mice typically show elevated mortality, associated with massive and chronic infiltration of leukocytes, suggesting that TGF-β1 is an important immunosuppressor[491,492]. Among its anti-inflammatory functions, TGF-β1 downregulates the expression of IL-1β and TNF[493,494]. The early death of *Tgfb1-KO* mice has been associated with overactivation of T cells. Accordingly, constitutive overexpression of TGF-β1 in T cells under the control of the *Il2* gene promoter protected *Tgfb1-KO* mice from early death, allowing the study of the cytokine during homeostasis[495,496].

Within the adult CNS, microglia are the main source of *Tgfb1* mRNA in mice[154]. Microglia-derived TGF-β1 release acts in autocrine manner to preserve gene expression and function of resting microglia [193,230]. Deletion of the *Tgfb1* gene in all cells but T cells, to avoid early mouse lethality, revealed that microglia have an altered phenotype in the absence of the immunosuppressive cytokine, characterized among other things by a reduction in expression of the P2Y12 protein[193]. Interestingly, microglia rely on TGF-β signaling and its downstream enhancer SMAD to recruit PU.1 transcription factor, maintaining the homeostatic microglia state[232]. Deletion of *Tgfbr2* specifically in microglia resulted in reduced microglial ramifications, a sign of microglial activation, enhanced proliferation and production of proinflammatory cytokines[193,230].

Following SCI, TGF-β1 production was associated with neurons and immune cells, including microglia[89,497–499]. TGF-β1 neutralization either with a single or continuous treatment affected the astrocytic response, reducing their migration and reactivity[500,501]. Acute treatment with anti-TGF-β1 reduced the formation of fibrotic tissue[500], whereas continuous blockage of TGF-β1 augmented microglial/macrophage response, as demonstrated by the increase in expression of Iba1 and ED-1 markers, a response correlated with improved locomotor recovery[501]. Injection of TGF-β1 results in prominent gliosis[485,500,502], which we know can reduce axonal plasticity[108]. Interestingly, the administration of Taxol, a drug that inhibits TGF-β1/SMAD signaling, reduced tissue scarring, enhanced the sprouting of serotoninergic axons, and improved locomotor recovery after SCI[503]. The same study demonstrated that Taxol reduced the production of inhibitory molecules by astrocytes[503]. Altogether, these data suggest that TGF-β1 production following SCI particularly affects astrogliosis, promoting the formation of scarring tissue.

1.6.4. IGF-1

Insulin growth factor (IGF)-1, IGF-2 and insulin itself form the insulin family. IGF-1 consists in a 7.5-kDa protein formed by 57 amino acids[504–506]. Each protein of the family shows preferential affinity for different receptors. The IGF receptor type 1, IGF-1R, binds with greater affinity to IGF-1 than IGF-2 and insulin, by 10- and 250-times, respectively[507]. IGF-1R is a tyrosine kinase receptor that, following binding to IGF-1, induces an autophosphorylation that results in activation of the insulin receptor substrates (IRS)[192,505,506,508]. In return, IRS activate phosphatidylinositol 3-kinase (PI3K), which then phosphorylates serine/threonine protein kinase (AKT). AKT can activate several pathways including phosphoinositide-dependent protein kinase (PDK), mammalian target of rapamycin (mTOR), forkhead Box O (FOXO) transcription factors, and cAMP-responsive element binding protein (CREB), all of which regulate cellular metabolism, survival, proliferation and migration processes, among others[509–518]. IGF-1R also signals through the mitogen-activated protein kinases (MAPK) and extracellular signal-regulated kinases (ERK), promoting cellular proliferation in different cell types[258,509,510,519,520].

IGF-1 regulates a plethora biological processes in various tissues and organs. The production of IGF-1 is particularly important during embryogenesis. *Igf1-KO* mice have reduced survival rates after birth when compared to WT littermates, most likely due to the reduced maturation of various tissues[504,513,521–523]. Survivors are smaller in size with reduced brain size, an observation correlated with a reduced number of neurons[504,524–527]. Two major sources of IGF-1 have been identified thus far. First, the liver, which releases IGF-1 into the plasma, allowing it to cross the BBB and influence CNS resident cells[510,528,529]. Resident cells of the CNS is the second major source, as shown by *in situ* hybridization experiments[505,510,518,530,531]. IGF-1 can form complexes with several insulin growth factor binding proteins (IGFBP), namely IGFBP1-7, in the blood circulation or within tissues. IGFBPs can modify the characteristics and biodisponibility of IGF-1. In the blood, IGF-1 mainly binds to IGFBP3 and IGFBP5[532,533]. Although the liver production of IGF-1 is important, during brain development, the autocrine production seems to be determinant, as demonstrated by the fact that liver-specific *Igf1-KO* mice have a normal growth rate and normal organ sizes despite having 75% less IGF-1 in their plasma[532]. The generation double-

KO mice that combined liver-specific deficiency in *Igf1-KO* with deficiency in the acid-labile subunit, a protein subunit that stabilizes the binding of IGF-1 with the IGFBP3 complex in serum, resulted in greater reduction in IGF-1 plasma levels, thus conferring reduced tissue maturation and mouse size[532].

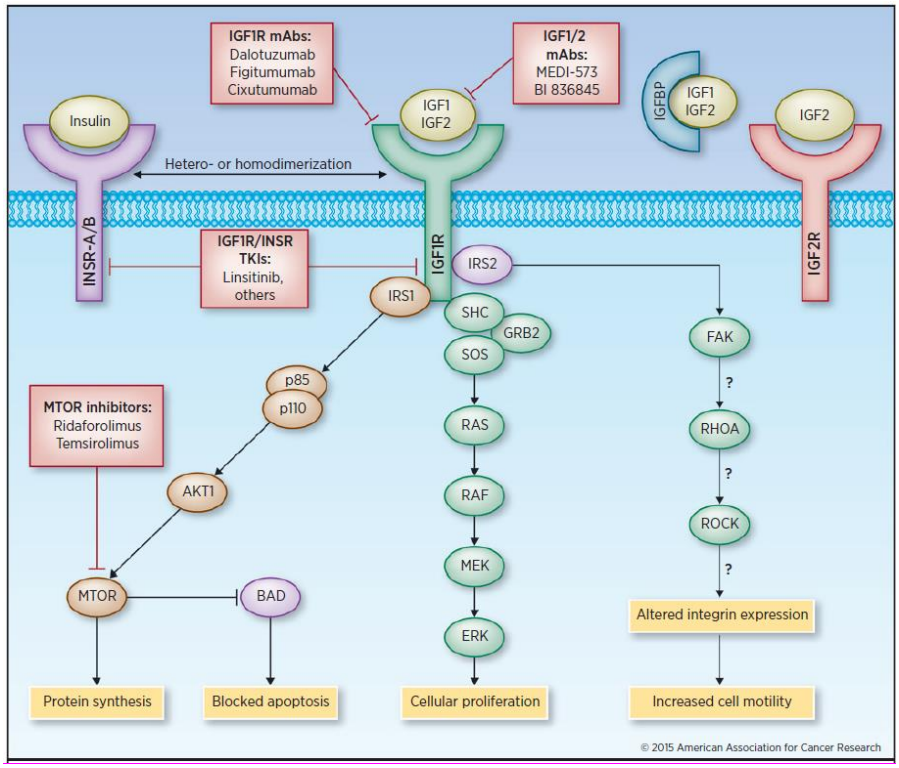

Figure 1.6. IGF-1 signaling pathway.
IGF-1 signaling pathway, obtained from REF[534].

IGF-1 is mainly produced during CNS embryonic development. IGF-1 is implicated in different processes of CNS maturation. In the adult CNS, IGF-1 production is reduced and restricted to certain areas, including neurogenic niches where they regulate neurogenesis[531,535]. Accordingly, *Igf1-KO* mice have a reduced brain size, which is correlated with a reduction in neurogenesis, total neurons, total oligodendrocytes, and myelinated areas[526,536]. On the contrary, overexpression of *Igf1* results in increased myelination and enhanced brain size[537]. The increased presence of IGF-1 is associated with increased neuronal counts in medullary nuclei and increased neurogenesis correlated with more synaptic buttons

per neuron in the hippocampus[538,539]. *In vitro*, stimulation of embryonic progenitors with IGF-1 promotes proliferation[540,541]. Moreover, IGF-1 regulates oligodendrocyte maturation and astrocyte migration/proliferation[89,542–544]. The production of *Igf1* in the CNS relies on neurons and glia[14,195,545]. *Igf1* is highly produced by early and pre-microglia during embryonic CNS development, but downregulated in these cells during adulthood[14]. Notably, microglia-derived IGF-1 promotes neuronal survival in cortical layer V, as demonstrated by the fact that depletion of microglia and microglia-specific deletion of the *Igf1* gene both resulted in increased neuronal apoptosis in this region[195]. Stimulation of neurons *in vitro* with IGF-1 favors axonal outgrowth[123,546,547]. During development, IGF-1 regulates corticospinal tract (CST) axon growth from the cortex to the spinal cord[123]. Accordingly, microglia depletion altered axonal outgrowth and pathfinding during embryogenesis[18]. Although the injection of IGF-1 failed to promote CST axon regrowth following CNS injury in the adult[548,549], the combination of IGF-1 with osteopontin, a protein that enhances IGF-1R phosphorylation in CST neurons, favored axonal sprouting in animal models of stroke and spinal cord dorsal hemisection[549].

IGF-1 is highly upregulated following stroke, traumatic brain injury (TBI) and SCI[89,550–554]. IGF-1 upregulation regulates several cellular processes following CNS injury, including proliferation, survival, migration and plasticity events in different cell subtypes. IGF-1 administration either by a central or peripheral route protected neurons from apoptosis, as well as reduced infarct volumes following stroke[555,556]. In support of this, genetic overexpression of *Igf1* in astrocytes enhanced neuronal survival and improved cognitive function following TBI[557]. Astrocytes use IGF-1 to enhance their proliferation and migration. Glioblastoma, which consists in uncontrolled astrocyte proliferation, require IGF-1 to expand and proliferate[558,559]. Blocking IGF-1 derived from tumor-associated macrophages (TAMs) using the chemical compound OSI-906 in combination with the CSF1R antagonist BLZ945 inhibited glioblastoma expansion, expanding survival rates following tumor inoculation[559].

1.7. Hypothesis and research objectives

SCI induces a plethora of responses such as inflammation, leukocyte recruitment and polarization, glial scarring, tissue repair and plasticity. Many of these events are regulated by inflammatory cytokines. Previous studies have suggested that immune cells, particularly microglia, the resident macrophages of the CNS, may play a pivotal role in SCI outcome. But since the response of microglia and MDMs has often been confused, we still do not know which cell type is doing what and how. Thus, our general **research objective** was to elucidate the role of microglia in SCI. We **hypothesized** that the microglial response is highly regulated to protect the injured spinal cord from inflammation and to facilitate tissue repair and functional recovery.

1.7.1. Role of microglia in SCI

In Chapter 1, we characterized the microglial response following SCI. The confusion behind the role of this particular cell type motivated us to clearly elucidate the function of microglia in the context of SCI. The generation of *Cx3cr1*^{creER} mice provided us with a great tool to visualize and distinguish microglia from MDMs[291]. Additionally, the use of CSF1R inhibitors allowed us to eradicate microglia from the CNS and to understand their function following SCI[17].

Hypothesis:

The microglial response is highly regulated to protect the injured spinal cord from inflammation and to facilitate tissue repair and functional recovery.

Experimental objectives:

- To localize microglia and compare their dynamics with the one of MDMs after SCI.
- To characterize the microglial response and possible interactions between microglia and astrocytes during formation of the glial scar.
- To investigate the effect of microglia depletion on glial scar formation and functional recovery after SCI.

- To study the response of microglia and functional recovery after SCI following exogenous delivery of recombinant MCSF.

1.7.2. Role of the IL-1 cytokine system in SCI

In Chapter 2, we characterized the function of IL-1α and IL-1β following SCI. Both cytokines belong to IL-1 superfamily and are initiators of the inflammatory response. IL-1α expression is restricted to microglia, whereas IL-1β is expressed by infiltrating myeloid cells[70]. We used different transgenic mouse models to elucidate the role of both cytokines in SCI[70].

Hypothesis:

IL-1α deficiency reduces inflammation and secondary tissue damage, thus ameliorating functional recovery after SCI.

Experimental objectives:

- To characterize IL-1α and IL-1β expression following SCI.
- To identify the main cellular source(s) of IL-1α and IL-1β during their peak of expression after SCI.
- To evaluate functional recovery in the absence of IL-1α and IL-1β after SCI.
- To study consequences of IL-1α and IL-1β secondary tissue damage and the loss of neurons and oligodendrocytes in the injured spinal cord.
- To assess secondary tissue damage and functional recovery in SCI mice treated with an antagonist of IL-1R signaling, anakinra.

Chapter 1:

Microglia are an essential component of the neuroprotective scar that forms after spinal cord injury

Victor Bellver-Landete[1], Floriane Bretheau[1], Benoit Mailhot[1], Nicolas Vallières[1], Martine Lessard[1], Marie-Eve Janelle[2], Nathalie Vernoux[1], Marie-Ève Tremblay[1], Tobias Fuehrmann[3], Molly S. Shoichet[3] and Steve Lacroix[1]*

[1]Axe neurosciences du Centre de recherche du Centre hospitalier universitaire (CHU) de Québec–Université Laval et Département de médecine moléculaire de l'Université Laval, Québec, QC, G1V 4G2, Canada; [2] Département de biologie-biotechnologie du Cégep de Lévis-Lauzon, Lévis, QC, Canada, G6V 6Z9; [3]Department of Chemical Engineering & Applied Chemistry, University of Toronto, Toronto, ON, M5S 3E1, Canada

Keywords: Astrocytic scar, CSF1R, fibrotic scar, hydrogel, IGF-1, M-CSF, microglia depletion, neuroinflammation, PLX5622, secondary degeneration.

2.1. Résumé

Le rôle des microglies lors d'une lésion de la moelle épinière (LME) reste incompris et souvent confus avec celui des macrophages dérivés du sang (MDMs). Dans cet article, nous utilisons une lignée de souris transgéniques fluorescentes permettant de visualiser spécifiquement les microglies et des drogues servant à éliminer celles-ci afin de mieux comprendre leurs réactions et rôles à la suite d'une LME. Nous avons observé que la microglie est très dynamique et prolifère abondamment durant la première semaine, s'accumulant autour du site lésionnel. À cet endroit, les microglies actives se positionnent à la jonction entre les leucocytes dérivés du sang et les astrocytes qui prolifèrent et qui forment la cicatrice gliale en réponse aux facteurs relâchés par les microglies elles-mêmes, comme par exemple le facteur de croissance 1 ressemblant à l'insuline (IGF-1). L'élimination des microglies après une LME entraine une perturbation dans la formation de la cicatrice gliale, permettant du même coup la migration des MDMs hors de la zone lésée. Ceci a pour effet de réduire la survie des neurones et des oligodendrocytes et de perturber le recouvrement des fonctions locomotrices. Par ailleurs, une prolifération microgliale induite via un traitement local au M-CSF a pour effet de réduire la taille de la lésion et d'améliorer le recouvrement des fonctions motrices. Ainsi, nos résultats définissent la microglie comme un composant cellulaire important de la cicatrice qui se développe après une LME afin de protéger le tissu neuronal.

2.2. Abstract

The role of microglia in spinal cord injury (SCI) remains poorly understood and is often confused with the response of macrophages. Here, we use specific transgenic mouse lines and depleting agents to understand the response of microglia after SCI. We find that microglia are highly dynamic and proliferate extensively during the first two weeks, accumulating around the lesion. There, activated microglia position themselves at the interface between infiltrating leukocytes and astrocytes, which proliferate and form a scar in response to microglia-derived factors, such as IGF-1. Depletion of microglia after SCI causes disruption of glial scar formation, enhances parenchymal immune infiltrates, reduces neuronal and oligodendrocyte survival, and impairs locomotor recovery. Conversely, increased microglial proliferation, induced by local M-CSF delivery, reduces lesion size and enhances functional recovery. Altogether, our results identify microglia as a key cellular component of the scar that develops after SCI to protect neural tissue.

2.3. Introduction

Microglia derive from primitive yolk sac progenitors that arise during embryogenesis [1, 2, 3]. They are maintained after birth and into adulthood by self-renewal [4, 5], independently from bone marrow-derived hematopoietic stem cells (HSCs) and their differentiated progeny (e.g. monocyte-derived macrophages, MDMs) [6, 7]. After a CNS injury, blood-derived monocytes are massively recruited in the tissue where they differentiate into macrophages and adopt many of the markers and behaviors of microglia. These similarities have complicated the development of efficient prediction tools to discriminate between them. As a consequence, they are still referred to as microglia/macrophages in the neuroscience literature, and accordingly, their individual roles remain to be clarified.

Recent advances in genetic fate mapping and conditional gene targeting have allowed the study of the specific biology of microglia in various experimental contexts, including SCI [8]. This, together with the newly-developed strategies to specifically eliminate microglia [9], has moved forward knowledge about these cells substantially. For example, the application of some of these advances to a mouse model of stroke has led to the discovery that microglia can protect neurons through the regulation of calcium levels [10]. In contrast, the elimination of microglia in mouse models of Alzheimer's disease and Tau pathology reduced disease progression [11, 12]. Thus, depending on the context, microglia may exert diverging roles. Whether these cells are beneficial or deleterious after SCI remains unexplored.

Here, we took advantage of *Cx3cr1*^{creER} mice [13], a mouse line that allows with an adequate regimen of tamoxifen to label microglia while excluding nearly all MDMs. Our results show that microglia are highly dynamic and proliferate extensively during the first week post-SCI. Notably, we reveal that microglia form a dense cellular interface at the border of the lesion between reactive astrocytes and infiltrating MDMs, which we hereafter refer to as the "microglial scar". Microglia depletion experiments using PLX5622, a CSF1R inhibitor that crosses the blood-spinal cord barrier (BSCB), demonstrated that the absence of microglia in the context of SCI disrupts the organization of the astrocytic scar, reduces the number of neurons and oligodendrocytes at the site of injury, and impairs functional recovery. The timing of the beneficial effects of microglia was estimated to be during the first week post-

SCI. Accordingly, CNS delivery of M-CSF during that critical period boosted microglial proliferation and enhanced locomotor recovery. In light of these data, we conclude that microglia are an important component of the protective scar that forms after SCI.

2.4. Results

2.4.1. Microglia rapidly accumulate around the site of SCI

To distinguish microglia from MDMs, we took advantage of Cx3cr1^{creER}::R26-TdT mice, and the slow turnover of microglia [4, 5]. Mice received tamoxifen treatment one month before SCI to activate the inducible Cre for recombination of TdT floxed (Supplementary Figure 1a). As expected from our previous work [14], nearly all (99.6 ± 0.2 %) CD11b$^+$ cells in the spinal cord parenchyma expressed TdT (Supplementary Figure 1b-c). In contrast, only a few CD11b$^+$ cells in the blood, spleen and bone marrow were TdT$^+$, with average colocalization percentages of 3.8 ± 1.7 %, 6.7 ± 1.6 % and 2.4 ± 0.2 %, respectively (Supplementary Figure 1d-f). Thus, inducible Cx3cr1^{creER}::R26-TdT mice are a good tool to study microglia in SCI.

To understand the dynamics of the microglial response after SCI, we first quantified the total number of TdT$^+$ microglia both in normal conditions and at 1, 4, 7, 14 and 35 days post-injury (dpi) (Fig. 1a-g & Supplementary Figure 2). In the uninjured thoracic spinal cord of Cx3cr1^{creER}::R26-TdT mice, we counted an average of 85.9 ± 4.6 microglia per mm^2. Following a moderate contusive SCI, only 28.8 ± 1.9 microglia per mm^2 were left at the lesion epicenter at 1 dpi, which corresponds to a 67% reduction in cell numbers. Hardly any TdT$^+$ microglia were observed in the lesion core at this early time point, suggesting that they underwent rapid cell death. Despite the fact that the impactor tip measures 1.25 mm of diameter, microglia were lost across several spinal cord segments rostrocaudally. This microglial cell loss ranged from approximately 20% to 65% at rostrocaudal distances up to 6 mm from the lesion epicenter (Fig. 1g-h), and was mediated in part through apoptosis (Fig. 1i-k). At that time, residual microglia still expressed the purinergic receptor P2ry12 (Supplementary Figure 3), a receptor implicated in microglia recruitment during the early acute phase of CNS injury [15]. Accordingly, we noticed a retraction of microglial processes as early as day 1. Expression levels of the lysosome-associated glycoprotein CD68, a marker of phagocytosis, remained low in TdT$^+$ microglia at 1dpi (Supplementary Figure 4). However, the situation changed at day 4, as we counted 119.1 ± 15.0 microglia per mm^2 at the lesion epicenter, which represents a 4-fold increase in the number of TdT$^+$ microglia compared to day 1 (Fig. 1g). Microglia around the lesion epicenter exhibited a round morphology,

downregulation of P2ry12 and a strong upregulation of CD68 (Supplementary Figures 3-4), which points to a potential increase in their phagocytic activity starting around 4 dpi. The number of microglia continued to increase at the lesion epicenter over time, reaching up to 1204.61 ± 137.8 cells/mm^2 at 14 dpi. Nearly all microglia observed in these areas were TdT$^+$ CD68^{hi} P2Y12^{neg} (Supplementary Figures 3-4). A similar trend was seen in the surrounding tissue (400-800 µm) of the lesion epicenter up to 35 dpi, after which the total number of microglia (i.e. 673.91 ± 62.4 cells/mm^2 at the lesion epicenter) started to decrease compared to day 14 (Fig. 1g). Interestingly, TdT$^+$ microglia started to gradually increase their expression of P2ry12 and decrease their expression of CD68 from day 14 up to day 35 (Supplementary Figures 3-4), suggesting a partial return to homeostasis. In sum, our data indicate that microglia are rapidly recruited around the site of SCI, where they accumulate extensively during the subacute phase and adopt an activated state that is eventually partially resolved during the intermediate/chronic phases.

2.4.2. Microglia proliferate extensively during the subacute phase of SCI

Under normal circumstances, the adult microglial population remains stable in the brain throughout life by coupled cell death and cell proliferation [4], but little is known about its dynamic in the spinal cord and how it reacts following SCI. Here, we report that 0.6 ± 0.1 microglia/mm^2 (0.58% of total) are proliferating in the normal thoracic spinal cord of Cx3cr1^{creER}::R26-TdT mice, as revealed by the co-expression of TdT and the cell proliferation marker Ki67. One day after SCI, no significant changes were observed in terms of microglial cell proliferation compared to the uninjured spinal cord (Fig. 1l-m). Strikingly, about 50% of microglia at the lesion epicenter expressed Ki67 at 4 dpi. As shown in Supplementary Movie 1, proliferating TdT$^+$ Ki67$^+$ microglia were round-shaped. The peak proliferation of microglia, in terms of absolute numbers, was observed at day 7 (Fig. 1l, n-p). At 14 and 35 dpi, only a few (2-6%) microglia were still expressing Ki67, suggesting that microglial proliferation was mostly inhibited by then. Together, these results show that microglia are highly dynamic after SCI, not only through their recruitment and activation, but also through their ability to rapidly proliferate and surround the site of SCI during the subacute phase.

2.4.3. Depletion of microglia reduces locomotor recovery after SCI

Yolk sac progenitors are at the origin of specialized tissue-resident macrophages, including microglia, and depend on colony-stimulating factor 1 receptor (CSF1R) signaling for their survival [16]. Thus, to better understand the role of microglia and MDMs in SCI, we compared the effects of two novel CSF1R inhibitors from Plexxikon: 1) PLX5622, a drug that crosses the blood-brain barrier (BBB) and eradicates nearly all microglia in the brain [9, 10, 17, 18, 19], and 2) PLX73086, a CSF1R inhibitor that does not deplete resident microglia because of its low BBB penetration (Dr. Andrey Rymar, Plexxikon, personal communication). Treatment of uninjured C57BL/6 mice with PLX5622 for 3 weeks resulted in depletion of 97.9 ± 0.6% of spinal cord microglia (Fig. 2a-d & Supplementary Figure 5). In contrast, PLX73086 did not affect the microglial population. To examine the effects of the two CSF1R inhibitors on peripheral immune cells, we next performed a cytometric analysis of leukocyte subsets in the blood, spleen and bone marrow. No changes were observed after 3 weeks of treatment with the different diets (Supplementary Figure 6a-c). Altogether, these data indicate that PLX5622 can be used to selectively and nearly completely eliminate spinal cord microglia without significantly affecting peripheral leukocyte counts under steady state in vivo conditions in mice.

To examine the long-term effect of continuous PLX5622 treatment on microglia depletion, we counted the number of microglia per mm^2 at 1, 7 and 14 days post-SCI (Fig. 2e-h). Mice were fed chow containing either PLX5622, PLX73086 or vehicle (without gavage) starting 3 weeks before SCI and until time of sacrifice. Again, treatment of C57BL/6 or $Cx3cr1^{creER}$::R26-TdT mice with PLX5622 eliminated virtually all microglia at each of the above time points. Although no changes were observed at day 1 and day 14 between PLX73086-treated mice and those fed the control diet (Fig. 2e, g), we found that the total number of TdT^+ microglia at the lesion epicenter was reduced by nearly half at 7 dpi in animals that received PLX73086 (Fig. 2f). This might be due to a temporary breakdown of the BSCB, which allowed PLX73086 to enter the spinal cord parenchyma and to negatively affect microglial cell survival. In accordance, we detected an increased accumulation of

fluorescein isothiocyanate (FITC)-conjugated Lycopersicon esculentum agglutinin (LEA) lectin from day 1 to day 7 post-SCI at the lesion site, but not at 14 dpi (Fig. 2i).

At 1 dpi, a slight neutropenia was observed in C57BL/6 mice treated with PLX5622 or PLX73086 compared to those fed with the control diet (Supplementary Figure 6d). However, the number of infiltrating neutrophils at the site of SCI was similar between all groups at this time (Fig. 2j). No changes in blood leukocyte numbers were observed between groups at 7 and 14 dpi (Supplementary Figure 6e-f), except for a slight and transient decrease in the B cell counts at day 7. Treatment of LysM-eGFP mice with CSF1R inhibitors highlighted a transient reduction in the number of myeloid cells at the lesion epicenter in PLX5622-treated mice that was overcome by day 14 (Fig. 2k). Treatment with PLX73086 had no impact on the number of neutrophils and $LysM^+$ cells at the lesion site compared to control treatment (Fig. 2j-k). We interpret that the delayed myeloid cell recruitment in the injured spinal cord of PLX5622-treated mice was caused by the absence of microglia rather than a direct effect on peripheral leukocytes. Overall, these results indicate that PLX5622 can be used to eradicate virtually all spinal cord microglia after SCI with minimal direct effects on leukocytes.

We next investigated the role of microglia in functional recovery after SCI. Chow containing either PLX5622, PLX73086 or no drug (control) was given to C57BL/6 mice starting 3 weeks prior to SCI and then maintained for an additional 5 weeks (Fig. 3a). Similar to uninjured mice that received the control diet, microglia-depleted uninjured animals showed no gross locomotor deficits at the beginning of behavioral testing, as illustrated by the perfect BMS scores and subscores at day 0. No difference was found in terms of BMS score between the PLX73086 and control groups at any of the time points analyzed after SCI (Fig. 3b). However, mice depleted in microglia (PLX5622) exhibited impaired locomotor recovery compared to mice treated with PLX73086 or the control diet at 3, 7, 14, 28 and 35 dpi (Fig. 3b). Statistical differences in the BMS subscores between PLX5622-treated mice and animals of the other groups were detected starting from day 7 up to day 35 (Fig. 3c). At 35 dpi, the average subscore of PLX5622-depleted mice was 2.9 ± 0.6 compared to 4.5 ± 0.2 for PLX73086-treated mice and 5.4 ± 0.2 for mice fed the control diet. These results indicate that microglia play an essential role in recovery from SCI.

2.4.4. The beneficial actions of microglia occur during week 1 post-SCI

Recent work has established that the microglia-depleted brain repopulates within one week through local proliferation of residual microglia [20]. We reasoned that we could take advantage of this observation to study the time window during which the neuroprotective and/or neurorepair effects of microglia occur after SCI. We first evaluated the time course of repopulation of microglia in the spinal cord (Supplementary Figure 7). Cx3cr1^{creER}::R26-TdT mice were fed ad libitum for one week with the appropriate treatment. At this time, we counted 75.9 ± 7.9 TdT$^+$ microglia per mm^2 in the thoracic spinal cord of mice fed the control diet compared to 4 ± 0.6 in those treated with PLX5622 (94.7% depletion). The dynamic of the microglial repopulation was then assessed by switching the PLX5622 group to the control diet (Supplementary Figure 7a-m). The diet change resulted in a rapid increase in the number of microglia in the uninjured spinal cord, going from 4.0 ± 0.6 TdT$^+$ cells per mm^2 at day 0 to 15.8 ± 2.0 at day 2 and 35.3 ± 2.8 at day 3. By day 7 of withdrawal of CSF1R inhibition, the microglial population had completely recovered, with an average count of 99.5 ± 2.3 cells per mm^2, exceeding by ~30% the microglia numbers counted in control mice (Supplementary Figure 7m). Repopulated TdT$^+$ cells, observed after 7 days of drug withdrawal, had a ramified morphology and expressed CD11b and Iba1 (Supplementary Figure 7i-l, n), confirming that they are mature microglia. Only few (2.3 ± 1.7%) of the repopulated CD11b$^+$ Iba1$^+$ cells were TdT^{neg} at 7 days post-withdrawal. This indicates that microglia were repopulated from cells in which the Cx3cr1 gene promoter was active (i.e. TdT$^+$) at the time of tamoxifen treatment, confirming that adult spinal cord microglia are capable of self-renewal. A similar trend was also seen in C57BL/6 mice, in which the total number of P2ry12$^+$ microglia, after a repopulation period of 7 days, exceeded that of untreated mice by 54% (116.5 ± 5.4 P2ry12$^+$ cells/mm^2 compared to 75.7 ± 2.1 P2ry12$^+$ cells/mm^2).

As described above, spinal cord microglia of adult naïve mice are in low proliferative state (Supplementary Figure 7o). However, 2 and 3 days after PLX5622 removal, 93.5% and 87.4% of the TdT$^+$ microglia, respectively, were actively proliferating based on Ki67 expression. Few TdT^{neg} cells also proliferated simultaneously to microglia proliferation but at a reduced rate. Multiple immunofluorescence labeling revealed that the non-microglia proliferating cells were mostly of the oligodendrocyte lineage, with 6.1 ± 0.9 and 6.7 ± 1.9

Olig2^{+} TdT^{neg} Ki67^{+} cells/mm^{2} at 2 and 3 days, respectively (Supplementary Figure 7p). GFAP-positive astrocytes, CD206^{+} perivascular macrophages, CD13^{+} pericytes, and CD45^{+} TdT^{-} blood-derived leukocytes accounted for less than 1% of the Ki67^{+} cells. Therefore, our results indicate that residual microglia proliferate extensively and can repopulate the entire spinal cord microglial population within 7 days.

We next sought to determine when the beneficial effects of microglia occur after SCI, as this is critical for the development of a therapeutic approach targeting microglia. For that purpose, C57BL/6 mice were fed PLX5622 for 3 weeks, before switching to a control diet at the time of SCI (Fig. 3d), resulting in microglia depletion at the time of injury but not afterwards. No differences were found in behavioral outcomes between groups (Fig. 3e-f). As microglial repopulation requires about a week to be completed after cessation of treatment with the CSF1R inhibitor (Supplementary Figure 7i-m), we next hypothesized that the beneficial effects of microglia might take place during the first week post-SCI. Since injured mice eat significantly less during the first few days, separate groups of mice were force-fed with either PLX5622 or vehicle by gavage from the time of SCI up to day 7 (Fig. 3g), in addition to the ad libitum access to the drug-containing chow. Importantly, PLX5622-gavaged mice showed impaired locomotor recovery on the BMS scale compared to control mice (Fig. 3h-i). In contrast, SCI mice that were started on the PLX5622 diet at day 3 displayed locomotor scores similar to those observed in the PLX73086 and control groups (Fig. 3j-l). Altogether, these data indicate that activated, proliferating microglia are crucial for protecting/repairing the injured spinal cord and that their beneficial effects take place during the first week post-SCI.

2.4.5. A microglial scar forms at the astrocyte–immune cell interface

It was recently proposed that cytokines released by activated microglia in response to CNS injury or disease determine whether astrocytes will have neurotoxic or pro-survival effects [21]. Thus, we next investigated whether microglia play an important role in the formation of the astrocytic scar that develops during the subacute/chronic phases of SCI and which can influence axonal regeneration and functional recovery. As neutrophils and MDMs rapidly accumulate in the injured spinal cord and share common markers with microglia, Cx3cr1^{creER}::R26-TdT::LysM-eGFP reporter mice were initially used to perform an

immunofluorescence and ultrastructural characterization of glial scar formation over time (Supplementary Figure 8a). We found that TdT^+ microglia accumulate mainly around the lesion site, where they make direct contacts with $GFAP^+$ astrocytes, especially their distal processes, and also with blood-derived $LysM^+$ cells (Fig. 4a-g, Supplementary Figures 8b-e & 9). This microglial interaction with $GFAP^+$ astrocytes and blood-derived $LysM^+$ cells was most apparent starting at 14 dpi and persisted until at least day 35. As described above, nearly half of the microglia detected at the rim of the lesion were actively proliferating at day 7, a response that returned near baseline by day 14 (Fig. 4h). This translated into an increased number of TdT^+ microglia at the lesion epicenter at 14 dpi (Fig. 4i). However, we noted that the lesion itself was predominantly occupied by $LysM^+$ neutrophils/MDMs and PDGFR-ß$^+$ pericytes rather than TdT^+ microglia (Fig. 4j-l). These results indicate that microglia synergize with reactive astrocytes, and perhaps as well with pericytes, to isolate infiltrating immune cells at the core of the lesion. We named this phenomenon "microglial scar" as an analogy to the astroglial-fibrotic scar that develops after SCI and limits the spread of inflammatory cells, and at the same time influences regeneration of the severed axons [22, 23].

Since a residual fraction of peripheral myeloid cells express TdT in Cx3cr1^{creER}::R26-TdT (Supplementary Figure 1b), we further validated our microglial scar concept in chimeras resulting from the transplantation of β-actin-eGFP bone marrow cells into lethally irradiated Cx3cr1^{creER}::R26-TdT mice (Fig. 5a). Fourteen days after SCI, the microglial scar was still prominent and primarily consisted of TdT^+ microglia, with infiltrating bone marrow-derived ($eGFP^+$) cells located at the core of the lesion (Fig. 5b-e). In contrast, very few TdT^+ cells were seen at the rim of the lesion when Cx3cr1^{creER}::R26-TdT mice were used as bone marrow donors for recipient C57BL/6 mice (Fig. 5f-h). Indeed, we found ~25 times less TdT^+ cells in Cx3cr1^{creER}::R26-TdT → WT mice (49.5 ± 8.0 cells/mm^2) compared to Cx3cr1^{creER}::R26-TdT mice (1204.61 ± 137.8 TdT^+ cells/mm^2, Fig. 1 e, g) at 14 dpi. This suggests that cells from the periphery contribute minimally (less than 4%) to the total TdT^+ cell number in experiments using inducible Cx3cr1^{creER}::R26-TdT mice. Additionally, we inflicted SCI in Flt3-cre::R26-TdT mice (Supplementary Figure 8f), in which TdT is expressed in HSCs and their progeny (including MDMs and neutrophils), but not microglia [16]. At 14 dpi, a dense layer of $CD11b^+$ TdT $(Flt3)^{neg}$ cells was clearly detectable at the interface between $GFAP^+$ astrocytic end-feet on the outside of the lesion and $CD11b^+$ TdT

(Flt3)$^+$ blood-derived myeloid cells inside the lesion (Supplementary Figure 8g-j). This once again indicates a minimal contribution of blood-derived myeloid cells to the microglial scar that rapidly forms after SCI.

To eliminate the possibility that long-living TdT$^+$ perivascular and/or meningeal macrophages could be at the origin of the microglial scar, immunofluorescence staining was performed to detect the co-expression of TdT and markers of perivascular and meningeal macrophages. CNS border-associated macrophages were defined based on expression of macrophage mannose receptor (CD206) and major histocompatibility complex class II (MHCII) [24, 25]. Although some TdT$^+$ microglia at the rim of the lesion were CD206$^+$ at 14 dpi, they weakly expressed CD206 compared to perivascular and meningeal macrophages (Fig. 5i-o & Supplementary Figure 10a-c). We failed to detect MHCII expression on TdT$^+$ microglia (Fig. 5p & Supplementary Figure 10d-e). Instead, the MHCII signal was restricted to TdT^{neg} myeloid cells that infiltrated the lesion core, as well as perivascular and meningeal macrophages. In sum, our results demonstrate that a microglial scar, consisting of primarily proliferating microglia, forms at the border of the lesion after SCI.

2.4.6. Microglia induce astrocytic scar formation via IGF-1

Adequate astrocyte reactivity and glial scar formation have been shown to be vital for recovery of neurological functions after SCI [26, 27]. Strikingly, we observed that astrocytes located just outside of the lesion core formed a less compact scar when microglia were depleted using PLX5622 compared to the control treatment at 14 dpi (Fig. 6a-d). Notably, GFAP$^+$ astrocytes were oriented randomly and not aligned in any particular direction in PLX5622-treated SCI mice. This disorganized astroglial scar was accompanied by an increased infiltration of blood-derived myeloid cells inside the spinal cord parenchyma, outside of the primary lesion. Since glial scar borders that surround the site of SCI are typically formed by newly proliferated astrocytes [28], we next investigated whether microglial depletion was associated with changes in astrocytic proliferation. To enable accurate counting of proliferating (BrdU$^+$) astrocytes, these cells were identified based on expression of Sox9, a nuclear protein exclusively expressed by astrocytes in the adult CNS (except for ependymal cells) [29]. As shown in Figure 6e-k, the number Sox9$^+$ BrdU$^+$ astrocytes at the

lesion epicenter and in adjacent areas was reduced by ~40-55% in PLX5622-treated mice compared to the control group at 7 dpi. This suggests that, after SCI, microglia release molecules that trigger astrocyte proliferation and astrocyte scar formation.

Given the recent demonstration that the astrocyte response is determined by cytokines released by activated microglia in models of neuroinflammation (LPS) and CNS injury (optic nerve crush) [21], we studied the expression of cytokines identified as confirmed or potential inducers of A1 (TNF, IL-1α, IL-1β, IL-6) and A2 (TGF-β1, IGF-1) phenotypes using in situ hybridization (ISH). From 7 to 14 dpi, the period during which we observed the greatest proliferation of astrocytes and formation of the astroglial scar, mRNA transcripts for the proinflammatory cytokines IL-1α, IL-1β, IL-6, and TNF-α were weakly expressed at the lesion epicenter (Fig. 7a-d). In contrast, we detected strong expression of TGF-β1 and IGF-1 mRNAs at these times (Fig. 7e-l). The spatial distribution of TGF-β1- and IGF-1-expressing cells correlated with the microglial scar, with more ISH signal at the lesion border than at the lesion center. Accordingly, selective depletion of microglia resulted in a decrease of TGF-β1 and IGF-1 mRNA signals. To further demonstrate the involvement of microglia-derived TGF-β1 and IGF-1 in the formation of the astrocytic scar, we treated primary astrocytes with recombinant forms of these proteins. As shown in Figure 7m-n, treatment with IGF-1, but not TGF-β1, induced the proliferation of astrocytes (BrdU incorporation) and their migration towards the site of injury (scratch assay). Immunolabeling for IGF-1 in tissue sections from Cx3cr1^{creER}::R26-TdT mice confirmed that scar-forming TdT^{+} microglia are the principal cellular source of this factor at 7 dpi (Fig. 7o-q). Accordingly, in vivo inhibition of the IGF-1 receptor using an antagonist, OSI-906 [30], resulted in reduced expression of the astrocyte-specific marker Sox9 in the injured spinal cord of C57BL/6 mice (Fig. 7r). Thus, microglia-derived IGF-1 triggers astrocyte proliferation and promotes astrocyte scar formation after SCI.

Since reactive astrocytes were previously shown to exert protective functions after SCI [26], we next aimed to determine whether microglial depletion affects tissue damage. Quantification revealed that disrupted glial scar formation in PLX5622-treated mice is correlated with an increase of the lesion core area at 7 days post-SCI (Fig. 8a-c). Although no significant differences were observed between groups regarding the lesion core area at 14

and 35 dpi, we detected the presence of several secondary satellite lesions outside of the primary lesion in the spinal cord parenchyma of microglia-depleted mice (Fig. 8d-i). Secondary satellite lesions were devoid of neuronal elements (NF-H^+) and instead filled by blood-derived myeloid cells ($CD11b^+$ $LysM^+$) and PDGFRβ^+ pericytes/fibroblasts (Fig. 8j-k). Together, these results indicate that microglia play an important role in the formation of the astroglial scar after SCI, which is at least partly mediated by IGF-1, and that failure to carry out this function results in widespread inflammation and the appearance of satellite lesions.

2.4.7. Microglia prevent death of neurons and oligodendrocytes after SCI

Having established that the lesion load was increased and functional recovery worse in microglia-depleted mice at 35 days post-SCI, we next determined whether microglial elimination would influence the survival of neurons and oligodendrocytes. No differences in numbers of HuC/HuD^+ neurons and $Olig2^+$ $CC1^+$ mature oligodendrocytes were seen between groups in the absence of injury (Fig. 8l, p). However, there were fewer neurons and oligodendrocytes in spinal cord sections spanning the lesion site in the PLX5622 group compared with the other groups at 35 dpi (Fig. 8m-o, q). As expected, this difference resolved at distances >1.0 mm from the lesion site, thus suggesting that microglia are necessary for the survival of neurons and oligodendrocytes following an insult. Altogether, our results indicate that microglia play a neuroprotective role during SCI.

2.4.8. Boosting microglial proliferation enhances recovery after SCI

The above results demonstrate the importance of the microglial response in scar formation, protection of neural tissue and functional recovery after SCI. We therefore asked whether an increased microglial population would be beneficial on the outcome of SCI. As we observed that 7 days after the end of PLX5622 regimen the microglial population exceeded the one observed in homeostatic conditions (Supplementary Figure 11a-c), we subjected microglia-repopulated C57BL/6 mice to SCI (Supplementary Figure 11d). Although these mice had ~50% more microglia in their spinal cord at the time of injury, they exhibited no motor benefit

(Supplementary Figure 11e-f). These results suggest that microglial density at the time of injury is not the limiting factor in recovery.

Since we previously demonstrated that microglia exert their beneficial effects during the first week post-SCI, coinciding with their maximal proliferation rate (Fig. 1m), we hypothesized that artificially increasing their proliferative response right after the injury and continuously during the first week would lead to improvements. Given the importance of CSF1R signaling in microglia development [1], we tested whether M-CSF injection in the cisterna magna would induce microglial proliferation throughout the spinal cord. As shown in Figure 9a, treatment with M-CSF induced a dose-dependent effect on microglia proliferation, increasing by ~20-25% the number of $CD11b^{+}$ $P2ry12^{+}$ microglia in the thoracic spinal cord. Notably, this effect lasted for at least one week. To target the lesion site rather than the entire spinal cord, we incorporated M-CSF into a bioresorbable hydrogel that was injected into the intrathecal space at the site of SCI (Fig. 9b). Previous work has established that the hyaluronan-methyl cellulose hydrogel can provide sustained drug release for 3-7 days [31, 32, 33]. Despite the fact that treating $Cx3cr1^{creER}$::R26-TdT mice with the M-CSF-based hydrogel resulted in a non-significant trend towards a higher number of TdT^{+} microglia (Fig. 9c), it was sufficient to reduce the lesion area rostral to the epicenter at 7 dpi (Fig. 9d). In addition, the M-CSF-delivering hydrogels improved locomotor recovery from day 7 to day 21 after SCI when compared with PBS-based hydrogels (Fig. 9e-f). This suggests that enhancing the proliferation of microglia limits tissue loss and functional deficits following SCI through regulation of scar tissue formation. Altogether, our results demonstrate the importance of microglia in protecting the spinal cord after injury.

2.5. Discussion

The role of microglia in SCI has remained obscure for decades. Here, we took advantage of newly-developed genetic mouse models, in particular the *Cx3cr1*^{creER} mouse strain, and depletion strategies (e.g. the CSF1R inhibitor PLX5622) that allow us to target microglia specifically to study their role in the context of traumatic SCI. We found that microglia proliferate extensively and accumulate around the site of contusion at 7 days, forming a dense scar at the interface between the fibrotic scar and the yet-to-be-formed astrocytic scar. Notably, the near-complete elimination of spinal cord microglia by PLX5622 treatment led to a reduction in IGF-1 production, a disorganized astroglial scar and the appearance of satellite lesions filled with blood-derived inflammatory cells. This was accompanied by an increased loss of neurons and oligodendrocytes at the site of SCI, as well as greater tissue damage and impairment in locomotor function. The comparison of two CSF1R inhibitors with different BSCB permeability (given at various times before and after SCI) provided strong evidence that the protective function of microglia takes place during the first week post-SCI, matching the peak of proliferation of microglia. Accordingly, local delivery of the microglial proliferation factor, M-CSF, at the site of contusion significantly improved locomotor recovery compared to vehicle controls.

We initially predicted, based on previous SCI studies using radiation bone marrow chimeras, that MDMs would infiltrate almost exclusively the core of the lesion, while microglia would be found both within spared CNS tissue and the lesion itself [34, 35]. However, genetic fate mapping using *Cx3cr1*^{creER}::*R26-TdT* and *Cx3cr1*^{creER}::*R26-TdT*::*LysM*-eGFP mouse lines revealed that microglia at the site of trauma rapidly die after SCI. Additionally, we found that microglia that surround the lesion site rapidly become activated and proliferate extensively, forming a previously undescribed scar tissue, which we now refer to as the microglial scar. Our findings also contrast with those of Shecther and colleagues who reported that MDMs are restricted to the margins of the lesion and excluded from the center of the lesion [36]. Rather, the margins (borders) of the lesion are entirely occupied by microglia and pericytes/fibroblasts, whereas MDMs are confined to the center of the lesion. This once again shows that, although radiation bone marrow chimeras remain a useful tool, data generated

using them must be interpreted with care because: i) whole-body irradiation harms the blood-CNS barriers and impairs the proliferative capacity of microglia [37], and ii) HSCs and their progenitors are artificially introduced in the bloodstream as a result of the bone marrow transplant, thus creating a bias towards cells of the hematopoietic compartment [38, 39]. Using animal models that did not introduce such artifacts, we can conclude that blood-derived myeloid cells that infiltrate the injured spinal cord remain at the center of the lesion, where they are confined by surrounding tissue consisting of the microglial, fibrotic, and astrocytic scars.

As initially observed in the brain [9], continuous treatment with the CSF1R inhibitor PLX5622 resulted in the depletion of spinal cord microglia (99.6%), that was in our hands more efficient than *Cx3cr1*^{creER}::*R26-iDTR* transgenic mice (77.9%), in which diphtheria toxin (DT) has to be injected to induce cell death [40]. The PLX5622 treatment also avoided the occurrence of the undesired cytokine storm described by Bruttger and colleagues using the iDTR model [37], thus making it a better model to study the role of microglia. We found that the recruitment of MDMs is delayed in the injured spinal cord of PLX5622-treated mice during the acute phase. This finding is consistent with our previous observation that physically injured microglia release damage-associated molecular patterns (DAMPs), such as IL-1α, that initiate sterile neuroinflammation after SCI [41].

Historically, microglial activation in the injured CNS was generally perceived as harmful to both neurons and oligodendrocytes because of the release of high amounts of proinflammatory cytokines, proteases and reactive oxygen species. Supporting this view is the recent discovery that cytokines derived from activated microglia, such as IL-1α, TNF and C1q, determine whether astrocytes will have neurotoxic or pro-survival effects in various neurodegenerative disorders [21]. Accordingly, deletion of either of the genes encoding IL-1α, TNF and C1q in the context of SCI has been associated with an improved locomotor recovery [41, 42, 43]. However, the data here show that the elimination of microglia leads to aberrant growth factor production (e.g. IGF-1) and glial scar formation, increased neuronal and oligodendrocyte death, as well as reduced locomotor performance. In line with our results is a recent stroke study, where microglia depletion using PLX3397, a CSF1R inhibitor that also targets c-KIT and FLT3, increased neuronal death and infarct size in the brain [10]. This once

again reinforces the idea that the overall net effect of microglia after CNS injury is neuroprotection. Although the early infiltration of blood-derived myeloid cells at sites of SCI was previously associated with neurotoxicity [44, 45, 46], we cannot rule out the possibility that these cells may have contributed to the functional recovery effect seen in PLX5622-treated mice. If it were to be the case, we argue that it would be under the positive influence of microglia as evidence here indicates that the reduction in myeloid cell infiltration was a direct cause of the absence of microglia. In the context of CNS injury, therapies targeting microglia should therefore be aimed at enhancing their neuroprotective function and/or reducing their neurotoxicity rather than complete microglia eradication.

We uncovered that microglia regulate the astrocytic response, in part, through IGF-1. The fact that activated, proliferating microglia are an important source of IGF-1 following a CNS insult is line with findings of Lalancette-Hébert et al. in a mouse model of ischemic stroke [47]. There is also ample *in vitro* evidence that IGF-1 modulates astrocyte proliferation and the migratory ability of these cells towards a lesion [48, 49]. It should be noted, however, that TGF-β1 at the concentration tested in the present study and elsewhere was found not to be mitogenic for astrocytes [50, 51]. Still, a role for microglia-derived TGF-β1 in scar formation remains plausible because this cytokine was found to influence astrocytes by acting in synergy with other cytokines and growth factors [51], and as likely to occur in the complex *in vivo* setting of CNS injury where TGF-β1 neutralization reduces scarring [52, 53, 54]. It will therefore be of interest in future work to validate the relevance of these cytokines and their receptors, individually or in combination, in animal models of SCI using cell-specific conditional gene targeting strategies.

In the absence of microglia, glial scar formation was perturbed, and this resulted in an increased presence of infiltrating blood-derived myeloid cells around the site of trauma. Satellite lesions filled with inflammatory cells have been reported before following depletion of reactive astrocytes [26], as well as in mice with conditional deletion of the *Stat3* gene from astrocytes after SCI [27, 55]. Given the importance of astrocytic Stat3 activation in glial scar formation, we speculate that cytokines of the IL-10 families could be additional candidate upstream mediators of these effects (for review, see [56]). Taken together with the finding that

microglia-derived cytokines, such as IGF-1, regulate astrocyte function in pathological conditions [21], our results indicate that activated microglia trigger scar formation after SCI.

The identification of the first week post-SCI as the time window for the beneficial effect of microglia suggests that treatments targeting these cells should be initiated promptly. This therapeutic time window is in line with clinical trials that focus on immunomodulators as potential treatments for SCI [57, 58, 59, 60]. We also provide evidence that microglia proliferate actively during this period, and that boosting their proliferative response during the early acute phase of SCI using a hydrogel-based M-CSF delivery system further enhances functional recovery.

In light of the current data, we conclude that activated, proliferating microglia play a key role in the formation of the scar that develops after SCI, and that these multicellular interactions serve to sequester blood-derived immune cells in the lesion core, thus protecting non-injured neurons and oligodendrocytes from inflammation-mediated tissue damage.

2.6. Materials and methods

2.6.1. Animals

A total of 394 mice were used in this study. C57BL/6N mice were purchased from Charles River Laboratories at 8-10 weeks of age. *Cx3cr1*^{creER}::*Rosa26(R26)-TdT* transgenic mice were generated as before [14], and bred with *LysM*-eGFP knock-in mice created by Dr. T. Graf (Center for Genomic Regulation, Barcelona, Spain) to obtain *Cx3cr1*^{creER}::*R26-TdT*::*LysM*-eGFP. Breeders for *Flt3*-cre mice were obtained from Drs. Thomas Boehm and Conrad C. Bleul, Max Planck Institute, Freiburg, Germany. All mice were bred in-house at the Animal Research Facility of the Centre de recherche du Centre hospitalier universitaire de Québec–Université Laval. Mice had free access to food and water at all time. All animal procedures were approved by the Centre de recherche du CHU de Québec–Université Laval Animal Care Committee and conducted in compliance with relevant ethical regulations and guidelines of the Canadian Council on Animal Care.

2.6.2. Tamoxifen treatment

To induce recombination in *Cx3cr1*^{creER}::*R26-TdT* and *Cx3cr1*^{creER}::*R26-TdT*::*LysM*-eGFP mouse lines, mice were treated orally with 10 mg of tamoxifen (dissolved in 1:10 ethanol/corn oil) twice at 2-day intervals starting at postnatal day (P) 30-32. The animals were then allowed a resting period of 28 days prior to SCI to allow sufficient time for the turnover of MDMs and near disappearance of TdT^+ cells in the blood, spleen and bone marrow.

2.6.3. Spinal cord injury (SCI)

Mice were anesthetized with isoflurane and underwent a laminectomy at vertebral level T9-10, which corresponds to spinal segment T10-11. Briefly, the vertebral column was stabilized and a contusion of 50 kdyn was performed using the Infinite Horizon SCI device (Precision Systems & Instrumentation). Overlying muscular layers were then sutured and cutaneous layers stapled. Post-operatively, animals received manual bladder evacuation twice daily to

prevent urinary tract infections. Depending on the experiment performed, SCI mice were killed by transcardiac perfusion at 1, 4, 7, 14 and 35 days post-contusion.

2.6.4. Microglia depletion

To eliminate microglia, mice were fed PLX5622 (1200 ppm) or PLX73086 (200 ppm) provided by Plexxikon and formulated into AIN-76A chow from Research Diets Inc. For gavage experiments, mice received PLX5622 at 90 mg/kg once a day for 7 consecutive days, starting immediately after SCI. PLX5622 was diluted in 5% DMSO, 0.5 % hydroxypropyl methyl cellulose and 1% polysorbate 80. An equal volume of vehicle was used as control.

2.6.5. Systemic intravascular lectin injections

To visualize blood-perfused microvessels and determine the time course and magnitude of BSCB permeability after SCI, mice were injected in the tail vein with FITC-conjugated LEA lectin (100 µg/100 µl, Sigma-Aldrich Canada Ltd.) 10 minutes prior to transcardial perfusion.

2.6.6. Bromodeoxyuridine (BrdU) injections

To label proliferating cells, mice were intraperitoneally injected once daily with BrdU (50 mg/kg of body weight in 0.9% saline) for 6 consecutive days, starting on day 1 after SCI.

2.6.7. In vivo IGF-1R inhibition

To determine whether IGF-1/IGF-1R signaling is involved in astrocytic scar formation, mice were orally administered with OSI-906 (also known as Linsitinib, Selleckchem), a CNS-penetrant pharmacological inhibitor of IGF-1R [30]. OSI-906 was formulated daily at 4 mg/ml in 25 mM tartaric acid with shaking and sonication for 15 min and then given by gavage once a day for 7 consecutive days at 40 mg/kg, starting immediately after SCI.

2.6.8. Intra-cisterna magna M-CSF injections

In the experiment in which we studied the effects of central M-CSF treatment on the proliferation of spinal cord microglia, mice were injected intra-cisterna magna (i.c.m.) with

recombinant murine M-CSF (PreproTech) at various doses ranging from 25 to 250 ng/µl in PBS. The i.c.m. treatment consisted of a single injection using a pulled-glass micropipette connected to a 10-µl Hamilton syringe.

2.6.9. Tissue processing

For the purpose of histology and immunofluorescence experiments, mice were overdosed with a mixture of ketamine-xylazine and transcardially perfused with PBS followed by 1% PFA, pH 7.4, in PBS. Spinal cords were dissected out and then immersed for two days in a PBS solution containing 20% sucrose for cryoprotection. For each animal, a spinal cord segment of 12 mm centered over the lesion site was cut in 7 series of 14 µm-thick coronal sections using a cryostat. For experiments involving ISH, mice were transcardially perfused with a 0.9% saline solution followed by 4% PFA, pH 9.5, in borax buffer. Spinal cords were post-fixed for an additional 2 days in 4% PFA, and then placed overnight in a 4% PFA-borax/10% sucrose solution. Thirty-µm-thick cryostat coronal sections were collected directly onto slides that have a permanent positive charged surface (Leica Biosystems) and stored at –20 °C until ISH was performed.

2.6.10. Immunofluorescence and confocal imaging

Immunofluorescence labeling was performed according to our previously published method [61]. Primary antibodies used in this study are of the following sources (catalog numbers in parentheses) and were used at the indicated dilutions: rat anti-BrdU (1:750, Abcam, ab6326), mouse anti-CC1 (1:500, Abcam, ab16794), rat anti-CD11b (1:250, AbD Serotec, MCA711), goat anti-CD13 (1:100, R&D Systems, AF2335), rat anti-CD45 (1:500, BD Biosciences, 553076), rat anti-CD68 (1:2500, AbD Serotec, MCA1957), goat anti-CD206 (1:50, R&D Systems, AF2535), rabbit anti-cleaved caspase-3 (Asp175) (1:250, Cell Signaling Technology, 9661), rat anti-GFAP (1:1000, Invitrogen, 13-0300), rabbit anti-GFAP (1:750, Dako, Z0334), mouse anti-HuC/HuD (1:80, Thermo Fisher Scientific, A-21271), goat anti-iba1 (1:1000, Novus Biologicals, NB100-1028), goat anti-IGF-1 (1:10, R&D Systems, AF791), rabbit anti-Ki67 (1:200, Abcam, ab15580), rat anti-Ly6G (1:2000, BD Biosciences, 551459), chicken anti-neurofilament H (NF-H, 1:500, EMD millipore, AB5539), goat anti-

Olig-2 (1:400, R&D Systems, AF-2418), rabbit anti-P2ry12 (1:500, Anaspec, AS-55043A), rabbit anti-PDGFRβ (1:750, Abcam, ab32570), and rabbit anti-Sox9 (1:1000, Millipore, AB5535). For Ki67 immunofluorescence, antigen retrieval was performed using sodium citrate buffer at 95ºC for 5 min. For BrdU, tissue sections were treated with HCl (2.0 N) for 30 min at 37 °C followed by 0.1M sodium borate (pH 8.5) for 10 min at room temperature. Alexa Fluor secondary antibodies from Thermo Fisher Scientific (1:250 dilution) or Vector Laboratories (1:500) were used for multicolor immunofluorescence imaging, whereas 4', 6-diamidino-2-phenylindole, dilactate (DAPI; 1 µg/ml, Thermo Fisher Scientific) was used for nuclear counterstaining. Sections were imaged on a Zeiss LSM 800 confocal microscope system equipped with 405, 488 nm, 561 nm, and 640 nm lasers. Confocal images were acquired using a Zeiss Axiocam 506 Mono camera and mosaics created using the Zen 2.3 software (Blue edition).

2.6.11. In situ hybridization (ISH)

ISH was carried out to detect mRNAs coding for IL-1α, IL-1ß, IL-6, TNF, TGF-β1 and IGF-1, following our previously published method [62]. Primer pairs and enzymes used for riboprobe synthesis are listed in Supplementary Table 1.

2.6.12. Quantitative analyses

For the quantification of microglia (TdT^+ or $CD11b^+$ $P2yr12^+$ or $CD11b^+$ TdT^+), proliferating microglia ($Ki67^+$ TdT^+), neutrophils ($Ly6G^+$), blood-derived myeloid cells ($LysM^+$), astrocytes ($Sox9^+$), neurons (HuC/HuD^+), oligodendrocytes ($Olig\text{-}2^+$), proliferating oligodendrocytes/OPCs ($Ki67^+$ $Olig\text{-}2^+$), proliferating astrocytes ($BrdU^+$ $Sox9^+$ or $Ki67^+$ $GFAP^+$), proliferating perivascular macrophages ($Ki67^+$ $CD206^+$), proliferating pericytes ($Ki67^+$ $CD13^+$), and proliferating leukocytes ($Ki67^+$ $CD45^+$ TdT^-), the total number of immunolabeled cells per cross section was counted at 20× magnification using mosaics created from 6-12 overlapping confocal images or images obtained using a Zeiss Slide Scanner Axio Scan.Z1. A threshold was applied to the resulting images to trace the contour of the coronal section and a grid of 50 µm × 50 µm positioned over the spinal cord either using ImageJ2 (version 1.51d) or BIOQUANT Life Science software (v. 18.5, Bioquant

Image Analysis Corporation). Immunolabeled cells with a DAPI-stained nucleus were then manually counted. Results were presented as the total number of positive cells per cross-section, the average number of positive cells per mm^2 of tissue section, the percentage of cells that expressed specific markers (Ki67), or the mean area under the curve (AUC) of the number of cells per mm^2 in a predetermined distance range (Sox9).

For the quantification of the BSCB permeability, the proportional area of tissue stained with the FITC-LEA lectin within the entire coronal section at the lesion epicenter was measured using images taken at 20× magnification with the Zeiss Slide Scanner Axio Scan.Z1. Thresholding values in Fiji (version 1.52h, National Institutes of Health, NIH) were chosen such that only labeled product resulted in measurable pixels on the digitized images. Contrast between positive signal and background was maximized and held constant between all images. Data were expressed as the proportional area of the tissue section occupied by FITC staining. Proportional area of tissue occupied by GFAP (astrocytes), TdT (microglia) and PDGFRβ (pericytes/fibroblasts) immunolabeling was measured in increments of 40 µm relative to the distance from astrocytic endfeet. The area of tissue occupied by immunostaining in each sampling region was measured using the BIOQUANT Life Science software on video images of tissue sections transmitted by a high-resolution Retiga QICAM fast color 1394 camera (1392 x 1040 pixels, QImaging) installed on a Nikon Eclipse 80i microscope. Thresholding values in BIOQUANT Life Science were chosen such that only immunolabeled product resulted in measurable pixels on the digitized image. Contrast between immunolabeling and background was maximized and held constant between all specimen. Data were presented as the proportional area of the sampling region occupied by immunolabeling.

The calculation of areas of tissue damage after SCI was performed on 1 series of adjacent sections within a predetermined spinal cord segment, including the lesion epicenter and surrounding sections in both directions (i.e., rostral and caudal). Fourteen-µm-thick coronal sections were first immunostained for GFAP as well as LysM, NF-H and/or PDGFRβ. Sections were then counterstained with DAPI and confocal mosaics prepared as described above. For each section, the outline of the core and satellite lesions were separately traced at 20× magnification and areas measured using ImageJ2. Both types of lesions were surrounded

by GFAP-positive astrocytic processes. However, satellite lesions were adjacent to the lesion core and defined as the absence of normal spinal cord architecture and presence of blood-derived myeloid cells ($CD11b^+$) and pericytes ($PDGFR\beta^+$).

The average density of ISH signal was measured within the entire cross-section at the lesion epicenter. Mean grey values (MGV, ranging from 1 to 256 bits) were measured under dark-field illumination on video images of tissue sections transmitted by the Retiga camera, using the BIOQUANT Life Science software. Mean grey values were corrected for the average background signal, which was measured in three boxes of 50H x 50W µm (80H x 80W pixels) placed in regions where no positive signal was observed. ISH data were expressed as an average MGV of the section.

All quantifications were done blind with respect to the identity of the animals.

2.6.13. Biological sample collection and processing for cytometry

Animals were anesthetized with a mixture of 400 mg/kg ketamine and 40 mg/kg xylazine. Blood was collected via cardiac puncture using a 22-gauge syringe and immediately transferred into EDTA-coated microtubes (Sarstedt). Blood samples were then put on slow rotation at room temperature until processing. Prior to collection of the spleen and femurs, animals were transcardially perfused with cold Hanks' balanced salt solution (HBSS) to remove blood from the vasculature.

Spleens were harvested from anesthetized animals and placed in HBSS (without Ca^{2+}/Mg^{2+}). Spleens were homogenized and passed through a 70-µm nylon mesh strainer (BD Biosciences). Erythrocyte lysis was performed using the ACK buffer. The cell suspension was passed on a second 70-µm nylon mesh strainer and the cell count measured.

For the bone marrow, animals were anesthetized and their left femurs isolated and flushed with HBSS (without Ca^{2+}/Mg^{2+}) + 2% FBS using a 25-gauge needle. Erythrocytes were lysed using the ACK buffer (NH_4Cl 150 mM, potassium bicarbonate 10 mM, EDTA 0.01 mM). Cells were manually counted with a hemocytometer (Hausser Scientific).

2.6.14. Flow cytometry

Cells freshly isolated from the blood, spleen and bone marrow of SCI mice were analyzed using flow cytometry. In brief, red blood cells were first lysed and the remaining cells incubated with Mouse Fc Block (i.e., purified anti-mouse CD16/CD32; BD Biosciences) for 15 min at 4^{o}C to prevent nonspecific binding. Multicolor immunolabeling was then performed for 30 min at 4^{o}C using the following fluorescently conjugated primary antibodies: PerCP-conjugated anti-CD45 (1:50 dilution), Alexa 700-conjugated anti-CD11b (1:50), BD HorizonTM V450-conjugated anti-Ly6C (1:83), PE-Cy7-conjugated anti-Ly6G (1:50), APC-conjugated anti-CD3e (1:50) and Alexa 488-conjugated anti-B220 (1:50) (all from BD Biosciences; for a full description of these primary antibodies, please refer to our published work [63]). Cells were analyzed using FlowJo software (v. 9.2; Tree Star Inc.) on a FACS LSRII flow cytometer (BD Biosciences). Cells were identified as follows: $CD45^{hi}$ $CD11b^{+}$ $Ly6C^{+}$ $Ly6G^{+}$ cells were considered as neutrophils, $CD45^{hi}$ $CD11b^{+}$ $Ly6C^{hi}$ $Ly6G^{-}$ cells as $Ly6C^{high}$ monocytes (also known as M1 monocytes or monocyte-derived M1 macrophages), $CD45^{hi}$ $CD11b^{+}$ $Ly6C^{lo}$ $Ly6G^{-}$ cells as $Ly6C^{low}$ monocytes (or M2 monocytes), $CD45^{hi}$ $CD11b^{-}$ $B220^{+}$ $CD3e^{-}$ cells as B cells, and $CD45^{hi}$ $CD11b^{-}$ $B220^{-}$ $CD3e^{+}$ cells as T cells.

2.6.15. Behavioral analysis

Recovery of locomotor function after SCI was quantified in an open field using the Basso Mouse Scale (BMS), according to the method developed by Basso and colleagues [64]. All groups of mice exhibited similar parameters in terms of the impact force and spinal cord tissue displacement prior to BMS testing. All behavioral analyses were done blind with respect to the identity of the animals.

2.6.16. Immunoelectron microscopy

Mice were anesthetized with sodium pentobarbital (80mg/kg, intraperitoneally) and perfused with 3.5% acrolein followed by 4% PFA. Fifty-micrometer-thick coronal sections of the spinal cord were cut in sodium phosphate buffer (50 mM, pH 7.4) using a Leica VT1000S vibratome (Leica Biosystems) and stored at -20^{o}C in cryoprotectant until use. Spinal cord sections were rinsed in PBS (50 mM, pH 7.4) and then quenched with 0.3% hydrogen

peroxide (H_2O_2) for 5 min followed by 0.1% sodium borohydride ($NaBH_4$) for 30 min. Afterwards, sections were rinsed three times in PBS and incubated for 1h in blocking buffer (5% fetal bovine serum, 3% bovine serum albumin, 0.01% Triton X-100) and then overnight with a primary anti-GFAP antibody (1:1000 dilution, Thermo Fisher Scientific). The next day, sections were rinsed three times in PBS and incubated for 2h with secondary antibody conjugated to biotin (1:500, Vector Laboratories) and for 1h with Vectastain® Avidin-Biotin Complex Staining kit (Vector Laboratories). Sections were developed in a Tris buffer solution (TBS; 0.05M, pH 7.4) containing 0.05% diaminobenzidine and 0.015% H_2O_2 and then rinsed with PBS and incubated overnight with a primary anti-RFP antibody (1:1000, Rockland). The next day, sections were rinsed in TBS and incubated overnight with secondary antibody conjugated to gold (1.4 nm Nanogold goat anti-rabbit, 1:50, Nanoprobes). Then the sections were washed three times with TBS and twice with 3% sodium acetate. Using the HQ Silver Enhancement kit (Nanoprobes), the staining was revealed at room temperature for 1 min and rinsed quickly with sodium acetate followed by three 5-min washes with PBS. The sections were post-fixed with 1% osmium tetroxide, dehydrated using sequential alcohol baths followed by propylene oxide. Sections were embedded in Durcupan resin (Sigma-Aldrich Canada Ltd.) between ACLAR sheets at 55°C for 3 days. Ultrathin sections were generated at ~65 nm using a Leica UC7 ultramicrotome. Images were acquired at 1900× or 4800× magnification using a FEI Tecnai Spirit G2 transmission electron microscope (Thermo Fisher Scientific) operating at 80kV and equipped with a Hamamatsu ORCA-HR digital camera (10 MP).

2.6.17. Production of bone marrow chimeras

Recipient mice (*Cx3cr1*^{creER}::*R26-TdT* or C57BL/6 mice) were exposed to a total body γ-irradiation with a single dose of 7.5 Gy using a cesium-173 source (Gammacell 40 Exactor, MDS Nordion) to destroy hematopoietic stem cells. Recipients were then injected in the tail vein with a total of 9×10^6 bone marrow cells freshly isolated from either β-actin-GFP or *Cx3cr1*^{creER}::*R26-TdT* donors, as described before [14]. Briefly, femurs and tibias were harvested from euthanized donor mice and flushed with HBSS (without Ca^{2+}/Mg^{2+}) + 2% FBS using a 25-gauge needle. After the bone marrow transplantation, mice were kept in sterile cages and treated for 2 weeks with antibiotics (2.5 mL of Septra (GlaxoSmithKline)

in 200 mL of drinking water), and let to recover an additional 8 weeks (for a total of 70 days) before being subjected to SCI.

2.6.18. Proliferation and scratch wound assays

Primary cultures of mouse astrocytes were prepared from the cortex of P0-P1 pups, as described in [65], and used from passages 3 to 4. Cells were grown in complete Dulbecco's Modified Eagle Medium (DMEM) either on glass coverslips coated with poly-L-lysine (0.1 mg/ml) in 24-well plates (for the proliferation assay) or directly into 24-well plates (for the scratch wound assay) at a density of 200,000 cells/well. After 1 day in culture for the proliferation assay and two days for scratch wound assay, cells were starved for 18 hours after reaching a confluence level of ~70%. The proliferation assay was initiated by the addition of either recombinant mouse (rm) TGF-β1 (50 ng/ml, dissolved in PBS containing 4 mM HCl; R&D Systems), rmIGF-1 (760 ng/ml, dissolved in PBS; R&D Systems) or their respective vehicle. Six hours before the end of the experiment (48 hours after growth factor addition), a single dose of 10 µM bromodeoxyuridine (BrdU; Sigma-Aldrich Canada Ltd.) was added to each well. The BrdU labeling solution was then removed and cells washed several times with PBS. Cells were next fixed with 4% PFA for 15 min, permeabilized in PBS/0.1% Triton X-100 for 20 min, treated with HCl (2.0 N) for 20 min at 37 °C followed by 0.1M sodium borate (pH 8.5) for 30 min at room temperature, and then immunostained for BrdU. The total number of proliferating cells was counted on images taken at 10× magnification, using the "Co-localization and Analyze Particles" plugin in Fiji. Data were expressed as number of $BrdU^+$ $YO\text{-}PRO\text{-}1^+$ cells per mm^2. For the scratch wound assay, confluent cells were starved for 18 hours and a linear scratch made in the cell monolayer using a 10-µl sterile pipette tip. Complete DMEM was used to wash the cells three times, after which the growth factors identified above were added in 0.2% serum medium. The closure of the wound was monitored using a Zeiss Axio Observer.Z1 Inverted Microscope equipped with an AxioCam MRm digital camera and an incubation chamber by imaging each well every 4 hours over 48 hours. The phase-contrast images were analyzed by measuring the closure percentage of the scratch, relative to the initial width (t = 0), at various times following exposure to the factors under study.

2.6.19. Subdural hydrogel implantation

Hydrogels containing particular M-CSF were prepared as in [31]. Briefly, methlycellulose (310 kDa, Shin-Etsu) and hyaluronan (1200-1900 kDa, FMC) were dissolved in ddH_2O, sterile filtered, lyophilized (Labconco) under sterile conditions, and stored at 4 °C until use. An initial particulate dispersion was produced by mixing M-CSF powder into 0.5% w/v methlycellulose solution. Drug loaded hydrogels were prepared by physical blending hyaluronan (HA, 1.6 x 10^6 g/mol), methylcellulose (3 x 10^5 g/mol), and methylcellulose containing M-CSF in artificial cerebrospinal fluid (aCSF: 148 mM NaCl, 3 mM KCl, 0.8 mM $MgCl_2$, 1.4 mM $CaCl_2$, 1.5 mM Na_2HPO_4, 0.2 mM NaH_2PO_4 in ddH_2O, pH adjusted to 7.4, filter sterilized at 0.2 µm) for a final composition of 1.4% w/v HA, 3% w/v MC, and 0.5 µg/µl M-CSF. Components were dispersed in aCSF using a dual asymmetric centrifugal mixer (Flacktek Inc.) and dissolved overnight at 4 °C. On the day of the hydrogel implantation, a 5-µl Hamilton syringe (32-gauge needle with a pre-bent blunt tip) was filled with either M-CSF-loaded or PBS-loaded hydrogels. A needle was then used to gently puncture the dura at the level of the contusion injury and 2 µl of hydrogel injected subdurally immediately following SCI.

2.6.20. Statistical Analysis

Statistical evaluations were performed with one- or two-way ANOVA or repeated-measures ANOVA, as indicated in figure legends. Post-ANOVA comparisons were made using the Bonferroni correction. All statistical analyses were performed using the GraphPad Prism software (GraphPad Software Inc.). A p value < 0.05 was considered as statistically significant.

2.6.21. Data availability

The data that support the findings of this study are available from the corresponding author upon reasonable request.

2.7. Acknowledgments

This study was supported by grants from the International Foundation for Research in Paraplegia (P161 to S.L.), the Wings for Life Spinal Cord Research Foundation (WFL-CA-006/11 to S.L.), and the Canadian Institute of Health Research (Foundation Grant to M.S.S). M.E.J. is supported by the Research Support Program for College Teachers-Researchers of the Fonds de recherche en santé–Québec. We thank Nadia Fortin for her invaluable technical assistance and TransBIOTech–Centre de recherche et de transfert en biotechnologies for giving us access to their inverted fluorescence microscope. We also thank Plexxikon Inc. for providing us with the PLX5622 and PLX73086 compounds, and Drs. Brian L. West and Andrey Rymar for their guidance on how to use these drugs effectively in rodents. We are grateful to Drs. Bleul and Boehm for providing the *Flt3*-Cre mice.

2.8. Author contributions

V.B.-L. conceived the study, designed and performed most of the experiments, analyzed the data, drafted the figures and wrote the manuscript. F.B. designed and performed in vitro experiments, performed immunofluorescence, microscopy imaging and quantitative analyses, and commented on the manuscript. B.M. performed the in vivo permeability assay and related quantitative analysis and commented on the manuscript. N.Vallières performed in situ hybridization, immunofluorescence and flow cytometry experiments, acquired microscopy images, performed quantitative analyses and edited all figures. M.L. generated bone marrow chimeras, performed in vitro and in vivo immunofluorescence, flow cytometry experiments and quantitative analyses. M.-E.J. performed in vitro assays and related analyses. N.Vernoux performed immunoelectron microscopy. M.-È.T. performed immunoelectron microscopy and commented on the manuscript. T.F. prepared the hydrogels, trained staff for the subdural implantation and commented on the manuscript. M.S.S. provided the hydrogels and commented on the manuscript. S.L. conceived the study, designed the experiments, supervised the overall project and wrote the manuscript.

2.9. References

1. Ginhoux F, *et al.* Fate mapping analysis reveals that adult microglia derive from primitive macrophages. *Science* **330**, 841-845 (2010).
2. Schulz C, *et al.* A lineage of myeloid cells independent of Myb and hematopoietic stem cells. *Science* **336**, 86-90 (2012).
3. Kierdorf K, *et al.* Microglia emerge from erythromyeloid precursors via Pu.1- and Irf8-dependent pathways. *Nat Neurosci* **16**, 273-280 (2013).
4. Askew K, *et al.* Coupled Proliferation and Apoptosis Maintain the Rapid Turnover of Microglia in the Adult Brain. *Cell Rep* **18**, 391-405 (2017).
5. Tay TL, *et al.* A new fate mapping system reveals context-dependent random or clonal expansion of microglia. *Nat Neurosci* **20**, 793-803 (2017).
6. Hoeffel G, *et al.* C-Myb(+) erythro-myeloid progenitor-derived fetal monocytes give rise to adult tissue-resident macrophages. *Immunity* **42**, 665-678 (2015).
7. Sheng J, Ruedl C, Karjalainen K. Most Tissue-Resident Macrophages Except Microglia Are Derived from Fetal Hematopoietic Stem Cells. *Immunity* **43**, 382-393 (2015).
8. David S, Kroner A, Greenhalgh AD, Zarruk JG, Lopez-Vales R. Myeloid cell responses after spinal cord injury. *J Neuroimmunol* **321**, 97-108 (2018).
9. Elmore MR, *et al.* Colony-stimulating factor 1 receptor signaling is necessary for microglia viability, unmasking a microglia progenitor cell in the adult brain. *Neuron* **82**, 380-397 (2014).
10. Szalay G, *et al.* Microglia protect against brain injury and their selective elimination dysregulates neuronal network activity after stroke. *Nat Commun* **7**, 11499 (2016).

11. Asai H, *et al.* Depletion of microglia and inhibition of exosome synthesis halt tau propagation. *Nat Neurosci* **18**, 1584-1593 (2015).
12. Spangenberg EE, *et al.* Eliminating microglia in Alzheimer's mice prevents neuronal loss without modulating amyloid-beta pathology. *Brain* **139**, 1265-1281 (2016).
13. Yona S, *et al.* Fate mapping reveals origins and dynamics of monocytes and tissue macrophages under homeostasis. *Immunity* **38**, 79-91 (2013).
14. Levesque SA, *et al.* Myeloid cell transmigration across the CNS vasculature triggers IL-1beta-driven neuroinflammation during autoimmune encephalomyelitis in mice. *J Exp Med* **213**, 929-949 (2016).
15. Haynes SE, *et al.* The P2Y12 receptor regulates microglial activation by extracellular nucleotides. *Nat Neurosci* **9**, 1512-1519 (2006).
16. Gomez Perdiguero E, *et al.* Tissue-resident macrophages originate from yolk-sac-derived erythro-myeloid progenitors. *Nature* **518**, 547-551 (2015).
17. Rice RA, *et al.* Elimination of Microglia Improves Functional Outcomes Following Extensive Neuronal Loss in the Hippocampus. *J Neurosci* **35**, 9977-9989 (2015).
18. Cavnar MJ, *et al.* KIT oncogene inhibition drives intratumoral macrophage M2 polarization. *J Exp Med* **210**, 2873-2886 (2013).
19. Dagher NN, *et al.* Colony-stimulating factor 1 receptor inhibition prevents microglial plaque association and improves cognition in 3xTg-AD mice. *J Neuroinflammation* **12**, 139 (2015).
20. Huang Y, *et al.* Repopulated microglia are solely derived from the proliferation of residual microglia after acute depletion. *Nat Neurosci* **21**, 530-540 (2018).
21. Liddelow SA, *et al.* Neurotoxic reactive astrocytes are induced by activated microglia. *Nature* **541**, 481-487 (2017).

22. Sofroniew MV. Astrocyte barriers to neurotoxic inflammation. *Nat Rev Neurosci* **16**, 249-263 (2015).
23. Cregg JM, Depaul MA, Filous AR, Lang BT, Tran A, Silver J. Functional regeneration beyond the glial scar. *Exp Neurol* **253C**, 197-207 (2014).
24. Zeisel A, *et al.* Brain structure. Cell types in the mouse cortex and hippocampus revealed by single-cell RNA-seq. *Science* **347**, 1138-1142 (2015).
25. Mrdjen D, *et al.* High-Dimensional Single-Cell Mapping of Central Nervous System Immune Cells Reveals Distinct Myeloid Subsets in Health, Aging, and Disease. *Immunity* **48**, 599 (2018).
26. Faulkner JR, Herrmann JE, Woo MJ, Tansey KE, Doan NB, Sofroniew MV. Reactive astrocytes protect tissue and preserve function after spinal cord injury. *J Neurosci* **24**, 2143-2155 (2004).
27. Okada S, *et al.* Conditional ablation of Stat3 or Socs3 discloses a dual role for reactive astrocytes after spinal cord injury. *Nat Med* **12**, 829-834 (2006).
28. Wanner IB, *et al.* Glial scar borders are formed by newly proliferated, elongated astrocytes that interact to corral inflammatory and fibrotic cells via STAT3-dependent mechanisms after spinal cord injury. *J Neurosci* **33**, 12870-12886 (2013).
29. Sun W, *et al.* SOX9 Is an Astrocyte-Specific Nuclear Marker in the Adult Brain Outside the Neurogenic Regions. *J Neurosci* **37**, 4493-4507 (2017).
30. Quail DF, *et al.* The tumor microenvironment underlies acquired resistance to CSF-1R inhibition in gliomas. *Science* **352**, aad3018 (2016).
31. Caicco MJ, Cooke MJ, Wang Y, Tuladhar A, Morshead CM, Shoichet MS. A hydrogel composite system for sustained epi-cortical delivery of Cyclosporin A to the brain for treatment of stroke. *J Control Release* **166**, 197-202 (2013).

32. Kang CE, Poon PC, Tator CH, Shoichet MS. A new paradigm for local and sustained release of therapeutic molecules to the injured spinal cord for neuroprotection and tissue repair. *Tissue Eng Part A* **15**, 595-604 (2009).
33. Elliott Donaghue I, Tator CH, Shoichet MS. Sustained delivery of bioactive neurotrophin-3 to the injured spinal cord. *Biomater Sci* **3**, 65-72 (2015).
34. Popovich PG, Hickey WF. Bone marrow chimeric rats reveal the unique distribution of resident and recruited macrophages in the contused rat spinal cord. *J Neuropathol Exp Neurol* **60**, 676-685. (2001).
35. Donnelly DJ, *et al.* Deficient CX3CR1 signaling promotes recovery after mouse spinal cord injury by limiting the recruitment and activation of Ly6Clo/iNOS+ macrophages. *J Neurosci* **31**, 9910-9922 (2011).
36. Shechter R, *et al.* Infiltrating blood-derived macrophages are vital cells playing an anti-inflammatory role in recovery from spinal cord injury in mice. *PLoS Med* **6**, e1000113 (2009).
37. Bruttger J, *et al.* Genetic Cell Ablation Reveals Clusters of Local Self-Renewing Microglia in the Mammalian Central Nervous System. *Immunity* **43**, 92-106 (2015).
38. Mildner A, *et al.* Microglia in the adult brain arise from Ly-6ChiCCR2+ monocytes only under defined host conditions. *Nat Neurosci* **10**, 1544-1553 (2007).
39. Ajami B, Bennett JL, Krieger C, Tetzlaff W, Rossi FM. Local self-renewal can sustain CNS microglia maintenance and function throughout adult life. *Nat Neurosci* **10**, 1538-1543 (2007).
40. Parkhurst CN, *et al.* Microglia promote learning-dependent synapse formation through brain-derived neurotrophic factor. *Cell* **155**, 1596-1609 (2013).

41. Bastien D, *et al.* IL-1alpha gene deletion protects oligodendrocytes after spinal cord injury through upregulation of the survival factor Tox3. *J Neurosci* **35**, 10715-10730 (2015).
42. Galvan MD, *et al.* Deficiency in complement C1q improves histological and functional locomotor outcome after spinal cord injury. *J Neurosci* **28**, 13876-13888 (2008).
43. Kroner A, Greenhalgh AD, Zarruk JG, Passos Dos Santos R, Gaestel M, David S. TNF and increased intracellular iron alter macrophage polarization to a detrimental M1 phenotype in the injured spinal cord. *Neuron* **83**, 1098-1116 (2014).
44. Blight AR. Effects of silica on the outcome from experimental spinal cord injury: implication of macrophages in secondary tissue damage. *Neuroscience* **60**, 263-273. (1994).
45. Popovich PG, Guan Z, Wei P, Huitinga I, van Rooijen N, Stokes BT. Depletion of hematogenous macrophages promotes partial hindlimb recovery and neuroanatomical repair after experimental spinal cord injury. *Exp Neurol* **158**, 351-365. (1999).
46. Kigerl KA, Gensel JC, Ankeny DP, Alexander JK, Donnelly DJ, Popovich PG. Identification of two distinct macrophage subsets with divergent effects causing either neurotoxicity or regeneration in the injured mouse spinal cord. *J Neurosci* **29**, 13435-13444 (2009).
47. Lalancette-Hebert M, Gowing G, Simard A, Weng YC, Kriz J. Selective ablation of proliferating microglial cells exacerbates ischemic injury in the brain. *J Neurosci* **27**, 2596-2605 (2007).
48. Tranque PA, Calle R, Naftolin F, Robbins R. Involvement of protein kinase-C in the mitogenic effect of insulin-like growth factor-I on rat astrocytes. *Endocrinology* **131**, 1948-1954 (1992).

49. Faber-Elman A, Solomon A, Abraham JA, Marikovsky M, Schwartz M. Involvement of wound-associated factors in rat brain astrocyte migratory response to axonal injury: in vitro simulation. *J Clin Invest* **97**, 162-171. (1996).
50. Lindholm D, Castren E, Kiefer R, Zafra F, Thoenen H. Transforming growth factor-beta 1 in the rat brain: increase after injury and inhibition of astrocyte proliferation. *J Cell Biol* **117**, 395-400 (1992).
51. Hunter KE, Sporn MB, Davies AM. Transforming growth factor-betas inhibit mitogen-stimulated proliferation of astrocytes. *Glia* **7**, 203-211 (1993).
52. Logan A, Berry M, Gonzalez AM, Frautschy SA, Sporn MB, Baird A. Effects of transforming growth factor beta 1 on scar production in the injured central nervous system of the rat. *Eur J Neurosci* **6**, 355-363 (1994).
53. Kohta M, Kohmura E, Yamashita T. Inhibition of TGF-beta1 promotes functional recovery after spinal cord injury. *Neurosci Res* **65**, 393-401 (2009).
54. Hellal F, *et al.* Microtubule stabilization reduces scarring and causes axon regeneration after spinal cord injury. *Science* **331**, 928-931 (2011).
55. Herrmann JE, *et al.* STAT3 is a critical regulator of astrogliosis and scar formation after spinal cord injury. *J Neurosci* **28**, 7231-7243 (2008).
56. Bastien D, Lacroix S. Cytokine pathways regulating glial and leukocyte function after spinal cord and peripheral nerve injury. *Exp Neurol* **258**, 62-77 (2014).
57. Bracken MB, *et al.* Methylprednisolone or naloxone treatment after acute spinal cord injury: 1-year follow-up data. Results of the second National Acute Spinal Cord Injury Study. *J Neurosurg* **76**, 23-31. (1992).

58. Bracken MB, *et al.* A randomized, controlled trial of methylprednisolone or naloxone in the treatment of acute spinal-cord injury. Results of the Second National Acute Spinal Cord Injury Study [see comments]. *N Engl J Med* **322**, 1405-1411 (1990).
59. Bracken MB, *et al.* Administration of methylprednisolone for 24 or 48 hours or tirilazad mesylate for 48 hours in the treatment of acute spinal cord injury. Results of the Third National Acute Spinal Cord Injury Randomized Controlled Trial. National Acute Spinal Cord Injury Study. *Jama* **277**, 1597-1604 (1997).
60. Casha S, Zygun D, McGowan MD, Bains I, Yong VW, Hurlbert RJ. Results of a phase II placebo-controlled randomized trial of minocycline in acute spinal cord injury. *Brain* **135**, 1224-1236 (2012).
61. Pineau I, Lacroix S. Proinflammatory cytokine synthesis in the injured mouse spinal cord: Multiphasic expression pattern and identification of the cell types involved. *J Comp Neurol* **500**, 267-285 (2007).
62. Boivin A, *et al.* Toll-like receptor signaling is critical for Wallerian degeneration and functional recovery after peripheral nerve injury. *J Neurosci* **27**, 12565-12576 (2007).
63. Pare A, *et al.* IL-1beta enables CNS access to CCR2(hi) monocytes and the generation of pathogenic cells through GM-CSF released by CNS endothelial cells. *Proc Natl Acad Sci U S A* **115**, E1194-E1203 (2018).
64. Basso DM, Fisher LC, Anderson AJ, Jakeman LB, McTigue DM, Popovich PG. Basso Mouse Scale for locomotion detects differences in recovery after spinal cord injury in five common mouse strains. *J Neurotrauma* **23**, 635-659 (2006).
65. Schildge S, Bohrer C, Beck K, Schachtrup C. Isolation and culture of mouse cortical astrocytes. Journal of visualized experiments : JoVE, (2013).

2.10. Figures

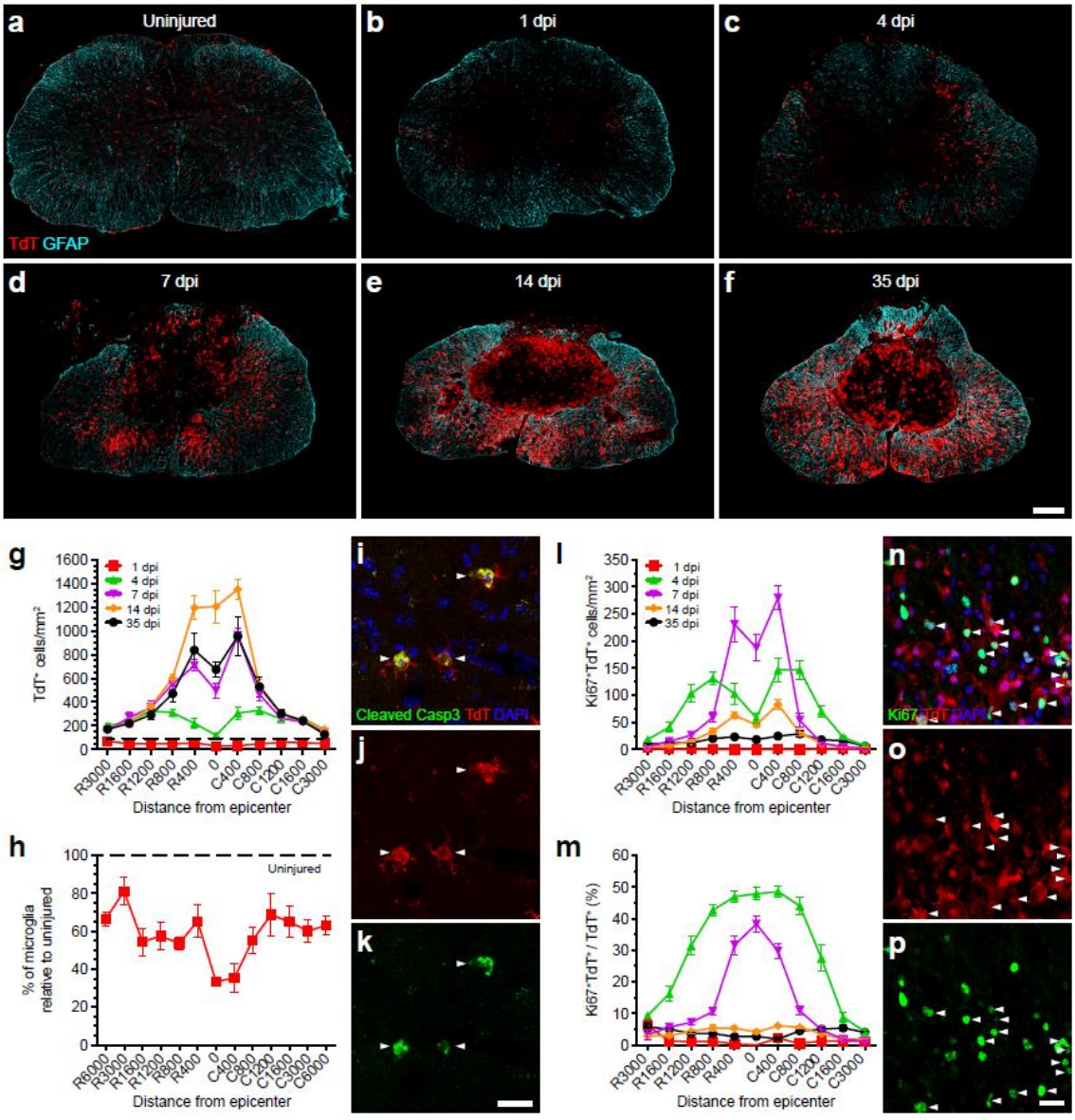

Figure 2.1. Microglia proliferate extensively and accumulate at the lesion border after SCI. (**a-f**) Confocal immunofluorescence microscopy of representative spinal cord sections showing the spatio-temporal distribution of microglia (TdT, red) and astrocytes (GFAP, cyan) in an uninjured *Cx3cr1*^{creER}::*R26-TdT* transgenic mouse (**a**), as well as at the lesion epicenter at 1 (**b**), 4 (**c**), 7 (**d**), 14 (**e**), and 35 (**f**) days post-injury (dpi). (**g**) Quantification of the total number of TdT^{+} microglia per mm^{2} of tissue in spinal cord sections taken both rostral (R) and caudal (C) to the lesion epicenter at 1 (red line), 4 (green), 7 (violet), 14 (orange) and 35 (black) dpi (n=6-8 mice per group/time point).

Data from uninjured mice are shown with the dotted black line. (**h**) Percentage of surviving TdT$^+$ microglia at day 1 post-SCI relative to the uninjured group. (**i-k**) Confocal immunofluorescence images showing expression of the apoptotic marker cleaved caspase-3 (Casp3, green) in TdT$^+$ microglia (red) at 1 dpi. Nuclear staining (DAPI) is shown in blue, while white arrowheads indicate co-localization of cleaved Casp3, TdT and DAPI. (**l**) Quantification of the number of actively proliferating microglia (TdT$^+$ Ki67$^+$ cells) at 1, 4, 7, 14 and 35 dpi (n=7-8 mice per group). (**m**) Percentage of TdT$^+$ microglia undergoing proliferation after SCI (n=7-8 per group). (**n-p**) Confocal immunofluorescence microscopy showing that TdT$^+$ microglia (red) are actively proliferating at 7 dpi, as demonstrated by their expression of the proliferation marker Ki67 (green). DAPI is shown in blue, while white arrowheads indicate co-localization of TdT, Ki67 and DAPI staining. Data are expressed as mean ± SEM. Scale bars: (**a-f**, in **f**) 200 µm; (**i-k**, in **k**) 20 µm; (**n-p**, in **p**) 20 µm.

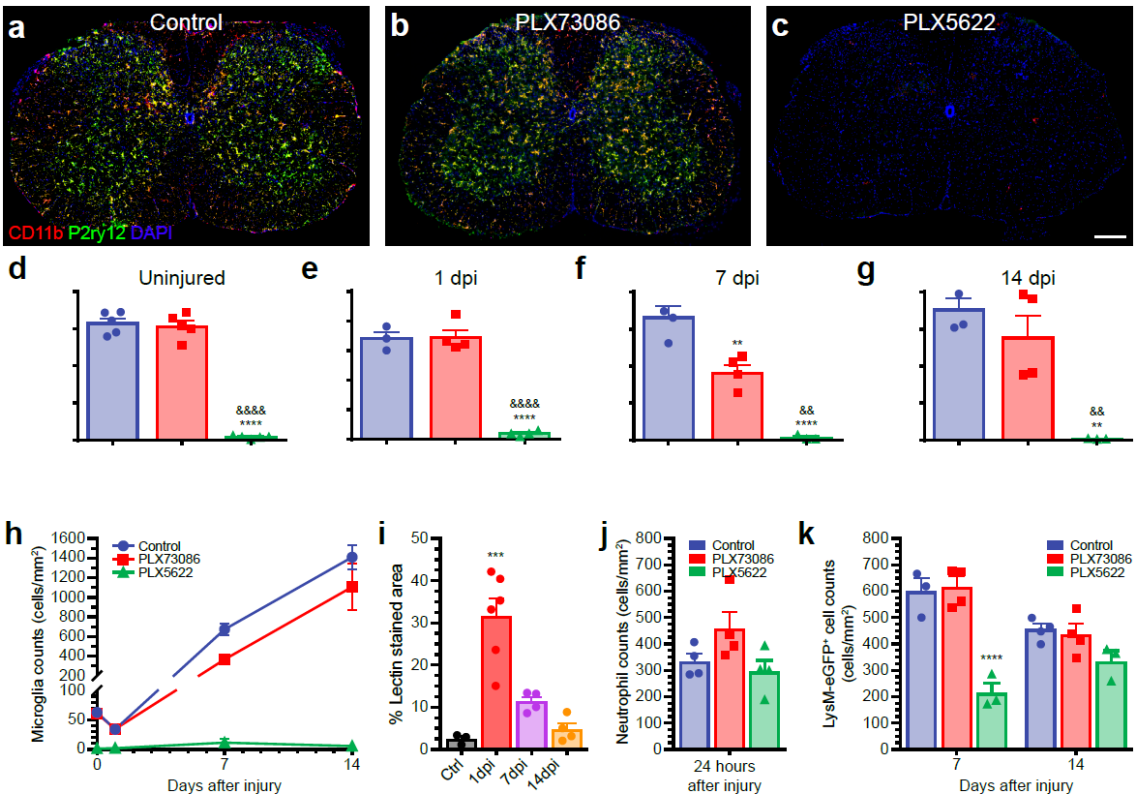

Figure 2.2. The CSF1R inhibitor PLX5622, but not PLX73086, crosses the blood-spinal cord barrier to deplete virtually all microglia.

(**a-c**) Representative confocal images of CD11b and P2ry12 immunostainings showing the almost complete elimination of microglia in the spinal cord of naïve (uninjured) C57BL/6 mice after treatment with the CSF1R inhibitor PLX5622 compared to those fed PLX73086 or the control diet. Mice were killed after 21 days of treatment. (**d-h**) Quantification of microglia in the spinal cord of

uninjured C57BL/6 mice treated with PLX5622, PLX73086 or the control diet (**d**), as well as at the lesion epicenter in *Cx3cr1*^{creER}::*R26-TdT* mice killed at 1 (**e**), 7 (**f**), and 14 (**g**) days post-injury (dpi) (n=4-5 mice per group/time point). (**i**) Quantification of the proportional area of spinal cord tissue permeable to FITC-conjugated lectin injected intravenously prior to tissue fixation. (**j**) Quantification of $Ly6G^+$ neutrophils at the lesion epicenter at day 1 post-SCI in mice treated with either PLX5622, PLX73086 or the control chow (n=4-5 per group). (**k**) Quantification of the number of granulo-myelomonocytic cells at the lesion epicenter at 7 and 14 dpi in *Cx3cr1*^{creER}::*R26-TdT*::*LysM*-eGFP mice treated with either PLX5622, PLX73086 or the control diet (n=4-5 mice per group/time point). For all injured mice, treatment was initiated 3 weeks before SCI and continued until sacrifice. Data are expressed as mean ± SEM. ** $p < 0.01$, *** $p < 0.001$, **** $p < 0.0001$, PLX5622 or 1 dpi compared to the control group; and $^{\&\&}$ $p < 0.01$, $^{\&\&\&\&}$ $p < 0.0001$, PLX5622 compared with the PLX73086 group. Statistical analysis was performed using a one-way (**d-g, i-j**) or two-way (**k**) ANOVA followed by a Bonferroni's post hoc test. Scale bar: (**a-c**, in **c**) 200 µm.

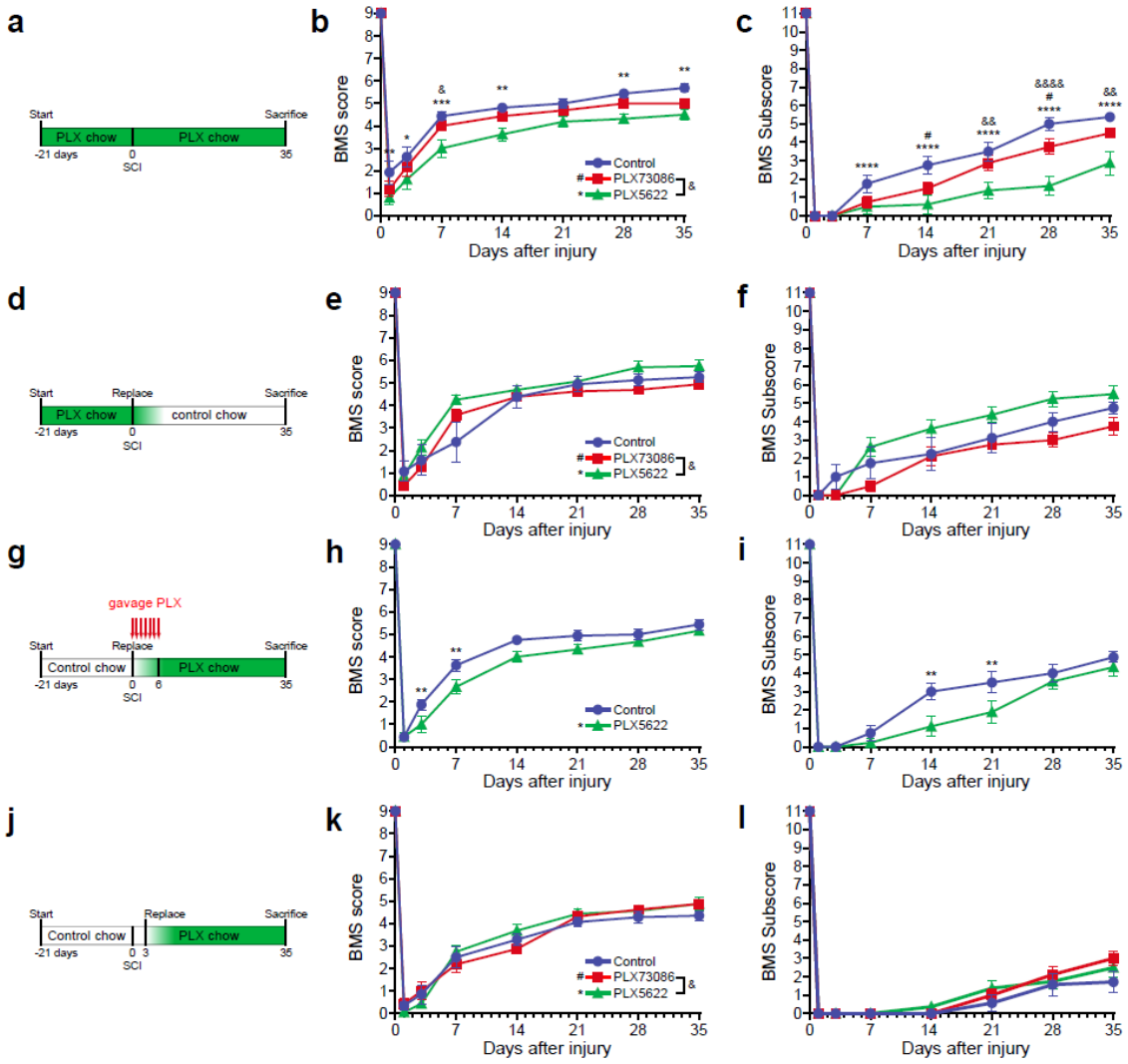

Figure 2.3. Microglia play a key role in recovery of locomotor function during the first week post-SCI.

(**a**, **d**, **g**, **j**) Schematics of experimental design showing the timeline of microglia depletion, spinal cord contusion, behavioral testing using the basso mouse scale (BMS), and sacrifice. CSF1R inhibitors and vehicle were administered in the diet or by oral gavage, as indicated. (**b-c**, **e-f**, **h-i**, **k-l**) Locomotor function was assessed using the BMS score (**b**, **e**, **h**, **k**) and BMS subscore (**c**, **f**, **i**, **l**) over a 35-day period after SCI (n=8 mice per group). Data are expressed as mean ± SEM. * $p < 0.05$, ** $p < 0.01$, *** $p < 0.001$, **** $p < 0.0001$, PLX5622 versus the control group; $^{\#}$ $p < 0.05$, PLX73086 versus the control group; and $^{\&}$ $p < 0.05$, $^{\&\&}$ $p < 0.01$, $^{\&\&\&\&}$ $p < 0.0001$, PLX5622 compared to PLX73086. Statistical analysis was performed using a two-way repeated-measures ANOVA followed by a Bonferroni's post hoc test.

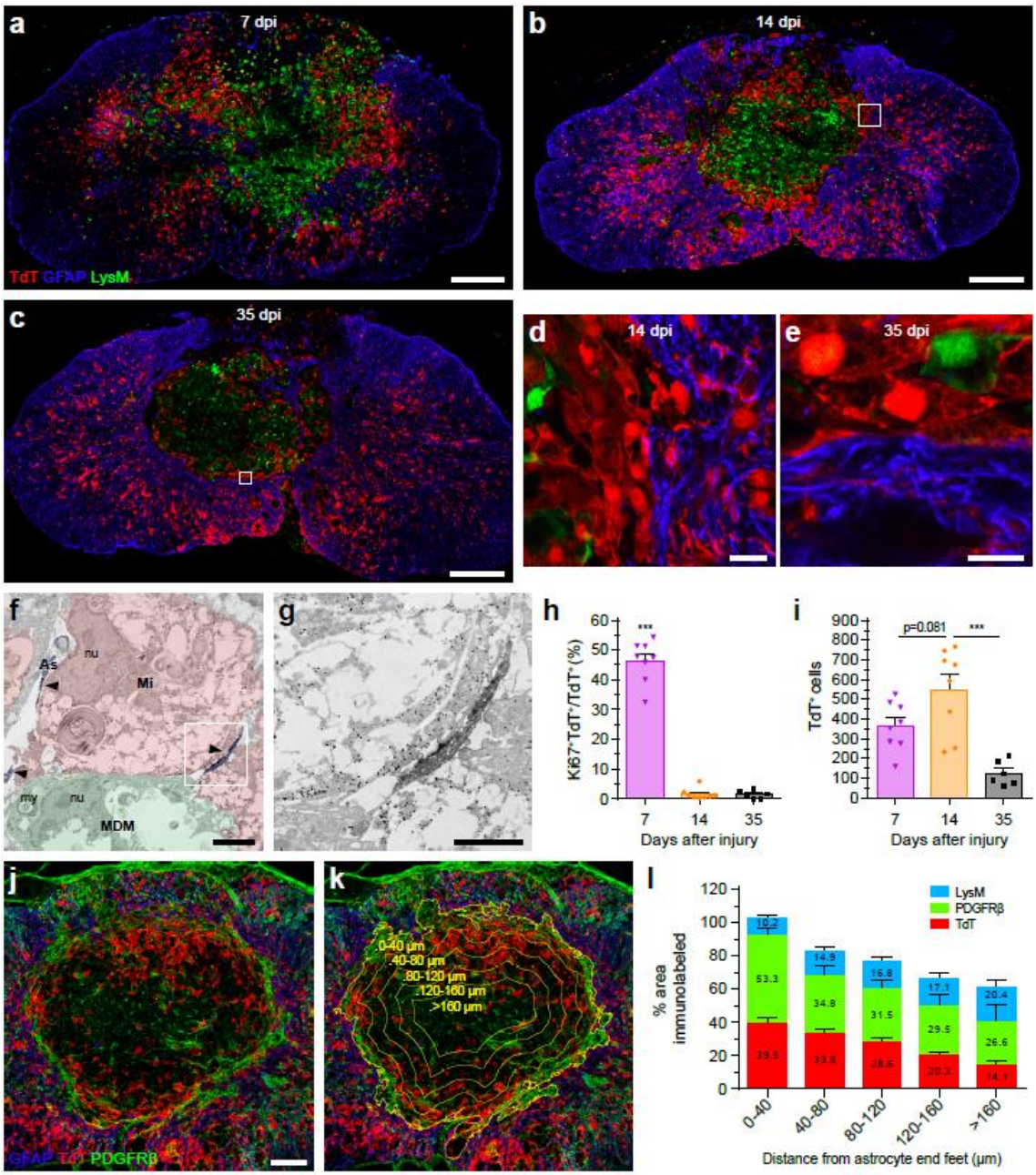

Figure 2.4. A microglial scar forms at the interface between the astrocytic and fibrotic scars. (**a-e**) Confocal immunofluorescence microscopy of representative spinal cord sections taken at the lesion epicenter at 7 (**a**), 14 (**b**, **d**), and 35 (**c**, **e**) days post-injury (dpi) showing formation of the microglial scar, characterized by the accumulation of TdT^+ microglia (red) at the lesion borders, over time. The microglial scar is shown in relation to the infiltration of blood-derived myeloid cells (LysM-$eGFP^+$, green) and formation of the astroglial scar (GFAP-immunoreactive astrocytes, blue). Panels (**d**) and (**e**) are insets of panels (**b**) and (**c**), respectively, showing close-ups of the microglial scar in *Cx3cr1*^{creER}::*R26-TdT*::*LysM*-eGFP mice at 14 and 35 dpi. (**f-g**) Immunoelectron microscopy images

showing a gold-labeled microglia (Mi) (dense black dots, highlighted in red) located at the lesion border making direct contacts with immunolabeled astrocytic endfeet (As) (diffuse black, highlighted in blue and pointed by arrowheads) and a monocyte-derived macrophage (MDM, highlighted in green). The intimate relationship between the microglia and distal astrocytic processes is shown at high magnification in the inset (**g**). nu = nucleus, my = myelin debris. (**h**) Percentage of microglia (TdT^+) that are actively proliferating ($Ki67^+$ TdT^+) at the lesion epicenter at 7, 14 and 35 dpi. (**i**) Counts of microglia (TdT^+) at the lesion epicenter at 7, 14 and 35 dpi. (**j**-**k**) Confocal images showing the presence of TdT^+ microglia (red), $PDGFR\beta^+$ pericytes/fibroblasts (green) and $GFAP^+$ astrocytes (blue) at the lesion epicenter at 14 dpi. The distance from astrocyte endfeet is depicted by the yellow lines and indicated (**k**). (**l**) Percentage area occupied by microglia (TdT^+, red bars in the histogram), pericytes/fibroblasts (PDGFRβ, green) and blood-derived myeloid cells (LysM-$eGFP^+$, blue) as a function of distance from astrocyte endfeet (n= 4-9 mice). Data are expressed as mean ± SEM. * $p < 0.05$, ** $p < 0.01$, *** $p < 0.001$, compared to the other time points. Statistical analysis was performed using a one-way ANOVA followed by a Bonferroni's post hoc test. Scale bars: (**a-c**) 200 µm; (**d-e**) 20 µm; (**f**) 5 µm; (**g**) 2 µm; (**j**-**k**) 100 µm.

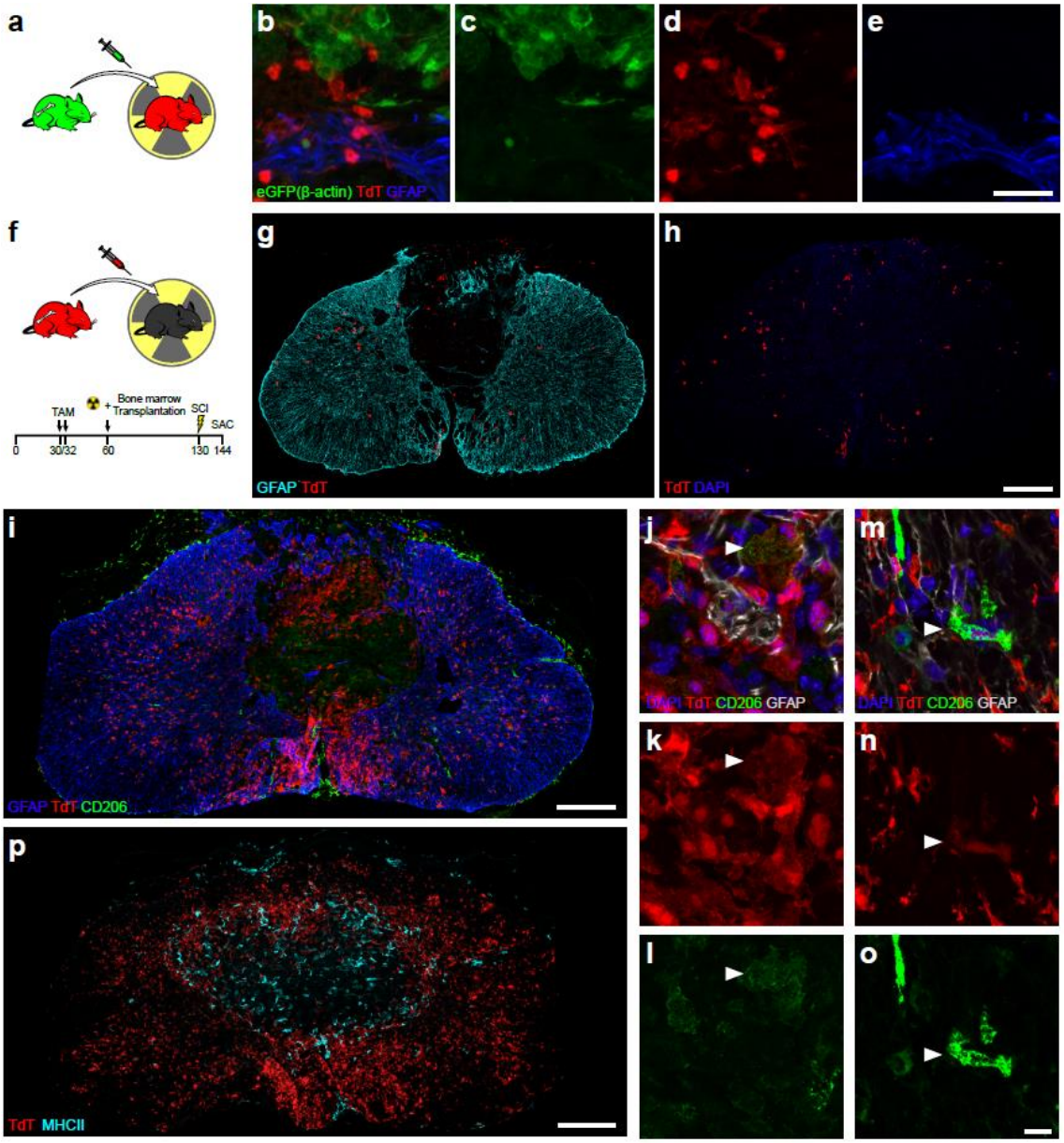

Figure 2.5. The microglial scar is mainly composed of microglia, with few scattered blood-derived myeloid cells and CNS border-associated macrophages.

(**a**) Schematic diagram showing the protocol used to generate radiation bone marrow chimeras in which microglia express TdT and bone marrow-derived cells the GFP reporter. (**b-e**) Representative confocal images showing the microglial scar formed of TdT^{+} microglia (red), some of which are in close apposition with GFAP-immunoreactive astrocyte endfeet (blue) on one side and bone marrow-derived cells ($eGFP^{+}$, green) on the other side at 14 days post-SCI. (**f**) Schematic of experimental procedure and timeline to generate bone marrow chimeras in which *Cx3cr1*^{creER}::*R26-TdT* mice were used as bone marrow donors for irradiated recipient C57BL/6 mice. (**g-h**) Representative confocal

images showing the virtual absence of bone marrow-derived TdT^{+} cells (red) medial to the astrocytic scar (as defined by GFAP^{+} astrocyte endfeet in blue), where the microglial scar normally develops, at 14 days post-SCI in *Cx3cr1*^{creER}::*R26-TdT* → WT chimeric mice. (**i-o**) Confocal images showing the absence (or very weak expression) of CD206 (green) in microglia (TdT^{+}, red) forming the microglial scar at the lesion borders at 14 days post-SCI. In contrast, border-associated macrophages express high levels of the CD206 protein. (**p**) Representative confocal image showing the absence of colocalization between TdT (red) and MHCII (cyan) in the injured spinal cord of a *Cx3cr1*^{creER}::*R26-TdT* mouse at 14 days. Scale bars: (**b-e**, in **e**) 20 µm, (**g-h**, in **h**) 200 µm, (**i**, **p**) 200 µm, (**j-o**, in **o**) 10 µm.

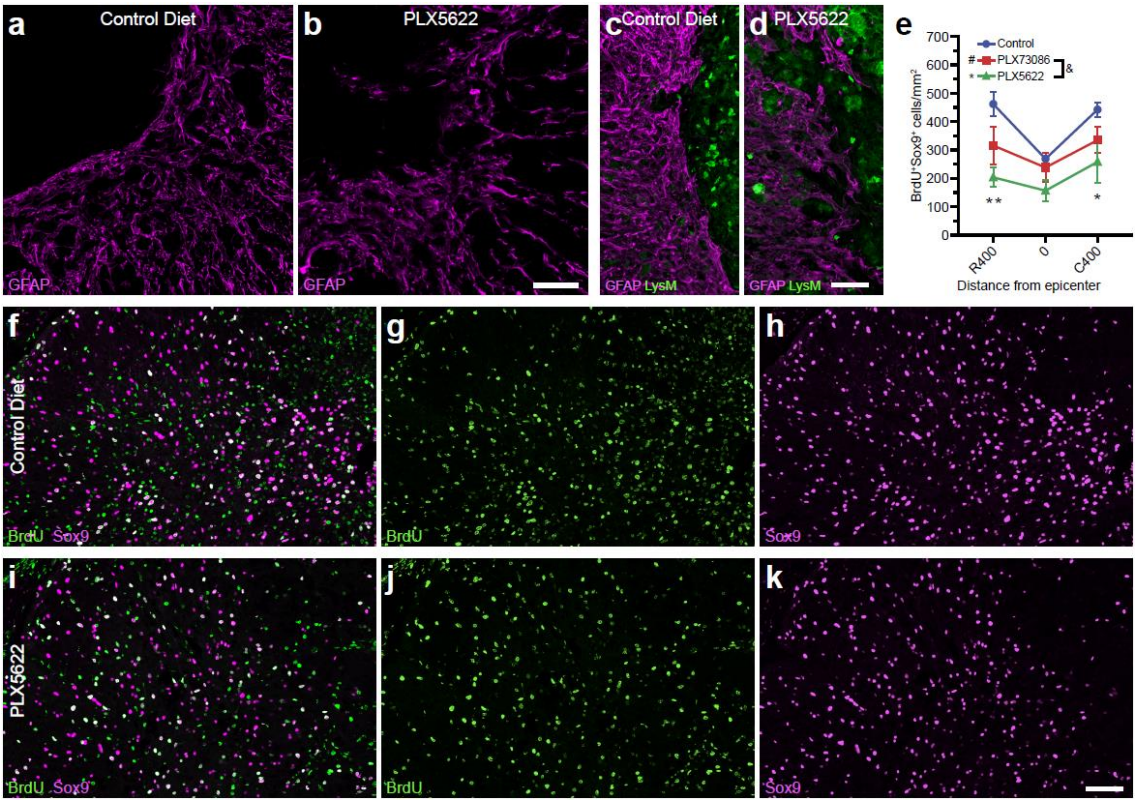

Figure 2.6. The elimination of microglia results in a reduced proliferation of astrocytes and disorganized astrocytic scar at the lesion border.

(**a-d**) Confocal immunofluorescence microscopy of astrocytes (GFAP, purple) in spinal cord sections taken at the lesion epicenter in *Cx3cr1*^{creER}::*R26-TdT*::*LysM*-eGFP mice at 14 days post-injury (dpi). In mice fed with the control diet (**a**, **c**), astrocytes adjacent to the site of SCI exhibit elongated processes oriented parallel to the lesion border, thus forming a compact scar. This astrocytic response was compromised in mice depleted of microglia *using* PLX5622 (**b, d**), and associated with clusters of blood-derived myeloid cells (*LysM-eGFP*$^{+}$, *green cells in* ***d***) spreading outside of

the lesion core. (**e**) Total counts of $Sox9^+$ $BrdU^+$ cells at the epicenter and both rostral (R) and caudal (C) to the lesion at 7 dpi in mice fed the control diet (blue), PLX73086 (red) or PLX5622 (green) (n=4 mice per group). (**f-k**) Representative confocal images showing the proliferation of astrocytes ($Sox9^+$, purple cells), as demonstrated by their incorporation of BrdU (green cells), in mice treated with PLX5622 (**f-h**) or the control diet (**i-k**) and killed at 7 dpi. Data are expressed as mean ± SEM. * $p < 0.05$, ** $p < 0.01$, PLX5622 versus the control group. Statistical analysis was performed using a two-way ANOVA followed by a Bonferroni's post hoc test. Scale bars: (**a-b**, in **b**) 50 µm, (**c-d**, in **d**) 50 µm, (**f-k**, in **k**) 50 µm.

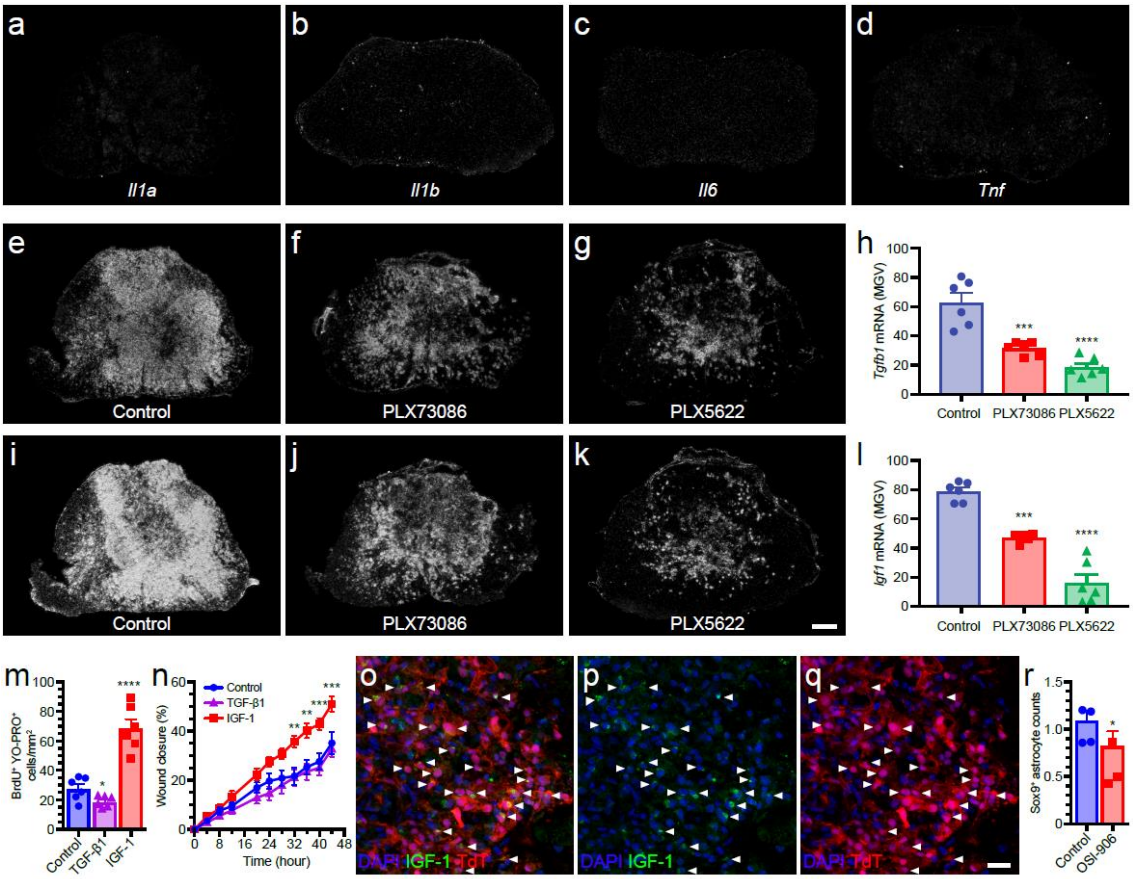

Figure 2.7. Microglia-derived IGF-1 is a potent mitogen for astrocytes and inducer of astrocytic migration towards an injured area.

(**a-d**) *In situ* hybridization (ISH) signal for the proinflammatory cytokines IL-1α, IL-1β, IL-6 and TNF in the injured mouse spinal cord (lesion epicenter) at 7 days post-SCI (dpi). (**e-g**, **i-k**) Representative darkfield photomicrographs showing expression of *Tgfb1* and *Igf1* mRNAs at the lesion epicenter at 7 dpi in C57BL/6 mice fed the control diet, PLX73086 or PLX5622. (**h**, **l**) Quantification of ISH signal (in mean grey values, MGV) for TGF-β1 (**h**) and IGF-1 (**l**) at the lesion

epicenter in mice treated with vehicle (Control, blue bars), PLX73086 (red bars) or PLX5622 (green bars) (n=6 per group). (**m**) Quantification of the number of $BrdU^+$ YO-PRO-1^+ nuclear profiles following treatment of primary astrocyte cultures with either TGF-β1, IGF-1 or control solution (n=6 per group). (**n**) Quantification of the wound closure response in the different groups (n=6 per group). (**o-q**) Representative immunofluorescence images showing the expression of IGF-1 (green signal, **o-p**) by TdT^+ microglia (red cells, **o** and **q**) accumulating at the lesion border at 7 dpi. White arrowheads indicate co-localization of IGF-1, TdT, and DAPI (blue). (**r**) Quantification of $Sox9^+$ astrocytes, expressed as the AUC of the total number of $Sox9^+$ cells (x 10^3 per mm^3) from 800 µm rostral to 800 µm caudal to the epicenter, in the injured spinal cord of C57BL/6 mice treated with the IGF-1R antagonist OSI-906 (red bar) or the vehicle solution (Control, blue bar) (n=4 per group). Data are expressed as mean ± SEM. * $p < 0.05$, ** $p < 0.01$, *** $p < 0.001$, **** $p < 0.0001$, compared to the control group. Statistical analysis was performed using either a one-way (**h**, **l-m**) or two-way (**n**) ANOVA followed by a Bonferroni's post hoc test, or a Student's t-test (**r**). Scale bars: (**a-g** & **i-k**, in **k**) 200 µm, (**o-q**, in **q**) 20 µm.

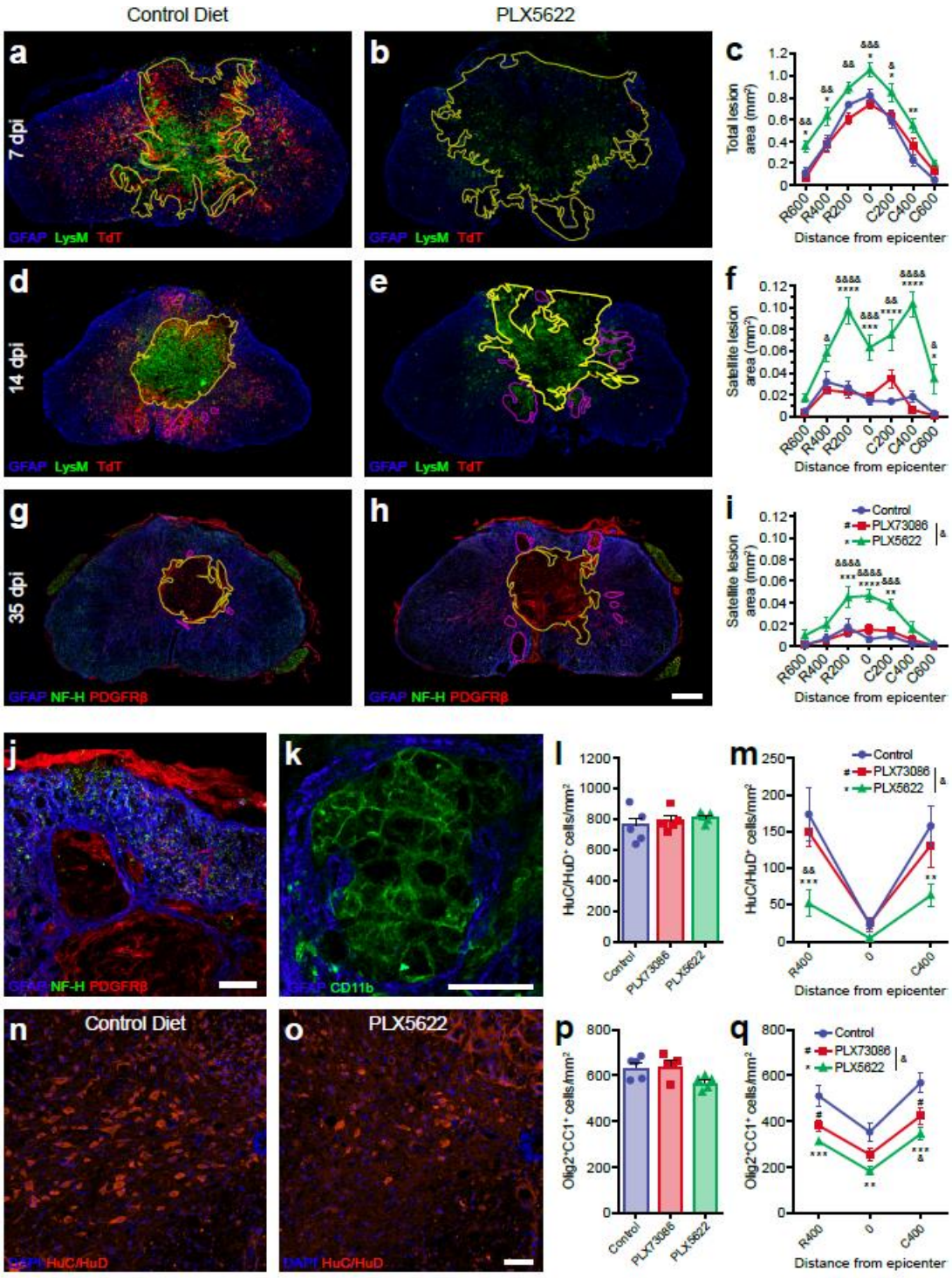

Figure 2.8. Microglial depletion results in an increased loss of neurons and oligodendrocytes leading to greater tissue damage after SCI.

(**a-b**, **d-e**, **g-h**, **j-k**) Confocal immunofluorescence of astrocytes (GFAP$^+$, blue), microglia (TdT$^+$, red cells in **a-b**, **d-e**), blood-derived myeloid cells (LysM-eGFP$^+$ or CD11b$^+$, green cells in **a-b**, **d-e**, **k**), neurons/axons (NF-H$^+$, green in **g-h**, **j**) and pericytes/fibroblasts (PDGFRβ$^+$, red cells in **g-h**, **j**) at the

lesion epicenter at 7 (**a-b**), 14 (**d-e**) and 35 (**g-h**) dpi. Yellow and purple lines respectively delineate the contours of the primary (core) and satellite lesions, which were surrounded by astrocytic endfeet and characterized by the absence *of* neuronal elements and presence of cells *of* non-CNS origin *(*blood-derived myeloid cells, pericytes and fibroblasts). Satellite lesions are shown in a microglia-depleted mouse at 35 dpi (**j-k**). (**c**) Quantification of the total lesion area at 7 dpi in mice fed the control diet (blue), PLX73086 (red) or PLX5622 (green) (n=5-6 mice/group). (**f**, **i**) Quantification of the total area occupied by satellite lesions at 14 (**f**) and 35 (**i**) dpi (n=5-7/group). (**l-m**) Quantification of the number of neurons (HuC/HuD^{+}) in the uninjured spinal cord (**l**), as well as rostral (R) and caudal (C) to the epicenter (**m**), in mice treated with PLX5622, PLX73086 or control at 35 dpi (n=5-8/group). (**n-o**) Representative confocal images taken at the lesion epicenter at 35 dpi immunostained for HuC/HuD (red). DAPI is shown in blue. (**p**, **q**) Quantification of the number of oligodendrocytes (Olig2^{+} CC1^{+}) in the uninjured (**p**) and injured (**q**) spinal cord of mice treated with PLX5622, PLX73086 or control at 35 dpi (n=5-8/group). Data are expressed as mean ± SEM. * $p < 0.05$, ** $p < 0.01$, *** $p < 0.001$, **** $p < 0.0001$, PLX5622 versus control; $^{\#}$ $p < 0.05$, PLX73086 versus control; and $^{\&}$ $p < 0.05$, $^{\&\&}$ $p < 0.01$, $^{\&\&\&}$ $p < 0.001$, $^{\&\&\&\&}$ $p < 0.0001$, PLX5622 compared to PLX73086. Statistical analysis was performed using a two-way ANOVA followed by a Bonferroni's post hoc test. Scale bars: (**a-b, d-e, g-h** in **h**) 200 µm, (**j-k**) 50 µm, (**n-o**, in **o**) 50 µm.

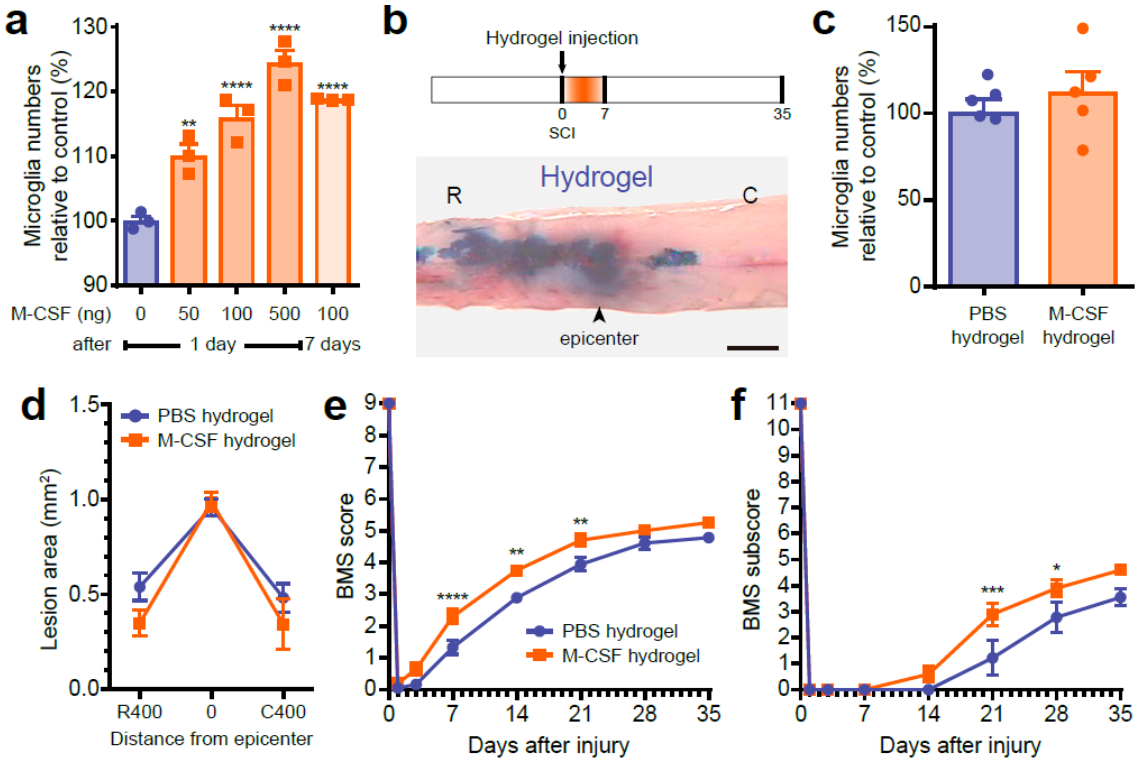

Figure 2.9. Hydrogel delivery of M-CSF at the site of SCI boosted microglial proliferation and enhanced functional recovery.

(**a**) Quantification of the number of microglia ($CD11b^+$ $P2ry12^+$) in the thoracic spinal cord following intra-cisterna magna injection of recombinant murine M-CSF at various doses (n=3 mice per group). (**b**) Schematic of the experimental design showing the timeline of spinal cord contusion (SCI), hydrogel injection, behavioral testing using the basso mouse scale (BMS), and sacrifice. Below the schematic is a picture showing how much a hydrogel loaded with Evans blue spreads following subdural injection at the site of SCI. (**c**) Quantification of the number of microglia (TdT^+) at the lesion epicenter at 7 days post-injury (dpi) in *Cx3cr1*^{creER}::*R26-TdT* mice treated with either M-CSF-based (orange bar) or PBS-based (blue) hydrogels (n=5 mice per group). (**d**) Quantitative analysis of the total lesion area at the lesion epicenter and both rostral (R) and caudal (C) at 7 dpi in mice treated with M-CSF (orange) or PBS (blue) in hydrogels (n= 9-15 mice per group). (**e-f**) Assessment of locomotor recovery using the BMS (**e**) and BMS subscore (**f**) showed that hydrogel delivery of M-CSF increased functional recovery after SCI (n=9-10 mice per group). Data are expressed as mean ± SEM. * $p < 0.05$, ** $p < 0.01$, *** $p < 0.001$, **** $p < 0.0001$, M-CSF-loaded hydrogel compared with PBS-loaded hydrogel. Statistical analysis was performed using a one-way (**a**, **c**), two-way (**d**) or two-way repeated-measures (**e-f**) ANOVA followed by a Bonferroni's post hoc test.

2.11. Supplemental Figures

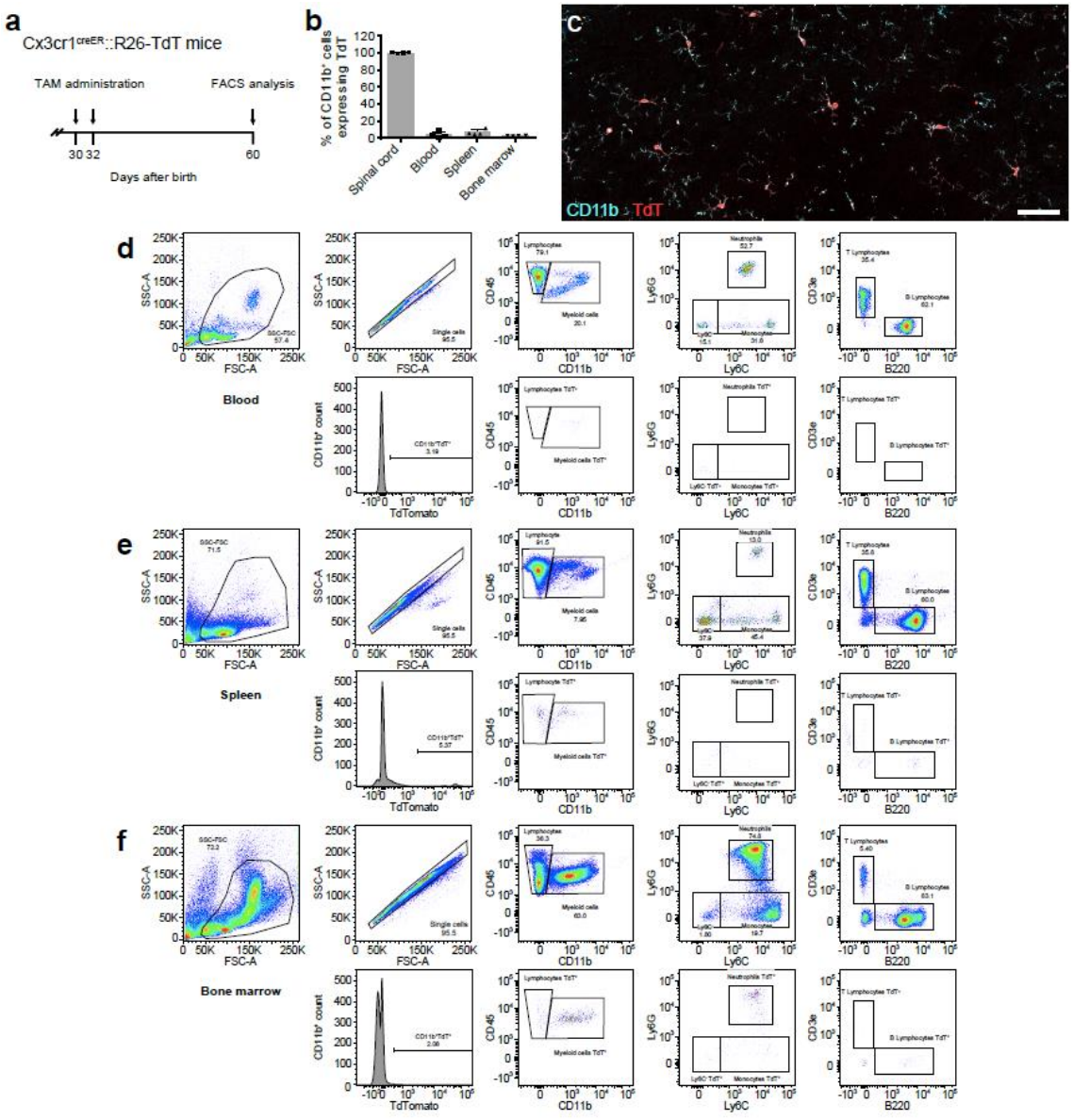

Supplementary Figure 2.1. Adequate regimen of tamoxifen treatment in inducible Cx3cr1creER::R26-TdT mice allows to specifically target microglia, while leaving monocytes and tissue-resident macrophages almost unaffected

(**a**) Schematic diagram of experimental design showing the timeline of tamoxifen (TAM) treatment and FACS analysis relative to the age of *Cx3cr1*creER::*R26*-TdT mice. Transgenic mice were administered tamoxifen at postnatal day (P) 30 and 32 and then allowed to recover for 28 days prior to SCI to allow sufficient time for the turnover of MDMs and near disappearance of TdT+ cells in the blood, spleen and bone marrow. (**b**) Percentage of myeloid cells expressing the TdT fluorescent

reporter 28 days following the last TAM injection. Note that virtually all CNS-resident myeloid cells are TdT+, while only few (if any) myeloid cells in the blood, spleen and bone marrow express TdT (n=4 mice). (**c**) Confocal image showing the colocalization of CD11b (green) and TdT (red) proteins in the spinal cord of a *Cx3cr1*creER::*R26*-TdT mouse at 28 days post-tamoxifen treatment. (**d-f**) Gating strategy used to identify immune cell subsets in the blood (**d**), spleen (**e**) and bone marrow (**f**) of *Cx3cr1*creER::*R26*-TdT mice. For each panel from (**d**) to (**f**), the second row of plots shows the gating strategy used to identify TdT+ cells. **** p <0.0001, spinal cord versus peripheral fluids/tissues. Statistical analysis was performed using a one-way ANOVA followed by a Bonferroni's post hoc test. Scale bar: (**c**) 200 µm.

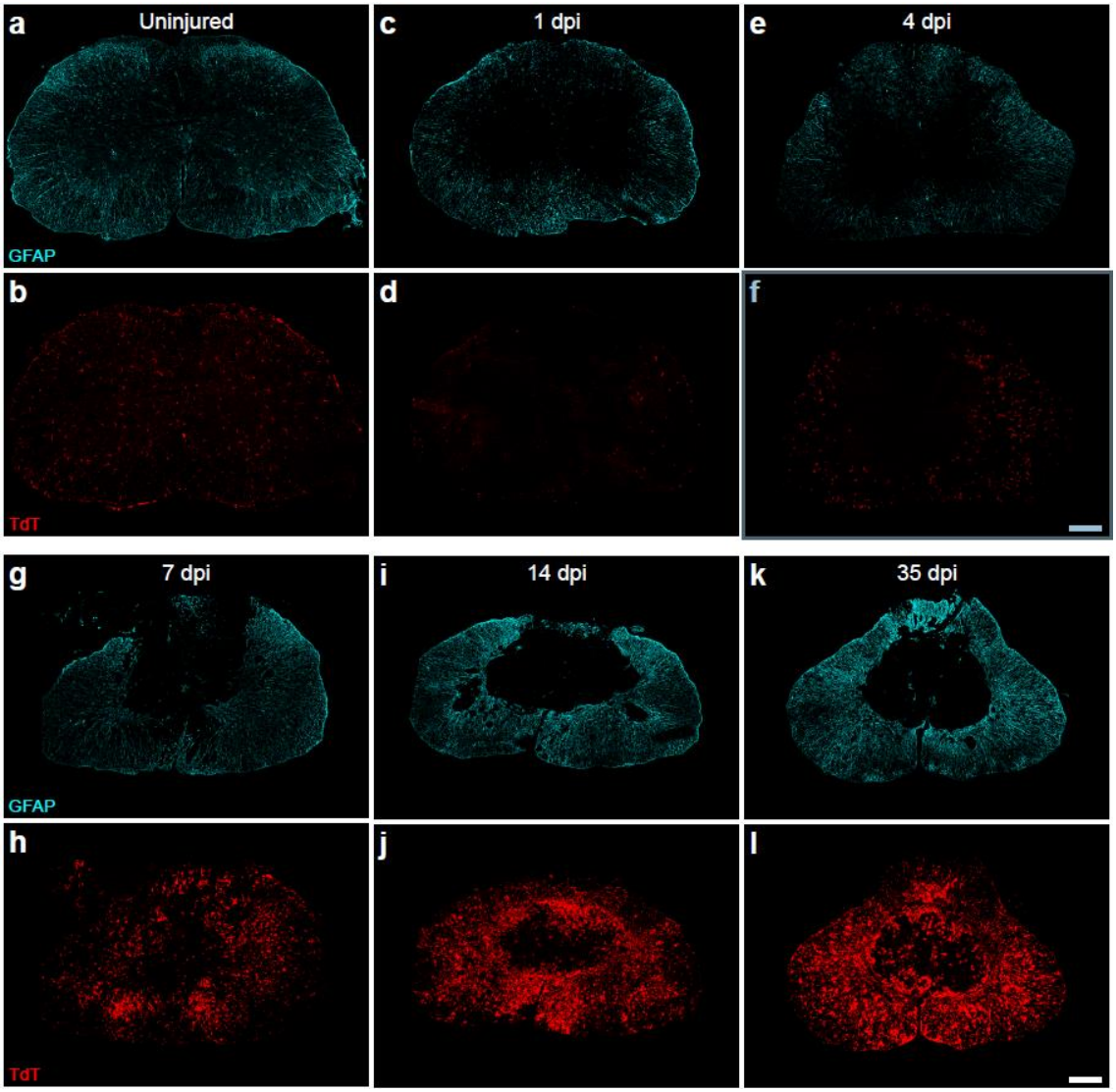

Supplementary Figure 2.2. Microglia proliferate extensively and accumulate at the lesion border after SCI

(**a-l**) Individual color channels are displayed for the merged confocal images shown in Fig. 1a-f. Depicted are representative confocal immunofluorescence photomicrographs of spinal cord sections showing the spatio-temporal distribution of microglia (TdT, red) and astrocytes (GFAP, cyan) in an uninjured *Cx3cr1*creER::*R26-TdT* transgenic mouse (**a-b**), as well as at the lesion epicenter at 1 (**c-d**), 4 (**e-f**), 7 (**g-h**), 14 (**i-j**), and 35 (**k-l**) days post-injury (dpi). Scale bars: (**a-l**, in **f** and **l**) 200 μm.

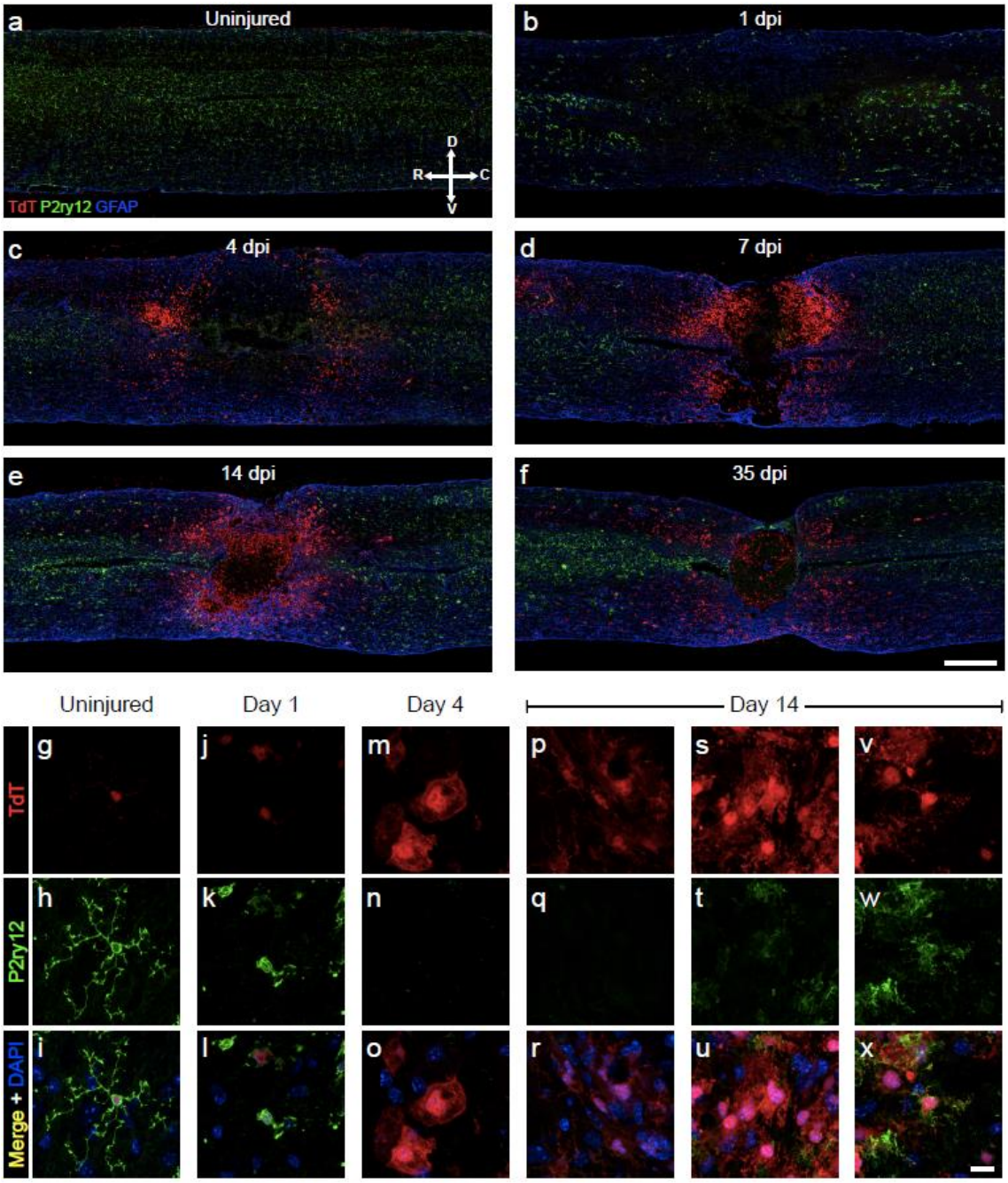

Supplementary Figure 2.3. Microglia rapidly downregulate P2ry12 after SCI and regain expression over time

(**a-r**) Confocal immunofluorescence microscopy of representative sagittal sections showing the expression of P2ry12 (green) by TdT+ microglia (red) in the uninjured spinal cord of *Cx3cr1*creER::*R26*-TdT transgenic mice (**a, g-i**), as well as at the lesion epicenter in *Cx3cr1*creER::*R26*-TdT mice killed at 1 (**b, j-l**), 4 (**c, m-o**), 7 (**d**), 14 (**e, p-x**), and 35 (**f**) days post-injury (dpi). Astrocytes (GFAP+) are shown in blue in panels (**a-f**), while DAPI (blue) is shown instead in panels (**g-x**). Note the re-expression of the P2ry12 protein in some TdT+ microglia at the lesion epicenter starting at day 14 post-SCI. Scale bars: (**a-f,** in **f**) 400 μm, (**g-x,** in **x**) 10 μm.

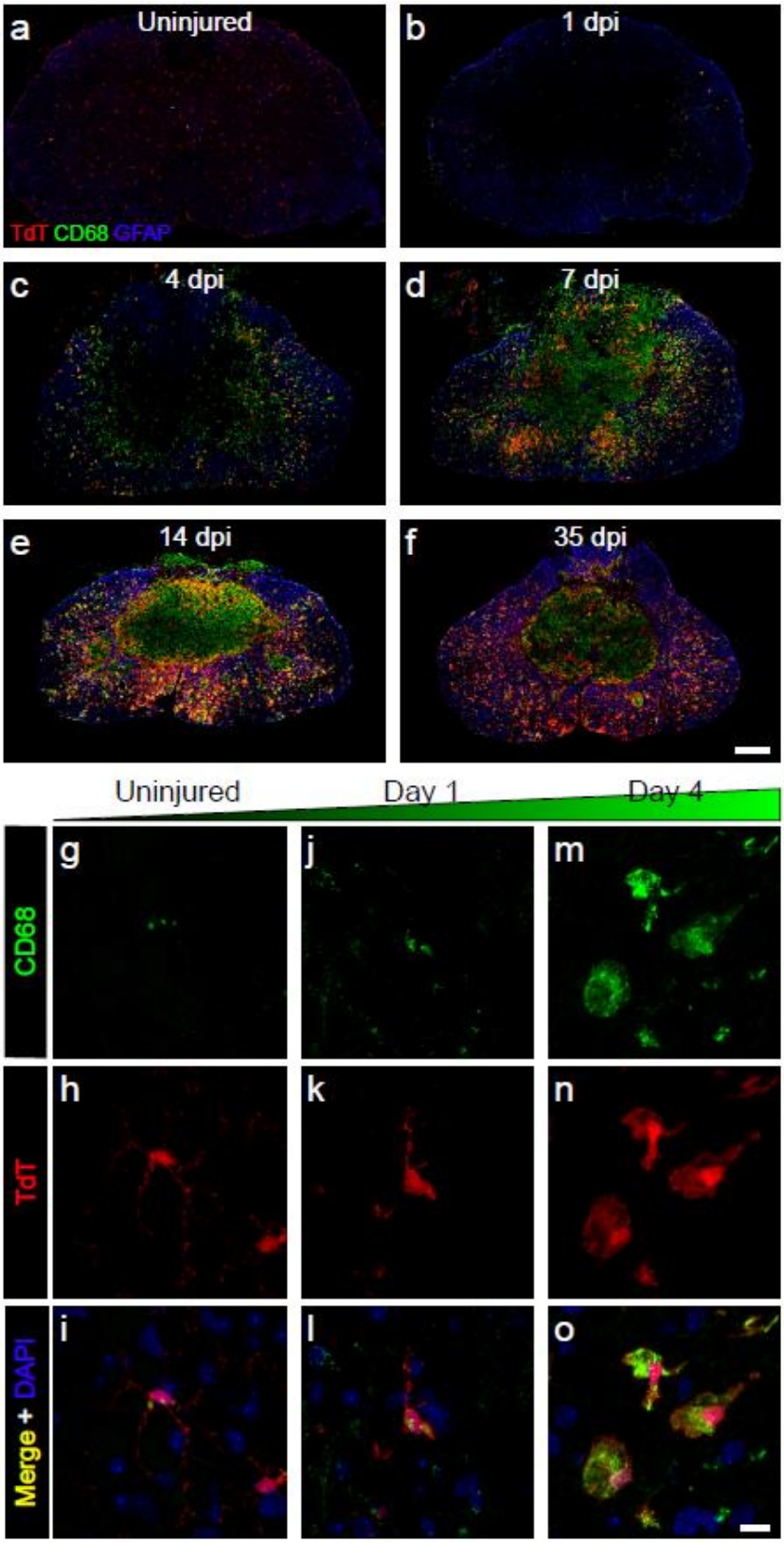

Supplementary Figure 2.4. Microglia rapidly upregulate CD68 after SCI

(**a-o**) Confocal immunofluorescence microscopy of representative spinal cord sections showing the expression of CD68 (green) by TdT+ microglia (red) in the uninjured spinal cord of *Cx3cr1*creER::*R26*-TdT transgenic mice (**a, g-i**), as well as at the lesion epicenter in *Cx3cr1*creER::*R26*-TdT mice killed at 1 (**b, j-k**), 4 (**c, m-o**), 7 (**d**), 14 (**e**), and 35 (**f**) days post-injury (dpi). Astrocytes (GFAP+) are shown in blue in panels (**a-f**), while DAPI (blue) is shown instead in panels (**g-o**). Scale bars: (**a-f,** in **f**) 200 μm, (**g-o**, in **o**) 10 μm.

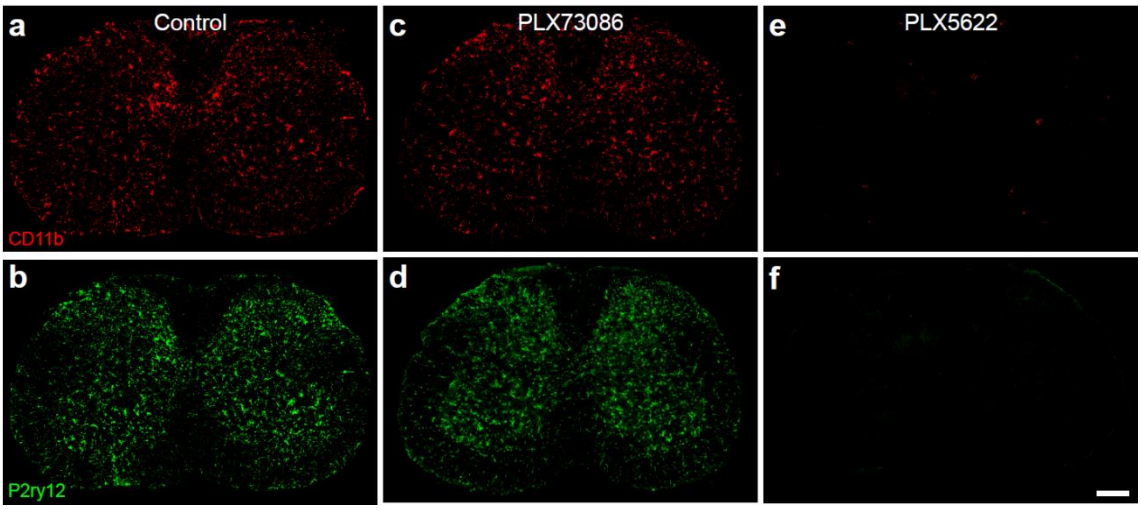

Supplementary Figure 2.5. The CSF1R inhibitor PLX5622, but not PLX73086, crosses the intact blood-spinal cord barrier to deplete virtually all microglia

(**a-c**) Individual color channels are displayed for the merged confocal images shown in Fig. 2a-c. Depicted are representative confocal images of CD11b and P2ry12 immunostainings showing the almost complete elimination of microglia in the spinal cord of naïve (uninjured) C57BL/6 mice after treatment with the CSF1R inhibitor PLX5622 compared to those fed PLX73086 or the control diet. Mice were killed after 21 days of treatment. Scale bar: (**a-f**, in **f**) 200 μm.

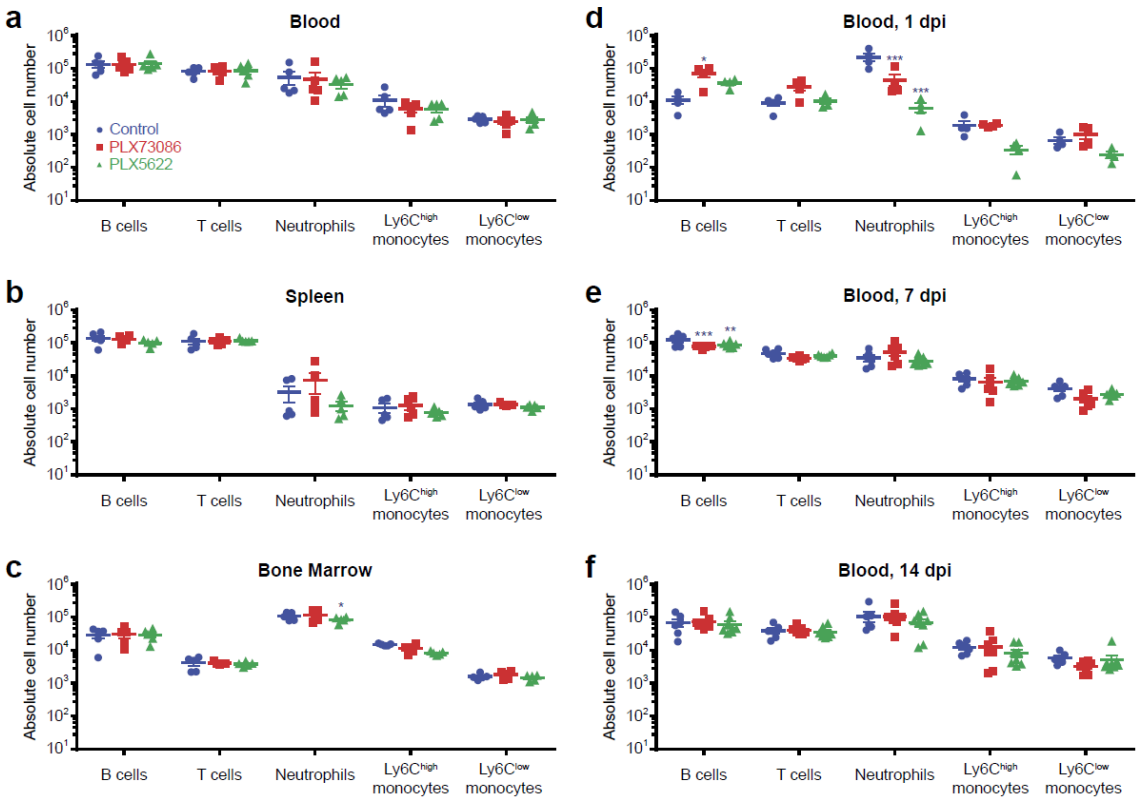

Supplementary Figure 2.6. Treatment with CSF1R inhibitors barely affects the number of peripheral immune cells

(**a-f**) Absolute numbers of immune cells in the blood (**a, d-f**), spleen (**b**), and bone marrow (**c**) of uninjured (**a-c**) and spinal cord injured (**d-f**) mice following 3 weeks of treatment with either PLX5622, PLX73086 or control diet (n=4-8 mice per group per time point). No changes in cell numbers were detected, except a small and transient blood neutropenia at day 1 post-SCI in mice fed CSF1R inhibitors. Note that treatments were continued until the time of sacrifice. Data are expressed as mean ± SEM. * p <0.05, *** p <0.001, compared to the control group. Statistical analysis was performed using a two-way ANOVA followed by a Bonferroni's post hoc test.

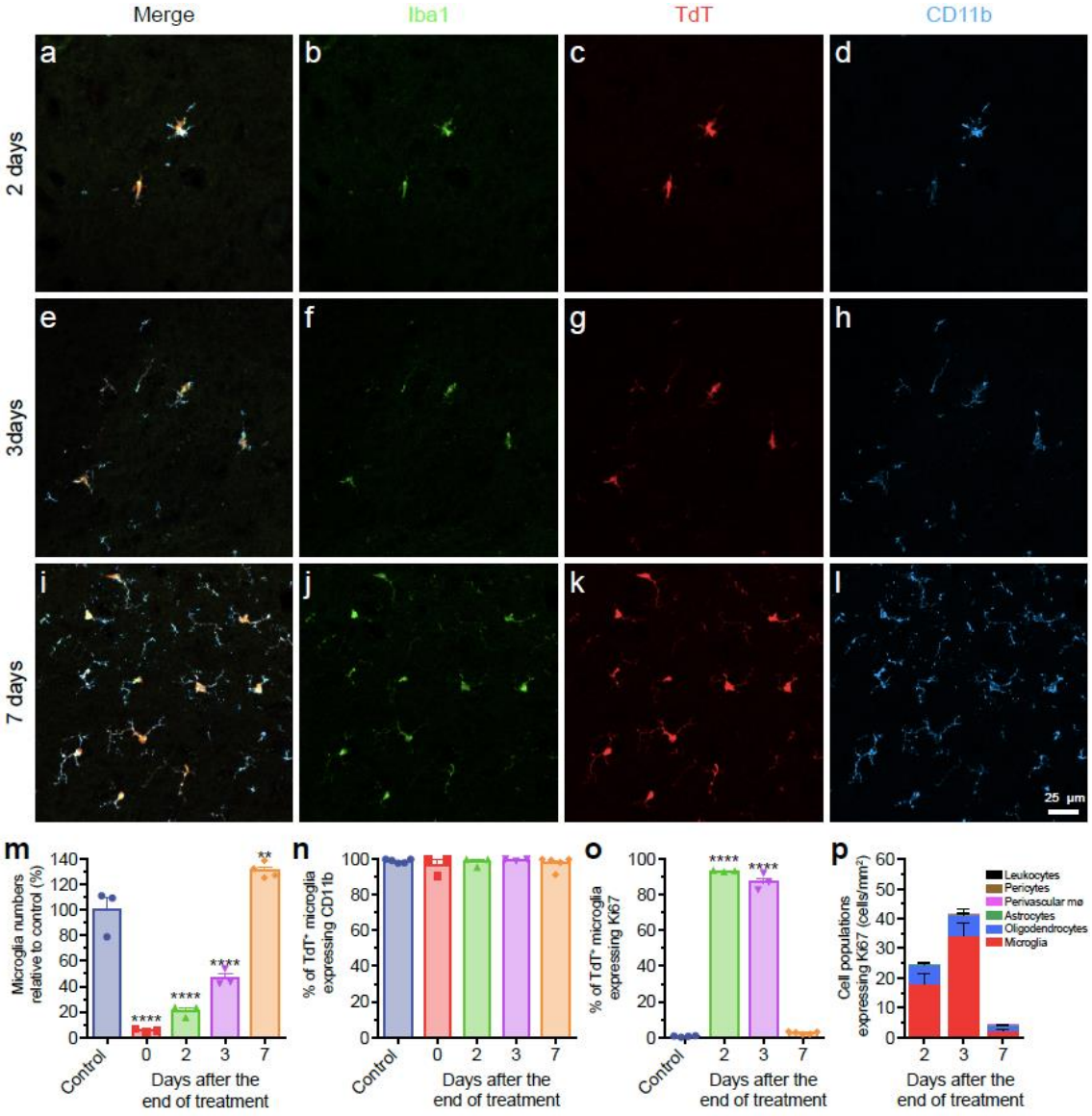

Supplementary Figure 2.7. Microglia proliferate extensively and repopulate the entire spinal cord after one week of cessation of PLX5622 treatment

(**a-l**) Representative confocal images showing CD11b (blue), Iba1 (green), and TdT (red) signals in the uninjured spinal cord of *Cx3cr1*creER::*R26*-TdT mice at 2 (**a-d**), 3 (**e-h**), and 7 (**i-l**) days after cessation of treatment with PLX5622. Nuclear staining (DAPI) is shown in turquoise. (**m**) Quantification of the number of TdT+ microglia in the normal thoracic spinal cord (control, blue bar), after 1 week of continuous treatment with PLX5622 (referred to as day 0 in the graph, (red), as well as 2 (green), 3 (purple) and 7 (orange) days after cessation of PLX5622 treatment (n=3-5 mice per group and per time point). (**n-o**) Percentage of spinal cord microglia (TdT+) expressing CD11b (**n**) and the proliferation marker Ki67 (**o**) at various times after cessation of PLX5622 treatment. (**p**) Number of microglia (TdT+, red bars), oligodendrocytes/OPCs (Olig2+, blue), astrocytes (GFAP+,

green), perivascular macrophages (perivascular mø, CD206+; purple), pericytes (CD13+, brown), and blood-derived leukocytes (CD45+ TdTneg, black) expressing Ki67 at various times after cessation of PLX5622 treatment. * p <0.05, ** p <0.01, *** p <0.001, **** p <0.0001, compared to the control group. Statistical analysis was performed using a one-way ANOVA followed by a Bonferroni's post hoc test. Scale bar: (**a-l**, in **l**) 200 μm.

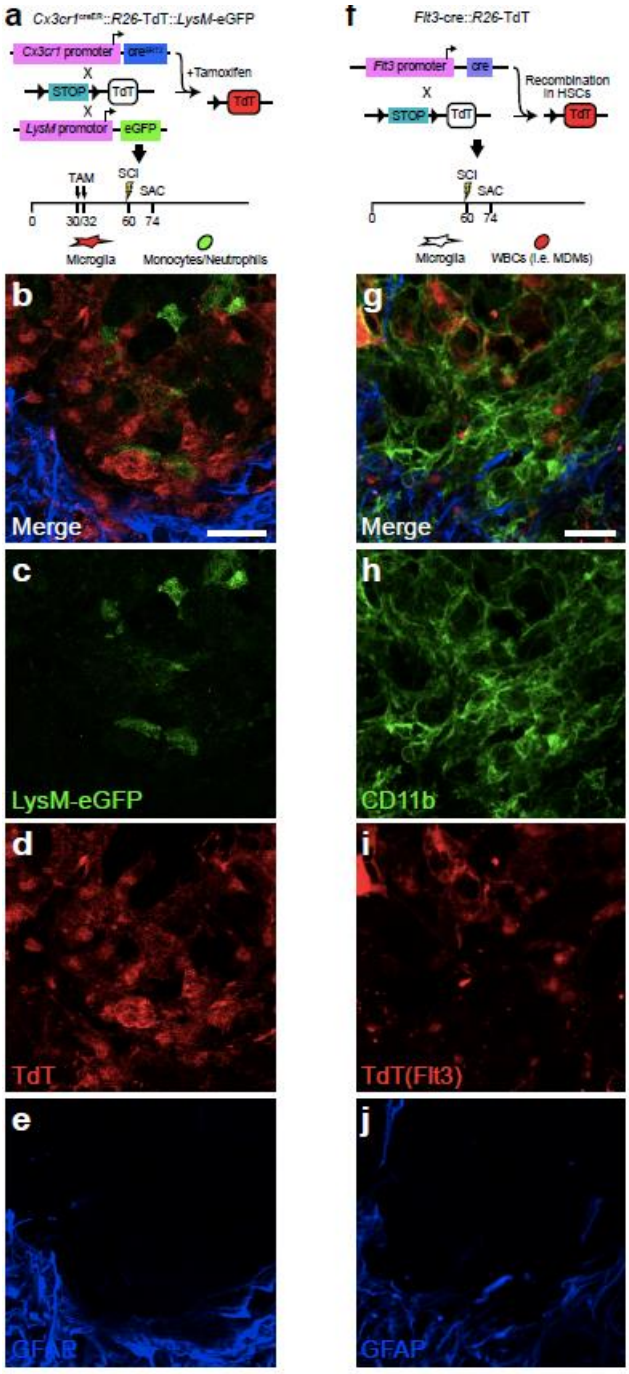

Supplementary Figure 2.8. Fate-mapping analysis reveals that microglia form a scar between reactive astrocytes and infiltrated peripheral immune cells after SCI

(**a**) Schematic diagram showing the strategy of breeding to obtain *Cx3cr1creER::R26-TdT*::*LysM*-eGFP mice, and the timeline of tamoxifen treatment, spinal cord contusion (SCI) and sacrifice (SAC). (**b-e**) Representative confocal images showing the microglial scar formed of TdT+ microglia (red cells), some of which are in direct contact with GFAP-immunoreactive astrocyte endfeet (blue) on one side and LysM-eGFP+ blood-derived myeloid cells (green cells) on the other side at 14 days post-SCI. (**f**) Schematic diagram showing the breeding strategy to obtain *Flt3-cre::R26-TdT* mice, in which TdT is expressed in hematopoietic stem cells (HSCs) and their progeny (e.g. monocyte-derived macrophages, MDMs), but not microglia. (**g-j**) Representative confocal images showing the microglial scar formed of CD11b+ Flt3neg microglia (green cells), making close contact with astrocyte endfeet (GFAP+, blue) and infiltrating MDMs (CD11b+ Flt3+, green cells with red nuclei) at 14 days post-SCI. Scale bars: (**b-e**, in **e**) 20 μm, (**g-j**, in **j**) 20 μm.

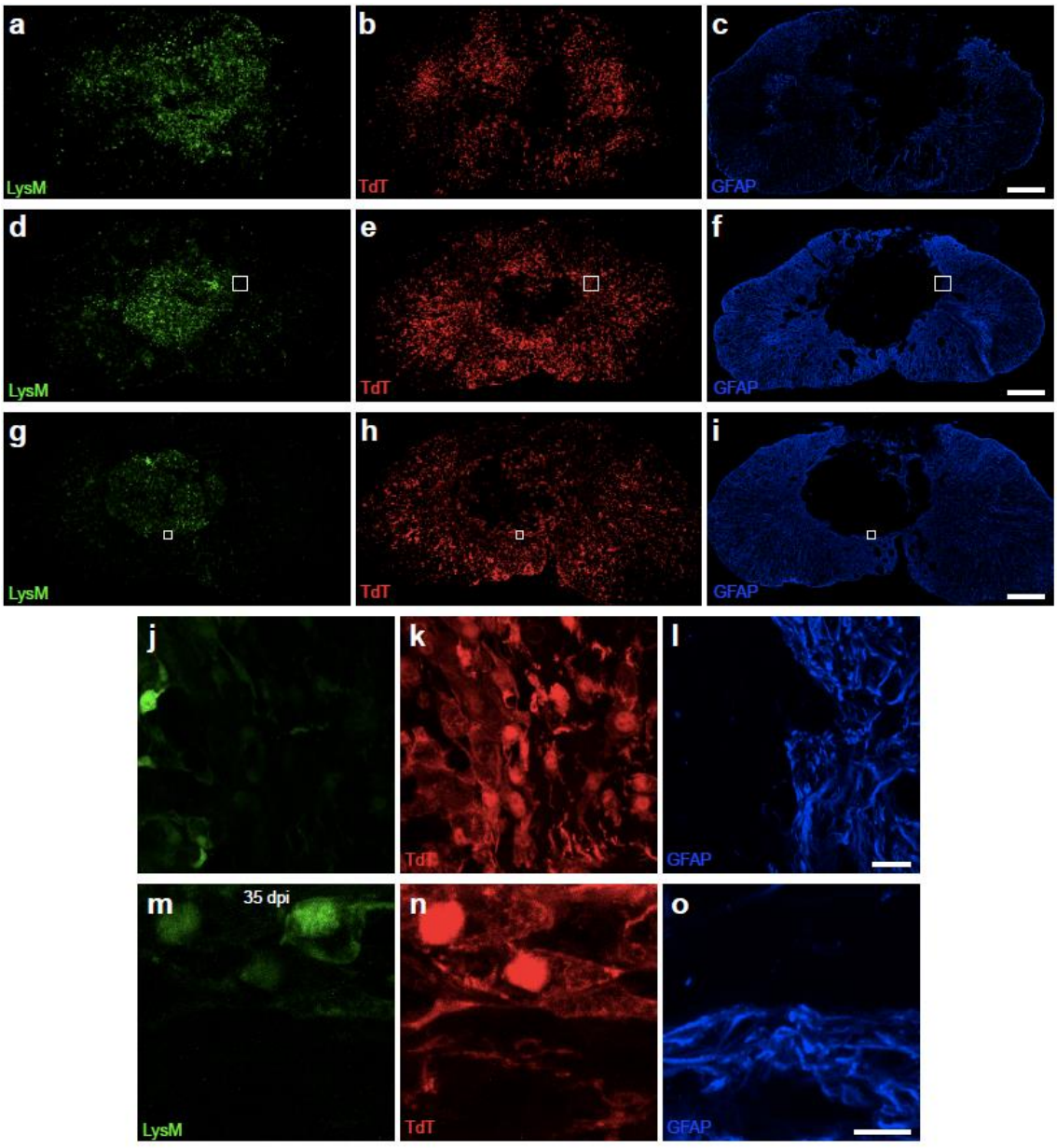

Supplementary Figure 2.9. A microglial scar forms at the interface between reactive astrocytes and blood-derived myeloid cells that infiltrate the lesion site

(**a-o**) Individual color channels are displayed for the merged confocal images shown in Fig. 4a-e. Depicted are representative confocal immunofluorescence photomicrographs of spinal cord sections taken at the lesion epicenter at 7 (**a-c**), 14 (**d-f, j-l**), and 35 (**g-i, m-o**) days post-injury (dpi) showing formation of the microglial scar, characterized by the accumulation of TdT+ microglia (red) at the lesion borders, over time. The microglial scar is shown in relation to the infiltration of blood-derived myeloid cells (LysM-eGFP+, green) and formation of the astroglial scar (GFAP-immunoreactive astrocytes, blue). Panels (**j-l**) and (**m-o**) are insets of panels (**d-f**) and (**g-i**), respectively, showing

close-ups of the microglial scar in *Cx3cr1*creER::*R26-TdT*::*LysM*-eGFP mice at 14 and 35 dpi. Scale bars: (**a-i**) 200 µm; (**j-o**) 20 µm.

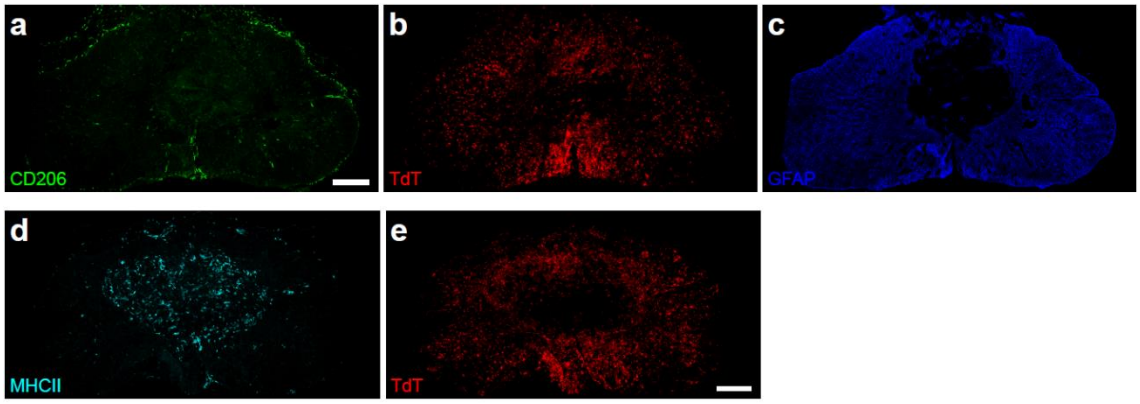

Supplementary Figure 2.10. The microglial scar is mainly composed of microglia with the presence of only few scattered CNS border-associated macrophages

(**a-c**) Individual color channels are displayed for the merged confocal image shown in Fig. 5i. Depicted are representative confocal immunofluorescence photomicrographs showing the absence (or very weak expression) of CD206 (green) in microglia (TdT+, red) forming the microglial scar at the lesion borders at 14 days post-SCI. In contrast, border-associated macrophages express high levels of the CD206 protein. (**d-e**) Individual color channels are displayed for the merged confocal image shown in Fig. 5p. Depicted are representative confocal image showing the absence of colocalization between TdT (red) and MHCII (cyan) in the injured spinal cord of a *Cx3cr1*creER::*R26-TdT* mouse at 14 days. Scale bars: **(a-c**, in **c**) 200 µm, (**d-e**, in **e**) 200 µm.

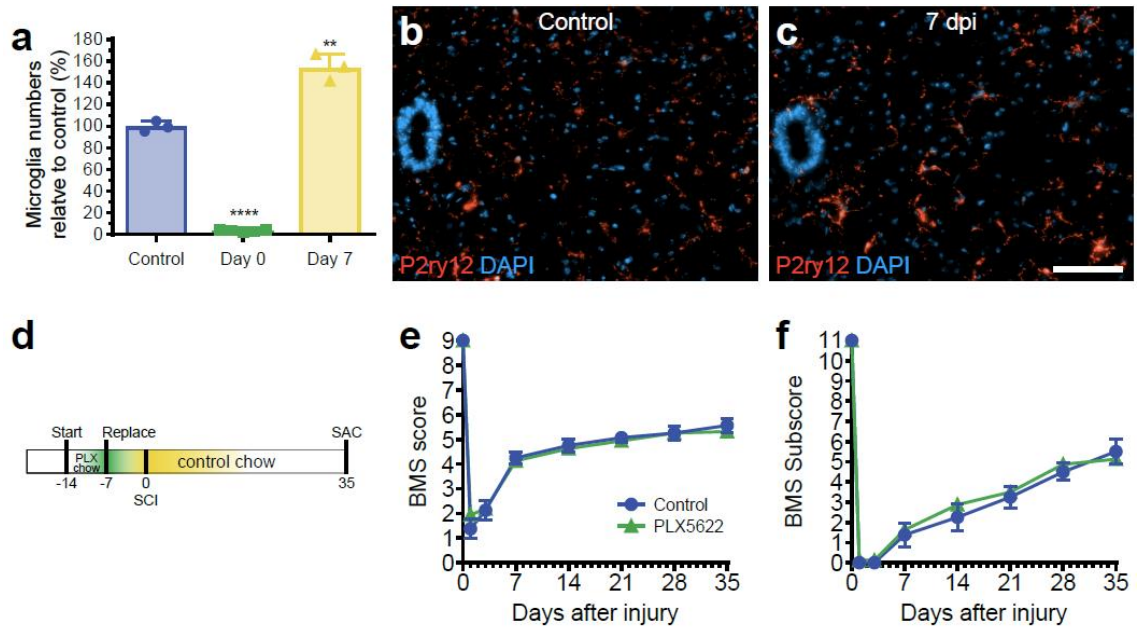

Supplementary Figure 2.11. Mice with more microglia in their spinal cord at the time of injury recover locomotor function similar to that of SCI mice on the control diet

(**a**) Quantification of the number of microglia (P2ry12+) in the uninjured thoracic spinal cord of C57BL/6 mice (control, blue bar in the histogram), as well as in mice treated with PLX5622 for 1 week and then switched to the control diet for 0 (green) or 7 (yellow) days (n=3-5 mice per group). (**b-c**) Representative confocal images of P2ry12 immunostaining showing the increased number of spinal cord microglia after switching C57BL/6 mice from the PLX5622 diet to control chow for 7 days. (**d**) Schematic diagram of experimental design showing the timeline of treatment (PLX5622 versus control chow), spinal cord contusion (SCI) and sacrifice (SAC). (**e-f**) Assessment of locomotor recovery using the BMS (**e**) and BMS subscore (**f**) (n=8 mice per group). ** $p < 0.01$, **** $p < 0.0001$, compared to the control group. Statistical analysis was performed using a one-way ANOVA (**a**) or a two-way repeated-measures ANOVA (**e-f**) followed by a Bonferroni's post hoc test. Scale bar: (**b-c,** in **c**) 50 μm.

2.12. Tables

Symbol	Gene Name	Genbank Accession Numbers	Position	Size (bp)	Linearization		Transcription	
					Antisense	Sense	Antisense	Sense
Igf1	Insulin-like growth factor 1	NM_184052	1338-1856	868	HindIII	XhoI	T7	SP6
Il1a	Interleukin 1 alpha	NM_010554	270-1985	1715	XhoI	BamHI	SP6	T7
Il1b	Interleukin 1 beta	M15131	1-1339	1358	KpnI	XhoI	T7	SP6
Il6	Interleukin 6	J03783		600	KpnI	HindIII	T3	T7
Tnf	Tumor necrosis factor	NM_013693	426-844	419	XhoI	HindIII	SP6	T7
Tgfb1	Transforming growth factor, beta 1	BC013738	315-1487	1173	EcoRI	XhoI	T3	T7

Table 2.1 List of cDNA used for *in situ* hybridization

Chapter 2:

IL-1α gene deletion protects oligodendrocytes after spinal cord injury through upregulation of the survival factor Tox3

Dominic Bastien[a], Victor Bellver Landete[a], Martine Lessard[a], Nicolas Vallières[a], Mathieu Champagne[a], Akira Takashima[b], Marie-Ève Tremblay[a], Yannick Doyon[a], and Steve Lacroix[a,1]

[a]Centre de recherche du Centre hospitalier universitaire (CHU) de Québec - CHUL et Département de médecine moléculaire de l'Université Laval, Québec, Canada; [b]Department of Medical Microbiology and Immunology, University of Toledo College of Medicine, Toledo, OH, USA.

Keywords: Neuroimmunology, cytokine, hypoxia, nervous system, macrophage, microglia, monocyte, neutrophil, neurodegeneration, oligodendrocyte progenitor cells.

3.1. Résumé

Les lésions de la moelle épinière (LME) entraînent la relâche de signaux de danger par les cellules nécrotiques, un processus qui mène à la neuroinflammation. Des études suggèrent que l'inflammation joue un rôle dans les dommages mais aussi dans la réparation du tissu nerveux. Dans notre étude, nous avons étudié la synthèse, la relâche et les fonctions de l'IL-1α et l'IL-1β dans la neuroinflammation, les dommages tissulaires et la récupération locomotrice suite à une LME. Nous avons démontré que les microglies situées au site de lésion expriment rapidement l'IL-1α, tandis que les neutrophiles ($Ly6G^{+}$ $7/4^{+}$) et les macrophages dérivés des monocytes infiltrants ($Ly6C^{hi}$ $7/4^{+}$) produisent l'IL-1β. Bien que l'infiltration de ces 2 types cellulaires fut également réduite chez les souris *Il1a*$^{-/-}$ et *Il1b*$^{-/-}$ comparées aux souris sauvages, les souris *Il1a*$^{-/-}$ présentaient une plus grande amélioration locomotrice dès le jour 1 post-LME. Cette récupération a persistée à travers le temps et corrèle avec un volume lésionnel plus petit. L'analyse du transcriptome des cellules du tissu nerveux au 1 jour post-LME a permis d'identifier 18 transcrits différentiellement régulés chez les souris *Il1a*$^{-/-}$ comparativement aux souris *Il1b*$^{-/-}$ et sauvages, parmi lesquels se retrouve le facteur de survie cellulaire TOX3. En absence d'IL-1α, les souris ont présenté des niveaux plus élevés de TOX3 dans leurs oligodendrocytes et ce dès le jour 10 post-natal, un effet qui a persisté jusqu'à l'âge adulte. L'analyse de la moelle épinière en développement de souris sauvages a révélé que les niveaux d'ARNm de l'IL-1α, mais pas ceux de l'IL-1β, augmentent drastiquement entre les jours P5 et P10, coïncidant avec une période critique de l'activation microgliale et de l'initiation de la myélinisation. Chez les souris *Il1a*$^{-/-}$ adultes, la survie des oligodendrocytes fut significativement plus élevée comparativement aux souris *Il1b*$^{-/-}$ et sauvages au jour 1 post-LME. Nous avons donc démontré pour la première fois que l'absence de l'IL-1α chez la souris réduit l'expression du facteur de survie TOX3 chez les oligodendrocytes, suggérant que l'inhibition de cette cytokine pourrait réduire la dégénérescence suite à un traumatisme du système nerveux central ou certaines maladies neurodégénératives.

3.2. Abstract

Spinal cord injury (SCI) causes the release of danger signals by stressed and dying cells, a process that leads to neuroinflammation. Evidence suggests that inflammation plays a role in both damage and repair of injured neural tissue. We show that microglia at sites of SCI rapidly express the alarmin IL-1α, and that infiltrating neutrophils and macrophages subsequently produce IL-1β. Infiltration of these cells is dramatically reduced in both *IL-1α*$^{-/-}$ and *IL-1β*$^{-/-}$ mice, but only *IL-1α*$^{-/-}$ mice showed rapid (at day 1) and persistent improvements in locomotion associated with reduced lesion volume. Similarly, intrathecal administration of the IL-1 receptor antagonist anakinra restored locomotor function post-SCI. Transcriptome analysis of SCI tissue at day 1 identified the survival factor Tox3 as being differentially regulated exclusively in *IL-1α*$^{-/-}$ mice compared with *IL-1β*$^{-/-}$ and wild-type mice. Accordingly, *IL-1α*$^{-/-}$ mice have markedly increased Tox3 levels in their oligodendrocytes, beginning at postnatal day (P) 10 and persisting through adulthood. At P10, the spinal cord of *IL-1α*$^{-/-}$ mice showed a transient increase in mature oligodendrocyte numbers, coinciding with increased IL-1α expression in wild-type animals. In adult mice, *IL-1α* deletion is accompanied by increased oligodendrocyte survival after SCI. TOX3 overexpression in human oligodendrocytes reduced cellular death under conditions mimicking SCI. These results suggest that IL-1α-mediated Tox3 suppression during the early phase of CNS insult plays a crucial role in secondary degeneration.

3.3. Introduction

Spinal cord injury (SCI) can lead to loss of motor and sensory function in the lower and/or upper limbs. At the site of injury, the pathology is divided into two major chronological events: the primary and secondary lesions. The second wave of tissue destruction that follows the primary mechanical insult is believed to be caused by a complex series of events leading to apoptosis, including ischemia, vascular damage, glutamate excitotoxicity, ionic dysregulation, inflammation, free radical generation, and cytokine and protease production (David and Lacroix, 2005). Damage to the CNS is associated with an almost immediate response of microglia (Davalos et al., 2005). Astrocytes, the main cellular component of the glial scar, also react quickly by exhibiting changes in gene expression, hypertrophy, and process extension (Sofroniew, 2009). The glial scar has been shown to have both protective and detrimental functions in the context of SCI (Faulkner et al., 2004; Brambilla et al., 2005; Brambilla et al., 2009).

Innate immune cells such as neutrophils and monocytes are rapidly recruited at sites of SCI (Fleming et al., 2006; Stirling and Yong, 2008; Pineau et al., 2010; Lee et al., 2011; Thawer et al., 2013). Evidence suggests that these cells could play a key role in both damage and repair of neural tissue after an injury or ischemia (Barrette et al., 2008; Kigerl et al., 2009; Shechter et al., 2009; Stirling et al., 2009; Allen et al., 2012). The apparent contradictions between these studies may be due to the fact that different subsets of immune cells have divergent effects causing either neurotoxicity or regeneration in the injured spinal cord (David and Kroner, 2011; Bastien and Lacroix, 2014; Plemel et al., 2014). A better understanding of the roles of the various subsets of immune cells and the identification of the endogenous factors stimulating their recruitment is key for the development of efficient immunotherapies.

One important family of cytokines playing a key role in neurodegeneration is the interleukin (Il)-1 family (Allan and Rothwell, 2001; Allan et al., 2005). Two of the members of this large family, IL-1α and IL-1β, exert similar proinflammatory actions by binding to the IL-1 type 1 receptor (IL-1r1). Both IL-1α and IL-1β produced by tissue resident macrophages are required for neutrophil recruitment during cell death-induced sterile inflammation (Chen

et al., 2007), (Kono et al., 2010). However, the function of IL-1β has been studied more thoroughly because of its importance in the development and progression of a number of autoinflammatory and CNS diseases (Allan et al., 2005; Dinarello, 2011). Apart from its role in the initiation of gliosis and inflammation (Basu et al., 2002), studies have linked IL-1β to the production of growth factors by CNS resident cells in various disease and injury models (Herx et al., 2000; Albrecht et al., 2002; Albrecht et al., 2003; Amankulor et al., 2009). Other evidence indicates that IL-1β likely plays an important role in CNS remyelination by regulating multiple stages of oligodendrocyte development (Mason et al., 2001).

Here, we sought to determine whether cytokines of the IL-1 family are an endogenous signal initiating neuroinflammation after traumatic SCI. We uncovered a dual role for IL-1α not only in triggering inflammation in the injured spinal cord, but also in suppressing the expression of the survival factor TOX high mobility group box family member 3 (Tox3) in oligodendrocytes. Overexpression of this transcription factor gave remarkable protection against cell death. Thus, blocking this cytokine may be a promising therapeutic avenue to prevent loss of CNS cells following SCI and other neurodegenerative conditions.

3.4. Materials and methods

3.4.1. Animals

A total of 308 mice of either sex were used in this study. C57BL/6 mice, used as controls, were purchased from Charles River Laboratories. IL-1α-, IL-1β-, and IL-1α/β-knockout (KO) were obtained from Dr. Yoichiro Iwakura (Institute of Medical Science, University of Tokyo, Japan) and have been previously described (Horai et al., 1998). Breeders for the p*Il1b*-DsRed transgenic mouse line were obtained from Dr. Akira Takashima (University of Toledo College of Medicine, Toledo, OH) and bred in-house at the Animal Research Facility of the CHUL Research Center and genotyped according to the method published by

Matsushima *et al.* (Matsushima et al., 2010). Finally, Cx3cr1-eGFP transgenic mice were purchased from The Jackson Laboratory. All mice had free access to food and water.

3.4.2. Spinal cord injury and animal treatment

C57BL/6 (n = 75), IL-1α-KO (n = 64), IL-1β-KO (n = 60), IL-1α/β-KO (n = 13), p*Il1b*-DsRed (n = 6) and Cx3cr1-eGFP (n = 18) adult mice were anesthetized with isoflurane and underwent a laminectomy at vertebral level T9-10, which corresponds to spinal segment T10-11. Briefly, the vertebral column was stabilized and a contusion of 50 kdyn was performed using the Infinite Horizon SCI device (Precision Systems & Instrumentation). Animals used for quantification of immune cells, either by immunofluorescence (IF) or flow cytometry, received a 70-kdyn injury. Overlying muscular layers were then sutured and cutaneous layers stapled. Post-operatively, animals received manual bladder evacuation twice daily to prevent urinary tract infections. Depending on the experiment performed, SCI mice were killed by transcardiac perfusion at 1, 3, 4, 6, 12 and 24 hours, and 3, 4 and 38 days post-contusion. C57BL/6 (n = 37), IL-1α-KO (n = 12) and IL-1β-KO (n = 12) neonatal mice were killed by either decapitation under ice anesthesia for pups of 1, 3, 7, 10 and 14 days of age, or transcardiac perfusion under deep anesthesia induced with ketamine-xylazine for mice at postnatal day (P) 18 and 30.

In the experiment in which we studied the effects of treatment with the IL-1r1 antagonist anakinra (Kineret®, 100 mg/0.67 ml in prefilled syringes; Swedish Orphan Biovitrum AB) on functional recovery after SCI, mice were injected either intravenously (i.v.; anakinra diluted to a final concentration of 20 µg/µL in PBS, for a dose of 100 mg/kg per injection) or intrathecally (i.t.; 33 mg/kg in 5 µl PBS). The 3-day i.v. treatment consisted

of injections at 6, 24 and 48 hours post-SCI, whereas the 7-day i.v. treatment consisted of injections made at the time of injury, 2 hours after and then every day until day 7. The i.t. treatment consisted of a single injection into the cisterna magna performed 15 minutes after SCI using a pulled-glass micropipette connected to a 10-µl Hamilton syringe. All surgical procedures and treatments were approved by the Laval University Animal Care Committee and conducted in accordance with guidelines of the Canadian Council on Animal Care.

3.4.3. Flow cytometry

Cells freshly isolated from the spinal cord of injured mice were analyzed using flow cytometry following our previously published method (de Rivero Vaccari et al., 2012). Briefly, animals were transcardially perfused with cold Hanks' balanced salt solution (HBSS) to remove blood from the vasculature, their spinal cords dissected out, and a 1-cm segment centered at the site of the lesion isolated and mechanically homogenized with a small tissue grinder. Cells were filtered through a 40-µm nylon mesh cell strainer (BD Biosciences), centrifuged at 200g for 10 minutes, washed once with HBSS, and resuspended with HBSS containing 20% fetal bovine serum (FBS; Sigma-Aldrich Canada Ltd.). For multicolor immunofluorescent labeling, cells were incubated with Mouse Fc Block (i.e., purified anti-mouse CD16/CD32; BD Biosciences) for 5 minutes in order to prevent nonspecific binding, followed by labeling for 30 min at room temperature with the following fluorescently conjugated primary antibodies: PerCP-conjugated anti-CD45 (1:33 dilution, BD Biosciences), BD HorizonTM V450-conjugated anti-CD11b (1:66, BD Biosciences), FITC-conjugated anti-Ly6C (1:100, BD Biosciences), PE-Cy7-conjugated anti-Ly6G (1:100, BD Biosciences), and APC-conjugated anti-F4/80 (1:20, AbD Serotec) (for a full description of these primary antibodies, please refer to our published work (Nadeau et al., 2011)). Cells

were analyzed using FlowJo software (v. 9.2; Tree Star Inc.) on a FACS LSRII flow cytometer (BD Biosciences). Blood-derived myeloid cells were identified based on their expression of CD45, CD11b, Ly6C, Ly6G and F4/80, as follows: $CD45^{hi}$ $CD11b^{+}$ $Ly6C^{+}$ $Ly6G^{+}$ $F4/80^{-}$ cells were considered as neutrophils and $CD45^{hi}$ $CD11b^{+}$ $Ly6C^{hi}$ $Ly6G^{-}$ $F4/80^{+}$ cells as monocyte-derived M1 macrophages (de Rivero Vaccari et al., 2012).

3.4.4. Tissue processing and histology

Spinal cords were collected and prepared as previously described (Pineau and Lacroix, 2007). Briefly, mice were overdosed with a mixture of ketamine-xylazine and transcardiacally perfused with 4% paraformaldehyde (PFA), pH 7.4, in PBS. Spinal cords were dissected out and placed overnight in a PBS/30% sucrose solution. For each animal, a spinal cord segment of 12 mm centered over the lesion site was cut in 7 series of 14-µm-thick coronal sections using a cryostat. For immunohistochemistry against 7/4 (also referred to as Ly6B, see (Rosas et al., 2010)) and Ly6G, mice were perfused with 0.9% saline solution followed by 4% PFA, pH 9.5, in borax buffer. Spinal cords were dissected out, post-fixed for 2 days, and placed overnight in a 4% PFA-borax/10% sucrose solution until processing using a cryostat set at 30 µm thickness. All sections were collected directly onto Surgipath X-tra® slides having a permanent positive charged surface (Leica Microsystems Canada) and stored at -20 °C until use. To identify the lesion epicenter and quantify lesion volume, one series of adjacent sections was immunostained using a rabbit anti-GFAP (mouse) antibody (1:750 dilution, Dako Canada Inc.) and then counterstained with 4', 6-diamidino-2-phenylindole, dilactate (DAPI; 1 µg/ml, Life Technologies Inc.) and FluoroMyelin™ red fluorescent myelin stain (1:300, Life Technologies Inc.).

3.4.5. Immunohistochemistry and quantification

Cells expressing IL-1α were identified by confocal IF labeling using a goat anti-mouse IL-1α polyclonal antibody (1:100 dilution, R&D Systems Inc.), and co-localized with the myeloid cell marker CD11b (1:250, AbD Serotec) or markers of microglia such as ionized calcium-binding adaptor molecule 1 (Iba1; 1:750, Wako Chemicals USA) and the GFP reporter expressed under the control of the *Cx3cr1* promoter (Cx3cr1-eGFP transgenic mice). The astroglial scar was visualized using the anti-GFAP antibody described above. Alexa Fluor® secondary antibody conjugates (1:250, Life Technologies Inc.) were used as secondary antibodies, whereas DAPI was used for nuclear counterstaining.

Immunofluorescence labeling was performed according to our previously published methods (de Rivero Vaccari et al., 2012). Sections were observed and imaged on an Olympus IX81 Fluoview FV1000 confocal microscope system equipped with 488 nm, 543 nm, and 633 nm lasers (Olympus Canada Inc.). Quantification of double-labeled cells was performed manually at 40× using the Olympus confocal microscope. Results were presented as the total number of IL-1α-positive (+) cells per cross-section or the percent of IL-1α^{+} cells that expressed each of the two microglial markers (Iba1, GFP).

Tox3 protein expression was visualized by confocal IF microscopy using a rabbit polyclonal anti-Tox3 antibody (1:100 dilution, Novus Biologicals Canada ULC). Colocalization of Tox3 in neurons, oligodendrocytes and endothelial cells was performed using the neuron-specific markers NeuN (1:250, EMD Millipore) and HuC/HuD (1:80, Life Technologies Inc.), the oligodendrocyte marker CC1 (also referred to as anti-APC; 1:500,

Abcam) and the endothelial cell marker CD31 (also referred to as PECAM-1; 1:750, BD Biosciences), respectively. For the quantification of $NeuN^+$ neurons and $CC1^+$ oligodendrocytes expressing or not Tox3, the number of labeled cells was estimated by the optical fractionator method using the Bioquant Nova Prime software (Bioquant Image Analysis Corporation) on video images transmitted by a high-resolution Retiga QICAM fast color 1394 camera (1392 × 1040 pixels, QImaging) installed on a Nikon Eclipse 80i microscope. For this, the outline of the spinal cord gray matter (for the quantification of neurons) or white matter (for the quantification of oligodendrocytes) was traced at 10× and then sampled at 40× magnification. The counting parameters were as follows: sampling grid size, 150 × 150 µm (except for P3 mice, for which a sampling grid of 100 × 100 µm was used instead); counting frame size, 50 × 50 µm, and; dissector height, 14 µm. Cells were counted only if their nuclei laid within the dissector area, did not intersect forbidden lines, and came into the focus as the optical plane moved through the height of the dissector. Quantification was performed on a total of 9 equally spaced sections (294 µm apart) spanning 3 mm centered at the lesion epicenter, since we noted in our previous work that the lesion normally extends over approximately 3 mm in mice that received a 50-kdyn SCI contusion. For each section, the total number of positively-stained cells was calculated by multiplying the total volume of the spinal cord gray or white matter, as measured using the Bioquant Nova Prime software, by the average number of cells per mm^3. A relative number of cells that survived the trauma was then estimated by adding the total number of positively-stained cells counted in each of the 9 sections encompassing the lesion.

Immunoperoxidase labeling using the anti-7/4 antibody (1:800 dilution, AbD Serotec) was performed to detect both neutrophils and proinflammatory M1 macrophages in the spinal

cord of injured mice, as this antibody was recently shown to be specific for detecting these two cell types in SCI tissue (de Rivero Vaccari et al., 2012). Immunoperoxidase labeling was performed on spinal cord tissue sections directly mounted onto slides using CoverWell incubation chambers (Life Technologies Inc.) and our previously published protocol (Pineau and Lacroix, 2007), with the only difference that sections were pre-treated for 15 minutes with proteinase K to improve immunolabeling efficiency. Following immunoperoxidase labeling, tissue sections were counterstained with Luxol Fast blue (LFB) to visualize damaged areas. For the quantification of neutrophils and M1 macrophages, the outline of the coronal section was traced at 10× magnification, as described above, and a grid of 50 µm × 50 µm positioned over the spinal cord using the Bioquant Nova Prime software. All $7/4^+$ cells were then counted at 20× magnification. Results were expressed as an average number of positive cells per coronal section.

All quantifications were done blind with respect to the identity of the animals and the epineurial layer excluded from analyses.

3.4.6. Lesion volume analysis

The calculation of areas of tissue damage and lesion volume after SCI was performed on 1 series of adjacent sections within a predetermined spinal cord segment, including the lesion epicenter and sections located up to approximately 1.5 mm distal to the center of the lesion in both directions (i.e., rostral and caudal). Fourteen-µm-thick coronal sections were first immunostained for GFAP and then counterstained with DAPI and FluoroMyelin^{TM} to visualize the glial scar and identify gray and white matter sparing, respectively. The analysis was performed using the BioQuant Nova Prime computerized image analysis system

(Bioquant Topographer XP plug-in). In each section, the total area of the coronal section was first determined by manually tracing the contour at low magnification. Next, the outline of necrotic and damaged tissue was traced at higher magnifications. Areas where normal spinal cord architecture was absent and areas containing cellular and myelin debris surrounded by the astroglial scar were considered as areas of tissue damage. The Bioquant Topographer program was then used to reconstruct the injured spinal cord and measure lesion volume.

3.4.7. Toluidine blue staining and g-ratio analysis

The method used was previously described by Tremblay et al. (Tremblay et al., 2010). Mice were perfused with a solution of 3.5% acrolein followed by 4% PFA in 0.1 M phosphate buffer (pH 7.4). Two-mm-thick cross-sections of the thoracic spinal cord were left to post-fix for 2 hours at 4°C in 4% PFA and then cut at a thickness of 50 µm using a vibratome (VT1000S; Leica Microsystems). Fifty-µm-thick sections were next treated with 1% osmium tetroxide and dehydrated into ascending concentrations of ethanol followed by propylene oxide. The tissue was embedded into Durcupan resin and sections cut at a thickness of 1 µm using an ultramicrotome (UC7; Leica Microsystems) and histology diamond knife. Semi-thin sections were collected directly onto slides, stained with 0.1% toludine blue in sodium borate and coverslipped. G-ratios were determined by dividing the axon diameter by the axon + myelin diameter. Quantification was performed on a total of 200 myelinated axons per animal. Half of the axons were imaged at 100× magnification in the ascending sensory tract (AST) of the dorsal column and the other half in the lateral descending rubrospinal tract (RST).

3.4.8. Microarray analysis

Spinal cord segments of 6 mm-long centered over the lesion were rapidly dissected, frozen in liquid nitrogen, and stored at -80°C until RNA extraction. Total RNA was isolated by TRI Reagent and purified with the GenElute mammalian total RNA miniprep kit (Sigma-Aldrich Canada Ltd.). Two hundred nanograms of total RNA was labeled using the Ambion® WT Expression Kit protocol, as described by the manufacturer (Affymetrix, Santa Clara, CA). The quality of total RNA, cDNA synthesis, cRNA amplification, and cDNA fragmentation was monitored by microcapillary electrophoresis (Bioanalyzer 2100, Agilent Technologies). Five µg of fragmented single-stranded cDNA was hybridized for 16 hours at 45°C with constant rotation on a GeneChip® Mouse Gene 1.0 ST Array (Affymetrix). After hybridization, microarrays (n = 12) were processed using the Affymetrix GeneChip Fluidic Station 450 (protocol FS450_0007). In brief, staining was made with streptavidin-conjugated phycoerythrin (SAPE; Affymetrix), followed by amplification with a biotinylated anti-streptavidin antibody (Affymetrix), and by a second round of SAPE staining. Microarrays were scanned using a GeneChip Scanner 3000 7G (Affymetrix) enabled for high-resolution scanning. Images were extracted with the GeneChip Operating Software (Affymetrix GCOS v1.4). Quality control of microarrays was performed using the AffyQCReport software (Gautier et al., 2004).

Background subtraction and normalization of probe set intensities was performed using the method of Robust Multiarray Analysis (RMA) described by Irizarry *et al.* (Irizarry et al., 2003). To identify differentially expressed genes, gene expression intensity was compared using an ANOVA test with a significance threshold < 0.001 and fold change of ≥ 1.5, and a Bayes smoothing approach developed for a low number of replicates (Smyth,

2004). False discovery rate (FDR) < 0.2 was used to adjust for multiple testing. This analysis was performed using the AffylmGUI Graphical User Interface for the LIMMA microarray package (Wettenhall et al., 2006), and Partek Genomics Suite (Partek Incorporated). All microarray data compliant with the MIAME guidelines (http://www.mged.org/) were deposited in the Gene Expression Omnibus (GEO) database (http://www.ncbi.nlm.nih.gov/geo/), Accession Number (to be determined after publication acceptance).

3.4.9. Real time quantitative RT-PCR (qRT-PCR)

Total RNA was isolated from spinal cords (exsanguinated) using the TRIzol method following the manufacturer's protocol (Life Technologies Inc.). RNA quantity and quality were assessed using the RNA 6000 Nano LabChip and Agilent Bioanalyzer 2100. First-strand cDNA synthesis was accomplished using 5 µg of isolated RNA in a reaction containing 200 U of SuperScript^{TM} III RNase H-Reverse Transcriptase (Life Technologies Inc.), 300 ng of oligo-dT18, 50 ng of random hexamers, 50 mM Tris-HCl pH 8.3, 75 mM KCl, 3 mM $MgCl^2$, 500 uM deoxynucleotides triphosphate, 5 mM dithiothreitol, and 40 U of Protector RNase inhibitor (Roche Diagnostics) in a final volume of 50 µl. The reaction was incubated at 25°C for 10 min and then at 50°C for 1 h, and a PCR purification kit (Qiagen) was used to purify cDNA (Life Technologies Inc.). Equal amounts of cDNA were amplified in duplicate in a final volume of 10 µl containing 5 µL of 2X LightCycler 480 SYBRGreen I Master (Roche Diagnostics), 0.5 µM of forward and reverse primers and 2 µL of cDNA (10 ng/µl). The primer pairs were: *Il1a*, 5'-acctgcaacaggaagtaaaatttga-3' and 5'-actgaacctgaccgtacactcctcccgacgagtaggc-3'; *Il1b*, 5'-actgaacctgaccgtacaaaatgccacctttgacagtgat-3' and 5'-cgtcaacttcaaagaacaggtcat-3'; *Tox3*, 5'-

cctttcagactctcagcgatcc-3' and 5'-ctggcggtactgtgacacttgt-3'; *18S*, 5'-actgaacctgaccgtacacggtacagtgaaactgcgaatg-3' and 5'-ccaaaggaaccataactgatttaatga-3'; and *Gapdh*, 5'-acgggaagctcactggcatgg-3' and 5'-atgcctgcttcaccaccttcttg-3'. The sequences chosen were selected to match only the intended gene using the GeneTools software (BioTools Inc.), and verified by BLAST analysis in GenBank. Amplification was performed using the LightCycler 480 (Roche Diagnostics) and the following conditions: 2 minutes at 50°C, 4 minutes at 95°C, followed by 45 cycles of 10 seconds at 95°C (denaturation), 10 seconds at 60°C (annealing), 12 seconds at 72°C (elongation), and 5 seconds at 74°C (reading). Amplification efficiencies were validated and normalized to *18S* or *Gapdh* and relative amounts of mRNA levels calculated using the standard curve method.

3.4.10. Behavioral analysis

Recovery of locomotor function after SCI was quantified in an open field using the Basso Mouse Scale (BMS), according to the method developed by Basso et al. (Basso et al., 2006). All behavioral analyses were done blind with respect to the identity of the animals.

3.4.11. Cell culture and transfection

The human oligodendrocyte cell line MO3.13 was obtained from Dr. Nathalie Arbour (Centre hospitalier de l'Université de Montréal, Montréal, QC, Canada). Cells were maintained in Dubelcco's modified Eagle's medium (DMEM) without sodium pyruvate (Life Technologies Inc.) supplemented with 10% fetal bovine serum (FBS), 1X penicillin-streptomycin (Pen-Srep) and L-glutamine (2mM). The pCMV6 vector into which was cloned the open reading frame of the human Tox3 transcript variant 1 fused to C-terminal c-Myc and DDK tags was purchased from OriGene (Cat. No. RC218824; OriGene Technologies

Inc.). Cells were plated 1 day prior to transfection at 30,000 cells/well (24-well plate) and transfected with 0.5 μg of DNA using lipofectamine 3000 (Life Technologies Inc.), according to the manufacturer's instructions. Cells were trypsinized 48h post-transfection and 750 μg/ml of G418 (Geneticin®; Life Technologies Inc.) was added to the media for selection. After 2 weeks of selection, cells were passaged and cultured in medium containing a reduced concentration of G418 (500 μg/ml).

3.4.12. Hypoxia and *in vitro* cytotoxic assay

To study the effect of TOX3 overexpression on cell survival, MO3.13 and TOX3-transfected MO3.13 cells were cultured in hypoxic conditions and cell viability measured using the XTT colorimetric assay (Roche Diagnostics), according to the manufacturer's instructions. In brief, cells were plated at a density of 25,000 cells per well in a 24-well-plate 1 day prior to the experiment. For normoxic conditions, cells were maintained in DMEM with FBS, Pen-Strep and L-glutamine, as previously described. For hypoxic conditions, cells were cultured in DMEM, without glucose, supplemented with FBS, Pen-Strep and L-glutamine. Hypoxic culture was performed in a sealed anaerobic chamber under vacuum to remove oxygen (5% CO_2). Normoxic and hypoxic conditions were maintained for 24 hours, after which cells were incubated for another 4 hours with the XTT reagent at culture conditions and absorbances measured at 490 and 690 nm (reference wavelenght) using the Infinite® 200 Pro multimode reader (Tecan Group Ltd.).

3.4.13. Immunoblotting

For quantification of protein levels, cells were plated at a density of 10,000 cells per cm^2 and grown for 2 days prior to protein extraction. Cells were then harvested, rinsed in PBS and

lysed for 30 minutes on ice in lysis buffer (20 mM HEPES pH 7.9, 300 mM KCl, 10% Glycerol, 0.1% NP-40, 1 mM DTT) containing a protease inhibitor cocktail (Sigma-Aldrich Canada Ltd.). The cell lysate was then centrifuged and the supernatant collected. Ten µg of proteins were boiled and electrophoresed on SDS-polyacrylamide gel, followed by blotting on PVDF membranes (PerkinElmer). Membranes were blocked for 1 hour with 5% dry milk in TBST buffer (50mM Tris-HCL pH 8.0, 150mM NaCl, 0.05% Tween-20) and then incubated overnight in 5% milk/TBST solution containing the rabbit anti-TOX3 antibody (1:500 dilution, Novus Biologicals Canada ULC). A mouse monoclonal anti-GAPDH antibody (1:5,000, Applied Biological Materials Inc.) was used as a protein loading control and internal standard. Membranes were incubated with secondary antibodies conjugated to horseradish peroxidase (1:2,500, Vector Laboratories Inc.) and cross-reactive bands visualized by chemiluminescence (PerkinElmer).

3.4.14. Statistical Analysis

Statistical evaluations were performed with one- or two-way ANOVA or repeated-measures ANOVA. Post-ANOVA comparisons were made using the Bonferroni correction. A student's t-test was performed for the statistical analysis of g-ratios and cell viability assay. All statistical analyses were performed using the GraphPad Prism software (GraphPad Software Inc.). A p value < 0.05 was considered as statistically significant.

3.5. Results

3.5.1. IL-1α protein expression in the injured spinal cord precedes IL-1β and is localized in microglia at the site of injury

Previous work has suggested that IL-1α released by cells undergoing necrosis could induce sterile inflammation (Chen et al., 2007; Cohen et al., 2010; Rider et al., 2011). We thus investigated whether IL-1α protein expression could be detected early in the injured mouse spinal cord by confocal IF microscopy. While no IL-1α expression was observed in the spinal cord of adult naïve (uninjured) mice, IL-1α immunostaining became detectable in cells of the spinal cord as early as 4 hours post-SCI, with the presence of 38 ± 6 cells at the lesion epicenter (Fig. 1a-b). This number had decreased to 15 ± 1 cells by 24 hours (Fig. 1a-b). At 4 hours post-SCI, IL-1α^+ cells were mainly found at the lesion epicenter and surrounding damaged areas. On very rare occasions, a few IL-1α^+ cells were found proximal or distal to the lesion site, while at 24 hours all IL-1α^+ cells were physically contained within the contusion site. It should be noted that most of them had a ramified morphology reminiscent of microglia (Fig. 1c-e). No IL-1α-positive (+) cells were seen at 1 hour or 3 days after injury (data not shown). In these experiments, immunostaining was performed using a polyclonal anti-IL-1α antibody directed against the N-terminal (AA 6-166) part of murine IL-1α, thus recognizing both the mature and precursor forms of the cytokine. This analysis revealed that the IL-1α protein was detected in the cell nucleus as well as in the cytoplasm (Fig. 1c-e).

Taking advantage of transgenic Cx3cr1-eGFP$^{+/-}$ mice in which the GFP reporter coding sequence is inserted in place of coding exons of the Cx3cr1 gene and is highly transcribed in microglia, we confirmed that the vast majority of IL-1α^+ cells colocalized with GFP-expressing cells following SCI, with an average colocalization percentage of 95 ± 1% at 4 hours (Fig. 1c-e). IL-1α^+ cells also colocalized with the myeloid cell marker CD11b and the microglia/macrophage marker Iba1. At 4 hours post-SCI, a time that precedes the entry of blood-derived macrophages, colocalization of the IL-1α protein with the Iba1 marker was

estimated to be 96 ± 1%, indicating that microglia is the main source of IL-1α early after the SCI.

To examine IL-1β production, we took advantage of p*Il1b*-DsRed transgenic mice in which the DsRed fluorescent protein gene is expressed under the control of the *Il1b* gene promoter (p*Il1b*). No DsRed expression was detected in the spinal cord of uninjured mice (data not shown). Time-course experiments showed that DsRed marker expression was almost completely absent at 4 hours, but increased thereafter to reach a peak at 24 hours post-SCI (Fig. 1f). As for IL-1α$^+$ cells, IL-1β-DsRed$^+$ cells localized almost exclusively within the lesion site. However, the morphological characteristics of these cells differed drastically, as IL-1α$^+$ cells were typically ramified and arborized, whereas IL-1β-DsRed$^+$ cells were round. As seen in Fig. 1g, DsRed$^+$ cells colocalized with 7/4-expressing cells (i.e. neutrophils and monocyte-derived M1 macrophages), but only in rare occasions with Iba1-expressing microglia. Taken together, these results indicate that microglia located as sites of SCI rapidly (< 4 hours) respond to injury by expressing IL-1α, and that neutrophils and M1 monocytes that infiltrate the lesion site starting at 6 hours further contribute to the IL-1 response by producing IL-1β.

3.5.2. Infiltration of neutrophils and proinflammatory "M1" macrophages is equally reduced in the injured spinal cord of IL-1α- and IL-1β-KO mice

To determine to what extent these cytokines are responsible for the early recruitment of innate immune cells at sites of injury, we quantified the number of neutrophils and monocyte-derived macrophages expressing the 7/4 antigen, which is specifically expressed at the surface of both cell populations, but not in resident microglia (de Rivero Vaccari et al., 2012).

At 12 h after SCI, 1123 ± 72 cells immunopositive for 7/4 were counted at the lesion epicenter in wild-type (WT) mice (Fig. 2a). This number was reduced by 69%, 58% and 79% in IL-1α-, IL-1β- and IL-1α/β-KO mice, respectively, with an average of 347 ± 79, 470 ± 45 and 237 ± 114 cells at the lesion epicenter. Similarly, the number of Ly6G$^+$ neutrophils was reduced by ~65%, 48% and 78% in IL-1α-, IL-1β- and IL-1α/β-KO mice, respectively, compared with WT animals (Fig. 2b). To validate immunohistochemical data, cells were

isolated from the spinal cord of contused mice at 12 hours and then characterized and quantified by flow cytometry based on their expression of the following cell-surface markers: CD45, CD11b, Ly6C, Ly6G, and F4/80. As shown in Fig. 2c-e, flow cytometry data confirmed the significantly reduced presence of neutrophils ($CD45^{hi}$ $CD11b^{+}$ $Ly6C^{+}$ $Ly6G^{+}$ $F4/80^{-}$) and monocyte-derived M1 macrophages ($CD45^{hi}$ $CD11b^{+}$ $Ly6C^{hi}$ $Ly6G^{-}$ $F4/80^{+}$) in SCI mice lacking IL-1α and/or IL-1β. The number of microglia ($CD45^{dim}$ $CD11b^{+}$ $Ly6C^{-}$ $Ly6G^{-}$ $F4/80^{+}$) did not significantly differ between groups (data not shown).

Altogether, these results suggest that cytokines of the IL-1 family are important regulators of the infiltration of innate immune cells of the granulomonocytic lineage after SCI.

3.5.3. Improved functional recovery and histopathological outcome in mice harboring deletion of the *Il1a* gene after SCI

Neuroinflammation is considered as one of the leading causes of secondary bystander damage in the injured spinal cord. Therefore, we next investigated whether the absence of the *Il1a* or *Il1b* gene affects neuropathology in SCI. Evaluation was performed in an open field using the 9-point BMS scale and the 11-point BMS subscore (Basso et al., 2006). Naïve IL-1α-KO, IL-1β-KO and WT mice all performed flawlessly and received perfect scores on the BMS and BMS subscore scales. The situation was however different after a moderate (50 kdyn) traumatic SCI. As shown in Fig. 3a, IL-1α- and IL-1β-KO mice recovered significantly better than WT mice at 1 and 3 days post-SCI. Unlike IL-1β-KO mice, IL-1α-KO performed significantly better than WT mice at 7 and 14 days as well. At day 14, more than 90% of IL-1α-KO were mostly coordinated and had parallel paw position at initial contact (score ≥ 7 on the BMS), compared to 0% and 10% in WT and IL-1β-KO mice, respectively. The average BMS subscore of IL-1α-KO mice was 8.3 ± 0.4 compared with 5.4 ± 0.3 for WT and 4.7 ± 0.6 for IL-1β-KO mice at 14 days post-SCI (Fig. 3b). The extent and reproducibility of the early locomotor recovery seen at day 1 post-SCI in IL-1α-KO mice compared with the other two groups is best demonstrated by a dot plot showing individual BMS scores of all mice included in the experiments (n=27 mice per group) (Fig. 3c). Importantly, we found that deficiency in IL-1β attenuates production of IL-1α, but not the opposite, in the normal and

injured spinal cord (Fig. 4). This raises the possibility that some of the effects seen in IL-1β-KO mice compared to WT may be due to a reduction in IL-1α production.

Strikingly, lesion volume was also reduced in IL-1α-KO mice compared to IL-1β-KO and WT mice at day 35 post-SCI as judged by GFAP immunostaining which delimits the lesion frontier (Fig. 3d). Together, these results suggest that deletion of the *Il1a* gene contributes to better functional recovery by reducing lesion volume after SCI.

3.5.4. Intrathecal antagonism of IL-1 receptor promotes early locomotor recovery after SCI

We postulated that blockade of the signaling receptor for IL-1α, IL-1r1, early after SCI would improve recovery and locomotor function. We therefore compared the effectiveness of the most widely used inhibitor of IL-1 signaling, anakinra (a recombinant formulation of the natural IL-1r1 antagonist), given through two different routes of administration (i.v. vs. i.t.). Remarkably, a single i.t. injection of anakinra given approximately 15 minutes after the injury was effective at reducing behavioural dysfunction (Fig. 3e-f). In contrast, repeated i.v. injections of anakinra post-SCI in C57BL/6 mice failed to improve functional recovery. These data support our evidence that IL-1α is centrally produced and exerts its effects in the vicinity of the SCI lesion. Furthermore, it strongly suggests that continuous i.t. infusion or repeated i.t. injections of anti-IL-1α therapies could be an efficient way to prevent cell death and functional loss after CNS insult.

3.5.5. Increased expression of Tox3 during spinal cord development and after adult SCI in IL-1α-KO mice

To investigate the mechanism by which IL-1α mediates its detrimental effect after traumatic SCI, we analyzed the transcriptome of the injured spinal cord of IL-1α-KO, IL-1β-KO and WT mice at 24 hours after injury using GeneChip microarrays. This time point was selected because it corresponds to the earliest time at which functional recovery was detected in IL-1α-KO mice compared to the other mouse lines. As expected, transcripts from genes involved in neuroinflammation were found to be differentially regulated in the two IL-1-KO mouse

lines compared to WT after SCI (data not shown). Surprisingly, this analysis also identified 18 genes differentially regulated in IL-1α-KO compared with IL-1β-KO and WT mice with no reported role in neuroinflammation (Table 1). Among those genes, the neuronal survival factor Tox3, a member of the high-mobility group box (HMGB) family of transcription factors that protects neurons from apoptotic cell death when overexpressed *in vitro* (Dittmer et al., 2011), figured prominently and was studied in greater detail.

We first confirmed using qRT-PCR that Tox3 is significantly upregulated in IL-1α-KO mice compared with IL-1β-KO and WT mice at 24 hours post-SCI, consistent with our microarray data (Fig. 5a-b). Using IF confocal microscopy, we observed that the Tox3 protein is weakly expressed in the spinal cord of WT mice under normal conditions. Nevertheless, co-staining of Tox3 with various makers of CNS cells, such as the neuronal marker NeuN and the mature oligodendrocyte marker CC1, revealed that the Tox3 signal is mainly localized in the nucleus of neurons and oligodendrocytes (Fig. 5c-d). Tox3 staining was also associated with $CD31^+$ endothelial cells, but the contribution of this cell population to the beneficial effect of IL-1α deficiency was ruled out by showing that endothelial cell survival and spinal microvascular perfusion are unaltered in IL-1α-KO mice after SCI (data not shown). Importantly, quantification of Tox3 immunostaining revealed that protein levels of the survival factor were markedly increased in the spinal cord of adult naïve IL-1α-KO mice compared with IL-1β-KO and WT mice (Fig. 5e). The overexpression concerned mainly neurons and oligodendrocytes, with an approximate 130% and 200% increase in signal intensity in these two cell types, respectively. This also translated into higher numbers of neurons and oligodendrocytes expressing Tox3 in the adult spinal cord of naïve IL-1α-KO mice (Fig. 5f). On average, we counted 151 ± 15 $NeuN^+$ $Tox3^+$ cells per section in the gray matter of IL-1α-KO mice compared to 59 ± 8 and 74 ± 8 in IL-1β-KO and WT mice, respectively. The same also applied to oligodendrocytes, for which we counted 242 ± 8 $CC1^+$ $Tox3^+$ cells per section in the white matter of naïve IL-1α-KO mice compared to 110 ± 16 and 98 ± 7 in IL-1β-KO and WT mice, respectively. The total numbers of $NeuN^+$ neurons and mature $CC1^+$ oligodendrocytes were similar between the three mouse strains under normal, uninjured conditions (data not shown). Importantly, deletion of IL-1 genes did not result in any differences in myelin thickness or axon calibre, as demonstrated by

measurements of g-ratios in the spinal cord AST and RST (Fig. 5g-j). As expected, g-ratios were positively correlated with axon diameter in both IL-1α/β-KO and C57BL/6 mice (Fig. 5i-j). Axons in the AST of IL-1α/β-KO mice had an average g-ratio of 0.67 compared to 0.65 in C57BL/6 mice, while axons in the RST had g-ratios of 0.69 and 0.68 in IL-1α/β-KO and C57BL/6 mice, respectively. Together, these results suggest that the absence of IL-1α could mediate protection of spinal cord neurons and/or oligodendrocytes by a mechanism distinct from its known inflammatory activities, potentially involving Tox3.

To determine whether Tox3 overexpression occurs during a specific period of CNS development or later during adulthood, we performed immunostaining for Tox3 and measured protein levels in the developing spinal cord of naïve IL-1α-KO, IL-1β-KO and WT mice. As shown in Fig. 6, Tox3 protein levels were increased in the spinal cord of IL-1α-KO mice compared with IL-1β-KO and WT mice during the postnatal period. Importantly, this overexpression translated into much higher numbers of $CC1^+$ oligodendrocytes expressing Tox3 in the spinal cord of naïve IL-1α-KO mice than the other two groups of mice from P10 up to P30 (Fig. 6a-b). At P10, we counted as many as 102 ± 30 $CC1^+$ $Tox3^+$ oligodendrocytes per cross-section in the spinal cord white matter of IL-1α-KO mice compared to only 4 ± 4 and 6 ± 4 in IL-1β-KO and WT mice, respectively. This represents a ~20- to 30-fold increase in the number of oligodendrocytes expressing Tox3 in response to deletion of the *Il1a* gene. Interestingly, IL-1α null spinal cords also contained increased numbers of mature oligodendrocytes at P10 (Fig. 6c). However, numbers of white matter $CC1^+$ cells returned to control levels by P18. In contrast, the total number of $NeuN^+$ neurons per cross-section remained similar in all three mouse lines at all time points investigated postnatally, despite seeing an increased number of $NeuN^+$ $Tox3^+$ neurons in IL-1α-KO mice compared to IL-1β-KO and C57BL/6 mice at P10 and a trend toward significance at P18 (data not shown). Together, these results suggest that IL-1α represses Tox3 in spinal cord oligodendrocytes during early postnatal development, at around P10, which corresponds to the beginning of the myelination process in the mouse spinal cord.

To confirm that IL-1α is normally produced during this developmental phase, we next measured mRNA levels for *Il1a* and *Il1b* in the spinal cord of C57BL/6 mice at various times postnatally (between P1 and P30) by real-time qRT-PCR. mRNA levels for *Il1a*, and to a

much lower extent *Il1b*, were found to be robustly increased between P10 and P18 (Fig. 6d). Taken together, our findings indicate that deletion of the *Il1a* gene promotes oligodendrocyte survival in the developing mouse spinal cord. It also raises the possibility that IL-1α inhibition may protect oligodendrocytes from secondary cell death after traumatic SCI in adult mice through upregulation of Tox3.

3.5.6. Oligodendrocytes from mice lacking IL-1α upregulate the survival factor Tox3 and are protected from SCI-induced death

To investigate whether Tox3 overexpression persists in adult spinal cord neurons and oligodendrocytes following injury, we next performed dual immunostaining for Tox3 and neuron- or oligodendrocyte-specific markers (Fig. 7a). Intriguingly, Tox3 overexpression in IL-1α-KO mice was maintained in oligodendrocytes but completely lost in neurons at 24 hours after SCI, thus suggesting that the former cell type is more likely to be protected from injury. To determine whether more neurons and oligodendrocytes were protected from SCI in IL-1α-KO mice, and whether Tox3-expressing neurons/oligodendrocytes were more likely to be protected from injury-induced death, we counted these cells in spinal cord sections spanning the entire rostro-caudal extent of the lesion (i.e., ~3 mm centered at the lesion epicenter). As expected, fewer $NeuN^+$ neurons and $CC1^+$ oligodendrocytes were detected in the injured compared with uninjured spinal cord, independently of the mouse line (data not shown). On average, the neuronal and oligodendroglial cell loss in IL-1β-KO and WT (C57BL/6) mice was estimated to be around 50% at 24 hours post-SCI. Importantly, the total numbers of $CC1^+$ oligodendrocytes, but not $NeuN^+$ neurons, were significantly higher (by more than 20%) in the injured spinal cord of IL-1α-KO mice at this time (Fig. 7b). In IL-1α-KO mice, a total of 2656 ± 210 neurons and 3283 ± 209 oligodendrocytes survived the injury compared to 2746 ± 186 and 2680 ± 135 in IL-1β-KO mice and 2759 ± 167 and 2707 ± 133 in WT mice. Another important observation is that 75% of the $CC1^+$ oligodendrocytes that overexpress Tox3 survived the injury in IL-1α-KO mice (Fig. 7c), while the survival rate of $CC1^+$ $Tox3^-$ oligodendrocytes was around 40% in these same animals (Fig. 7c). $CC1^+$ $Tox3^+$ oligodendrocytes normally account for 35% of the total number of $CC1^+$ oligodendrocytes in the uninjured spinal cord of IL-1α-KO mice. Importantly, the acute protection response of

oligodendrocytes resulting from *Il1a* gene deletion was maintained up to at least 14 days post-SCI, with a trend toward significance at day 35 (Fig. 7d). Collectively, these data suggest that Tox3 overexpression is protective in SCI and that $CC1^+$ $Tox3^+$ oligodendrocytes have a greater capacity to survive the hypoxic, ischemic and inflammatory conditions of the lesion.

3.5.7. TOX3 overexpression protects human oligodendrocytes from hypoxia-induced apoptotic cell death

Oligodendrocytes are essential to axon myelination as well as neuronal support in the CNS (Oluich et al., 2012). After SCI, a considerable amount of oligodendrocytes located close to the trauma are lost through apoptosis, in part due to the hypoxic-ischemic conditions (McTigue and Tripathi, 2008). The consequences of that cell death are the demyelination of multiple axons accompanied by the loss of axonal conduction, thus resulting in severe functional impairments in the acute phase of SCI. To further explore the role of Tox3 in oligodendrocyte survival, we next examined the effect of TOX3 overexpression in the human oligodendroglial cell line MO3.13. First, we established that human MO3.13 oligodendrocytes constitutively express the endogenous TOX3 protein (67.5 kDa) (Fig. 8a), and are therefore endowed with the necessary machinery to respond to this potential protective factor. TOX3 was then overexpressed in MO3.13 cells by transfection of a vector encoding human TOX3 fused to a Myc-DDK tag. Immunoblotting using the anti-TOX3 antibody confirmed overexpression of tagged-TOX3 (98 kDa) in the cell line and the unchanged expression of endogenous TOX3 (Fig. 8a-b). The molecular weights of the endogenous and tagged forms of the TOX3 protein are in agreement with those reported by Dittmer et al. (Dittmer et al., 2011). The oligodendrocyte cultures were next subjected to 24 hours of hypoxia and cell viability was evaluated using the XTT assay. Importantly, MO3.13 oligodendrocytes overexpressing TOX3 survived in greater numbers (63 ± 4%) than either GFP-transfected (44 ± 5%) or untransfected cells (41 ± 2%) (Fig. 8c), thus supporting again a protective effect of TOX3 overexpression against cell death.

Taken all together, our results indicate that IL-1α blockade protects oligodendrocytes against cell death after injury through a mechanism involving overexpression of the nuclear survival factor Tox3.

3.6. Discussion

In this study, we show that deletion of the *Il1a* gene in mice results in decreased lesion volume and improved functional outcome after SCI, an effect that we ascribe to an increased survival of oligodendrocytes in damaged areas. Our data indicate that IL-1α is rapidly produced by resident microglia after SCI, in line with a recent report from Luheshi *et al.* using an ischemic brain injury model in mice (Luheshi et al., 2011). Specifically, we found that IL-1α is produced and/or released at sites of trauma, and that IL-1α production by microglia precedes both the infiltration of blood-derived innate immune cells, which we found are the main cellular source of IL-1β, and secondary damage to oligodendrocytes. Importantly, the infiltration of neutrophils and monocyte-derived macrophages is severely compromised in the injured spinal cord of IL-1α-KO mice. Our results thus support the growing body of evidence that IL-1α is a damage-associated molecular pattern (DAMP) molecule released by stressed or dying cells, thus enabling the recruitment of innate immune cells (Chen et al., 2007; Eigenbrod et al., 2008). However, the loss of oligodendrocytes at sites of SCI appears to be independent of the infiltration of neutrophils and macrophages, as the recruitment of these two cell populations was equally reduced in both IL-1α- and IL-1β-KO mice despite the fact that IL-1α null mutants exhibited better locomotor recovery. Another key new finding of this study is the discovery that the survival factor Tox3 is overexpressed in oligodendrocytes as a result of deletion of the *Il1a* gene, and that this overexpression occurs during the early postnatal period and lasts for the lifetime of the IL-1α-KO mouse. Furthermore, oligodendrocytes overexpressing Tox3 in the spinal cord of IL-1α-KO mice survived better than those not expressing Tox3 (in these same animals), as well as those of IL-1β-KO and WT mice after SCI *in vivo*. Accordingly, *in vitro* data suggest that overexpression of the *TOX3* gene in human oligodendrocytes enhances cell survival under hypoxic conditions.

Cohen *et al.* have recently reported that IL-1α associates with the chromatin and is released with the cytoplasmic content as a result of necrotic cell death, but not apoptotic cell death, following which it stimulates myeloid cell recruitment (Cohen et al., 2010). Although our results indicate that IL-1α is released by microglia and initiates inflammation after SCI,

we do not know whether this inflammatory response mediates secondary (bystander) damage. Interestingly, the Allan group has recently shown that neutrophils acquire potentially neurotoxic properties upon transmigration across IL-1-stimulated blood-brain barrier (Allen et al., 2012). This particular study suggested that neurotoxicity could be mediated by the action of neutrophil-derived proteases that are released in association with decondensed DNA, referred to as neutrophil extracellular traps (NETs). In addition, monocyte-derived M1 macrophages identified by their production of proinflammatory mediators are present in the injured spinal cord and neurotoxic when co-cultured with primary neurons (Kigerl et al., 2009). A recent cell depletion study in SCI mice has further revealed that preventing the recruitment of both neutrophils and monocytes is beneficial for functional recovery (Lee et al., 2011). The evidence provided here, however, suggests that microglia rather than neutrophils and M1 macrophages are involved in the death of oligodendrocytes. Future studies will therefore be required to determine whether microglia or other immune cells which rapidly infiltrate sites of SCI in response to IL-1α are those that contribute to secondary tissue damage.

Pro-IL-1α and pro-IL-1β are expressed as 31-kDa polypeptides. Despite long-standing evidence that the precursor form of IL-1α is biologically active, in contrast to pro-IL-1β, recent studies have challenged this view by showing that pro-IL-1α has minimal activity, but its cleavage into a 17-kDa fragment by proteases such as calpain or granzyme B enhanced biological activity by up to 10-50 fold *in vitro* and *in vivo* (Afonina et al., 2011; Zheng et al., 2013). The processing and secretion of IL-1β is regulated by inflammasomes (Lamkanfi and Dixit, 2012), and we now know that this is also partially the case for IL-1α, at least in the context of exposition to microbial pathogen-associated molecular pattern (PAMP) molecules (Gross et al., 2012). Here, we show that IL-1α is rapidly (within 4 hours) produced by resident microglia after SCI, and that innate immune cells that are subsequently recruited from the blood into sites of injury further amplify inflammation by producing IL-1β. It remains unknown whether the effects of IL-1α on inflammation and secondary degeneration are mediated by the proform or mature form of the cytokine. Assuming the latter, it would of great interest to identify the mechanism involved in IL-1α maturation in the context of CNS injury, especially since inhibitors of specific inflammasomes, caspase-1 and calpain are currently being developed and tested in the clinic for other

indications/disorders (Pietsch et al., 2010; Dinarello, 2011; Lopez-Castejon and Pelegrin, 2012).

It is important to keep in mind that the IL-1β reporter mouse line has some limitations despite being a powerful tool to study IL-1β protein expression *in vivo*. One of these limitations is the slightly delayed kinetics of DsRed expression compared to IL-1β protein expression, with a lag time reported to be between 3-12 hours depending on the model (Matsushima et al., 2010). Another limitation is that the assessment of IL-1β protein production through visualization of DsRed can only be done during the induction phase of inflammation, because a certain level of fluorescence must be reached for cell detection and because the half-life and clearance of the two molecules could slightly differ. This and the fact that different species were used (rats versus mice) may explain why a previous study has shown that neurons are the earliest source of IL-1β (de Rivero Vaccari et al., 2008), whereas we failed to detect DsRed expression (i.e., IL-1β promoter activation) in these cells after SCI.

The most important conclusion that can be drawn from the comparison of IL-1α- and IL-1β-KO mice is that despite showing a similarly reduced inflammatory response after SCI, IL-1α-KO mice exhibited better recovery of locomotor abilities and had reduced lesion volume. This, combined with the early functional recovery seen at day 1 in IL-1α-KO mice, suggests that these mutant animals are protected from SCI-induced neurodegeneration rather than benefiting from improved regenerative abilities. It also suggests that the improved functional recovery in injured IL-1α-KO mice is unlikely to be mediated by innate immune cells recruited from the blood. Still, we cannot completely rule out the possibility that the absence of IL-1α or IL-1β could have differentially affected the expression of specific proinflammatory and cytotoxic effectors by the remaining immune cells recruited at the lesion site. However, it must be pointed out that our microarray study failed to detect significant changes in expression levels of inflammatory genes between the two IL-1 mouse strains at day 1 post-SCI.

We found that a single i.t., but not i.v., injection of anakinra given immediately after SCI improved locomotor recovery during the first week post-treatment. This suggests that the drug either does not cross the blood-spinal cord barrier after SCI, or does so only weakly.

Galea and colleagues have reported a slow passive penetration of anakinra into the CNS and a large variability in concentrations measured in cerebrospinal fluid (CSF) when injected i.v. at experimentally therapeutic concentrations (Galea et al., 2011). They estimated that only 1.6 ± 0.4% of i.v. administered anakinra crossed into the CSF of patients with subarachnoid haemorrhage. Anakinra levels were found to rapidly decrease in plasma following cessation of i.v. treatment (half-life of 33 ± 9 minutes). In contrast, anakinra was more stable in the CSF, with an estimated half-life of 238 minutes (Galea et al., 2011). Similarly, a rat imaging study reported a low uptake of radiolabelled IL-1ra in the normal brain because of the rapid metabolism and excretion of anakinra (Cawthorne et al., 2011). As our data imply, administering anakinra directly into the CSF, which irrigates the spinal cord parenchyma, rather than systemically, may prove to be more efficient therapeutically. Intrathecal drug delivery in patients with SCI is an achievable goal, as demonstrated by the anti-Nogo clinical trial (Zorner and Schwab, 2010). Another alternative to achieve experimentally therapeutic CSF concentrations might be to systemically inject a high loading dose followed by maintenance therapy. A randomized phase II study conducted in acute stroke patients showed that an i.v. bolus dose of 100 mg of recombinant human IL-1RA followed by continuous i.v. infusion at 2 mg/kg/h over 72 hours is safe and exhibited improved clinical outcome (Emsley et al., 2005). Whether a similar i.v. regimen in SCI mice would result in superior outcomes compared with the i.t. route remains to be investigated.

In contrast to the function of IL-1α, which remains uncertain, the role of IL-1β has been relatively well studied in the context of CNS injury (Allan and Rothwell, 2001; Allan et al., 2005). It has been proposed that IL-1 proteins have identical biological functions given that both cytokines bind and activate the same cell surface receptor, IL-1r1, although a role for IL-1r2 in the regulation of IL-1α activity post-necrosis has recently been highlighted (Zheng et al., 2013). Thus, it may come as a surprise that IL-1β-KO mice did not recover locomotor function to the extent of IL-1α-KO mice after SCI. This could suggest that IL-1α mediates CNS cell loss independently of IL-1r1, through a yet unidentified receptor. Interestingly, a novel isoform of the IL-1r1 accessory protein, IL-1racpb, containing a variant TIR domain and whose expression is restricted to CNS neurons has recently been implicated in neuroprotection in animal models of neuroinflammation (Smith et al., 2009). Nguyen *et al.* later reported that IL-1α-induced, but not IL-1β-induced, p38 phosphorylation is

significantly reduced in primary neuronal cultures from IL-1racpb-KO mice (Nguyen et al., 2011). This is convincing evidence that supports the idea that IL-1α has specific effects within the CNS. Here, we have extended this work by identifying 18 genes that are regulated by IL-1α, but not by IL-1β, and through the demonstration that IL-1α regulates oligodendrocyte survival after SCI. It is important to note that the study by Smith *et al.* assessed *Il1racpb* mRNA expression in purified neurons, microglia and astrocytes, but not in oligodendrocytes. It is therefore possible that IL-1α may exert its effects on oligodendrocytes through a receptor other than IL-1r1, such as IL-1racpb.

Our genome-wide transcriptome analysis identified 18 genes as significantly up- or down-regulated in IL-1α-KO mice compared with IL-1β-KO and WT mice, among which is the transcript coding for Tox3. Tox3 was recently shown to regulate Ca^{2+}-dependent transcription in neurons through interaction with the cAMP-response-element-binding protein (CREB) (Yuan et al., 2009). Dittmer *et al.* have since established that Tox3 is predominantly expressed in the CNS where it acts as a neuronal survival factor (Dittmer et al., 2011). It was demonstrated that Tox3 overexpression *in vitro* protects neurons from cell death via the upregulation of anti-apoptotic genes and downregulation of pro-apoptotic genes. Here, our data show the presence of almost 3 times more neurons and oligodendrocytes expressing Tox3 in the spinal cord of naïve IL-1α-KO mice compared to IL-1β-KO and WT mice, but this difference did not translate into an increased neuronal survival in IL-1α-KO mice at day 1 post-SCI. Instead, deletion of the *Il1a* gene distinctively induced the survival of mature oligodendrocytes after SCI. Recently, Miron *et al.* unveiled that alternatively-activated M2 microglia/macrophages are important for oligodendrocyte differentiation and CNS remyelination (Miron et al., 2013). It will be of interest in future work to determine whether the absence of IL-1α could induce a phenotypic switch in microglial polarization during the early developmental period, thus leading to gene expression changes in oligodendrocytes.

In summary, we have established that deletion of the *Il1a* gene provides protection of oligodendrocytes from SCI via a mechanism that involves overexpression of the survival factor Tox3. Therefore, we propose that central inhibition of IL-1α or overexpression of Tox3 during the early acute phase of a CNS insult may be an effective means for preventing loss

of neurological function in SCI, and may be extended to a variety of other acute injuries such as ischemia and traumatic brain injuries.

3.7. Acknowledgments

This study was supported by grants from Wings for Life Spinal Cord Research Foundation (Project number 48, Contract number WFL-CA-006/11) and the Canadian Institutes of Health Research (Grant number MOP-84558) to S.L. Salary support for D.B., Y.D. and S.L. was provided by the Fonds de la recherche en santé du Québec. We thank Nadia Fortin, Kanchan Bisht and Samuel Boisjoly-Villeneuve for their invaluable technical assistance and Dr. David Gosselin for his critical review of this manuscript.

3.8. References

Afonina IS, Tynan GA, Logue SE, Cullen SP, Bots M, Luthi AU, Reeves EP, McElvaney NG, Medema JP, Lavelle EC, Martin SJ (2011) Granzyme B-dependent proteolysis acts as a switch to enhance the proinflammatory activity of IL-1alpha. Mol Cell 44:265-278.

Albrecht PJ, Dahl JP, Stoltzfus OK, Levenson R, Levison SW (2002) Ciliary neurotrophic factor activates spinal cord astrocytes, stimulating their production and release of fibroblast growth factor-2, to increase motor neuron survival. Exp Neurol 173:46-62.

Albrecht PJ, Murtie JC, Ness JK, Redwine JM, Enterline JR, Armstrong RC, Levison SW (2003) Astrocytes produce CNTF during the remyelination phase of viral-induced spinal cord demyelination to stimulate FGF-2 production. Neurobiol Dis 13:89-101.

Allan SM, Rothwell NJ (2001) Cytokines and acute neurodegeneration. Nat Rev Neurosci 2:734-744.

Allan SM, Tyrrell PJ, Rothwell NJ (2005) Interleukin-1 and neuronal injury. Nat Rev Immunol 5:629-640.

Allen C, Thornton P, Denes A, McColl BW, Pierozynski A, Monestier M, Pinteaux E, Rothwell NJ, Allan SM (2012) Neutrophil cerebrovascular transmigration triggers rapid neurotoxicity through release of proteases associated with decondensed DNA. J Immunol 189:381-392.

Amankulor NM, Hambardzumyan D, Pyonteck SM, Becher OJ, Joyce JA, Holland EC (2009) Sonic hedgehog pathway activation is induced by acute brain injury and regulated by injury-related inflammation. J Neurosci 29:10299-10308.

Barrette B, Hebert MA, Filali M, Lafortune K, Vallieres N, Gowing G, Julien JP, Lacroix S (2008) Requirement of myeloid cells for axon regeneration. J Neurosci 28:9363-9376.

Basso DM, Fisher LC, Anderson AJ, Jakeman LB, McTigue DM, Popovich PG (2006) Basso Mouse Scale for locomotion detects differences in recovery after spinal cord injury in five common mouse strains. J Neurotrauma 23:635-659.

Bastien D, Lacroix S (2014) Cytokine pathways regulating glial and leukocyte function after spinal cord and peripheral nerve injury. Exp Neurol 258:62-77.

Basu A, Krady JK, O'Malley M, Styren SD, DeKosky ST, Levison SW (2002) The type 1 interleukin-1 receptor is essential for the efficient activation of microglia and the induction of multiple proinflammatory mediators in response to brain injury. J Neurosci 22:6071-6082.

Brambilla R, Hurtado A, Persaud T, Esham K, Pearse DD, Oudega M, Bethea JR (2009) Transgenic inhibition of astroglial NF-kappaB leads to increased axonal sparing and sprouting following spinal cord injury. J Neurochem 110:765-778.

Brambilla R, Bracchi-Ricard V, Hu WH, Frydel B, Bramwell A, Karmally S, Green EJ, Bethea JR (2005) Inhibition of astroglial nuclear factor kappaB reduces inflammation and improves functional recovery after spinal cord injury. J Exp Med 202:145-156.

Cawthorne C, Prenant C, Smigova A, Julyan P, Maroy R, Herholz K, Rothwell N, Boutin H (2011) Biodistribution, pharmacokinetics and metabolism of interleukin-1 receptor antagonist (IL-1RA) using [(1)(8)F]-IL1RA and PET imaging in rats. Br J Pharmacol 162:659-672.

Chen CJ, Kono H, Golenbock D, Reed G, Akira S, Rock KL (2007) Identification of a key pathway required for the sterile inflammatory response triggered by dying cells. Nat Med 13:851-856.

Cohen I, Rider P, Carmi Y, Braiman A, Dotan S, White MR, Voronov E, Martin MU, Dinarello CA, Apte RN (2010) Differential release of chromatin-bound IL-1alpha discriminates between necrotic and apoptotic cell death by the ability to induce sterile inflammation. Proc Natl Acad Sci U S A 107:2574-2579.

Davalos D, Grutzendler J, Yang G, Kim JV, Zuo Y, Jung S, Littman DR, Dustin ML, Gan WB (2005) ATP mediates rapid microglial response to local brain injury in vivo. Nat Neurosci 8:752-758.

David S, Lacroix S (2005) Role of the Immune Response in Tissue Damage and Repair in the Injured Spinal Cord. In: Clinical Neuroimmunology, Second edition Edition (Antel J, Birnbaum G, Hartung HP, Vincent A, eds), pp 53-63. New York: Oxford University press.

David S, Kroner A (2011) Repertoire of microglial and macrophage responses after spinal cord injury. Nat Rev Neurosci 12:388-399.

de Rivero Vaccari JP, Lotocki G, Marcillo AE, Dietrich WD, Keane RW (2008) A molecular platform in neurons regulates inflammation after spinal cord injury. J Neurosci 28:3404-3414.

de Rivero Vaccari JP, Bastien D, Yurcisin G, Pineau I, Dietrich WD, De Koninck Y, Keane RW, Lacroix S (2012) P2X4 receptors influence inflammasome activation following spinal cord injury. J Neurosci 32:3058-3066.

Dinarello CA (2011) Interleukin-1 in the pathogenesis and treatment of inflammatory diseases. Blood 117:3720-3732.

Dittmer S, Kovacs Z, Yuan SH, Siszler G, Kogl M, Summer H, Geerts A, Golz S, Shioda T, Methner A (2011) TOX3 is a neuronal survival factor that induces transcription depending on the presence of CITED1 or phosphorylated CREB in the transcriptionally active complex. J Cell Sci 124:252-260.

Eigenbrod T, Park JH, Harder J, Iwakura Y, Nunez G (2008) Cutting edge: critical role for mesothelial cells in necrosis-induced inflammation through the recognition of IL-1 alpha released from dying cells. J Immunol 181:8194-8198.

Emsley HC, Smith CJ, Georgiou RF, Vail A, Hopkins SJ, Rothwell NJ, Tyrrell PJ, Acute Stroke I (2005) A randomised phase II study of interleukin-1 receptor antagonist in acute stroke patients. J Neurol Neurosurg Psychiatry 76:1366-1372.

Faulkner JR, Herrmann JE, Woo MJ, Tansey KE, Doan NB, Sofroniew MV (2004) Reactive astrocytes protect tissue and preserve function after spinal cord injury. J Neurosci 24:2143-2155.

Fleming JC, Norenberg MD, Ramsay DA, Dekaban GA, Marcillo AE, Saenz AD, Pasquale-Styles M, Dietrich WD, Weaver LC (2006) The cellular inflammatory response in human spinal cords after injury. Brain 129:3249-3269.

Galea J, Ogungbenro K, Hulme S, Greenhalgh A, Aarons L, Scarth S, Hutchinson P, Grainger S, King A, Hopkins SJ, Rothwell N, Tyrrell P (2011) Intravenous anakinra can achieve experimentally effective concentrations in the central nervous system within a therapeutic time window: results of a dose-ranging study. J Cereb Blood Flow Metab 31:439-447.

Gautier L, Cope L, Bolstad BM, Irizarry RA (2004) affy--analysis of Affymetrix GeneChip data at the probe level. Bioinformatics 20:307-315.

Gross O, Yazdi AS, Thomas CJ, Masin M, Heinz LX, Guarda G, Quadroni M, Drexler SK, Tschopp J (2012) Inflammasome activators induce interleukin-1alpha secretion via distinct pathways with differential requirement for the protease function of caspase-1. Immunity 36:388-400.

Herx LM, Rivest S, Yong VW (2000) Central nervous system-initiated inflammation and neurotrophism in trauma: IL-1 beta is required for the production of ciliary neurotrophic factor. J Immunol 165:2232-2239.

Horai R, Asano M, Sudo K, Kanuka H, Suzuki M, Nishihara M, Takahashi M, Iwakura Y (1998) Production of mice deficient in genes for interleukin (IL)-1alpha, IL-1beta, IL-1alpha/beta, and IL-1 receptor antagonist shows that IL-1beta is crucial in turpentine-induced fever development and glucocorticoid secretion. J Exp Med 187:1463-1475.

Irizarry RA, Hobbs B, Collin F, Beazer-Barclay YD, Antonellis KJ, Scherf U, Speed TP (2003) Exploration, normalization, and summaries of high density oligonucleotide array probe level data. Biostatistics 4:249-264.

Kigerl KA, Gensel JC, Ankeny DP, Alexander JK, Donnelly DJ, Popovich PG (2009) Identification of two distinct macrophage subsets with divergent effects causing either neurotoxicity or regeneration in the injured mouse spinal cord. J Neurosci 29:13435-13444.

Kono H, Karmarkar D, Iwakura Y, Rock KL (2010) Identification of the Cellular Sensor That Stimulates the Inflammatory Response to Sterile Cell Death. J Immunol.

Lamkanfi M, Dixit VM (2012) Inflammasomes and their roles in health and disease. Annu Rev Cell Dev Biol 28:137-161.

Lee SM, Rosen S, Weinstein P, van Rooijen N, Noble-Haeusslein LJ (2011) Prevention of both neutrophil and monocyte recruitment promotes recovery after spinal cord injury. J Neurotrauma 28:1893-1907.

Lopez-Castejon G, Pelegrin P (2012) Current status of inflammasome blockers as anti-inflammatory drugs. Expert opinion on investigational drugs 21:995-1007.

Luheshi NM, Kovacs KJ, Lopez-Castejon G, Brough D, Denes A (2011) Interleukin-1alpha expression precedes IL-1beta after ischemic brain injury and is localised to areas of focal neuronal loss and penumbral tissues. J Neuroinflammation 8:186.

Mason JL, Suzuki K, Chaplin DD, Matsushima GK (2001) Interleukin-1beta promotes repair of the CNS. J Neurosci 21:7046-7052.

Matsushima H, Ogawa Y, Miyazaki T, Tanaka H, Nishibu A, Takashima A (2010) Intravital imaging of IL-1beta production in skin. J Invest Dermatol 130:1571-1580.

McTigue DM, Tripathi RB (2008) The life, death, and replacement of oligodendrocytes in the adult CNS. J Neurochem 107:1-19.

Miron VE, Boyd A, Zhao JW, Yuen TJ, Ruckh JM, Shadrach JL, van Wijngaarden P, Wagers AJ, Williams A, Franklin RJ, ffrench-Constant C (2013) M2 microglia and macrophages drive oligodendrocyte differentiation during CNS remyelination. Nat Neurosci 16:1211-1218.

Nadeau S, Filali M, Zhang J, Kerr BJ, Rivest S, Soulet D, Iwakura Y, de Rivero Vaccari JP, Keane RW, Lacroix S (2011) Functional Recovery after Peripheral Nerve Injury is Dependent on the Pro-Inflammatory Cytokines IL-1{beta} and TNF: Implications for Neuropathic Pain. J Neurosci 31:12533-12542.

Nguyen L, Rothwell NJ, Pinteaux E, Boutin H (2011) Contribution of interleukin-1 receptor accessory protein B to interleukin-1 actions in neuronal cells. Neurosignals 19:222-230.

Oluich LJ, Stratton JA, Xing YL, Ng SW, Cate HS, Sah P, Windels F, Kilpatrick TJ, Merson TD (2012) Targeted ablation of oligodendrocytes induces axonal pathology independent of overt demyelination. J Neurosci 32:8317-8330.

Pietsch M, Chua KC, Abell AD (2010) Calpains: attractive targets for the development of synthetic inhibitors. Curr Top Med Chem 10:270-293.

Pineau I, Lacroix S (2007) Proinflammatory cytokine synthesis in the injured mouse spinal cord: Multiphasic expression pattern and identification of the cell types involved. J Comp Neurol 500:267-285.

Pineau I, Libo S, Bastien D, Lacroix S (2010) Astrocytes initiate inflammation in the injured mouse spinal cord by promoting the entry of neutrophils and inflammatory monocytes in an IL-1 receptor/MyD88-dependent fashion. Brain Behav Immun 24:540-553.

Plemel JR, Wee Yong V, Stirling DP (2014) Immune modulatory therapies for spinal cord injury - past, present and future. Exp Neurol 258:91-104.

Rider P, Carmi Y, Guttman O, Braiman A, Cohen I, Voronov E, White MR, Dinarello CA, Apte RN (2011) IL-1{alpha} and IL-1{beta} Recruit Different Myeloid Cells and Promote Different Stages of Sterile Inflammation. J Immunol 187:4835-4843.

Rosas M, Thomas B, Stacey M, Gordon S, Taylor PR (2010) The myeloid 7/4-antigen defines recently generated inflammatory macrophages and is synonymous with Ly-6B. J Leukoc Biol 88:169-180.

Shechter R, London A, Varol C, Raposo C, Cusimano M, Yovel G, Rolls A, Mack M, Pluchino S, Martino G, Jung S, Schwartz M (2009) Infiltrating blood-derived macrophages are vital cells playing an anti-inflammatory role in recovery from spinal cord injury in mice. PLoS Med 6:e1000113.

Smith DE, Lipsky BP, Russell C, Ketchem RR, Kirchner J, Hensley K, Huang Y, Friedman WJ, Boissonneault V, Plante MM, Rivest S, Sims JE (2009) A central nervous system-restricted isoform of the interleukin-1 receptor accessory protein modulates neuronal responses to interleukin-1. Immunity 30:817-831.

Smyth GK (2004) Linear models and empirical bayes methods for assessing differential expression in microarray experiments. Stat Appl Genet Mol Biol 3:Article3.

Sofroniew MV (2009) Molecular dissection of reactive astrogliosis and glial scar formation. Trends Neurosci 32:638-647.

Stirling DP, Yong VW (2008) Dynamics of the inflammatory response after murine spinal cord injury revealed by flow cytometry. J Neurosci Res 86:1944-1958.

Stirling DP, Liu S, Kubes P, Yong VW (2009) Depletion of Ly6G/Gr-1 leukocytes after spinal cord injury in mice alters wound healing and worsens neurological outcome. J Neurosci 29:753-764.

Thawer SG, Mawhinney L, Chadwick K, de Chickera SN, Weaver LC, Brown A, Dekaban GA (2013) Temporal changes in monocyte and macrophage subsets and microglial macrophages following spinal cord injury in the lys-egfp-ki mouse model. J Neuroimmunol 261:7-20.

Tremblay ME, Riad M, Majewska A (2010) Preparation of mouse brain tissue for immunoelectron microscopy. Journal of visualized experiments : JoVE.

Wettenhall JM, Simpson KM, Satterley K, Smyth GK (2006) affylmGUI: a graphical user interface for linear modeling of single channel microarray data. Bioinformatics 22:897-899.

Yuan SH, Qiu Z, Ghosh A (2009) TOX3 regulates calcium-dependent transcription in neurons. Proc Natl Acad Sci U S A 106:2909-2914.

Zheng Y, Humphry M, Maguire JJ, Bennett MR, Clarke MC (2013) Intracellular interleukin-1 receptor 2 binding prevents cleavage and activity of interleukin-1alpha, controlling necrosis-induced sterile inflammation. Immunity 38:285-295.

Zorner B, Schwab ME (2010) Anti-Nogo on the go: from animal models to a clinical trial. Ann N Y Acad Sci 1198 Suppl 1:E22-34.

3.9. Figures

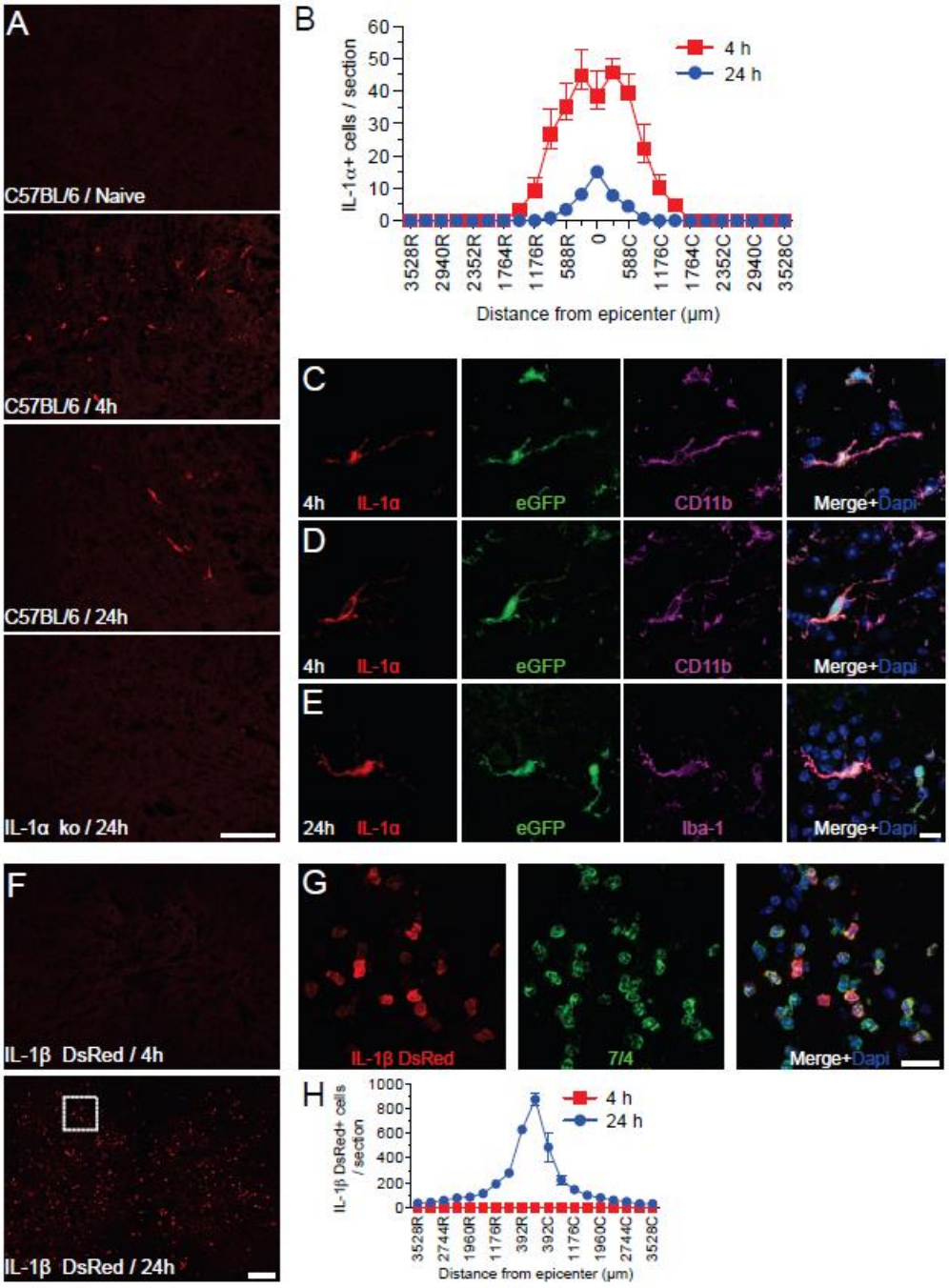

Figure 3.1. IL-1α protein expression in the injured spinal cord precedes IL-1β and is localized in microglia at the site of injury.

(a) Representative confocal photomicrographs showing IL-1α immunostaining (red) in the spinal cord of naïve and injured C57BL/6 mice at 4 and 24 hours (h) post-SCI (n=6-9 mice/time). Note that no

IL-1α signal was detected in the injured spinal cord of IL-1α-KO mice, thus confirming antibody specificity. (b) Quantification of IL-1α+ cells in spinal cord sections taken both rostral (R) and caudal (C) to the lesion epicenter at 4 and 24 h post-SCI. (c-e) Confocal photomicrographs showing co-localization of the IL-1α protein (red) with the myeloid cell marker CD11b (c-d, purple) and the microglial/macrophage markers Iba1 (e, purple) and Cx3cr1-eGFP (eGFP, green cells in panels c-e). The nuclear staining DAPI is shown in blue. Also shown is the percentage of IL-1α+ cells that express the microglia/macrophage markers Iba1 and Cx3cr1-eGFP. (f) Imaging of IL-1β-producing cells (red cells) in the injured spinal cord of pIl1b-DsRed transgenic mice at 4 and 24 h post-SCI. In these transgenic mice, the DsRed fluorescent reporter is expressed under the control of the Il1b gene promoter. (g) Confocal photomicrographs showing the co-localization of DsRed+ cells (red) with 7/4-expressing cells (green). (h) Quantification of DsRed+ cells in spinal cord sections taken both rostral (R) and caudal (C) to the lesion epicenter at 4 and 24 h post-SCI (n=3 mice/time). Scale bars: a, 100 µm; c-e (in e), 10 µm; f, 100 µm; g, 20 µm.

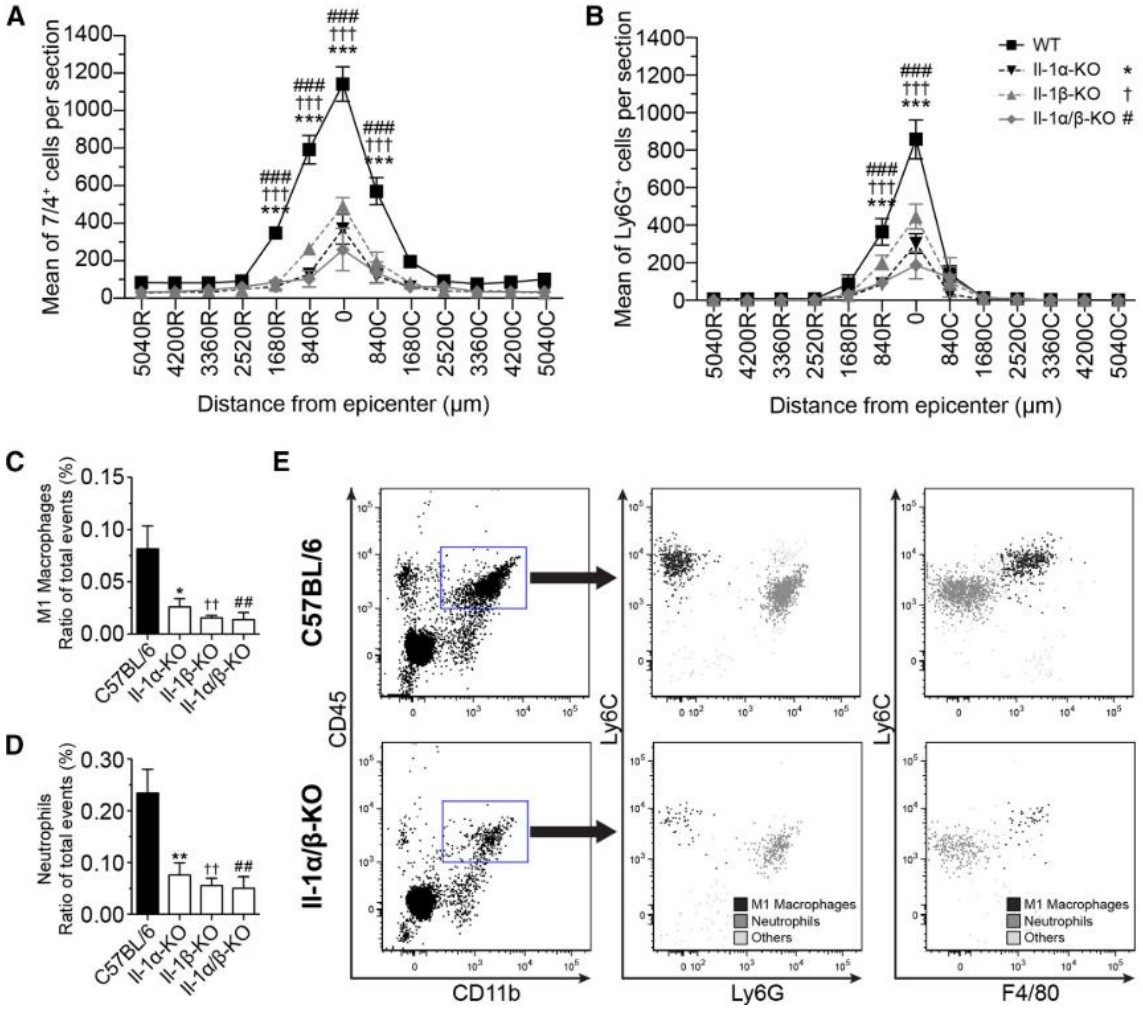

Figure 3.2. IL-1 deficiency reduces neutrophil and M1 monocyte infiltration in the injured spinal cord

(**a-b**) Quantification of the number of neutrophils and proinflammatory M1 macrophages, as visualized by 7/4 (**a**) and Ly6G (**b**) immunostaining, at various rostral (R) and caudal (C) distances from the lesion epicenter at 12 h after SCI (n=4-12 mice/group). (**c-d**) Quantification of the proportions of M1 macrophages (**c**) and neutrophils (**d**) relative to total events in KO and WT (C57BL/6) mice at 12 h after SCI. (**e**) Representative flow cytometry profiles showing the presence of neutrophils (black dots; $CD45^{hi}$ $CD11b^{+}$ $Ly6C^{+}$ $Ly6G^{+}$) and monocyte-derived M1 macrophages (dark gray dots; $CD45^{hi}$ $CD11b^{+}$ $Ly6C^{hi}$ $Ly6G^{-}$) in the spinal cord of a C57BL/6 and IL-1α/β-KO mouse at 12 h after SCI (date are representative of n= 4 mice). *, †, # $p < 0.05$; **, ††, ## $p < 0.01$; and ***, †††, ### $p < 0.001$, significant difference between KO and WT mice. Two-way repeated-measures ANOVA with Bonferroni's post-hoc test.

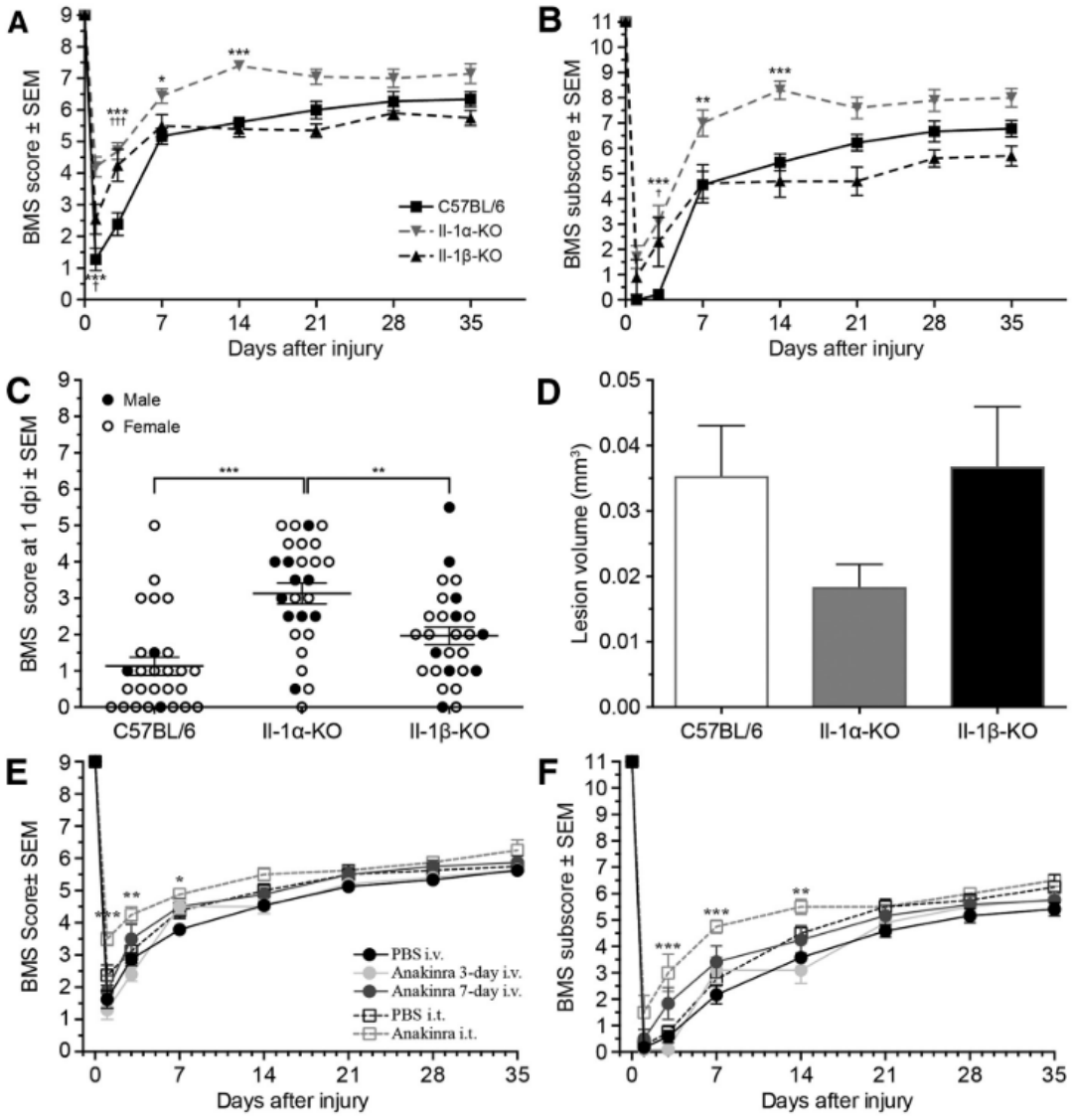

Figure 3.3. Recovery of locomotor function and spinal cord lesion volume are improved as a result of genetic or pharmacological IL-1α inhibition

(a-b) Locomotor function was assessed using the Basso mouse scale (BMS) (a) and BMS subscore (b) over a 35-day period after SCI (n= 8-10 mice per group). (c) Dot plot showing BMS scores assigned to individual mice of each mouse line at 1 day post-SCI (dpi) across all experiments performed (n = 27 mice per group). Males are shown in black filled circles and females in empty white circles. (d) IL-1α-KO mice had reduced spinal cord tissue damage at 35 days after injury (n= 8-10 per group). (e-f) Assessment of functional recovery using the BMS (e) and BMS subscore (f) showed that intrathecal (i.t.), but not intravenous (i.v.), anakinra treatment improves locomotion after SCI. Mice that received a single i.t. infusion

of the IL-1 receptor antagonist anakinra (33 mg/kg) had significantly higher BMS scores and subscores than those treated with anakinra i.v. (100 mg/kg) or PBS. Data are expressed as means ± SEM. *, † $p < 0.05$; **, †† $p < 0.01$; and ***, ††† $p < 0.001$. The analysis of variance was performed using two-way repeated-measures (a-b, e-f) or one-way (c-d) ANOVA followed by Bonferroni's *post-hoc* test.

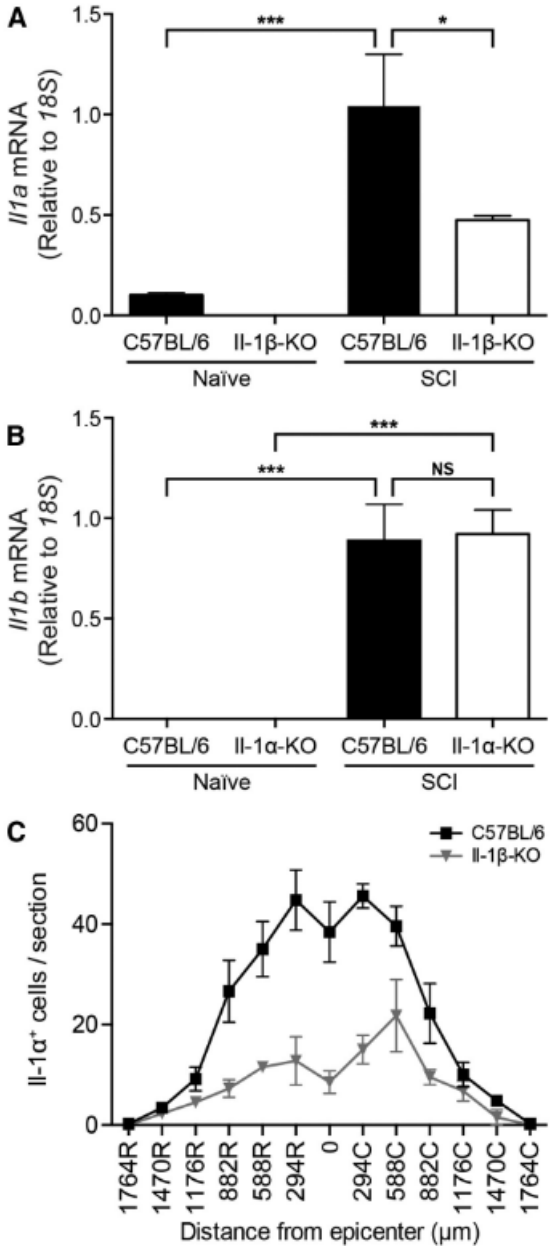

Figure 3.4. IL-1β-KO mice have reduced Il-1α levels in their spinal cord compared to WT mice, whereas IL-1α-KO mice express IL-1β normally

Analyses were performed on IL-1α and IL-1β single knockout animals to ascertain whether each of these genes could compensate for loss of the other under both naïve and injury conditions. (a-b) Quantitative real time RT-PCR (qRT-PCR) analysis shows decreased expression of *Il1a* mRNA in IL-1β-KO mice, while no changes in *Il1b* mRNA levels were detected in IL-1β-KO mice at day 1 post-SCI. The results were normalized to *18S* mRNA levels. (c) Quantification of IL-1α^+ cells in spinal cord sections taken both rostral (R) and caudal (C) to the lesion epicenter at 4 hours post-SCI in WT and IL-1β-KO mice. Data are expressed as means ± SEM. ***$p < 0.001$, *$p < 0.05$; one-way ANOVA with Bonferroni's post-hoc test.

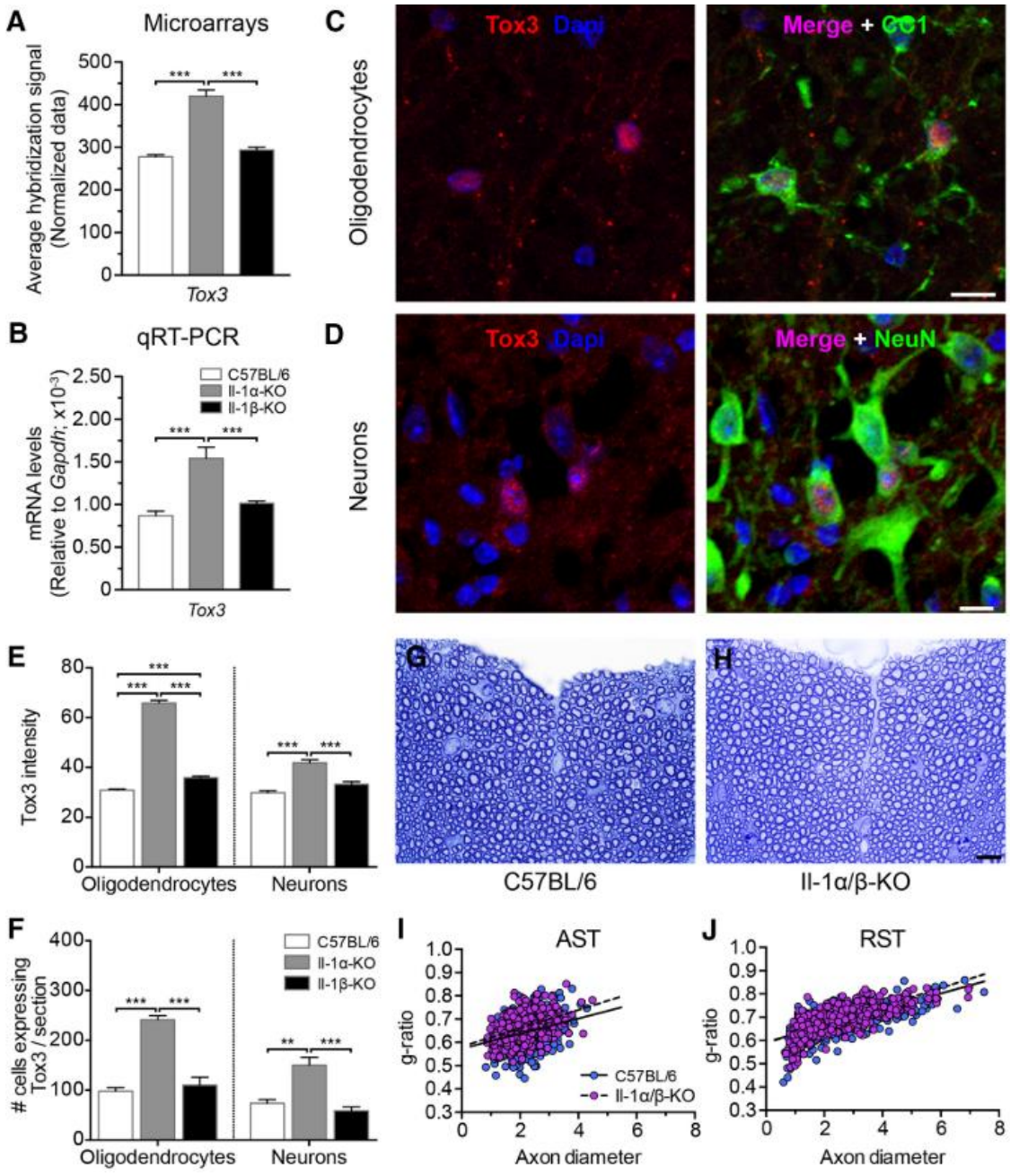

Figure 3.5. Expression of the survival factor Tox3 is increased in the injured spinal cord of IL-1α-KO mice

(a) Microarray analysis of gene expression shows that *Tox3* mRNA is differentially expressed (i.e. upregulated) in the spinal cord of IL-1α-KO mice compared with IL-1β-KO and C57BL/6 mice at day 1 post-SCI. Data are expressed as an average microarray hybridization signal (n = 4 mice per group). Normalization of probe set intensities was performed using the method of Robust Multiarray Analysis (RMA). (b) Quantitative real time RT-PCR (qRT-PCR) analysis confirms increased expression of *Tox3* in the injured spinal cord of IL-1α-KO at day 1 post-SCI. Data are expressed as a

ratio to *Gapdh* mRNA levels. (c-d) Confocal photomicrographs showing Tox3 immunostaining (red) in the spinal cord of a naïve C57BL/6 mouse. Note that the Tox3 protein is weakly expressed and localized specifically in the nucleus of oligodendrocytes ($CC1^+$, green cells in the upper right panel) and neurons ($NeuN^+$, green cells in the lower right panel) in adult C57BL/6 mice. The nuclear staining DAPI is shown in blue and the right-most panels are an overlay of the three colors. (e) Quantification of Tox3 immunostaining intensity in spinal cord oligodendrocytes and neurons of adult naïve mice from the three strains. (f) Quantification of the total number of $CC1^+$ oligodendrocytes and $NeuN^+$ neurons expressing Tox3 in the spinal cord white and gray matter, respectively, of naïve mice. (g-h) Representative high-magnification photomicrographs showing toluidine blue-stained semi-thin sections prepared from the spinal cord of adult naïve IL-1α/β-KO and C57BL/6 mice. The dorsal ascending sensory tract is shown in both images. (i-j) Scatter plots showing g-ratios as a function of axon diameter for naïve IL-1α/β-KO and C57BL/6 mice. G-ratios measurements were performed in the ascending sensory tract (AST) of the dorsal column (i) and lateral descending rubrospinal tract (RST, j) (200 axons/mouse; n = 5 mice per group). All data are expressed as means ± SEM. ***$p < 0.001$, **$p < 0.01$, *$p < 0.05$; one-way ANOVA with Bonferroni's post-hoc test. Scale bars: c-d, 10 µm; g-h (in h), 10 µm.

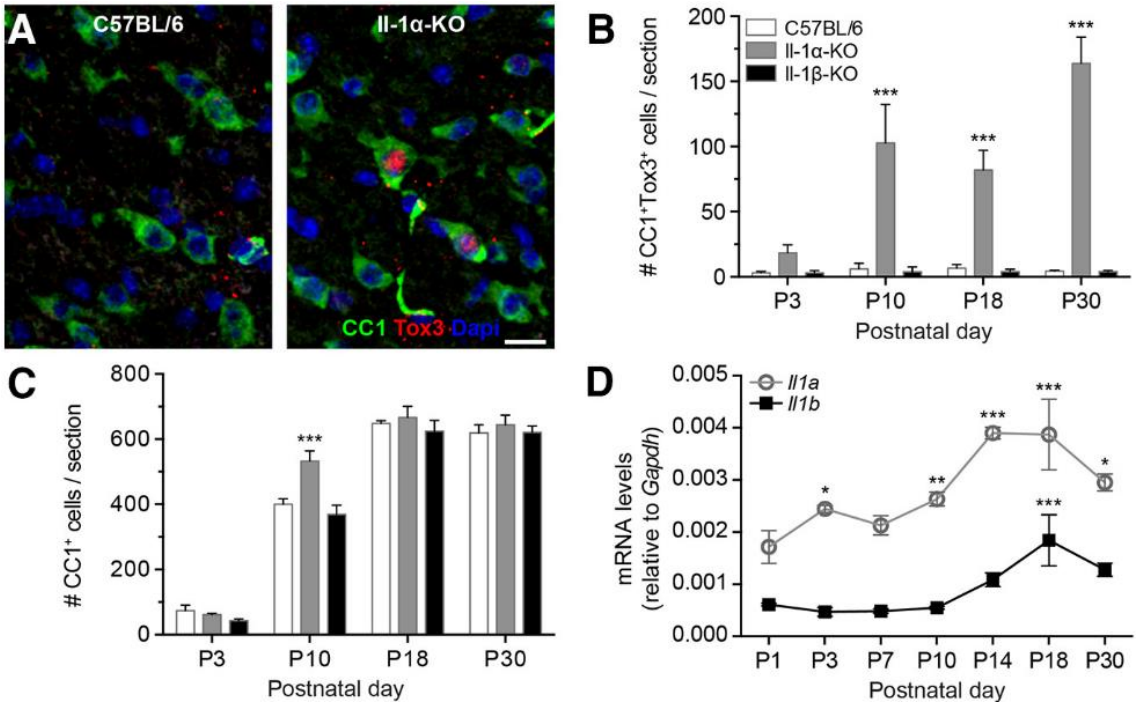

Figure 3.6. Tox3 overexpression in oligodendrocytes of IL-1α-KO mice occurs during spinal cord development

(a) Confocal photomicrographs showing the presence of Tox3 immunostaining (red) in spinal cord white matter oligodendrocytes ($CC1^+$ cells, green) of neonatal naïve IL-1α-KO mice, but not C57BL/6 mice, at postnatal day (P) 10. The nuclear staining DAPI is shown in blue. (b-c) Quantification of the total numbers of $CC1^+$ $Tox3^+$ (b) and $CC1^+$ (c) oligodendrocytes in the spinal cord white matter of IL-1α-KO, IL-1β-KO and C57BL/6 mice at P3, P10, P18 and P30. (d) Quantitative real time RT-PCR analysis confirms increased expression of *Il1a* mRNA, and to a lower degree *Il1b* mRNA, in the spinal cord of WT mice during the postnatal development period, at times that coincide with Tox3 overexpression in IL-1α-KO mice. Quantitative RT-PCR data are expressed as a ratio to *Gapdh* mRNA levels. ***$p < 0.001$, **$p < 0.01$, *$p < 0.05$; compared to both C57BL/6 and IL-1β-KO mice (b-c) or P1 mice (d), two-way ANOVA with Bonferroni's post-hoc test. Scale bar: a, 25 µm.

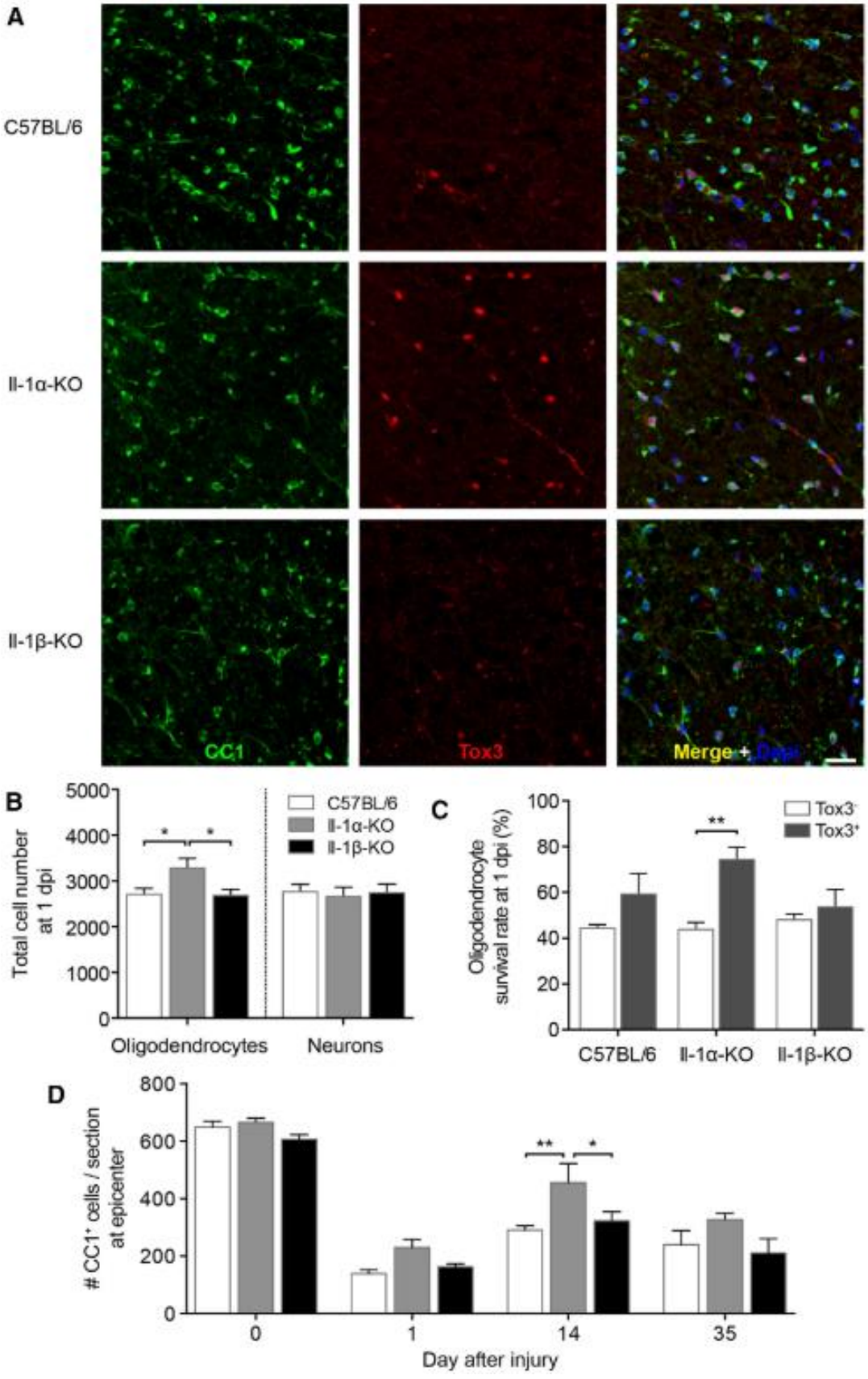
A
C57BL/6
Il-1α-KO
Il-1β-KO
CC1
Tox3
Merge + Dapi
B
Total cell number at 1 dpi
5000
4000
3000
2000
1000
0
C57BL/6
Il-1α-KO
Il-1β-KO
Oligodendrocytes
Neurons
C
Oligodendrocyte survival rate at 1 dpi (%)
100
80
60
40
20
0
Tox3⁻
Tox3⁺
C57BL/6
Il-1α-KO
Il-1β-KO
D
CC1⁺ cells / section at epicenter
800
600
400
200
0
0
1
14
35
Day after injury

Figure 3.7. IL-1α deficiency upregulates expression of the survival factor Tox3 in oligodendrocytes and protects these cells from death after SCI

(a) Representative confocal photomicrographs showing CC1 (green) and Tox3 (red) immunostainings in the injured spinal cord of C57BL/6 mice as well as IL-1α- and IL-1β-KO mice at 1 day post-injury (dpi). (b) Quantification of the total number of $CC1^+$ oligodendrocytes and $NeuN^+$ neurons in spinal cord sections spanning the entire rostro-caudal extent of the lesion (i.e. ~3 mm centered at the lesion epicenter) at 1 dpi. (c) Percentage of spinal cord white matter $CC1^+$ oligodendrocytes that survived the injury in relation to their expression of Tox3 for the three strains at 1 dpi. (d) Quantification of the total number of $CC1^+$ oligodendrocytes in the white matter of the spinal cord cross-section located at the lesion epicenter for all three mouse lines at 1, 14 and 35 dpi. Data in b-d are expressed as means ± SEM. ***$p < 0.001$, **$p < 0.01$, *$p < 0.05$. The analysis of variance was performed using a one-way (b-c) or two-way (d) ANOVA followed by Bonferroni's *post-hoc* test. Scale bar: a, 10 µm.

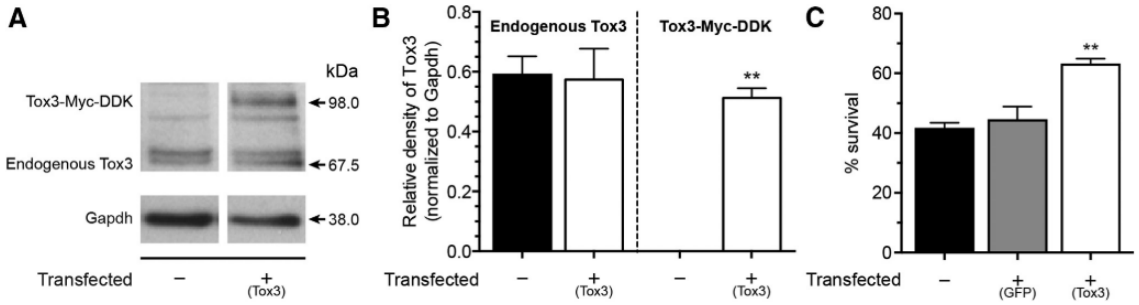

Figure 3.8. TOX3 overexpression protects human oligodendrocytes from hypoxia-induced cell death

(a) Immunoblotting using the anti-TOX3 antibody confirmed the presence of endogenous TOX3 (67.5 kDa) in untransfected and transfected human oligodendrocytes (MO3.13 cell line), as well as overexpression of TOX3-Myc-DDK (98 kDa) in stably transfected cells only. (b) Quantification of relative density of endogenous and tagged-TOX3 in untransfected and transfected MO3.13 cells. (c) Oligodendrocyte cultures were subjected to 24 hours of hypoxia and cell viability quantified using the XTT assay. Note that MO3.13 oligodendrocytes overexpressing TOX3 survived in greater numbers than untransfected cells. Data are expressed as means ± SEM. ** $p < 0.01$, *$p < 0.05$, compared with untransfected cells using a Student's t-test.

3.10. Tables

Gene name	Gene symbol	C57BL/6 Mean	C57BL/6 SD	Il-Lα-K0 Mean	Il-Lα-K0 SD	Il-Lα-K0 FC	Il-Lβ-K0 Mean	Il-Lβ-K0 SD	Il-Lβ-K0 FC
Short coiled-coil protein	Scoc	432.25	37.66	120.40	11.33	−3.59	408.36	14.52	−1.06
WD repeat and FYVE domain containing 1	Wdfy1	370.99	14.16	210.17	11.39	−1.77	370.91	21.73	−1.00
Phosphatidylserine decarboxylase, pseudogene 1	Pisd-ps1	883.29	122.76	556.31	39.28	−1.59	754.47	79.99	−1.17
RIKEN cDNA 4933436C20 gene	4933436C20Rik	163.97	11.31	108.85	6.72	−1.51	162.18	18.34	−1.01
ZNRD1 antisense RNA	Znrd1as	167.69	5.37	112.35	26.74	−1.49	190.08	14.97	1.13
ELMO domain containing 2	Elmod2	397.21	27.63	281.37	21.82	−1.41	395.99	15.78	−1.00
tRNA methyltransferase 6 homolog (*Saccharomyces cerevisiae*)	Trmt6	342.95	17.67	244.66	18.48	−1.40	331.38	33.56	−1.03
Methylthioribose-1-phosphate isomerase homolog (*S. cerevisiae*)	Mri1	343.01	24.14	258.44	6.92	−1.33	358.50	21.88	1.05
Growth arrest and DNA damage-inducible, γ interaction	Gadd45gip1	618.37	21.73	468.26	19.69	−1.32	630.84	15.87	1.02
G-protein-coupled receptor 34	Gpr34	61.08	7.96	76.42	5.80	1.25	60.86	4.34	−1.00
Coenzyme Q9 homolog (yeast)	Coq9	791.47	54.76	1089.57	55.82	1.38	802.91	43.05	1.01
Hydroxysteroid 11-β dehydrogenase 1	Hsd11b1	189.43	7.38	261.01	21.76	1.38	211.42	17.90	1.12
X-linked lymphocyte-regulated 3A	Xlr3a	60.63	9.09	89.50	10.82	1.48	61.51	6.70	1.01
X-linked lymphocyte-regulated 3C	Xlr3c	51.28	4.89	76.46	10.82	1.49	54.50	4.49	1.06
TOX high-mobility group box family member 3	Tox3	277.95	10.26	419.95	32.27	1.51	294.00	13.58	1.06
Ectonucleoside triphosphate diphosphohydrolase	Entpd4	1088.09	36.67	1770.74	37.56	1.63	1151.26	51.17	1.06
X-linked lymphocyte-regulated 3B	Xlr3b	42.24	3.92	70.96	12.43	1.68	46.81	5.98	1.11
Predicted gene 10002	Gm10002	23.45	0.45	102.69	8.83	4.38	23.35	1.24	−1.00

Affymetrix GeneChip microarrays were used to generate gene expression profiles of Il-1α-K0, Il-1β-K0, and C57BL/6 mice at day 1 post-SCI. FC, Fold change compared to the C57BL/6 control group. All mice in this analysis received a spinal cord injury.

Table 3.1. Transcripts differentially regulated in the spinal cords of Il1a-KO mice compared with Il1b-KO and C57BL/6 mice after SCI

Discussion & Conclusion

During the work of my thesis, we first tried to identify the dynamics of microglia following SCI, since the vast majority of the literature to date did not distinguish microglia cells from MDMs, and even merged both cell types under the name of microglia/macrophages. We first traced the dynamics of microglia after SCI, using the best transgenic mouse model available/described at the time that the project started. We described phenotypic changes occurring in microglia and MDMs based on their respective of cell-specific fluorescent markers. Multiple immunofluorescence staining suggested that microglia participate in the formation of the glial scar and sequestered MDMs at the core of the lesion. Microglia formed what we now referred to as the "microglial scar", based on my original idea, which consists in a layers of tightly-connected microglia at the rim of the lesion, at the interface between infiltrated MDMs and reactive astrocyte endfeet.

Furthermore, we uncovered some of the functions of microglia after SCI. For this, we used pharmacological approaches and transgenic mouse models to selectively deplete microglia. Pharmacological blockade of CSF-1R with a molecule that crosses the BBB, compared to a similar molecule that did not, revealed that microglia facilitate locomotor recovery following SCI. The first week post-SCI was identified as the time window when microglia exert most of their beneficial effects following SCI.

Lastly, we tried to modulate the microglial response in an attempt to identify the molecular mechanisms by which microglia mediate their beneficial effects. As a recent study (below) revealed that the astrocytic response is determined by cytokines released by activated microglia in models of neuroinflammation (LPS) and CNS injury (optic nerve crush), we also aimed at investigating the role of the cytokine IL-1α in SCI. Liddelow and colleagues have shown that proinflammatory cytokines IL-1α and TNF both induce a neurotoxic A1 phenotype, whereas anti-inflammatory cytokines such as TGF-β1 induced a neuroprotective A2 phenotype[149]. Along these lines, we first demonstrated that microglia are the main cellular

source of IL-1α following SCI. Importantly, we demonstrated that *Il1a-KO* mice are protected early on from SCI and found that oligodendrocytes have the tendency to survive better in these mice, via an anti-apoptotic mechanism that involves TOX3. Accordingly, the acute injection of anakinra, an IL-1R1 antagonist, directly into the CSF, protected mice from SCI. Thus, blocking signaling by proinflammatory cytokines such as IL-1α is promising therapy that may help reduce tissue loss and functional deficits after SCI. Based on studies involving microglia depletion strategies, in which we found that activated microglia release growth factors (e.g. IGF-1) and anti-inflammatory cytokines (e.g. TGF-β1) susceptible of helping tissue repair, we also tried to favor the beneficial effects of microglia. Although we failed to induce astrocyte proliferation, migration and scarring using recombinant TGF-β1, we found that IGF-1 promoted all of these responses, which may perhaps explain why microglia are beneficial after SCI. Although we identified IGF-1 as neuroprotective candidate, this growth factor could not be incorporated into an hydrogel to be locally delivered in a sustained manner at the site of SCI. We thus opted for a more general treatment (i.e. delivery of recombinant MCSF) known to induce microglia proliferation and targeted the first week post-SCI as therapeutic time window. MCSF incorporated into an hydrogel, which can provide a sustained release for at least 1 week[89], was placed at subdural level at the site of injury right after the contusion. Importantly, data showed improved locomotor recovery in SCI mice treated with MCSF. Therefore, modulating the microglial response, by favoring the release of pro-repair factors or blocking the release of neurotoxic molecules, appears to be a promising target,

In the following sections, I will discuss our most recent discoveries and put our work in perspective with the literature existing on the role of microglia in SCI. Finally, I will discuss the future directions and conclude.

4.1. The early microglial response following SCI

After SCI, many cells that reside in the spinal cord die as a consequence of the impact. Over the years, the microglial response has often been under- or over-estimated because of the confusion that exists with the response of MDMs[382]. Here, we found that the number of microglia is reduced between 20% to 60% along the entire rostro-caudal spinal cord axis by

24 hours post-injury[89]. The death of microglia is partially mediated by apoptosis, as demonstrated by the presence of cleaved caspase-3 in some of these cells. Although we cannot discard other mechanisms of cell death (e.g. necroptosis), we failed to detect the presence of markers such as RIKP3 and MLKL in microglia. Following the impact, activated microglia retract their cell processes and profoundly change their behavior[89]. Prior to our work, it was generally accepted that microglia rapidly migrate towards the site of injury, as it occurs following a laser-induced CNS lesion, following which microglia typically send their ramifications within literally minutes in direction of the gradient of ATP that is extracellularly released around the lesion[27,148]. However, a recent study suggested that excessive amounts of ATP in the tissue environment, as it occurs in the spinal cord parenchyma after injury, may impair the microglial response[560]. In this thesis, we clarified this ambiguity by showing that microglia undergo profound functional and phenotypic changes (e.g. loss of P2Y12 expression, gain of CD68 expression, switch from ramified to an ameboid morphology), and migrate towards the core of the lesion in a stepwise manner over the first week post-SCI[89].

During this early response, dead and dying microglia initiate the inflammatory response by releasing DAMPs. Indeed, we demonstrated that microglia release alarmins such as IL-1α as early as 4 hours post-SCI[70]. Among the functions of this early release of cytokines by activated microglia is the recruitment of blood-derived myeloid cells[89]. Accordingly, *Il1a-KO* showed reduced infiltration of myeloid cells (i.e. neutrophils and M1 monocytes) at 24h post-SCI compared to wild-type mice[89]. Thus, our findings confirm prior observation made in peripheral tissues, where the release of pro-IL-1α from necrotic cells was found to promote sterile inflammation and myeloid cell recruitment[72]. IL-1α also favored neutrophil recruitment in ischemic condition[71]. Thus, based on our finding that CNS blood vessels express IL-1R1[70,307], we hypothesize that IL-1α may activate endothelial cells to recruit myeloid cells. Interestingly, we showed a reduction in monocyte recruitment after SCI in microglia depletion experiments, highlighting the importance of these cells as well in myeloid cell recruitment[89].

4.2. The late microglial response

During my thesis work, we took advantage of the *Cx3cr1*^{Cre}::*Rosa26*-TdT mouse line to better understand the spatial and temporal distribution of microglia following SCI. We reveled that microglia surrounding the lesion epicenter adopt an ameboid phenotype starting at 4 days post-SCI, which is in drastic contrast to their ramified morphology at day 1[89]. Notably, not only the phenotype of microglia had changed at 4 days post-SCI, but also the microglial cell counts with numbers 4 times higher than at day 1. This accumulation of microglia around the primary site of contusion may be explained by the migration and/or proliferation of these cells. Supporting the latter, about 50% of all microglia were actively proliferating at 4 days post-SCI[89]. Further accumulation occurred during the following days, with a peak at 14 days post-SCI. At 35 days post-SCI, microgliosis had partially resolved and total microglia cell numbers were reduced by half compared to day 14. Although most cells still had an ameboid shape, some microglia had returned to a homeostatic phenotype, as defined by an increased in ramifications and an upregulation of P2y12 expression[89].

Importantly, we also revealed the spatio-temporal distribution of MDMs following SCI. Coinciding with the accumulation of microglia around the lesion site at 4 days post-SCI, myeloid cells were recruited from the blood at roughly the same time, as revealed by the presence of CD68^{+} TdT^{-} cells[89]. At 7 days post-SCI, total cell counts for microglia and infiltrated myeloid cells were similar at the epicenter[89]. Afterward, myeloid cells started to accumulate at the lesion core, while microglia accumulated in the penumbra. With the help of astrocytes and pericytes/fibroblasts, microglia formed a dense scar tissue that kept MDMs at the lesion core[89]. We determined that the mature microglial scar was fully formed by 14 days post-SCI, and maintained until at least day 35[89]. The identification of the microglial scar contrasts with the results of Shecther and colleagues who reported using radiation bone marrow chimeras that MDMs are restricted to the margins of the lesion and excluded from the center of the lesion[205]. Rather, we found that the margins (borders) of the lesion are entirely occupied by microglia and pericytes/fibroblasts, whereas MDMs are confined to the center of the lesion. This once again shows that, although radiation bone marrow chimeras remain a useful tool, data generated using them must be interpreted with care because: i)

whole-body irradiation harms the blood-CNS barriers and impairs the proliferative capacity of microglia[331], and ii) HSCs and their progenitors are artificially introduced in the bloodstream as a result of the bone marrow transplant, thus creating a bias towards cells of the hematopoietic compartment[21,561].

4.2.1. Microglia promote adequate glial scar formation

The formation of the glial scar is a key element in the prognosis of SCI. The interruption of astrocyte reactivity, using various genetic and pharmacological approaches, has been associated with enhanced myeloid cell infiltration and inflammatory events, increased neuronal death, and impaired locomotor recovery (please see the *Introduction* section on the role of the glial scar)[86,87,112].

During my thesis work, we identified microglia as one of the key regulators of the formation of the glial scar. Not only microglia directly interacted with astrocytes, but also released several factors, such as IGF-1, which regulated astrocyte proliferation/migration. The lack of microglia or inhibition of IGF-1 using a pharmacological inhibitor both impaired astrocyte proliferation and glial scar formation[89]. Interestingly, microglia depletion resulted in an increased presence of satellite lesion consisting of non-parenchymal tissue filled with infiltrating myeloid cells. Recently, Hong and collaborators showed that the injection of imidazole-poly(organophosphazenes) hydrogels reduced the number of cystic cavities and improved locomotor performance in SCI rats[562]. They associated the reduced cavitation to the interaction between the imidazole moiety and histamine receptors at the surface of microglia/macrophages. Our findings suggest that microglia rather than macrophages may account for these beneficial effects. Nonetheless, it will be of interest in future work to further investigate how signals derived from the microglial scar influence formation of the astroglial scar.

4.3. Future directions

4.3.1. *Il1a* gene deletion protects oligodendrocytes after spinal cord injury through upregulation of the survival factor Tox3

In the study presented in Chapter 3, we described the differences between *Il1a*- and *Il1b-KO* mice after SCI. Both cytokines were highly upregulated following SCI. Although IL-1α was mainly produced by microglia, IL-1β was expressed by infiltrated myeloid cells, peaking at day 1 post-SCI. *Il1b-KO* mice showed a reduction in myeloid cell infiltration, but the long-lasting locomotor recovery observed in *Il1a-KO* mice could not be seen in *Il1b-KO* mice[70]. We determined that the protective effect observed in the absence of the *Il1a* gene was associated with an upregulation of the survival factor TOX3 in oligodendrocytes. It was previously demonstrated that the upregulation of TOX3 in transfected neurons, namely the Neuro2a cell line, protected these cells from death upon tunicamycine exposure, a drug that causes reticulum endoplasmic stress[456]. Neurons were protected by the upregulation of anti-apoptotic genes, including *Bcl2* and *Bclxl*[456]. In the same vein, we also demonstrated that TOX3 overexpression in transfected oligodendrocytes, namely the MO3.13 cell line, protected these cells from ischemia[70]. However, we do not know at this point whether microglia-derived IL-1α has a direct or indirect effect on oligodendrocytes. Additional experiments will be required to investigate the effects of IL-1α on oligodendrocytes. In a recent study, Liddelow and collaborators demonstrated that IL-1α induced a neurotoxic A1 astrocyte phenotype[149]. Maybe those primed astrocytes induced oligodendrocyte cell death after SCI?

The fact that TOX3 was upregulated in oligodendrocytes of *Il1a-KO* mice during the postnatal developmental period suggests that microglia regulate oligodendrocyte functions during development. The IL-1 system has been proposed to modulate microglial cell dynamics within the CNS. Indeed, the IL-1α/IL1R1 interaction regulates microglial proliferation following microglia depletion[331]. Matcovich and collaborators revealed that the *Il1a* gene is significantly regulated by microglia during embryogenesis and postnatal brain development[14]. Therefore, many questions remain open regarding the role of the IL-1 system

in CNS development. One of these questions is whether microglia from *Il1a-KO* mice enhance their production of growth factors, such as IGF-1, during CNS development, thus affecting oligodendrocyte development? Another key question is whether IL-1α influences other cell types, such as astrocytes, which then regulate oligodendrocyte maturation and development?

During our investigations, we were also able to promote functional recovery after SCI through an acute injection of anakinra in the cisterna magna, but not intravenously. Another group also showed beneficial effects of chronic anakinra treatment after SCI[70,473]. The beneficial effects were associated with a reduction in cellular apoptosis at the lesion site[70,473]. The incorporation of anakinra in a gelatin sponge placed at the surface of the injured spinal cord promoted locomotor recovery in rats[474]. Although we considered that the beneficial effects observed were related to the protection of oligodendrocytes, further studies will be needed to confirm this hypothesis. During my thesis' work, we tried to achieve a sustained release of anakinra to increase its beneficial effects, but without any success. Although we found that delivery of anakinra *in vitro* using hydrogels blocked IL-1R1 signaling, we could not reproduce these findings in an *in vivo* SCI setting. Thus, many questions remain unanswered with regard to hydrogel drug delivery. Is the drug concentration released *in vitro* sufficient to block IL-1R1 signaling *in vivo*? If yes, is anakinra released fast enough from the hydrogels to interfere with IL-1α/IL-1R1 signaling before the 4-hour time point (i.e. peak of IL-1α production)? Does anakinra penetrate to deeper spinal cord levels (e.g. gray matter)?

4.3.2. Microglia are an essential component of the neuroprotective scar that forms after spinal cord injury

In the study presented in Chapter 2, we described the spatio-temporal distribution of microglia. Importantly, we identified several microglia phenotypes, which varied from the classical ramified microglia, which expressed P2Y12, to the ameboid microglia, which upregulated CD68. Recently, at least 3 different phenotypes have been described using single cell RNA-seq in Alzheimer's disease[210]. First, homeostatic microglia expressing markers such as *P2y12*, *Cx3cr1* and *Tmem119*. Second, damage-associated microglia (DAM) which downregulated homeostatic markers and upregulated markers such as *Axl*, *Apoe*, *Lyz2*, *Csf*,

Trem2, *Itgax*, *Cd63*, and which were associated to β-amyloid plaques. Lastly, a third phenotype found in between the two previous populations. The authors also suggested that DAM could be observed in many different CNS disorders. During my thesis work, we found that ameboid microglia downregulate TMEM119 at the protein level and upregulate markers such as CD11c, AXL and TREM2. Instead, MHCII was restricted to infiltrating myeloid cells and border-associated macrophages[89,309], thus suggesting that DAM are also present following SCI. What is the function of DAM after SCI? Are there more subsets of DAM after SCI? Are DAM in the proliferation phase? Are DAM found at 3 days similar to the ones detected at 14 days post-SCI, which correspond to the beginning of the chronic phase? Can we modulate these cells for beneficial purposes after SCI?

We showed that microglia rapidly proliferate during the first week post-SCI. As well, as other authors found before us, we demonstrated that microglia rapidly repopulate the CNS following cessation of exposure to the CSF1R antagonist PLX5622[17,89,219]. Bruttger and collaborators previously identified the IL-1α/IL1R1 interaction as a key signal for mediating microglia proliferation following prior cell depletion experiments[331]. As demonstrated in a model of peripheral nerve injury, MCSF/CSF1R signaling may also promote spinal cord microgliosis[336]. Thus, microglia proliferation is probably regulated by several different pathways. Several questions remain in that regard. What are these other signals that regulate microglia proliferation? Are the signals identified following pharmacologically-induced microglial cell depletion-repopulation similar to those that regulate repopulation in the context of CNS injury? Can these signalling pathways be harnessed to favor spinal cord repair and functional recovery?

During the microglia repopulation experiments using the CSF1R antagonist, we identified another cell type that proliferated along with microglia, i.e. oligodendrocytes. Oligodendrocytes are known to proliferate and differentiate into myelinating oligodendrocytes in the injured adult CNS. The myelinating capacity of newly-generated oligodendrocytes promotes motor learning during training[46]. Interestingly, several reports associated a poor prognosis of recovery after SCI to a reduced number of oligodendrocytes and extended areas of demyelination[70,89,127,563]. Therefore, enhancing the survival of oligodendrocytes and/or the production of OPCs seems to be a promising therapeutic avenue

for SCI. We demonstrated in Chapter 3 that microglia may affect oligodendrocyte survival by releasing IL-1α[70]. However, in the absence of microglia, oligodendrocyte numbers are reduced. Therefore, one may ask whether the reduction in oligodendrocyte numbers following microglia depletion is related to the exacerbation of tissue damage after SCI? Instead, could it be that the reduction was caused by a deficiency in the proliferative capacities of oligodendrocytes due to the absence of a key microglia-derived growth factor? In line with the second option, the identification of factors that influence oligodendrocyte cell proliferation in microglia repopulation experiments may be of great relevance for SCI.

We identified IGF-1 as one of the main microglia-derived factors that influence glial scar formation. Indeed, the stimulation of primary astrocytes *in vitro* with recombinant IGF-1 enhanced their proliferative capacity. On the contrary, the administration of OSI-906, an IGF-1R antagonist that crosses the BBB[559], inhibited astrocyte proliferation, but failed at influencing functional recovery. Importantly, the administration of IGF-1 either by the central or peripheral route protected neurons from apoptosis and reduced infarct volumes after stroke[555,556]. Genetic overexpression of IGF-1 in astrocytes enhanced neuronal survival and improved cognitive function following TBI[557]. Collectively, these findings suggest that the administration of IGF-1 could be an envisageable therapy after SCI. However, in our previous studies in which attempted to deliver IGF-1 in a sustained-fashion to the site of SCI, we failed to incorporate IGF-1 in hydrogels due to the electrostatic incompatibility between IGF-1 and the hydrogel. In future work, we propose to inject IGF-1 directly into mice, either by a central or peripheral route, in an attempt to promote functional recovery after SCI.

4.4. Conclusion

The overall work described in this thesis focuses on better understanding the role of microglia in SCI. We described several of the changes occurring in microglia following SCI. We uncovered a dual function of these cells with both beneficial and detrimental effects of microglia-derived factors. But overall, microglia appear to be beneficial. We identified microglia as key regulators of glial scar formation, which resulted in improved survival of neurons and oligodendrocytes after SCI. Finally, we identified new therapeutical avenues

that may help modulate the microglial response during the first week post-SCI, which was identified as the ideal therapeutic time window to target these cells.

References

1. Bradbury, E. J. & McMahon, S. B. Spinal cord repair strategies: why do they work? *Nat. Rev. Neurosci.* **7**, 644–653 (2006).

2. Ahuja, C. S. *et al.* Traumatic spinal cord injury. *Nat. Rev.* **3**, 17018 (2017).

3. Morell, P. & Quarles, R. H. Characteristic Composition of Myelin. in *Basic Neurochemistry: Molecular, Cellular and Medical Aspects.* (eds. Siegel, G. J., Agranoff, B. W., Albers, R. W., Fisher, S. K. & Uhler, M. D.) 1–8 (Lippincott-Raven, 1998).

4. Somjen, G. G. Nervenkitt: Notes on the history of the concept of neuroglia. *Glia* **1**, 2–9 (1988).

5. Virchow, R. Cellularpathologie in ihrer Begründung auf physiologische und pathologische Gewebelehre. Februar, März und April im Institut zu Berlin. (1858).

6. del Rio-Hortega, P. I. La microglia en estado normal. *Bol la soc esp biol* **9**, 68–120 (1919).

7. del Rio-Hortega, P. II. Intervención de la microglía en los procesos patologicos. *Bol la soc esp biol* **9**, 68–120 (1919).

8. del Rio-Hortega, P. III. Naturaleza probable de la microglia. *Bol la soc esp biol* **9**, 68–120 (1919).

9. del Rio-Hortega, P. IV. Poder fagocitario y movilidad de la microglia. *Bol la soc esp biol* **9**, 68–120 (1919).

10. Tremblay, M.-È. & Sierra, A. *Microglia in Health and Disease*. (Springer US, 2014). doi:10.1007/978-1-4939-1429-6

11. Ginhoux, F. *et al.* Fate Mapping Analysis Reveals That Adult Microglia Derive from

Primitive Macrophages. *Science (80-.).* **330**, 841–845 (2010).

12. Gomez Perdiguero, E. *et al.* Tissue-resident macrophages originate from yolk-sac-derived erythro-myeloid progenitors. *Nature* **518**, 547–551 (2015).

13. Alliot, F., Godin, I. & Pessac, B. Microglia derive from progenitors, originating from the yolk sac, and which proliferate in the brain. *Dev. Brain Res.* **117**, 145–152 (1999).

14. Matcovitch-Natan, O. *et al.* Microglia development follows a stepwise program to regulate brain homeostasis. *Science (80-.).* **353**, aad8670 (2016).

15. Kierdorf, K. *et al.* Microglia emerge from erythromyeloid precursors via Pu.1- and Irf8-dependent pathways. *Nat. Neurosci.* **16**, 273–280 (2013).

16. Erblich, B., Zhu, L., Etgen, A. M., Dobrenis, K. & Pollard, J. W. Absence of colony stimulation factor-1 receptor results in loss of microglia, disrupted brain development and olfactory deficits. *PLoS One* **6**, (2011).

17. Elmore, M. R. P. *et al.* Colony-stimulating factor 1 receptor signaling is necessary for microglia viability, unmasking a microglia progenitor cell in the adult brain. *Neuron* **82**, 380–97 (2014).

18. Squarzoni, P. *et al.* Microglia Modulate Wiring of the Embryonic Forebrain. *Cell Rep.* **8**, 1271–1279 (2014).

19. Lawson, L. J., Perry, V. H., Dri, P. & Gordon, S. Heterogeneity in the distribution and morphology of microglia in the normal adult mouse brain. *Neuroscience* **39**, 151–170 (1990).

20. Lawson L, P. H. and G. S. Turnover of resident microglia in the normal adult mouse. *Neuroscience* **48**, 405–415 (1992).

21. Ajami, B., Bennett, J. L., Krieger, C., Tetzlaff, W. & Rossi, F. M. V. Local self-renewal can sustain CNS microglia maintenance and function throughout adult life. *Nat. Neurosci.* **10**, 1538–1543 (2007).

22. Nimmerjahn, A., Kirchhoff, F. & Helmchen, F. Resting Microglial Cells Are Highly Dynamic Surveillants of Brain Parenchyma in Vivo. *Science (80-.).* **308**, 1314–1318 (2005).

23. Sierra, A. *et al.* Microglia shape adult hippocampal neurogenesis through apoptosis-coupled phagocytosis. *Cell Stem Cell* **7**, 483–495 (2010).

24. Tremblay, M.-E. E., Lowery, R. L. & Majewska, A. K. Microglial interactions with synapses are modulated by visual experience. *PLoS Biol.* **8**, e1000527 (2010).

25. Parkhurst, C. N. *et al.* Microglia promote learning-dependent synapse formation through brain-derived neurotrophic factor. *Cell* **155**, 1596–1609 (2013).

26. del Rio-Hortega, P. & Penfield, W. Cerebral Cicatrix: The Reaction of Neuroglia and Microglia to Brain Wounds. *Bull. Johns Hopkins Hosp.* **41**, 278–303 (1927).

27. Haynes, S. E. *et al.* The P2Y12 receptor regulates microglial activation by extracellular nucleotides. *Nat. Neurosci.* **9**, 1512–1519 (2006).

28. Kölliker, R. A. *Handbuch der Gewebelhre des Menchen für Aerzte und Studirende.* (Engelmann., 1852).

29. Bergmann, K. Notiz über einige Strukturverhältnisse des Cerebellums und Rückenmarks. *Z Med* **8**, 360–3 (1857).

30. Deiters, O. Untersuchungen über Gehirn und Rückenmark des Menschen und der Säugethiere. *Braunschweig: Vieweg* (1865).

31. Golgi, C. Contribuzione alla fina Anatomia degli organi centrali del sistema nervosos. *Riv. Clin. di Bol.* **2**, 38–46 (1872).

32. Kang, P. *et al.* Sox9 and NFIA Coordinate a Transcriptional Regulatory Cascade during the Initiation of Gliogenesis. *Neuron* **74**, 79–94 (2012).

33. Deneen, B. *et al.* The Transcription Factor NFIA Controls the Onset of Gliogenesis in the Developing Spinal Cord. *Neuron* **52**, 953–968 (2006).

34. Urayama, S. *et al.* Chromatin accessibility at a STAT3 target site is altered prior to astrocyte differentiation. *Cell Struct. Funct.* **38**, 55–66 (2013).

35. Muroyama, Y., Fujiwara, Y., Orkin, S. H. & Rowitch, D. H. Specification of astrocytes by bHLH protein SCL in a restricted region of the neural tube. *Nature* **438**, 360–363 (2005).

36. del Rio-Hortega, P. La glia de escasas radiaciones (oligodendroglía). *Bol la real soc esp hist nat* (1921).

37. del Rio-Hortega, P. ¿Son homologables la glía de escasas radiaciones y la célula de schawann? (1922).

38. del Rio-Hortega, P. Tercera aportacion al conocimiento morfologico e interpretacion funcional de la oligodendroglia. *Mem. Real Soc. Esp. Hist. Nat.* 5–122 (1928).

39. Stolt, C. C. *et al.* Terminal differentiation of myelin-forming oligodendrocytes depends on the transcription factor Sox10. *Genes Dev.* **16**, 165–170 (2002).

40. Stolt, C. C. *et al.* The Sox9 transcription factor determines glial fate choice in the developing spinal cord. *Genes Dev.* **17**, 1677–1689 (2003).

41. Stolt, C. C., Lommes, P., Friedrich, R. P. & Wegner, M. Transcription factors Sox8 and Sox10 perform non-equivalent roles during oligodendrocyte development despite functional redundancy. *Development* **131**, 2349–2358 (2004).

42. Kuspert, M., Hammer, A., Bosl, M. R. & Wegner, M. Olig2 regulates Sox10 expression in oligodendrocyte precursors through an evolutionary conserved distal enhancer. *Nucleic Acids Res.* **39**, 1280–1293 (2011).

43. Hornig, J. *et al.* The transcription factors Sox10 and Myrf define an essential regulatory network module in differentiating oligodendrocytes. *PLoS Genet.* **9**, e1003907 (2013).

44. Tsai, H. H. *et al.* Oligodendrocyte precursors migrate along vasculature in the

developing nervous system. *Science (80-.).* **351**, 379–384 (2016).

45. Marques, S. *et al.* Oligodendrocyte heterogeneity in the mouse juvenile and adult central nervous system. *Science (80-.).* **352**, 1326–1329 (2016).

46. McKenzie, I. A. *et al.* Motor skill learning requires active central myelination. *Science (80-.).* **346**, 318–322 (2014).

47. Vargas, M. E. & Barres, B. A. Why is Wallerian degeneration in the CNS so slow? *Annu. Rev. Neurosci.* **30**, 153–179 (2007).

48. David, S. & Lacroix, S. Molecular approaches to spinal cord repair. *Annu. Rev. Neurosci.* **26**, 411–440 (2003).

49. Benson, M. D. *et al.* Ephrin-B3 is a myelin-based inhibitor of neurite outgrowth. *Proc. Natl. Acad. Sci. U. S. A.* **102**, 10694–10699 (2005).

50. Moreau-Fauvarque, C. *et al.* The transmembrane semaphorin Sema4D/CD100, an inhibitor of axonal growth, is expressed on oligodendrocytes and upregulated after CNS lesion. *J. Neurosci.* **23**, 9229–9239 (2003).

51. Yiu, G. & He, Z. Glial inhibition of CNS axon regeneration. *Nat. Rev.* **7**, 617–627 (2006).

52. Shim, S.-O. *et al.* PlexinA2 limits recovery from corticospinal axotomy by mediating oligodendrocyte-derived Sema6A growth inhibition. *Mol. Cell. Neurosci.* **50**, 193–200 (2012).

53. Noonan, V. K. *et al.* Incidence and prevalence of spinal cord injury in Canada: A national perspective. *Neuroepidemiology* **38**, 219–226 (2012).

54. Krueger, H., Noonan, V. K., Trenaman, L. M., Joshi, P. & Rivers, C. S. The economic burden of traumatic spinal cord injury in Canada. *Chronic Dis. Inj. Can.* **33**, 113–122 (2013).

55. Tator, C. H. Update on the pathophysiology and pathology of acute spinal cord injury.

Brain Pathol. **5**, 407–413 (1995).

56. Anthes, D. L., Theriault, E. & Tator, C. H. Characterization of axonal ultrastructural pathology following experimental spinal cord compression injury. *Brain Res.* **702**, 1–16 (1995).

57. Losey, P. & Anthony, D. C. Impact of vasculature damage on the outcome of spinal cord injury: a novel collagenase-induced model may give new insights into the mechanisms involved. *Neural Regen. Res.* **9**, 1783–1786 (2014).

58. Fehlings, M. G. *et al.* A Clinical Practice Guideline for the Management of Patients With Acute Spinal Cord Injury and Central Cord Syndrome: Recommendations on the Timing (</=24 Hours Versus >24 Hours) of Decompressive Surgery. *Glob. spine J.* **7**, 195S-202S (2017).

59. Badhiwala, J. H., Ahuja, C. S. & Fehlings, M. G. Time is spine: a review of translational advances in spinal cord injury. *J. Neurosurg. Spine* **30**, 1–18 (2018).

60. Fehlings, M. G. & Perrin, R. G. The role and timing of early decompression for cervical spinal cord injury: update with a review of recent clinical evidence. *Injury* **36 Suppl 2**, B13-26 (2005).

61. Furlan, J. C., Noonan, V., Cadotte, D. W. & Fehlings, M. G. Timing of decompressive surgery of spinal cord after traumatic spinal cord injury: an evidence-based examination of pre-clinical and clinical studies. *J. Neurotrauma* **28**, 1371–1399 (2011).

62. Fehlings, M. G. & Wilson, J. R. Timing of surgical intervention in spinal trauma: what does the evidence indicate? *Spine* **35**, S159-60 (2010).

63. Kwon, B. K. *et al.* A grading system to evaluate objectively the strength of pre-clinical data of acute neuroprotective therapies for clinical translation in spinal cord injury. *J. Neurotrauma* **28**, 1525–1543 (2011).

64. Fehlings, M. G. *et al.* Early versus delayed decompression for traumatic cervical spinal

cord injury: results of the Surgical Timing in Acute Spinal Cord Injury Study (STASCIS). *PLoS One* **7**, e32037 (2012).

65. Fehlings, M. G. *et al.* A Clinical Practice Guideline for the Management of Patients With Acute Spinal Cord Injury: Recommendations on the Type and Timing of Anticoagulant Thromboprophylaxis. *Glob. spine J.* **7**, 212S-220S (2017).

66. Fehlings, M. G. *et al.* A Clinical Practice Guideline for the Management of Patients With Acute Spinal Cord Injury: Recommendations on the Role of Baseline Magnetic Resonance Imaging in Clinical Decision Making and Outcome Prediction. *Glob. spine J.* **7**, 221S-230S (2017).

67. Fehlings, M. G. *et al.* A Clinical Practice Guideline for the Management of Patients With Acute Spinal Cord Injury: Recommendations on the Use of Methylprednisolone Sodium Succinate. *Glob. spine J.* **7**, 203S-211S (2017).

68. Batchelor, P. E. *et al.* Meta-analysis of pre-clinical studies of early decompression in acute spinal cord injury: a battle of time and pressure. *PLoS One* **8**, e72659 (2013).

69. Matute, C. Characteristics of acute and chronic kainate excitotoxic damage to the optic nerve. *Proc. Natl. Acad. Sci. U. S. A.* **95**, 10229–10234 (1998).

70. Bastien, D. *et al.* Il-1α gene deletion protects oligodendrocytes after spinal cord injury through upregulation of the survival factor Tox3. *J. Neurosci.* **35**, 10715–10730 (2015).

71. Rider, P. *et al.* IL-1α and IL-1β recruit different myeloid cells and promote different stages of sterile inflammation. *J. Immunol.* **187**, 4835–43 (2011).

72. Cohen, I. *et al.* Differential release of chromatin-bound IL-1alpha discriminates between necrotic and apoptotic cell death by the ability to induce sterile inflammation. *Proc. Natl. Acad. Sci. U. S. A.* **107**, 2574–9 (2010).

73. Probert, L. & Selmaj, K. TNF and related molecules: trends in neuroscience and clinical applications. *J. Neuroimmunol.* **72**, 113–117 (1997).

74. Hopkins, S. J. & Rothwell, N. J. Cytokines and the nervous system. I: Expression and recognition. *Trends Neurosci.* **18**, 83–88 (1995).

75. Rothwell, N. J. & Hopkins, S. J. Cytokines and the nervous system II: Actions and mechanisms of action. *Trends Neurosci.* **18**, 130–136 (1995).

76. Pineau, I. & Lacroix, S. Proinflammatory Cytokine Synthesis in the Injured Mouse Spinal Cord : Multiphasic Expression Pattern and Identification of the Cell Types Involved. *J. Comp. Neurol.* **285**, 267–285 (2007).

77. de Rivero Vaccari, J. P., Lotocki, G., Marcillo, A. E., Dietrich, W. D. & Keane, R. W. A molecular platform in neurons regulates inflammation after spinal cord injury. *J. Neurosci.* **28**, 3404–3414 (2008).

78. Chatzipanteli, K. *et al.* Temporal and segmental distribution of constitutive and inducible nitric oxide synthases after traumatic spinal cord injury: effect of aminoguanidine treatment. *J. Neurotrauma* **19**, 639–651 (2002).

79. Colton, C. A. & Gilbert, D. L. Production of superoxide anions by a CNS macrophage, the microglia. *FEBS Lett.* **223**, 284–288 (1987).

80. Liu, D., Ling, X., Wen, J. & Liu, J. The role of reactive nitrogen species in secondary spinal cord injury: formation of nitric oxide, peroxynitrite, and nitrated protein. *J. Neurochem.* **75**, 2144–2154 (2000).

81. MacMicking, J. D., Willenborg, D. O., Weidemann, M. J., Rockett, K. A. & Cowden, W. B. Elevated secretion of reactive nitrogen and oxygen intermediates by inflammatory leukocytes in hyperacute experimental autoimmune encephalomyelitis: enhancement by the soluble products of encephalitogenic T cells. *J. Exp. Med.* **176**, 303–307 (1992).

82. Xiong, Y., Rabchevsky, A. G. & Hall, E. D. Role of peroxynitrite in secondary oxidative damage after spinal cord injury. *J. Neurochem.* **100**, 639–649 (2007).

83. Evans, T. J. & Cohen, J. Mediators: nitric oxide and other toxic oxygen species. *Curr.*

Top. Microbiol. Immunol. **216**, 189–207 (1996).

84. Lewen, A., Matz, P. & Chan, P. H. Free radical pathways in CNS injury. *J. Neurotrauma* **17**, 871–890 (2000).

85. Figley, S. A., Khosravi, R., Legasto, J. M., Tseng, Y.-F. & Fehlings, M. G. Characterization of vascular disruption and blood-spinal cord barrier permeability following traumatic spinal cord injury. *J. Neurotrauma* **31**, 541–552 (2014).

86. Okada, S. *et al.* Conditional ablation of Stat3 or Socs3 discloses a dual role for reactive astrocytes after spinal cord injury. *Nat. Med.* **12**, 829–834 (2006).

87. Faulkner, J. R. *et al.* Reactive astrocytes protect tissue and preserve function after spinal cord injury. *J. Neurosci.* **24**, 2143–55 (2004).

88. Lytle, J. M., Vicini, S. & Wrathall, J. R. Phenotypic changes in NG2+ cells after spinal cord injury. *J. Neurotrauma* **23**, 1726–38 (2006).

89. Bellver-Landete, V. *et al.* Microglia are an essential component of the neuroprotective scar that forms after spinal cord injury. *Nat. Commun.* **10**, 518 (2019).

90. Vanlandewijck, M. *et al.* A molecular atlas of cell types and zonation in the brain vasculature. *Nature* **554**, 475–480 (2018).

91. Thawer, S. G. *et al.* Temporal changes in monocyte and macrophage subsets and microglial macrophages following spinal cord injury in the Lys-Egfp-ki mouse model. *J. Neuroimmunol.* **261**, 7–20 (2013).

92. Liu, C. *et al.* Macrophages Mediate the Repair of Brain Vascular Rupture through Direct Physical Adhesion and Mechanical Traction. *Immunity* **44**, 1162–1176 (2016).

93. Corliss, B. A., Azimi, M. S., Munson, J. M., Peirce, S. M. & Murfee, W. L. Macrophages: An Inflammatory Link Between Angiogenesis and Lymphangiogenesis. *Microcirculation* **23**, 95–121 (2016).

94. Gliem, M., Schwaninger, M. & Jander, S. Biochimica et Biophysica Acta Protective

features of peripheral monocytes / macrophages in stroke ☆. *BBA - Mol. Basis Dis.* **1862**, 329–338 (2016).

95. Moriyama, Y., Takagi, N., Hashimura, K., Itokawa, C. & Tanonaka, K. Intravenous injection of neural progenitor cells facilitates angiogenesis after cerebral ischemia. *Brain Behav.* **3**, 43–53 (2013).

96. Chu, H. X. *et al.* Evidence That Ly6C(hi) Monocytes are Protective in Acute Ischemic Stroke by Promoting M2 Macrophage Polarization. *Stroke* **46**, 1929–1937 (2015).

97. Dudvarski Stankovic, N., Teodorczyk, M., Ploen, R., Zipp, F. & Schmidt, M. H. H. Microglia-blood vessel interactions: a double-edged sword in brain pathologies. *Acta Neuropathol.* **131**, 347–363 (2016).

98. Greenhalgh, A. D. *et al.* Peripherally derived macrophages modulate microglial function to reduce inflammation after CNS injury. *PLOS Biol.* **16**, e2005264 (2018).

99. Yu, S. *et al.* Angiogenic microspheres promote neural regeneration and motor function recovery after spinal cord injury in rats. *Sci. Rep.* **6**, 33428 (2016).

100. Yang, C. *et al.* β-Catenin signaling initiates the activation of astrocytes and its dysregulation contributes to the pathogenesis of astrocytomas. *Proc. Natl. Acad. Sci. U. S. A.* **109**, 6963–8 (2012).

101. Sofroniew, M. V. Astrocyte barriers to neurotoxic inflammation. *Nat. Rev. Neurosci.* **16**, 249–263 (2015).

102. Anderson, M. A. *et al.* Astrocyte scar formation aids central nervous system axon regeneration. *Nature* **532**, 195–200 (2016).

103. Herrmann, J. E. *et al.* STAT3 is a critical regulator of astrogliosis and scar formation after spinal cord injury. *J. Neurosci.* **28**, 7231–7243 (2008).

104. Anderson, M. A., Ao, Y. & Sofroniew, M. V. Heterogeneity of reactive astrocytes. *Neurosci. Lett.* **565**, 23–29 (2014).

105. Duncan, G. J. *et al.* Locomotor recovery following contusive spinal cord injury does not require oligodendrocyte remyelination. *Nat. Commun.* **9**, 3066 (2018).

106. Goritz, C. *et al.* A Pericyte Origin of Spinal Cord Scar Tissue. *Science (80-.).* **333**, 238–242 (2011).

107. Dias, D. O. *et al.* Reducing Pericyte-Derived Scarring Promotes Recovery after Spinal Cord Injury. *Cell* **173**, 153-165.e22 (2018).

108. Hara, M. *et al.* Interaction of reactive astrocytes with type I collagen induces astrocytic scar formation through the integrin-N-cadherin pathway after spinal cord injury. *Nat. Med.* **23**, 818–828 (2017).

109. Fleming, J. C. *et al.* The cellular inflammatory response in human spinal cords after injury. *Brain* **129**, 3249–3269 (2006).

110. Liu, Z. *et al.* Beneficial effects of gfap/vimentin reactive astrocytes for axonal remodeling and motor behavioral recovery in mice after stroke. *Glia* **62**, 2022–2033 (2014).

111. Li, L. *et al.* Protective role of reactive astrocytes in brain ischemia. *J. Cereb. Blood Flow Metab.* **28**, 468–481 (2008).

112. Pekny, M. *et al.* Abnormal reaction to central nervous system injury in mice lacking glial fibrillary acidic protein and vimentin. *J. Cell Biol.* **145**, 503–514 (1999).

113. Fouad, K., Pedersen, V., Schwab, M. E. & Brosamle, C. Cervical sprouting of corticospinal fibers after thoracic spinal cord injury accompanies shifts in evoked motor responses. *Curr. Biol.* **11**, 1766–1770 (2001).

114. Vavrek, R., Girgis, J., Tetzlaff, W., Hiebert, G. W. & Fouad, K. BDNF promotes connections of corticospinal neurons onto spared descending interneurons in spinal cord injured rats. *Brain* **129**, 1534–1545 (2006).

115. Sofroniew, M. V. Molecular dissection of reactive astrogliosis and glial scar

formation. *Trends Neurosci.* **32**, 638–647 (2009).

116. Cajal, S. R. *Degeneration and Regeneration of the Nervous System*. *R. M. May*, (Oxford Univ. Press, London, 1928).

117. Richardson, P. M., McGuinness, U. M. & Aguayo, A. J. Axons from CNS neurons regenerate into PNS grafts. *Nature* **284**, 264–265 (1980).

118. David, S. & Aguayo, A. J. Axonal elongation into peripheral nervous system 'bridges' after central nervous system injury in adult rats. *Science (80-.).* **214**, 931–933 (1981).

119. Smith, G. V & Stevenson, J. A. Peripheral nerve grafts lacking viable Schwann cells fail to support central nervous system axonal regeneration. *Exp. brain Res.* **69**, 299–306 (1988).

120. Hall, S. M. The effect of inhibiting Schwann cell mitosis on the re-innervation of acellular autografts in the peripheral nervous system of the mouse. *Neuropathol. Appl. Neurobiol.* **12**, 401–414 (1986).

121. Barrette, B. *et al.* Requirement of myeloid cells for axon regeneration. *J. Neurosci.* **28**, 9363–9376 (2008).

122. Cattin, A.-L. *et al.* Macrophage-Induced Blood Vessels Guide Schwann Cell-Mediated Regeneration of Peripheral Nerves. *Cell* **162**, 1127–1139 (2015).

123. Ozdinler, P. H. & Macklis, J. D. IGF-I specifically enhances axon outgrowth of corticospinal motor neurons. *Nat. Neurosci.* **9**, 1371–1381 (2006).

124. Alto, L. T. *et al.* Chemotropic guidance facilitates axonal regeneration and synapse formation after spinal cord injury. *Nat. Neurosci.* **12**, 1106–1113 (2009).

125. Deng, L.-X. *et al.* A novel growth-promoting pathway formed by GDNF-overexpressing Schwann cells promotes propriospinal axonal regeneration, synapse formation, and partial recovery of function after spinal cord injury. *J. Neurosci.* **33**, 5655–5667 (2013).

126. O'Shea, T. M., Burda, J. E. & Sofroniew, M. V. Cell biology of spinal cord injury and repair. *J. Clin. Invest.* **127**, 3259–3270 (2017).

127. Benson, M. D. *et al.* Terminal differentiation of myelin-forming oligodendrocytes depends on the transcription factor Sox10. *Genes Dev.* **16**, 165–170 (2003).

128. Schwab, M. E. & Strittmatter, S. M. Nogo limits neural plasticity and recovery from injury. *Curr. Opin. Neurobiol.* **27**, 53–60 (2014).

129. Cafferty, W. B. J. & Strittmatter, S. M. The Nogo-Nogo receptor pathway limits a spectrum of adult CNS axonal growth. *J. Neurosci.* **26**, 12242–12250 (2006).

130. Wang, X., Baughman, K. W., Basso, D. M. & Strittmatter, S. M. Delayed Nogo receptor therapy improves recovery from spinal cord contusion. *Ann. Neurol.* **60**, 540–549 (2006).

131. Savio, T. & Schwab, M. E. Rat CNS white matter, but not gray matter, is nonpermissive for neuronal cell adhesion and fiber outgrowth. *J. Neurosci.* **9**, 1126–1133 (1989).

132. Schwab, M. E. & Caroni, P. Oligodendrocytes and CNS myelin are nonpermissive substrates for neurite growth and fibroblast spreading in vitro. *J. Neurosci.* **8**, 2381–2393 (1988).

133. Lang, D. M., Rubin, B. P., Schwab, M. E. & Stuermer, C. A. CNS myelin and oligodendrocytes of the Xenopus spinal cord--but not optic nerve--are nonpermissive for axon growth. *J. Neurosci.* **15**, 99–109 (1995).

134. Wang, X. *et al.* Inhibition of Poly-ADP-Ribosylation Fails to Increase Axonal Regeneration or Improve Functional Recovery after Adult Mammalian CNS Injury. *eNeuro* **3**, (2016).

135. Huebner, E. A., Kim, B. G., Duffy, P. J., Brown, R. H. & Strittmatter, S. M. A multi-domain fragment of Nogo-A protein is a potent inhibitor of cortical axon regeneration via Nogo receptor 1. *J. Biol. Chem.* **286**, 18026–18036 (2011).

136. Cafferty, W. B. J., Duffy, P., Huebner, E. & Strittmatter, S. M. MAG and OMgp synergize with Nogo-A to restrict axonal growth and neurological recovery after spinal cord trauma. *J. Neurosci.* **30**, 6825–6837 (2010).

137. Duffy, P. *et al.* Rho-associated kinase II (ROCKII) limits axonal growth after trauma within the adult mouse spinal cord. *J. Neurosci.* **29**, 15266–15276 (2009).

138. Hu, F. *et al.* Nogo-A interacts with the Nogo-66 receptor through multiple sites to create an isoform-selective subnanomolar agonist. *J. Neurosci.* **25**, 5298–5304 (2005).

139. Schwab, M. E. Nogo and axon regeneration. *Curr. Opin. Neurobiol.* **14**, 118–124 (2004).

140. Schwab, M. E. Regeneration of lesioned CNS axons by neutralization of neurite growth inhibitors: a short review. *J. Neurotrauma* **9 Suppl 1**, S219-21 (1992).

141. Schwab, M. E. Myelin-associated inhibitors of neurite growth and regeneration in the CNS. *Trends Neurosci.* **13**, 452–456 (1990).

142. Cadelli, D. S. & Schwab, M. E. Myelin-associated inhibitors of neurite outgrowth and their role in CNS regeneration. *Ann. N. Y. Acad. Sci.* **633**, 234–240 (1991).

143. Freund, P. *et al.* Anti-Nogo-A antibody treatment promotes recovery of manual dexterity after unilateral cervical lesion in adult primates--re-examination and extension of behavioral data. *Eur. J. Neurosci.* **29**, 983–996 (2009).

144. Filbin, M. T. Myelin-associated inhibitors of axonal regeneration in the adult mammalian CNS. *Nat. Neurosci.* **4**, 703–713 (2003).

145. Silver, J. & Miller, J. H. Regeneration beyond the glial scar. *Nat. Neurosci.* **5**, 146–156 (2004).

146. Tom, V. J., Steinmetz, M. P., Miller, J. H., Doller, C. M. & Silver, J. Studies on the development and behavior of the dystrophic growth cone, the hallmark of regeneration failure, in an in vitro model of the glial scar and after spinal cord injury. *J. Neurosci.*

24, 6531–6539 (2004).

147. Bradbury, E., Moon, L. & Popat, R. Chondroitinase ABC promotes functional recovery after spinal cord injury. *Nature* **416**, (2002).

148. Davalos, D. *et al.* ATP mediates rapid microglial response to local brain injury in vivo. *Nat. Neurosci.* **8**, 752–758 (2005).

149. Liddelow, S. A. *et al.* Neurotoxic reactive astrocytes are induced by activated microglia. *Nature* **541**, 481–487 (2017).

150. Stirling, D. P., Liu, S., Kubes, P. & Yong, V. W. Depletion of Ly6G/Gr-1 leukocytes after spinal cord injury in mice alters wound healing and worsens neurological outcome. *J. Neurosci.* **29**, 753–764 (2009).

151. Lee, S. M., Rosen, S., Weinstein, P., van Rooijen, N. & Noble-Haeusslein, L. J. Prevention of both neutrophil and monocyte recruitment promotes recovery after spinal cord injury. *J. Neurotrauma* **28**, 1893–1907 (2011).

152. Yan, P. *et al.* Cellular localization of tumor necrosis factor-alpha following acute spinal cord injury in adult rats. *J. Neurotrauma* **18**, 563–568 (2001).

153. Yune, T. Y. *et al.* Increased production of tumor necrosis factor-alpha induces apoptosis after traumatic spinal cord injury in rats. *J. Neurotrauma* **20**, 207–219 (2003).

154. Zhang, Y. *et al.* An RNA-sequencing transcriptome and splicing database of glia, neurons, and vascular cells of the cerebral cortex. *J. Neurosci.* **34**, 11929–11947 (2014).

155. Kroner, A. *et al.* TNF and Increased Intracellular Iron Alter Macrophage Polarization to a Detrimental M1 Phenotype in the Injured Spinal Cord. *Neuron* 1–19 (2014). doi:10.1016/j.neuron.2014.07.027

156. Genovese, T. *et al.* TNF-alpha blockage in a mouse model of SCI: evidence for

improved outcome. *Shock* **29**, 32–41 (2008).

157. Chen, K.-B. *et al.* Tumor necrosis factor-alpha antagonist reduces apoptosis of neurons and oligodendroglia in rat spinal cord injury. *Spine (Phila. Pa. 1976).* **36**, 1350–1358 (2011).

158. Hajishengallis, G. & Lambris, J. D. Crosstalk pathways between Toll-like receptors and the complement system. *Trends Immunol.* **31**, 154–163 (2010).

159. Abe, T. *et al.* Local complement-targeted intervention in periodontitis: proof-of-concept using a C5a receptor (CD88) antagonist. *J. Immunol.* **189**, 5442–5448 (2012).

160. Brekke, O. L. *et al.* The effects of selective complement and CD14 inhibition on the E. coli-induced tissue factor mRNA upregulation, monocyte tissue factor expression, and tissue factor functional activity in human whole blood. *Adv. Exp. Med. Biol.* **735**, 123–136 (2013).

161. Alexander, J. J., Anderson, A. J., Barnum, S. R., Stevens, B. & Tenner, A. J. The complement cascade: Yin-Yang in neuroinflammation--neuro-protection and -degeneration. *J. Neurochem.* **107**, 1169–1187 (2008).

162. Ricklin, D. & Lambris, J. D. Complement in immune and inflammatory disorders: pathophysiological mechanisms. *J. Immunol.* **190**, 3831–3838 (2013).

163. Fonseca, M. I. *et al.* Cell-specific deletion of C1qa identifies microglia as the dominant source of C1q in mouse brain. *J. Neuroinflammation* **14**, 48 (2017).

164. Hong, S. *et al.* Complement and microglia mediate early synapse loss in Alzheimer mouse models. *Science (80-.).* **352**, 712–716 (2016).

165. Anderson, A. J., Robert, S., Huang, W., Young, W. & Cotman, C. W. Activation of complement pathways after contusion-induced spinal cord injury. *J. Neurotrauma* **21**, 1831–1846 (2004).

166. Rebhun, J., Madorsky, J. G. & Glovsky, M. M. Proteins of the complement system

and acute phase reactants in sera of patients with spinal cord injury. *Ann. Allergy* **66**, 335–338 (1991).

167. Galvan, M. D. *et al.* Deficiency in complement C1q improves histological and functional locomotor outcome after spinal cord injury. *J. Neurosci.* **28**, 13876–13888 (2008).

168. Peterson, S. L., Nguyen, H. X., Mendez, O. A. & Anderson, A. J. Complement protein C1q modulates neurite outgrowth in vitro and spinal cord axon regeneration in vivo. *J. Neurosci.* **35**, 4332–4349 (2015).

169. Mawhinney, L. A. *et al.* Differential detection and distribution of microglial and hematogenous macrophage populations in the injured spinal cord of lys-EGFP-ki transgenic mice. *J. Neuropathol. Exp. Neurol.* **71**, 180–197 (2012).

170. Prineas, J. Pathology of the early lesion in multiple sclerosis. *Hum. Pathol.* **6**, 531–554 (1975).

171. Prineas, J. W. & Connell, F. The fine structure of chronically active multiple sclerosis plaques. *Neurology* **28**, 68–75 (1978).

172. Nhong, M. *et al.* Monocyte recruitment and myelin removal are delayed following spinal cord injury in mice with CCR2 chemokine receptor deletion. *J. Neurosci. Res.* **68**, 691–702 (2002).

173. Kuhlmann, T. *et al.* Differential regulation of myelin phagocytosis by macrophages/microglia, involvement of target myelin, Fc receptors and activation by intravenous immunoglobulins. *J. Neurosci. Res.* **67**, 185–190 (2002).

174. Yamasaki, R. *et al.* Differential roles of microglia and monocytes in the inflamed central nervous system. *J. Exp. Med.* **211**, 1533–1549 (2014).

175. Kopper, T. J. & Gensel, J. C. Myelin as an inflammatory mediator: Myelin interactions with complement, macrophages, and microglia in spinal cord injury. *J. Neurosci. Res.* **96**, 969–977 (2018).

176. Hirata, K. & Kawabuchi, M. Myelin phagocytosis by macrophages and nonmacrophages during Wallerian degeneration. *Microsc. Res. Tech.* **57**, 541–547 (2002).

177. Rotshenker, S. Microglia and macrophage activation and the regulation of complement-receptor-3 (CR3/MAC-1)-mediated myelin phagocytosis in injury and disease. *J. Mol. Neurosci.* **21**, 65–72 (2003).

178. Neumann, H., Kotter, M. R. & Franklin, R. J. M. Debris clearance by microglia: an essential link between degeneration and regeneration. *Brain* **132**, 288–295 (2009).

179. Bogie, J. F. J. *et al.* Myelin-derived lipids modulate macrophage activity by liver X receptor activation. *PLoS One* **7**, e44998 (2012).

180. Durafourt, B. A. *et al.* Comparison of polarization properties of human adult microglia and blood-derived macrophages. *Glia* **60**, 717–727 (2012).

181. Bogie, J. F. J. *et al.* Myelin alters the inflammatory phenotype of macrophages by activating PPARs. *Acta Neuropathol. Commun.* **1**, 43 (2013).

182. Boven, L. A. *et al.* Myelin-laden macrophages are anti-inflammatory, consistent with foam cells in multiple sclerosis. *Brain* **129**, 517–526 (2006).

183. Sun, X. *et al.* Myelin activates FAK/Akt/NF-kappaB pathways and provokes CR3-dependent inflammatory response in murine system. *PLoS One* **5**, e9380 (2010).

184. van der Laan, L. J. *et al.* Macrophage phagocytosis of myelin in vitro determined by flow cytometry: phagocytosis is mediated by CR3 and induces production of tumor necrosis factor-alpha and nitric oxide. *J. Neuroimmunol.* **70**, 145–152 (1996).

185. van Rossum, D., Hilbert, S., Strassenburg, S., Hanisch, U.-K. & Bruck, W. Myelin-phagocytosing macrophages in isolated sciatic and optic nerves reveal a unique reactive phenotype. *Glia* **56**, 271–283 (2008).

186. Wang, Y. *et al.* TREM2 lipid sensing sustains the microglial response in an

Alzheimer's disease model. *Cell* **160**, 1061–1071 (2015).

187. Siddiqui, T. A., Lively, S. & Schlichter, L. C. Complex molecular and functional outcomes of single versus sequential cytokine stimulation of rat microglia. *J. Neuroinflammation* **13**, 66 (2016).

188. Liu, Y. *et al.* Suppression of microglial inflammatory activity by myelin phagocytosis: role of p47-PHOX-mediated generation of reactive oxygen species. *J. Neurosci.* **26**, 12904–12913 (2006).

189. Bruck, W. & Friede, R. L. L-fucosidase treatment blocks myelin phagocytosis by macrophages in vitro. *J. Neuroimmunol.* **27**, 217–227 (1990).

190. Bruck, W. & Friede, R. L. The role of complement in myelin phagocytosis during PNS wallerian degeneration. *J. Neurol. Sci.* **103**, 182–187 (1991).

191. Bruck, W. & Friede, R. L. Anti-macrophage CR3 antibody blocks myelin phagocytosis by macrophages in vitro. *Acta Neuropathol.* **80**, 415–418 (1990).

192. Vogel, D. Y. S. *et al.* Macrophages in inflammatory multiple sclerosis lesions have an intermediate activation status. *J. Neuroinflammation* **10**, 35 (2013).

193. Butovsky, O. *et al.* Identification of a unique TGF-β-dependent molecular and functional signature in microglia. *Nat. Neurosci.* **17**, 131–43 (2014).

194. Bohlen, C. J. *et al.* Diverse Requirements for Microglial Survival, Specification, and Function Revealed by Defined-Medium Cultures. *Neuron* **94**, 759-773.e8 (2017).

195. Ueno, M. *et al.* Layer V cortical neurons require microglial support for survival during postnatal development. *Nat. Neurosci.* **16**, 543–51 (2013).

196. Hoshiko, M., Arnoux, I., Avignone, E., Yamamoto, N. & Audinat, E. Deficiency of the Microglial Receptor CX3CR1 Impairs Postnatal Functional Development of Thalamocortical Synapses in the Barrel Cortex. *J. Neurosci.* **32**, 15106–15111 (2012).

197. Li, Y., Du, X.-F., Liu, C.-S., Wen, Z.-L. & Du, J.-L. Reciprocal regulation between

resting microglial dynamics and neuronal activity in vivo. *Dev. Cell* **23**, 1189–1202 (2012).

198. Pascual, O., Ben Achour, S., Rostaing, P., Triller, A. & Bessis, A. Microglia activation triggers astrocyte-mediated modulation of excitatory neurotransmission. *Proc. Natl. Acad. Sci. U. S. A.* **109**, E197-205 (2012).

199. Cunningham, C. L., Martinez-Cerdeno, V. & Noctor, S. C. Microglia Regulate the Number of Neural Precursor Cells in the Developing Cerebral Cortex. *J. Neurosci.* **33**, 4216–4233 (2013).

200. Kettenmann, H., Kirchhoff, F. & Verkhratsky, A. Microglia: new roles for the synaptic stripper. *Neuron* **77**, 10–18 (2013).

201. Paolicelli, R. C. *et al.* Synaptic pruning by microglia is necessary for normal brain development. *Science* **333**, 1456–1458 (2011).

202. Schafer, D. P. *et al.* Microglia sculpt postnatal neural circuits in an activity and complement-dependent manner. *Neuron* **74**, 691–705 (2012).

203. Prewitt, C. M., Niesman, I. R., Kane, C. J. & Houle, J. D. Activated macrophage/microglial cells can promote the regeneration of sensory axons into the injured spinal cord. *Exp. Neurol.* **148**, 433–443 (1997).

204. Ma, S.-F. *et al.* Adoptive transfer of M2 macrophages promotes locomotor recovery in adult rats after spinal cord injury. *Brain. Behav. Immun.* **45**, 157–170 (2015).

205. Shechter, R. *et al.* Infiltrating blood-derived macrophages are vital cells playing an anti-inflammatory role in recovery from spinal cord injury in mice. *PLoS Med.* **6**, (2009).

206. Rabchevsky, A. G. & Streit, W. J. Grafting of cultured microglial cells into the lesioned spinal cord of adult rats enhances neurite outgrowth. *J. Neurosci. Res.* **47**, 34–48 (1997).

207. Kigerl, K. a *et al.* Identification of two distinct macrophage subsets with divergent effects causing either neurotoxicity or regeneration in the injured mouse spinal cord. *J. Neurosci.* **29**, 13435–44 (2009).

208. Horn, K. P., Busch, S. A., Hawthorne, A. L., van Rooijen, N. & Silver, J. Another barrier to regeneration in the CNS: activated macrophages induce extensive retraction of dystrophic axons through direct physical interactions. *J. Neurosci.* **28**, 9330–9341 (2008).

209. Zhu, Y. *et al.* Neurobiology of Disease Hematogenous macrophage depletion reduces the fi brotic scar and increases axonal growth after spinal cord injury. *Neurobiol. Dis.* **74**, 114–125 (2015).

210. Keren-Shaul, H. *et al.* A Unique Microglia Type Associated with Restricting Development of Alzheimer's Disease. *Cell* **169**, 1276-1290.e17 (2017).

211. Godin, I. E., Garcia-Porrero, J. A., Coutinho, A., Dieterlen-Lievre, F. & Marcos, M. A. Para-aortic splanchnopleura from early mouse embryos contains B1a cell progenitors. *Nature* **364**, 67–70 (1993).

212. Medvinsky, A. L., Samoylina, N. L., Muller, A. M. & Dzierzak, E. A. An early pre-liver intraembryonic source of CFU-S in the developing mouse. *Nature* **364**, 64–67 (1993).

213. Orkin, S. H. & Zon, L. I. Hematopoiesis: An Evolving Paradigm for Stem Cell Biology. *Cell* **132**, 631–644 (2008).

214. Kumaravelu, P. *et al.* Quantitative developmental anatomy of definitive haematopoietic stem cells/long-term repopulating units (HSC/RUs): role of the aorta-gonad-mesonephros (AGM) region and the yolk sac in colonisation of the mouse embryonic liver. *Development* **129**, 4891–4899 (2002).

215. Naito, M., Takahashi, K. & Nishikawa, S. Development, differentiation, and maturation of macrophages in the fetal mouse liver. *J. Leukoc. Biol.* **48**, 27–37 (1990).

216. Kierdorf, K., Prinz, M., Geissmann, F. & Gomez Perdiguero, E. Development and function of tissue resident macrophages in mice. *Semin. Immunol.* **27**, 369–378 (2015).

217. Askew, K. *et al.* Coupled Proliferation and Apoptosis Maintain the Rapid Turnover of Microglia in the Adult Brain. *Cell Rep.* **18**, 391–405 (2017).

218. Tay, T. L. *et al.* A new fate mapping system reveals context-dependent random or clonal expansion of microglia. *Nat. Neurosci.* **20**, 793–803 (2017).

219. Huang, Y. *et al.* Repopulated microglia are solely derived from the proliferation of residual microglia after acute depletion. *Nat. Neurosci.* **21**, 530–540 (2018).

220. Reu, P. *et al.* The Lifespan and Turnover of Microglia in the Human Brain. *Cell Rep.* **20**, 779–784 (2017).

221. van Furth, R. & Cohn, Z. A. The origin and kinetics of mononuclear phagocytes. *J. Exp. Med.* **128**, 415–435 (1968).

222. Gordon, S. Biology of the macrophage. *J. Cell Sci. Suppl.* **4**, 267–286 (1986).

223. Ebert, R. H. & Florey, H. W. The Extravascular Development of the Monocyte Observed In vivo. *Br. J. Exp. Pathol.* **20**, 342–356 (1939).

224. Hashimoto, D. *et al.* Tissue-resident macrophages self-maintain locally throughout adult life with minimal contribution from circulating monocytes. *Immunity* **38**, 792–804 (2013).

225. Schulz, C. *et al.* A Lineage of Myeloid Cells Independent of Myb and Hematopoietic Stem Cells. *Science (80-.).* **336**, 86–90 (2012).

226. Geissmann, F., Jung, S. & Littman, D. R. Blood monocytes consist of two principal subsets with distinct migratory properties. *Immunity* **19**, 71–82 (2003).

227. December, C. *et al.* Development of Monocytes, Macrophages, and Dendritic Cells. (2010).

228. Askew, K. *et al.* Coupled Proliferation and Apoptosis Maintain the Rapid Turnover of Microglia in the Adult Brain. *Cell Rep.* **18**, 391–405 (2017).

229. Bruttger, J. *et al.* Genetic Cell Ablation Reveals Clusters of Local Self-Renewing Microglia in the Mammalian Central Nervous System. *Immunity* **43**, 92–106 (2015).

230. Buttgereit, A. *et al.* Sall1 is a transcriptional regulator defining microglia identity and function. *Nat. Immunol.* **17**, 1397–1406 (2016).

231. Deczkowska, A. *et al.* Disease-Associated Microglia: A Universal Immune Sensor of Neurodegeneration. *Cell* **173**, 1073–1081 (2018).

232. Gosselin, D. *et al.* Environment Drives Selection and Function of Enhancers Controlling Tissue-Specific Macrophage Identities. *Cell* **159**, 1327–1340 (2014).

233. Gosselin, D. *et al.* An environment-dependent transcriptional network specifies human microglia identity. *Science* **356**, (2017).

234. Wheeler, D. L., Sariol, A., Meyerholz, D. K. & Perlman, S. Microglia are required for protection against lethal coronavirus encephalitis in mice. *J. Clin. Invest.* **128**, 931–943 (2018).

235. Béchade, C., Cantaut-Belarif, Y. & Bessis, A. Microglial control of neuronal activity. *Front. Cell. Neurosci.* **7**, 32 (2013).

236. Schafer, D. P., Lehrman, E. K. & Stevens, B. The 'quad-partite' synapse: microglia-synapse interactions in the developing and mature CNS. *Glia* **61**, 24–36 (2013).

237. Konigsmark, B. W. & Sidman, R. L. Origin of brain macrophages in the mouse. *J. Neuropathol. Exp. Neurol.* **22**, 643–676 (1963).

238. Adrian, E. K. J. & Williams, M. G. Cell proliferation in injured spinal cord. An electron microscopic study. *J. Comp. Neurol.* **151**, 1–24 (1973).

239. Huntington, H. W. & Terry, R. D. The origin of the reactive cells in cerebral stab wounds. *J. Neuropathol. Exp. Neurol.* **25**, 646–653 (1966).

240. Kitamura, T., Hattori, H. & Fujita, S. Autoradiographic studies on histogenesis of brain macrophages in the mouse. *J. Neuropathol. Exp. Neurol.* **31**, 502–518 (1972).

241. Roessmann, U. & Friede, R. L. Entry of labeled monocytic cells into the central nervous system. *Acta Neuropathol.* **10**, 359–362 (1968).

242. Imamoto, K. & Leblond, C. P. Presence of labeled monocytes, macrophages and microglia in a stab wound of the brain following an injection of bone marrow cells labeled with 3H-uridine into rats. *J. Comp. Neurol.* **174**, 255–279 (1977).

243. Eglitis, M. A. & Mezey, E. Hematopoietic cells differentiate into both microglia and macroglia in the brains of adult mice. *Proc. Natl. Acad. Sci. U. S. A.* **94**, 4080–4085 (1997).

244. Priller, J. *et al.* Targeting gene-modified hematopoietic cells to the central nervous system: use of green fluorescent protein uncovers microglial engraftment. *Nat. Med.* **7**, 1356–1361 (2001).

245. Bechmann, I. *et al.* Circulating monocytic cells infiltrate layers of anterograde axonal degeneration where they transform into microglia. *FASEB J. Off. Publ. Fed. Am. Soc. Exp. Biol.* **19**, 647–649 (2005).

246. Simard, A. R., Soulet, D., Gowing, G., Julien, J.-P. & Rivest, S. Bone Marrow-Derived Microglia Play a Critical Role in Restricting Senile Plaque Formation in Alzheimer's Disease. *Neuron* **49**, 489–502 (2006).

247. Popovich, P. G., Wei, P. & Stokes, B. T. Cellular inflammatory response after spinal cord injury in Sprague-Dawley and Lewis rats. *J. Comp. Neurol.* **377**, 443–464 (1997).

248. Utans, U., Arceci, R. J., Yamashita, Y. & Russell, M. E. Cloning and characterization of allograft inflammatory factor-1: a novel macrophage factor identified in rat cardiac allografts with chronic rejection. *J. Clin. Invest.* **95**, 2954–2962 (1995).

249. Imai, Y., Ibata, I., Ito, D., Ohsawa, K. & Kohsaka, S. A novel gene iba1 in the major histocompatibility complex class III region encoding an EF hand protein expressed in

a monocytic lineage. *Biochem. Biophys. Res. Commun.* **224**, 855–862 (1996).

250. Ito, D. *et al.* Microglia-specific localisation of a novel calcium binding protein, Iba1. *Brain Res. Mol. Brain Res.* **57**, 1–9 (1998).

251. Kawai, T. & Akira, S. The role of pattern-recognition receptors in innate immunity: update on Toll-like receptors. *Nat. Immunol.* **11**, 373–384 (2010).

252. Takeuchi, O. & Akira, S. Pattern recognition receptors and inflammation. *Cell* **140**, 805–820 (2010).

253. Esen, N. & Kielian, T. Central role for MyD88 in the responses of microglia to pathogen-associated molecular patterns. *J. Immunol.* **176**, 6802–6811 (2006).

254. Kawagoe, T. *et al.* Sequential control of Toll-like receptor-dependent responses by IRAK1 and IRAK2. *Nat. Immunol.* **9**, 684–691 (2008).

255. Li, S., Strelow, A., Fontana, E. J. & Wesche, H. IRAK-4: a novel member of the IRAK family with the properties of an IRAK-kinase. *Proc. Natl. Acad. Sci. U. S. A.* **99**, 5567–5572 (2002).

256. Kozela, E. *et al.* Cannabinoids Delta(9)-tetrahydrocannabinol and cannabidiol differentially inhibit the lipopolysaccharide-activated NF-kappaB and interferon-beta/STAT proinflammatory pathways in BV-2 microglial cells. *J. Biol. Chem.* **285**, 1616–1626 (2010).

257. Deng, L. *et al.* Activation of the IkappaB kinase complex by TRAF6 requires a dimeric ubiquitin-conjugating enzyme complex and a unique polyubiquitin chain. *Cell* **103**, 351–361 (2000).

258. Cundiff, P. *et al.* ERK5 MAP kinase regulates neurogenin1 during cortical neurogenesis. *PLoS One* **4**, e5204 (2009).

259. Xia, Z.-P. *et al.* Direct activation of protein kinases by unanchored polyubiquitin chains. *Nature* **461**, 114–119 (2009).

260. Wang, C. *et al.* TAK1 is a ubiquitin-dependent kinase of MKK and IKK. *Nature* **412**, 346–351 (2001).

261. Bhoj, V. G. & Chen, Z. J. Ubiquitylation in innate and adaptive immunity. *Nature* **458**, 430–437 (2009).

262. Delhase, M., Hayakawa, M., Chen, Y. & Karin, M. Positive and negative regulation of IkappaB kinase activity through IKKbeta subunit phosphorylation. *Science* **284**, 309–313 (1999).

263. Holtman, I. R., Skola, D. & Glass, C. K. Transcriptional control of microglia phenotypes in health and disease. *J. Clin. Invest.* **127**, 3220–3229 (2017).

264. Hickey, W. F. & Kimura, H. Perivascular microglial cells of the CNS are bone marrow-derived and present antigen in vivo. *Science* **239**, 290–292 (1988).

265. Matsumoto, Y. & Fujiwara, M. Absence of donor-type major histocompatibility complex class I antigen-bearing microglia in the rat central nervous system of radiation bone marrow chimeras. *J. Neuroimmunol.* **17**, 71–82 (1987).

266. Massengale, M., Wagers, A. J., Vogel, H. & Weissman, I. L. Hematopoietic cells maintain hematopoietic fates upon entering the brain. *J. Exp. Med.* **201**, 1579–1589 (2005).

267. Nguyen, V., Gaber, M. W., Sontag, M. R. & Kiani, M. F. Late effects of ionizing radiation on the microvascular networks in normal tissue. *Radiat. Res.* **154**, 531–536 (2000).

268. Diserbo, M. *et al.* Blood-brain barrier permeability after gamma whole-body irradiation: an in vivo microdialysis study. *Can. J. Physiol. Pharmacol.* **80**, 670–678 (2002).

269. Li, Y.-Q., Chen, P., Jain, V., Reilly, R. M. & Wong, C. S. Early radiation-induced endothelial cell loss and blood-spinal cord barrier breakdown in the rat spinal cord. *Radiat. Res.* **161**, 143–152 (2004).

270. Kaya, M. *et al.* Effects of lipopolysaccharide on the radiation-induced changes in the blood-brain barrier and the astrocytes. *Brain Res.* **1019**, 105–112 (2004).

271. Akira, S., Uematsu, S. & Takeuchi, O. Pathogen recognition and innate immunity. *Cell* **124**, 783–801 (2006).

272. Erny, D. *et al.* Host microbiota constantly control maturation and function of microglia in the CNS. *Nat. Neurosci.* **18**, 965–977 (2015).

273. Wendeln, A.-C. *et al.* Innate immune memory in the brain shapes neurological disease hallmarks. *Nature* **556**, 332–338 (2018).

274. Lee, W. H., Sonntag, W. E., Mitschelen, M., Yan, H. & Lee, Y. W. Irradiation induces regionally specific alterations in pro-inflammatory environments in rat brain. *Int. J. Radiat. Biol.* **86**, 132–144 (2010).

275. Ljubimova, N. V, Levitman, M. K., Plotnikova, E. D. & Eidus, L. K. Endothelial cell population dynamics in rat brain after local irradiation. *Br. J. Radiol.* **64**, 934–940 (1991).

276. Roth, N. M., Sontag, M. R. & Kiani, M. F. Early effects of ionizing radiation on the microvascular networks in normal tissue. *Radiat. Res.* **151**, 270–277 (1999).

277. Lampron, A., Lessard, M. & Rivest, S. Effects of myeloablation, peripheral chimerism, and whole-body irradiation on the entry of bone marrow-derived cells into the brain. *Cell Transplant.* **21**, 1149–1159 (2012).

278. Lewis, C.-A. B. *et al.* Myelosuppressive conditioning using busulfan enables bone marrow cell accumulation in the spinal cord of a mouse model of amyotrophic lateral sclerosis. *PLoS One* **8**, e60661 (2013).

279. Kierdorf, K., Katzmarski, N., Haas, C. A. & Prinz, M. Bone marrow cell recruitment to the brain in the absence of irradiation or parabiosis bias. *PLoS One* **8**, e58544 (2013).

280. Capotondo, A. *et al.* Brain conditioning is instrumental for successful microglia reconstitution following hematopoietic stem cell transplantation. *Proc. Natl. Acad. Sci. U. S. A.* **109**, 15018–15023 (2012).

281. Wilkinson, F. L. *et al.* Busulfan conditioning enhances engraftment of hematopoietic donor-derived cells in the brain compared with irradiation. *Mol. Ther.* **21**, 868–876 (2013).

282. Liu, K. *et al.* Origin of dendritic cells in peripheral lymphoid organs of mice. *Nat. Immunol.* **8**, 578–583 (2007).

283. Ajami, B., Bennett, J. L., Krieger, C., McNagny, K. M. & Rossi, F. M. V. Infiltrating monocytes trigger EAE progression, but do not contribute to the resident microglia pool. *Nat. Neurosci.* **14**, 1142–1149 (2011).

284. Larochelle, A., Bellavance, M.-A., Michaud, J.-P. & Rivest, S. Bone marrow-derived macrophages and the CNS: An update on the use of experimental chimeric mouse models and bone marrow transplantation in neurological disorders. *Biochim. Biophys. Acta* **1862**, 310–322 (2016).

285. Bert, P. Expériences et Considérations Sur la Greffe Animale. *J Anat. Physiol.* **1**, 69–87 (1864).

286. Oehmichen, M., Gruninger, H., Saebisch, R. & Narita, Y. Transformation of blood monocytes into microglia and pericytes and their ability to proliferate. Experimental autoradiographical and enzyme histochemical studies with normal and damaged brain tissues of rabbits and rats. *Acta Neuropathol.* **23**, 200–218 (1973).

287. Kurz, H. & Christ, B. Embryonic CNS macrophages and microglia do not stem from circulating, but from extravascular precursors. *Glia* **22**, 98–102 (1998).

288. Li, T. *et al.* Proliferation of parenchymal microglia is the main source of microgliosis after ischaemic stroke. *Brain* **136**, 3578–3588 (2013).

289. Tashima, R. *et al.* Bone marrow-derived cells in the population of spinal microglia

after peripheral nerve injury. *Sci. Rep.* **6**, 23701 (2016).

290. Coull, J. A. M. *et al.* BDNF from microglia causes the shift in neuronal anion gradient underlying neuropathic pain. *Nature* **438**, 1017–1021 (2005).

291. Yona, S. *et al.* Fate Mapping Reveals Origins and Dynamics of Monocytes and Tissue Macrophages under Homeostasis. *Immunity* **38**, 79–91 (2013).

292. Rapalino, O. *et al.* Implantation of stimulated homologous macrophages results in partial recovery of paraplegic rats. *Nat. Biotechnol.* **4**, 814–821 (1998).

293. Schwartz, M. *et al.* Potential repair of rat spinal cord injuries using stimulated homologous macrophages. *Neurosurgery* **44**, 1041–1046 (1999).

294. Jung, S. *et al.* Analysis of fractalkine receptor CX(3)CR1 function by targeted deletion and green fluorescent protein reporter gene insertion. *Mol. Cell. Biol.* **20**, 4106–4114 (2000).

295. Boring, L. *et al.* Impaired monocyte migration and reduced type 1 (Th1) cytokine responses in C-C chemokine receptor 2 knockout mice. *J. Clin. Invest.* **100**, 2552–2561 (1997).

296. Saederup, N. *et al.* Selective chemokine receptor usage by central nervous system myeloid cells in CCR2-red fluorescent protein knock-in mice. *PLoS One* **5**, e13693 (2010).

297. Gu, N. *et al.* Spinal Microgliosis Due to Resident Microglial Proliferation Is Required for Pain Hypersensitivity after Peripheral Nerve Injury. *Cell Rep.* **16**, 605–614 (2016).

298. Yamasaki, R. *et al.* Differential roles of microglia and monocytes in the inflamed central nervous system. *J. Exp. Med.* **211**, 1533–1549 (2014).

299. Faust, N., Varas, F., Kelly, L. M., Heck, S. & Graf, T. Insertion of enhanced green fluorescent protein into the lysozyme gene creates mice with green fluorescent granulocytes and macrophages. *Blood* **96**, 719–726 (2000).

300. Howe, C. L., Lafrance-Corey, R. G., Sundsbak, R. S. & Lafrance, S. J. Inflammatory monocytes damage the hippocampus during acute picornavirus infection of the brain. *J. Neuroinflammation* **9**, 50 (2012).

301. Oweida, A. J., Dunn, E. A., Karlik, S. J., Dekaban, G. A. & Foster, P. J. Iron-oxide labeling of hematogenous macrophages in a model of experimental autoimmune encephalomyelitis and the contribution to signal loss in fast imaging employing steady state acquisition (FIESTA) images. *J. Magn. Reson. Imaging* **26**, 144–151 (2007).

302. Ricard, C. *et al.* Phenotypic dynamics of microglial and monocyte-derived cells in glioblastoma-bearing mice. *Sci. Rep.* **6**, 26381 (2016).

303. Zarruk, J. G., Greenhalgh, A. D. & David, S. Microglia and macrophages differ in their inflammatory profile after permanent brain ischemia. *Exp. Neurol.* **301**, 120–132 (2018).

304. Metzger, D., Clifford, J., Chiba, H. & Chambon, P. Conditional site-specific recombination in mammalian cells using a ligand-dependent chimeric Cre recombinase. *Proc Natl Acad Sci U S A* **92**, 6991–6995 (1995).

305. Goldmann, T. *et al.* A new type of microglia gene targeting shows TAK1 to be pivotal in CNS autoimmune inflammation. *Nat. Neurosci.* **16**, 1618–1626 (2013).

306. Gao, L. *et al.* Infiltration of circulating myeloid cells through CD95L contributes to neurodegeneration in mice. *J. Exp. Med.* **212**, 469–480 (2015).

307. Lévesque, S. *et al.* Myeloid cell transmigration across the CNS vasculature triggers Il-1β-driven neuroinflammation during autoimmune encephalomyelitis in mice. *J. Exp. Med.* **Accepted**, (2016).

308. Zeisel, A. *et al.* Cell types in the mouse cortex and hippocampus revealed by single-cell RNA-seq. *Science (80-.).* **347**, 1138–42 (2015).

309. Mrdjen, D. *et al.* High-Dimensional Single-Cell Mapping of Central Nervous System Immune Cells Reveals Distinct Myeloid Subsets in Health, Aging, and Disease.

Immunity **48**, 380-395.e6 (2018).

310. Wieghofer, P., Knobeloch, K.-P. & Prinz, M. Genetic targeting of microglia. *Glia* n/a-n/a (2014). doi:10.1002/glia.22727

311. Waisman, A., Ginhoux, F., Greter, M. & Bruttger, J. Homeostasis of Microglia in the Adult Brain: Review of Novel Microglia Depletion Systems. *Trends Immunol.* **36**, 625–636 (2015).

312. Stanley, E. R. & Heard, P. M. Factors regulating macrophage production and growth. Purification and some properties of the colony stimulating factor from medium conditioned by mouse L cells. *J. Biol. Chem.* **252**, 4305–4312 (1977).

313. Lin, H. *et al.* Discovery of a cytokine and its receptor by functional screening of the extracellular proteome. *Science* **320**, 807–811 (2008).

314. Nandi, S. *et al.* Receptor-type protein-tyrosine phosphatase zeta is a functional receptor for interleukin-34. *J. Biol. Chem.* **288**, 21972–21986 (2013).

315. von Holst, A., Sirko, S. & Faissner, A. The unique 473HD-Chondroitinsulfate epitope is expressed by radial glia and involved in neural precursor cell proliferation. *J. Neurosci.* **26**, 4082–4094 (2006).

316. Wei, S. *et al.* Functional overlap but differential expression of CSF-1 and IL-34 in their CSF-1 receptor-mediated regulation of myeloid cells. *J. Leukoc. Biol.* **88**, 495–505 (2010).

317. Nandi, S. *et al.* The CSF-1 receptor ligands IL-34 and CSF-1 exhibit distinct developmental brain expression patterns and regulate neural progenitor cell maintenance and maturation. *Dev. Biol.* **367**, 100–113 (2012).

318. Dai, X. M. *et al.* Targeted disruption of the mouse colony-stimulating factor 1 receptor gene results in osteopetrosis, mononuclear phagocyte deficiency, increased primitive progenitor cell frequencies, and reproductive defects. *Blood* **99**, 111–120 (2002).

319. Wang, Y. *et al.* IL-34 is a tissue-restricted ligand of CSF1R required for the development of Langerhans cells and microglia. *Nat. Immunol.* **13**, 753–760 (2012).

320. Greter, M. *et al.* Stroma-derived interleukin-34 controls the development and maintenance of langerhans cells and the maintenance of microglia. *Immunity* **37**, 1050–1060 (2012).

321. Caescu, C. I. *et al.* Colony stimulating factor-1 receptor signaling networks inhibit mouse macrophage inflammatory responses by induction of microRNA-21. *Blood* **125**, e1-13 (2015).

322. Cecchini, M. G. *et al.* Role of colony stimulating factor-1 in the establishment and regulation of tissue macrophages during postnatal development of the mouse. *Development* **120**, 1357–1372 (1994).

323. Wiktor-Jedrzejczak, W. *et al.* Total absence of colony-stimulating factor 1 in the macrophage-deficient osteopetrotic (op/op) mouse. *Proc. Natl. Acad. Sci. U. S. A.* **87**, 4828–4832 (1990).

324. Wiktor-Jedrzejczak, W. W., Ahmed, A., Szczylik, C. & Skelly, R. R. Hematological characterization of congenital osteopetrosis in op/op mouse. Possible mechanism for abnormal macrophage differentiation. *J. Exp. Med.* **156**, 1516–1527 (1982).

325. Felix, R. *et al.* Impairment of macrophage colony-stimulating factor production and lack of resident bone marrow macrophages in the osteopetrotic op/op mouse. *J. Bone Miner. Res.* **5**, 781–789 (1990).

326. Marks, S. C. J. & Lane, P. W. Osteopetrosis, a new recessive skeletal mutation on chromosome 12 of the mouse. *J. Hered.* **67**, 11–18 (1976).

327. Wang, Y., Berezovska, O. & Fedoroff, S. Expression of colony stimulating factor-1 receptor (CSF-1R) by CNS neurons in mice. *J. Neurosci. Res.* **57**, 616–632 (1999).

328. Chen, S.-K. *et al.* Hematopoietic origin of pathological grooming in Hoxb8 mutant mice. *Cell* **141**, 775–785 (2010).

329. Derecki, N. C. *et al.* Wild-type microglia arrest pathology in a mouse model of Rett syndrome. *Nature* **484**, 105–109 (2012).

330. Zhan, Y. *et al.* Deficient neuron-microglia signaling results in impaired functional brain connectivity and social behavior. *Nat. Neurosci.* **17**, 400–6 (2014).

331. Bruttger, J. *et al.* Genetic Cell Ablation Reveals Clusters of Local Self-Renewing Microglia in the Mammalian Central Nervous System. *Immunity* 1–15 (2015). doi:10.1016/j.immuni.2015.06.012

332. Chitu, V., Gokhan, S., Nandi, S., Mehler, M. F. & Stanley, E. R. Emerging roles for CSF-1 receptor and its ligands in the nervous system. *Trends Neurosci.* **39**, 378–393 (2016).

333. Chitu, V. *et al.* Phenotypic characterization of a Csf1r haploinsufficient mouse model of adult-onset leukodystrophy with axonal spheroids and pigmented glia (ALSP). *Neurobiol. Dis.* **74**, 219–228 (2015).

334. Lampron, a. *et al.* Inefficient clearance of myelin debris by microglia impairs remyelinating processes. *J. Exp. Med.* (2015). doi:10.1084/jem.20141656

335. Yao, Y. *et al.* Dynamics of spinal microglia repopulation following an acute depletion. *Sci. Rep.* **6**, 22839 (2016).

336. Guan, Z. *et al.* Injured sensory neuron–derived CSF1 induces microglial proliferation and DAP12-dependent pain. *Nat. Neurosci.* **19**, 94–101 (2015).

337. Reshef, R. *et al.* The role of microglia and their CX3CR1 signaling in adult neurogenesis in the olfactory bulb. *Elife* **6**, (2017).

338. Rice, R. A. *et al.* Elimination of Microglia Improves Functional Outcomes Following Extensive Neuronal Loss in the Hippocampus. *J. Neurosci.* **35**, 9977–9989 (2015).

339. Dagher, N. *et al.* Colony-stimulating factor 1 receptor inhibition prevents microglial plaque association and improves cognition in 3xTg-AD mice. *J. Neuroinflammation*

12, 1–14 (2015).

340. Asai, H. *et al.* Depletion of microglia and inhibition of exosome synthesis halt tau propagation. *Nat. Neurosci.* **18**, 1584–1593 (2015).

341. Zhu, C. *et al.* A neuroprotective role for microglia in prion diseases. *J. Exp. Med.* jem.20151000 (2016). doi:10.1084/jem.20151000

342. Acharya, M. M. *et al.* Elimination of microglia improves cognitive function following cranial irradiation. *Sci. Rep.* **6**, 31545 (2016).

343. Li, M. *et al.* Colony stimulating factor 1 receptor inhibition eliminates microglia and attenuates brain injury after intracerebral hemorrhage. *J. Cereb. Blood Flow Metab.* **1**, 1–13 (2016).

344. Louis, C. *et al.* Specific Contributions of CSF-1 and GM-CSF to the Dynamics of the Mononuclear Phagocyte System. *J. Immunol.* **195**, 134–144 (2015).

345. Naglich, J. G., Metherall, J. E., Russell, D. W. & Eidels, L. Expression cloning of a diphtheria toxin receptor: identity with a heparin-binding EGF-like growth factor precursor. *Cell* **69**, 1051–1061 (1992).

346. Middlebrook, J. L. & Dorland, R. B. Response of cultured mammalian cells to the exotoxins of Pseudomonas aeruginosa and Corynebacterium diphtheriae: differential cytotoxicity. *Can. J. Microbiol.* **23**, 183–189 (1977).

347. Pappenheimer, A. M. J., Harper, A. A., Moynihan, M. & Brockes, J. P. Diphtheria toxin and related proteins: effect of route of injection on toxicity and the determination of cytotoxicity for various cultured cells. *J. Infect. Dis.* **145**, 94–102 (1982).

348. Yamaizumi, M., Mekada, E., Uchida, T. & Okada, Y. One molecule of diphtheria toxin fragment A introduced into a cell can kill the cell. *Cell* **15**, 245–250 (1978).

349. Saito, M. *et al.* Diphtheria toxin receptor-mediated conditional and targeted cell ablation in transgenic mice. *Nat. Biotechnol.* **19**, 746–750 (2001).

350. Jung, S. *et al.* In vivo depletion of CD11c+ dendritic cells abrogates priming of CD8+ T cells by exogenous cell-associated antigens. *Immunity* **17**, 211–220 (2002).

351. Drazin, R., Kandel, J. & Collier, R. J. Structure and activity of diphtheria toxin. II. Attack by trypsin at a specific site within the intact toxin molecule. *J. Biol. Chem.* **246**, 1504–1510 (1971).

352. Gill, D. M. & Dinius, L. L. Observations on the structure of diphtheria toxin. *J. Biol. Chem.* **246**, 1485–1491 (1971).

353. Honjo, T., Nishizuka, Y., Kato, I. & Hayaishi, O. Adenosine diphosphate ribosylation of aminoacyl transferase II and inhibition of protein synthesis by diphtheria toxin. *J. Biol. Chem.* **246**, 4251–4260 (1971).

354. Buch, T. *et al.* A Cre-inducible diphtheria toxin receptor mediates cell lineage ablation after toxin administration. *Nat. Methods* **2**, 419–426 (2005).

355. Voehringer, D., Liang, H.-E. & Locksley, R. M. Homeostasis and effector function of lymphopenia-induced 'memory-like' T cells in constitutively T cell-depleted mice. *J. Immunol.* **180**, 4742–4753 (2008).

356. Peng, J. *et al.* Microglia and monocytes synergistically promote the transition from acute to chronic pain after nerve injury. *Nat. Commun.* **7**, 12029 (2016).

357. Elion, G. B. *et al.* Selectivity of action of an antiherpetic agent, 9-(2-hydroxyethoxymethyl) guanine. *Proc. Natl. Acad. Sci. U. S. A.* **74**, 5716–5720 (1977).

358. Fyfe, J. A., Keller, P. M., Furman, P. A., Miller, R. L. & Elion, G. B. Thymidine kinase from herpes simplex virus phosphorylates the new antiviral compound, 9-(2-hydroxyethoxymethyl)guanine. *J. Biol. Chem.* **253**, 8721–8727 (1978).

359. Furman, P. A., McGuirt, P. V, Keller, P. M., Fyfe, J. A. & Elion, G. B. Inhibition by acyclovir of cell growth and DNA synthesis of cells biochemically transformed with herpesvirus genetic information. *Virology* **102**, 420–430 (1980).

360. Heppner, F. L. *et al.* Experimental autoimmune encephalomyelitis repressed by microglial paralysis. *Nat. Med.* **11**, 146–152 (2005).

361. Gowing, G., Vallieres, L. & Julien, J.-P. Mouse model for ablation of proliferating microglia in acute CNS injuries. *Glia* **53**, 331–337 (2006).

362. Grathwohl, S. A. *et al.* Formation and maintenance of Alzheimer's disease beta-amyloid plaques in the absence of microglia. *Nat. Neurosci.* **12**, 1361–1363 (2009).

363. Mirrione, M. M. *et al.* Microglial ablation and lipopolysaccharide preconditioning affects pilocarpine-induced seizures in mice. *Neurobiol. Dis.* **39**, 85–97 (2010).

364. Varvel, N. H. *et al.* Microglial repopulation model reveals a robust homeostatic process for replacing CNS myeloid cells. *Proc. Natl. Acad. Sci. U. S. A.* **109**, 18150–18155 (2012).

365. Lalancette-Hebert, M., Gowing, G., Simard, A., Weng, Y. C. & Kriz, J. Selective ablation of proliferating microglial cells exacerbates ischemic injury in the brain. *J. Neurosci.* **27**, 2596–2605 (2007).

366. van Rooijen, N., Sanders, A. & van den Berg, T. K. Apoptosis of macrophages induced by liposome-mediated intracellular delivery of clodronate and propamidine. *J. Immunol. Methods* **193**, 93–99 (1996).

367. Van Rooijen, N. & Sanders, A. Liposome mediated depletion of macrophages: mechanism of action, preparation of liposomes and applications. *J. Immunol. Methods* **174**, 83–93 (1994).

368. Popovich, P. G. *et al.* Depletion of hematogenous macrophages promotes partial hindlimb recovery and neuroanatomical repair after experimental spinal cord injury. *Exp. Neurol.* **158**, 351–65 (1999).

369. Iannotti, C. A. *et al.* A combination immunomodulatory treatment promotes neuroprotection and locomotor recovery after contusion SCI. *Exp. Neurol.* **230**, 3–15 (2011).

370. Lee, J. C. *et al.* Replacement of microglial cells using Clodronate liposome and bone marrow transplantation in the central nervous system of SOD1(G93A) transgenic mice as an in vivo model of amyotrophic lateral sclerosis. *Biochem. Biophys. Res. Commun.* **418**, 359–365 (2012).

371. Hanafy, K. A. The role of microglia and the TLR4 pathway in neuronal apoptosis and vasospasm after subarachnoid hemorrhage. *J. Neuroinflammation* **10**, 83 (2013).

372. Hamada, Y. *et al.* Involvement of an intercellular adhesion molecule 1-dependent pathway in the pathogenesis of secondary changes after spinal cord injury in rats. *J. Neurochem.* **66**, 1525–1531 (1996).

373. Taoka, Y. *et al.* Role of neutrophils in spinal cord injury in the rat. *Neuroscience* **79**, 1177–1182 (1997).

374. Popovich, P. G., Wei, P. & Stokes, B. T. Cellular inflammatory response after spinal cord injury in Sprague-Dawley and Lewis rats. *J. Comp. Neurol.* **377**, 443–464 (1997).

375. Stirling, D. P. & Yong, V. W. Dynamics of the inflammatory response after murine spinal cord injury revealed by flow cytometry. *J. Neurosci. Res.* **86**, 1944–1958 (2008).

376. Beck, K. D. *et al.* Quantitative analysis of cellular inflammation after traumatic spinal cord injury: evidence for a multiphasic inflammatory response in the acute to chronic environment. *Brain* **133**, 433–447 (2010).

377. Saiwai, H. *et al.* Ly6C+ Ly6G- Myeloid-derived suppressor cells play a critical role in the resolution of acute inflammation and the subsequent tissue repair process after spinal cord injury. *J. Neurochem.* **125**, 74–88 (2013).

378. Zhou, X., He, X. & Ren, Y. Function of microglia and macrophages in secondary damage after spinal cord injury. *Neural Regen. Res.* **9**, 1787–95 (2014).

379. Schnell, L., Schneider, R., Berman, M. A., Perry, V. H. & Schwab, M. E. Lymphocyte recruitment following spinal cord injury in mice is altered by prior viral exposure. *Eur.*

J. Neurosci. **9**, 1000–1007 (1997).

380. Sroga, J. M., Jones, T. B., Kigerl, K. A., McGaughy, V. M. & Popovich, P. G. Rats and mice exhibit distinct inflammatory reactions after spinal cord injury. *J. Comp. Neurol.* **462**, 223–240 (2003).

381. Kigerl, K. A., McGaughy, V. M. & Popovich, P. G. Comparative analysis of lesion development and intraspinal inflammation in four strains of mice following spinal contusion injury. *J. Comp. Neurol.* **494**, 578–94 (2006).

382. Donnelly, D. J. & Popovich, P. G. Inflammation and its role in neuroprotection , axonal regeneration and functional recovery after spinal cord injury. *Exp. Neurol.* **209**, 378–388 (2008).

383. Wang, J. Neutrophils in tissue injury and repair. *Cell Tissue Res.* **371**, 531–539 (2018).

384. Pillay, J. *et al.* In vivo labeling with 2H2O reveals a human neutrophil lifespan of 5.4 days. *Blood* **116**, 625–627 (2010).

385. Semerad, C. L., Liu, F., Gregory, A. D., Stumpf, K. & Link, D. C. G-CSF is an essential regulator of neutrophil trafficking from the bone marrow to the blood. *Immunity* **17**, 413–423 (2002).

386. Roberts, A. W. G-CSF: a key regulator of neutrophil production, but that's not all! *Growth Factors* **23**, 33–41 (2005).

387. Borregaard, N. Neutrophils, from marrow to microbes. *Immunity* **33**, 657–670 (2010).

388. Yamanaka, R. *et al.* Impaired granulopoiesis, myelodysplasia, and early lethality in CCAAT/enhancer binding protein epsilon-deficient mice. *Proc. Natl. Acad. Sci. U. S. A.* **94**, 13187–13192 (1997).

389. Bedi, R., Du, J., Sharma, A. K., Gomes, I. & Ackerman, S. J. Human C/EBP-ε activator and repressor isoforms differentially reprogram myeloid lineage commitment and differentiation. *Blood* **113**, 317–327 (2009).

390. Jansen, J., Hanks, S., Thompson, J. M., Dugan, M. J. & Akard, L. P. Transplantation of hematopoietic stem cells from the peripheral blood. *J. Cell. Mol. Med.* **9**, 37–50 (2005).

391. Shechter, R. *et al.* Recruitment of Beneficial M2 Macrophages to Injured Spinal Cord Is Orchestrated by Remote Brain Choroid Plexus. *Immunity* **38**, 555–569 (2013).

392. Fleming, T. J., Fleming, M. L. & Malek, T. R. Selective expression of Ly-6G on myeloid lineage cells in mouse bone marrow. RB6-8C5 mAb to granulocyte-differentiation antigen (Gr-1) detects members of the Ly-6 family. *J. Immunol.* **151**, 2399–2408 (1993).

393. Urdzikova, L. *et al.* Transplantation of bone marrow stem cells as well as mobilization by granulocyte-colony stimulating factor promotes recovery after spinal cord injury in rats. *J. Neurotrauma* **23**, 1379–1391 (2006).

394. Kadota, R. *et al.* Granulocyte colony-stimulating factor (G-CSF) protects oligodendrocyte and promotes hindlimb functional recovery after spinal cord injury in rats. *PLoS One* **7**, e50391 (2012).

395. Nishio, Y. *et al.* Granulocyte colony-stimulating factor attenuates neuronal death and promotes functional recovery after spinal cord injury in mice. *J. Neuropathol. Exp. Neurol.* **66**, 724–731 (2007).

396. Schabitz, W.-R. *et al.* Neuroprotective effect of granulocyte colony-stimulating factor after focal cerebral ischemia. *Stroke* **34**, 745–751 (2003).

397. Chen, W.-F. *et al.* Intrathecally injected granulocyte colony-stimulating factor produced neuroprotective effects in spinal cord ischemia via the mitogen-activated protein kinase and Akt pathways. *Neuroscience* **153**, 31–43 (2008).

398. Volkman, A. & Gowans, J. L. The origin of macrophages from bone marrow in the rat. *Br. J. Exp. Pathol.* **46**, 62–70 (1965).

399. Villani, A.-C. *et al.* Single-cell RNA-seq reveals new types of human blood dendritic

cells, monocytes, and progenitors. *Science* **356**, (2017).

400. Gordon, S. & Taylor, P. R. Monocyte and macrophage heterogeneity. *Nat. Rev. Immunol.* **5**, 953–964 (2005).

401. Kuziel, W. A. *et al.* Severe reduction in leukocyte adhesion and monocyte extravasation in mice deficient in CC chemokine receptor 2. *Proc. Natl. Acad. Sci. U. S. A.* **94**, 12053–12058 (1997).

402. Kurihara, T., Warr, G., Loy, J. & Bravo, R. Defects in macrophage recruitment and host defense in mice lacking the CCR2 chemokine receptor. *J. Exp. Med.* **186**, 1757–1762 (1997).

403. Lu, B. *et al.* Abnormalities in monocyte recruitment and cytokine expression in monocyte chemoattractant protein 1-deficient mice. *J. Exp. Med.* **187**, 601–608 (1998).

404. Gu, L. *et al.* Absence of monocyte chemoattractant protein-1 reduces atherosclerosis in low density lipoprotein receptor-deficient mice. *Mol. Cell* **2**, 275–281 (1998).

405. Serbina, N. V, Salazar-Mather, T. P., Biron, C. A., Kuziel, W. A. & Pamer, E. G. TNF/iNOS-producing dendritic cells mediate innate immune defense against bacterial infection. *Immunity* **19**, 59–70 (2003).

406. Auffray, C., Sieweke, M. H. & Geissmann, F. Blood monocytes: development, heterogeneity, and relationship with dendritic cells. *Annu. Rev. Immunol.* **27**, 669–92 (2009).

407. Hanna, R. N. *et al.* The transcription factor NR4A1 (Nur77) controls bone marrow differentiation and the survival of Ly6C- monocytes. *Nat. Immunol.* **12**, 778–785 (2011).

408. Dal-Secco, D. *et al.* A dynamic spectrum of monocytes arising from the in situ reprogramming of CCR2 $^{+}$ monocytes at a site of sterile injury. *J. Exp. Med.* **212**, 447–456 (2015).

409. Francos-Quijorna, I., Amo-Aparicio, J., Martinez-Muriana, A. & Lopez-Vales, R. IL-4 drives microglia and macrophages toward a phenotype conducive for tissue repair and functional recovery after spinal cord injury. *Glia* **64**, 2079–2092 (2016).

410. Shichita, T. *et al.* MAFB prevents excess inflammation after ischemic stroke by accelerating clearance of damage signals through MSR1. *Nat. Med.* **23**, 723–732 (2017).

411. Rapalino, O. *et al.* Implantation of stimulated homologous macrophages results in partial recovery of paraplegic rats. *Nat. Med.* **4**, 814–821 (1998).

412. Giulian, D. & Robertson, C. Inhibition of mononuclear phagocytes reduces ischemic injury in the spinal cord. *Ann. Neurol.* **27**, 33–42 (1990).

413. Blight, A. R. Effects of silica on the outcome from experimental spinal cord injury: implication of macrophages in secondary tissue damage. *Neuroscience* **60**, 263–273 (1994).

414. Stirling, D. P. *et al.* Minocycline treatment reduces delayed oligodendrocyte death, attenuates axonal dieback, and improves functional outcome after spinal cord injury. *J. Neurosci.* **24**, 2182–2190 (2004).

415. Blomster, L. V. *et al.* Mobilisation of the splenic monocyte reservoir and peripheral CX3CR1 deficiency adversely affects recovery from spinal cord injury. *Exp. Neurol.* **247**, 226–240 (2013).

416. Donnelly, D. J. *et al.* Deficient CX3CR1 signaling promotes recovery after mouse spinal cord injury by limiting the recruitment and activation of Ly6Clo/iNOS+ macrophages. *J. Neurosci.* **31**, 9910–22 (2011).

417. Ankeny, D. P., Lucin, K. M., Sanders, V. M., Mcgaughy, V. M. & Popovich, P. G. Spinal cord injury triggers systemic autoimmunity : evidence for chronic B lymphocyte activation and lupus-like autoantibody synthesis. *J. Neurochem.* 1073–1087 (2006). doi:10.1111/j.1471-4159.2006.04147.x

418. Potas, J. R. *et al.* Augmented locomotor recovery after spinal cord injury in the athymic nude rat. *J. Neurotrauma* **23**, 660–673 (2006).

419. Fruman, D. A., Klee, C. B., Bierer, B. E. & Burakoff, S. J. Calcineurin phosphatase activity in T lymphocytes is inhibited by FK 506 and cyclosporin A. *Proc. Natl. Acad. Sci. U. S. A.* **89**, 3686–3690 (1992).

420. Lu, H.-Z., Wang, Y.-X., Zhou, J.-S., Wang, F.-C. & Hu, J.-G. Cyclosporin A increases recovery after spinal cord injury but does not improve myelination by oligodendrocyte progenitor cell transplantation. *BMC Neurosci.* **11**, 127 (2010).

421. Ibarra, A. *et al.* Effects of cyclosporin-A on immune response, tissue protection and motor function of rats subjected to spinal cord injury. *Brain Res.* **979**, 165–178 (2003).

422. McMahon, S. S. *et al.* Effect of cyclosporin A on functional recovery in the spinal cord following contusion injury. *J. Anat.* **215**, 267–279 (2009).

423. Lopez-Vales, R. *et al.* FK 506 reduces tissue damage and prevents functional deficit after spinal cord injury in the rat. *J. Neurosci. Res.* **81**, 827–836 (2005).

424. Madsen, J. R. *et al.* Tacrolimus (FK506) increases neuronal expression of GAP-43 and improves functional recovery after spinal cord injury in rats. *Exp. Neurol.* **154**, 673–683 (1998).

425. Nottingham, S., Knapp, P. & Springer, J. FK506 treatment inhibits caspase-3 activation and promotes oligodendroglial survival following traumatic spinal cord injury. *Exp. Neurol.* **177**, 242–251 (2002).

426. Lee, K. D. *et al.* FTY720 reduces inflammation and promotes functional recovery after spinal cord injury. *J. Neurotrauma* **26**, 2335–2344 (2009).

427. Norimatsu, Y. *et al.* FTY720 improves functional recovery after spinal cord injury by primarily nonimmunomodulatory mechanisms. *Am. J. Pathol.* **180**, 1625–1635 (2012).

428. Luchetti, S. *et al.* Comparison of immunopathology and locomotor recovery in C57BL/6, BUB/BnJ, and NOD-SCID mice after contusion spinal cord injury. *J. Neurotrauma* **27**, 411–421 (2010).

429. Wu, B. *et al.* Improved regeneration after spinal cord injury in mice lacking functional T- and B-lymphocytes. *Exp. Neurol.* **237**, 274–285 (2012).

430. Ankeny, D. P., Guan, Z. & Popovich, P. G. B cells produce pathogenic antibodies and impair recovery after spinal cord injury in mice. *J. Clin. Invest.* **119**, 2990–2999 (2009).

431. Moalem, G. *et al.* Autoimmune T cells protect neurons from secondary degeneration after central nervous system axotomy. *Nat. Med.* **5**, 49–55 (1999).

432. Hauben, E. *et al.* Passive or active immunization with myelin basic protein promotes recovery from spinal cord contusion. *J. Neurosci.* **20**, 6421–6430 (2000).

433. Yoles, E. *et al.* Protective autoimmunity is a physiological response to CNS trauma. *J. Neurosci.* **21**, 3740–3748 (2001).

434. Hauben, E. *et al.* Vaccination with a Nogo-A-derived peptide after incomplete spinal-cord injury promotes recovery via a T-cell-mediated neuroprotective response: comparison with other myelin antigens. *Proc. Natl. Acad. Sci. U. S. A.* **98**, 15173–15178 (2001).

435. Kipnis, J. *et al.* T cell immunity to copolymer 1 confers neuroprotection on the damaged optic nerve: possible therapy for optic neuropathies. *Proc. Natl. Acad. Sci. U. S. A.* **97**, 7446–7451 (2000).

436. Jones, T. B. *et al.* Passive or active immunization with myelin basic protein impairs neurological function and exacerbates neuropathology after spinal cord injury in rats. *J. Neurosci.* **24**, 3752–3761 (2004).

437. Na, S.-Y., Mracsko, E., Liesz, A., Hunig, T. & Veltkamp, R. Amplification of regulatory T cells using a CD28 superagonist reduces brain damage after ischemic

stroke in mice. *Stroke* **46**, 212–220 (2015).

438. Kassan, M., Galan, M., Partyka, M., Trebak, M. & Matrougui, K. Interleukin-10 released by CD4(+)CD25(+) natural regulatory T cells improves microvascular endothelial function through inhibition of NADPH oxidase activity in hypertensive mice. *Arterioscler. Thromb. Vasc. Biol.* **31**, 2534–2542 (2011).

439. Liesz, A. *et al.* Boosting regulatory T cells limits neuroinflammation in permanent cortical stroke. *J. Neurosci.* **33**, 17350–17362 (2013).

440. Chen, S. *et al.* Regulatory T cell in stroke: a new paradigm for immune regulation. *Clin. Dev. Immunol.* **2013**, 689827 (2013).

441. Chen, Y. *et al.* Mucosal tolerance to E-selectin provides cell-mediated protection against ischemic brain injury. *Proc. Natl. Acad. Sci. U. S. A.* **100**, 15107–15112 (2003).

442. Wang, M. *et al.* Albumin induces neuroprotection against ischemic stroke by altering Toll-like receptor 4 and regulatory T cells in mice. *CNS Neurol. Disord. Drug Targets* **12**, 220–227 (2013).

443. Garcia, J. M. *et al.* Role of Interleukin-10 in Acute Brain Injuries. *Front. Neurol.* **8**, 244 (2017).

444. Becker, K., Kindrick, D., McCarron, R., Hallenbeck, J. & Winn, R. Adoptive transfer of myelin basic protein-tolerized splenocytes to naive animals reduces infarct size: a role for lymphocytes in ischemic brain injury? *Stroke* **34**, 1809–1815 (2003).

445. Frenkel, D. *et al.* Neuroprotection by IL-10-producing MOG CD4+ T cells following ischemic stroke. *J. Neurol. Sci.* **233**, 125–132 (2005).

446. Zorner, B. & Schwab, M. E. Anti-Nogo on the go: from animal models to a clinical trial. *Ann. N. Y. Acad. Sci.* **1198 Suppl**, E22-34 (2010).

447. Pernet, V. & Schwab, M. E. The role of Nogo-A in axonal plasticity, regrowth and

repair. *Cell Tissue Res.* **349**, 97–104 (2012).

448. Mier, J. W. & Gallo, R. C. Purification and some characteristics of human T-cell growth factor from phytohemagglutinin-stimulated lymphocyte-conditioned media. *Proc. Natl. Acad. Sci. U. S. A.* **77**, 6134–6138 (1980).

449. Dinarello, C. A. Overview of the interleukin-1 family of ligands and receptors. *Semin. Immunol.* **25**, 389–393 (2013).

450. England, H., Summersgill, H. R., Edye, M. E., Rothwell, N. J. & Brough, D. Release of interleukin-1a or interleukin-1b depends on mechanism of cell death. *J. Biol. Chem.* **289**, 15942–15950 (2014).

451. Idan, C. *et al.* IL-1α is a DNA damage sensor linking genotoxic stress signaling to sterile inflammation and innate immunity. *Sci. Rep.* **5**, 14756 (2015).

452. Dinarello, C. a. Interleukin-1 in the pathogenesis and treatment of inflammatory diseases. *Blood* **117**, 3720–32 (2011).

453. Qian, J. *et al.* Interleukin-1R3 mediates interleukin-1-induced potassium current increase through fast activation of Akt kinase. *Proc. Natl. Acad. Sci. U. S. A.* **109**, 12189–94 (2012).

454. Yabuuchi, K., Minami, M., Katsumata, S. & Satoh, M. Localization of type I interleukin-1 receptor mRNA in the rat brain. *Mol. brain Res.* **27**, 27–36 (1994).

455. Luheshi, N. M., Kovács, K. J., Lopez-Castejon, G., Brough, D. & Denes, A. Interleukin-1α expression precedes IL-1β after ischemic brain injury and is localised to areas of focal neuronal loss and penumbral tissues. *J. Neuroinflammation* **8**, 186 (2011).

456. Dittmer, S. *et al.* TOX3 is a neuronal survival factor that induces transcription depending on the presence of CITED1 or phosphorylated CREB in the transcriptionally active complex. *J. Cell Sci.* **124**, 252–60 (2011).

457. Groß, O. *et al.* Inflammasome Activators Induce Interleukin-1α Secretion via Distinct Pathways with Differential Requirement for the Protease Function of Caspase-1. *Immunity* **36**, 388–400 (2012).

458. Takeda, K. & Akira, S. Toll-like receptors in innate immunity. *Int. Immunol.* **17**, 1–14 (2005).

459. Casanova, J.-L., Abel, L. & Quintana-Murci, L. Human TLRs and IL-1Rs in host defense: natural insights from evolutionary, epidemiological, and clinical genetics. *Annu. Rev. Immunol.* **29**, 447–491 (2011).

460. Masumoto, J. *et al.* ASC, a novel 22-kDa protein, aggregates during apoptosis of human promyelocytic leukemia HL-60 cells. *J. Biol. Chem.* **274**, 33835–33838 (1999).

461. Martinon, F., Burns, K. & Tschopp, J. The inflammasome: a molecular platform triggering activation of inflammatory caspases and processing of proIL-beta. *Mol. Cell* **10**, 417–26 (2002).

462. Mariathasan, S. *et al.* Differential activation of the inflammasome by caspase-1 adaptors ASC and Ipaf. *Nature* **430**, 213–218 (2004).

463. Madry, C. *et al.* Microglial Ramification, Surveillance, and Interleukin-1beta Release Are Regulated by the Two-Pore Domain K(+) Channel THIK-1. *Neuron* **97**, 299-312.e6 (2018).

464. Pare, A. *et al.* IL-1beta enables CNS access to CCR2(hi) monocytes and the generation of pathogenic cells through GM-CSF released by CNS endothelial cells. *Proc. Natl. Acad. Sci. U. S. A.* **115**, E1194–E1203 (2018).

465. Kaushik, D. K., Thounaojam, M. C., Kumawat, K. L., Gupta, M. & Basu, A. Interleukin-1?? orchestrates underlying inflammatory responses in microglia via Kr??ppel-like factor 4. *J. Neurochem.* **127**, 233–244 (2013).

466. Voronov, E. *et al.* Unique Versus Redundant Functions of IL-1α and IL-1β in the Tumor Microenvironment. *Front. Immunol.* **4**, 177 (2013).

467. Sato, A. *et al.* Interleukin-1 participates in the classical and alternative activation of microglia/macrophages after spinal cord injury. *J. Neuroinflammation* **9**, 65 (2012).

468. Perrin, F. E., Lacroix, S., Aviles-Trigueros, M. & David, S. Involvement of monocyte chemoattractant protein-1, macrophage inflammatory protein-1alpha and interleukin-1beta in Wallerian degeneration. *Brain* **128**, 854–866 (2005).

469. Dinarello, C. A., Simon, A. & van der Meer, J. W. M. Treating inflammation by blocking interleukin-1 in a broad spectrum of diseases. *Nat. Rev. Drug Discov.* **11**, 633–652 (2012).

470. Greenhalgh, A. D., Galea, J., Denes, A., Tyrrell, P. J. & Rothwell, N. J. Rapid brain penetration of interleukin-1 receptor antagonist in rat cerebral ischaemia: pharmacokinetics, distribution, protection. *Br. J. Pharmacol.* **160**, 153–159 (2010).

471. Galea, J. *et al.* Intravenous anakinra can achieve experimentally effective concentrations in the central nervous system within a therapeutic time window: results of a dose-ranging study. *J. Cereb. Blood Flow Metab.* **31**, 439–447 (2011).

472. Pradillo, J. M. *et al.* Delayed administration of interleukin-1 receptor antagonist reduces ischemic brain damage and inflammation in comorbid rats. *J. Cereb. Blood Flow Metab.* **32**, 1810–1819 (2012).

473. Nesic, O. *et al.* IL-1 receptor antagonist prevents apoptosis and caspase-3 activation after spinal cord injury. *J. Neurotrauma* **18**, 947–956 (2001).

474. Zong, S., Zeng, G., Wei, B., Xiong, C. & Zhao, Y. Beneficial effect of interleukin-1 receptor antagonist protein on spinal cord injury recovery in the rat. *Inflammation* **35**, 520–526 (2012).

475. Sriram, K. & O'Callaghan, J. P. Divergent roles for tumor necrosis factor-alpha in the brain. *J. Neuroimmune Pharmacol.* **2**, 140–153 (2007).

476. Karkkainen, I., Rybnikova, E., Pelto-Huikko, M. & Huovila, A. P. Metalloprotease-disintegrin (ADAM) genes are widely and differentially expressed in the adult CNS.

Mol. Cell. Neurosci. **15**, 547–560 (2000).

477. Cabal-Hierro, L. & Lazo, P. S. Signal transduction by tumor necrosis factor receptors. *Cell. Signal.* **24**, 1297–1305 (2012).

478. Micheau, O. & Tschopp, J. Induction of TNF receptor I-mediated apoptosis via two sequential signaling complexes. *Cell* **114**, 181–190 (2003).

479. Santello, M. & Volterra, A. TNFalpha in synaptic function: switching gears. *Trends Neurosci.* **35**, 638–647 (2012).

480. Bruce, A. J. *et al.* Altered neuronal and microglial responses to excitotoxic and ischemic brain injury in mice lacking TNF receptors. *Nat. Med.* **2**, 788–794 (1996).

481. Lambertsen, K. L. *et al.* Microglia protect neurons against ischemia by synthesis of tumor necrosis factor. *J. Neurosci.* **29**, 1319–1330 (2009).

482. Chi, L.-Y. *et al.* The dual role of tumor necrosis factor-alpha in the pathophysiology of spinal cord injury. *Neurosci. Lett.* **438**, 174–179 (2008).

483. Klass, B. R., Grobbelaar, A. O. & Rolfe, K. J. Transforming growth factor beta1 signalling, wound healing and repair: a multifunctional cytokine with clinical implications for wound repair, a delicate balance. *Postgrad. Med. J.* **85**, 9–14 (2009).

484. Okuda, K. *et al.* TGF-beta1 influences early gingival wound healing in rats: an immunohistochemical evaluation of stromal remodelling by extracellular matrix molecules and PCNA. *J. oral Pathol. Med. Off. Publ. Int. Assoc. Oral Pathol. Am. Acad. Oral Pathol.* **27**, 463–469 (1998).

485. Laping, N. J. *et al.* Transforming growth factor-beta 1 induces neuronal and astrocyte genes: tubulin alpha 1, glial fibrillary acidic protein and clusterin. *Neuroscience* **58**, 563–572 (1994).

486. Wrighton, K. H., Lin, X. & Feng, X.-H. Phospho-control of TGF-beta superfamily signaling. *Cell Res.* **19**, 8–20 (2009).

487. Wrighton, K. H., Lin, X., Yu, P. B. & Feng, X.-H. Transforming Growth Factor {beta} Can Stimulate Smad1 Phosphorylation Independently of Bone Morphogenic Protein Receptors. *J. Biol. Chem.* **284**, 9755–9763 (2009).

488. Liu, T. & Feng, X.-H. Regulation of TGF-beta signalling by protein phosphatases. *Biochem. J.* **430**, 191–198 (2010).

489. Bernabeu, C., Conley, B. A. & Vary, C. P. H. Novel biochemical pathways of endoglin in vascular cell physiology. *J. Cell. Biochem.* **102**, 1375–1388 (2007).

490. Ross, S. & Hill, C. S. How the Smads regulate transcription. *Int. J. Biochem. Cell Biol.* **40**, 383–408 (2008).

491. Kulkarni, A. B. *et al.* Transforming growth factor beta 1 null mutation in mice causes excessive inflammatory response and early death. *Proc. Natl. Acad. Sci. U. S. A.* **90**, 770–774 (1993).

492. Shull, M. M. *et al.* Targeted disruption of the mouse transforming growth factor-beta 1 gene results in multifocal inflammatory disease. *Nature* **359**, 693–699 (1992).

493. Turner, M. *et al.* Induction of the interleukin 1 receptor antagonist protein by transforming growth factor-beta. *Eur. J. Immunol.* **21**, 1635–1639 (1991).

494. Letterio, J. J. & Roberts, A. B. Regulation of immune responses by TGF-beta. *Annu. Rev. Immunol.* **16**, 137–161 (1998).

495. Gorelik, L. & Flavell, R. A. Transforming growth factor-beta in T-cell biology. *Nat. Rev. Immunol.* **2**, 46–53 (2002).

496. Carrier, Y., Yuan, J., Kuchroo, V. K. & Weiner, H. L. Th3 cells in peripheral tolerance. II. TGF-beta-transgenic Th3 cells rescue IL-2-deficient mice from autoimmunity. *J. Immunol.* **178**, 172–178 (2007).

497. Buss, A. *et al.* TGF-beta1 and TGF-beta2 expression after traumatic human spinal cord injury. *Spinal Cord* **46**, 364–371 (2008).

498. Lagord, C., Berry, M. & Logan, A. Expression of TGFbeta2 but not TGFbeta1 correlates with the deposition of scar tissue in the lesioned spinal cord. *Mol. Cell. Neurosci.* **20**, 69–92 (2002).

499. McTigue, D. M., Popovich, P. G., Morgan, T. E. & Stokes, B. T. Localization of transforming growth factor-beta1 and receptor mRNA after experimental spinal cord injury. *Exp. Neurol.* **163**, 220–230 (2000).

500. Logan, A. *et al.* Effects of transforming growth factor beta 1 on scar production in the injured central nervous system of the rat. *Eur. J. Neurosci.* **6**, 355–363 (1994).

501. Kohta, M., Kohmura, E. & Yamashita, T. Inhibition of TGF-beta1 promotes functional recovery after spinal cord injury. *Neurosci. Res.* **65**, 393–401 (2009).

502. Morgan, T. E. *et al.* Clusterin expression by astrocytes is influenced by transforming growth factor beta 1 and heterotypic cell interactions. *J. Neuroimmunol.* **58**, 101–110 (1995).

503. Hellal, F. *et al.* Microtubule stabilization reduces scarring and causes axon regeneration after spinal cord injury. *Science* **331**, 928–931 (2011).

504. Liu, J. P., Baker, J., Perkins, A. S., Robertson, E. J. & Efstratiadis, A. Mice carrying null mutations of the genes encoding insulin-like growth factor I (Igf-1) and type 1 IGF receptor (Igf1r). *Cell* **75**, 59–72 (1993).

505. Russo, V. C., Gluckman, P. D., Feldman, E. L. & Werther, G. A. The insulin-like growth factor system and its pleiotropic functions in brain. *Endocr. Rev.* **26**, 916–943 (2005).

506. Annunziata, M., Granata, R. & Ghigo, E. The IGF system. *Acta Diabetol.* **48**, 1–9 (2011).

507. Versteyhe, S. *et al.* IGF-I, IGF-II, and Insulin Stimulate Different Gene Expression Responses through Binding to the IGF-I Receptor. *Front. Endocrinol. (Lausanne).* **4**, 98 (2013).

508. Favelyukis, S., Till, J. H., Hubbard, S. R. & Miller, W. T. Structure and autoregulation of the insulin-like growth factor 1 receptor kinase. *Nat. Struct. Biol.* **8**, 1058–1063 (2001).

509. Bateman, J. M. & McNeill, H. Insulin/IGF signalling in neurogenesis. *Cell. Mol. Life Sci.* **63**, 1701–1705 (2006).

510. Fernandez, A. M. *et al.* Regulation of the phosphatase calcineurin by insulin-like growth factor I unveils a key role of astrocytes in Alzheimer's pathology. *Mol. Psychiatry* **17**, 705–718 (2012).

511. Fernandez, A. M. & Torres-Aleman, I. The many faces of insulin-like peptide signalling in the brain. *Nat. Rev. Neurosci.* **13**, 225–239 (2012).

512. O'Kusky, J. & Ye, P. Neurodevelopmental effects of insulin-like growth factor signaling. *Front. Neuroendocrinol.* **33**, 230–251 (2012).

513. Hurtado-Chong, A. *et al.* IGF-I promotes neuronal migration and positioning in the olfactory bulb and the exit of neuroblasts from the subventricular zone. *Eur. J. Neurosci.* **30**, 742–755 (2009).

514. Iwanami, A., Cloughesy, T. F. & Mischel, P. S. Striking the balance between PTEN and PDK1: it all depends on the cell context. *Genes Dev.* **23**, 1699–1704 (2009).

515. Onuma, T. A. *et al.* Regulation of temporal and spatial organization of newborn GnRH neurons by IGF signaling in zebrafish. *J. Neurosci.* **31**, 11814–11824 (2011).

516. Paliouras, G. N. *et al.* Mammalian target of rapamycin signaling is a key regulator of the transit-amplifying progenitor pool in the adult and aging forebrain. *J. Neurosci.* **32**, 15012–15026 (2012).

517. Pun, R. Y. K. *et al.* Excessive activation of mTOR in postnatally generated granule cells is sufficient to cause epilepsy. *Neuron* **75**, 1022–1034 (2012).

518. Bondy, C. A. & Cheng, C. M. Signaling by insulin-like growth factor 1 in brain. *Eur.*

J. Pharmacol. **490**, 25–31 (2004).

519. Baltensperger, K. *et al.* Binding of the Ras activator son of sevenless to insulin receptor substrate-1 signaling complexes. *Science* **260**, 1950–1952 (1993).

520. Skolnik, E. Y. *et al.* The function of GRB2 in linking the insulin receptor to Ras signaling pathways. *Science* **260**, 1953–1955 (1993).

521. Moreno-Barriuso, N., Lopez-Malpartida, A. V, de Pablo, F. & Pichel, J. G. Alterations in alveolar epithelium differentiation and vasculogenesis in lungs of LIF/IGF-I double deficient embryos. *Dev. Dyn.* **235**, 2040–2050 (2006).

522. Kappeler, L. *et al.* Brain IGF-1 receptors control mammalian growth and lifespan through a neuroendocrine mechanism. *PLoS Biol.* **6**, e254 (2008).

523. Pais, R. S. *et al.* Transcriptome analysis in prenatal IGF1-deficient mice identifies molecular pathways and target genes involved in distal lung differentiation. *PLoS One* **8**, e83028 (2013).

524. Baker, J., Liu, J. P., Robertson, E. J. & Efstratiadis, A. Role of insulin-like growth factors in embryonic and postnatal growth. *Cell* **75**, 73–82 (1993).

525. Powell-Braxton, L. *et al.* IGF-I is required for normal embryonic growth in mice. *Genes Dev.* **7**, 2609–2617 (1993).

526. Beck, K. D., Powell-Braxton, L., Widmer, H. R., Valverde, J. & Hefti, F. Igf1 gene disruption results in reduced brain size, CNS hypomyelination, and loss of hippocampal granule and striatal parvalbumin-containing neurons. *Neuron* **14**, 717–730 (1995).

527. Pichel, J. G. *et al.* Developmental cooperation of leukemia inhibitory factor and insulin-like growth factor I in mice is tissue-specific and essential for lung maturation involving the transcription factors Sp3 and TTF-1. *Mech. Dev.* **120**, 349–361 (2003).

528. Werner, H. & LeRoith, D. Insulin and insulin-like growth factor receptors in the brain:

physiological and pathological aspects. *Eur. Neuropsychopharmacol.* **24**, 1947–1953 (2014).

529. Nishijima, T. *et al.* Neuronal activity drives localized blood-brain-barrier transport of serum insulin-like growth factor-I into the CNS. *Neuron* **67**, 834–846 (2010).

530. Bartlett, W. P., Li, X. S., Williams, M. & Benkovic, S. Localization of insulin-like growth factor-1 mRNA in murine central nervous system during postnatal development. *Dev. Biol.* **147**, 239–250 (1991).

531. Bartlett, W. P., Li, X. S. & Williams, M. Expression of IGF-1 mRNA in the murine subventricular zone during postnatal development. *Brain Res. Mol. Brain Res.* **12**, 285–291 (1992).

532. Yakar, S. *et al.* Circulating levels of IGF-1 directly regulate bone growth and density. *J. Clin. Invest.* **110**, 771–781 (2002).

533. Ueki, I. *et al.* Inactivation of the acid labile subunit gene in mice results in mild retardation of postnatal growth despite profound disruptions in the circulating insulin-like growth factor system. *Proc. Natl. Acad. Sci. U. S. A.* **97**, 6868–6873 (2000).

534. Iams, W. T. & Lovly, C. M. Molecular pathways: Clinical applications and future direction of insulin-like growth factor-1 receptor pathway blockade. *Clin. Cancer Res.* **21**, 4270–4277 (2015).

535. Aberg, M. A., Aberg, N. D., Hedbacker, H., Oscarsson, J. & Eriksson, P. S. Peripheral infusion of IGF-I selectively induces neurogenesis in the adult rat hippocampus. *J. Neurosci.* **20**, 2896–2903 (2000).

536. Cheng, C. M. *et al.* Biochemical and morphometric analyses show that myelination in the insulin-like growth factor 1 null brain is proportionate to its neuronal composition. *J. Neurosci.* **18**, 5673–5681 (1998).

537. Carson, M. J., Behringer, R. R., Brinster, R. L. & McMorris, F. A. Insulin-like growth factor I increases brain growth and central nervous system myelination in transgenic

mice. *Neuron* **10**, 729–740 (1993).

538. Dentremont, K. D., Ye, P., D'Ercole, A. J. & O'Kusky, J. R. Increased insulin-like growth factor-I (IGF-I) expression during early postnatal development differentially increases neuron number and growth in medullary nuclei of the mouse. *Brain Res. Dev. Brain Res.* **114**, 135–141 (1999).

539. O'Kusky, J. R., Ye, P. & D'Ercole, A. J. Insulin-like growth factor-I promotes neurogenesis and synaptogenesis in the hippocampal dentate gyrus during postnatal development. *J. Neurosci.* **20**, 8435–8442 (2000).

540. DiCicco-Bloom, E. & Black, I. B. Insulin growth factors regulate the mitotic cycle in cultured rat sympathetic neuroblasts. *Proc. Natl. Acad. Sci. U. S. A.* **85**, 4066–4070 (1988).

541. Ye, P., Xing, Y., Dai, Z. & D'Ercole, A. J. In vivo actions of insulin-like growth factor-I (IGF-I) on cerebellum development in transgenic mice: evidence that IGF-I increases proliferation of granule cell progenitors. *Brain Res. Dev. Brain Res.* **95**, 44–54 (1996).

542. Faber-Elman, A., Solomon, A., Abraham, J. A., Marikovsky, M. & Schwartz, M. Involvement of wound-associated factors in rat brain astrocyte migratory response to axonal injury: in vitro simulation. *J. Clin. Invest.* **97**, 162–171 (1996).

543. Tranque, P. A., Calle, R., Naftolin, F. & Robbins, R. Involvement of protein kinase-C in the mitogenic effect of insulin-like growth factor-I on rat astrocytes. *Endocrinology* **131**, 1948–1954 (1992).

544. Kühl, N. M., De Keyser, J., De Vries, H. & Hoekstra, D. Insulin-like growth factor binding proteins-1 and -2 differentially inhibit rat oligodendrocyte precursor cell survival and differentiation in vitro. *J. Neurosci. Res.* **69**, 207–216 (2002).

545. Aguado, F. *et al.* Subcellular localization of insulin-like growth factor I (IGF-I) in Purkinje cells of the adult rat: an immunocytochemical study. *Neurosci. Lett.* **135**, 171–174 (1992).

546. Decourtye, L. *et al.* IGF-1 Induces GHRH Neuronal Axon Elongation during Early Postnatal Life in Mice. *PLoS One* **12**, e0170083 (2017).

547. Guo, C. *et al.* IGFBPL1 Regulates Axon Growth through IGF-1-mediated Signaling Cascades. *Sci. Rep.* **8**, 2054 (2018).

548. Hollis, E. R. 2nd, Lu, P., Blesch, A. & Tuszynski, M. H. IGF-I gene delivery promotes corticospinal neuronal survival but not regeneration after adult CNS injury. *Exp. Neurol.* **215**, 53–59 (2009).

549. Liu, Y. *et al.* A Sensitized IGF1 Treatment Restores Corticospinal Axon-Dependent Functions. *Neuron* **95**, 817-833.e4 (2017).

550. Beilharz, E. J. *et al.* Co-ordinated and cellular specific induction of the components of the IGF/IGFBP axis in the rat brain following hypoxic-ischemic injury. *Brain Res. Mol. Brain Res.* **59**, 119–134 (1998).

551. Li, X. S., Williams, M. & Bartlett, W. P. Induction of IGF-1 mRNA expression following traumatic injury to the postnatal brain. *Brain Res. Mol. Brain Res.* **57**, 92–96 (1998).

552. Sandberg Nordqvist, A. C. *et al.* Increase of insulin-like growth factor (IGF)-1, IGF binding protein-2 and -4 mRNAs following cerebral contusion. *Brain Res. Mol. Brain Res.* **38**, 285–293 (1996).

553. Walter, H. J., Berry, M., Hill, D. J. & Logan, A. Spatial and temporal changes in the insulin-like growth factor (IGF) axis indicate autocrine/paracrine actions of IGF-I within wounds of the rat brain. *Endocrinology* **138**, 3024–3034 (1997).

554. Yao, D. L. *et al.* Cryogenic spinal cord injury induces astrocytic gene expression of insulin-like growth factor I and insulin-like growth factor binding protein 2 during myelin regeneration. *J. Neurosci. Res.* **40**, 647–659 (1995).

555. Schabitz, W. R. *et al.* Delayed neuroprotective effect of insulin-like growth factor-i after experimental transient focal cerebral ischemia monitored with mri. *Stroke* **32**,

1226–1233 (2001).

556. Loddick, S. A. *et al.* Displacement of insulin-like growth factors from their binding proteins as a potential treatment for stroke. *Proc. Natl. Acad. Sci. U. S. A.* **95**, 1894–1898 (1998).

557. Madathil, S. K. *et al.* Astrocyte-Specific Overexpression of Insulin-Like Growth Factor-1 Protects Hippocampal Neurons and Reduces Behavioral Deficits following Traumatic Brain Injury in Mice. *PLoS One* **8**, e67204 (2013).

558. Rininsland, F. *et al.* Suppression of insulin-like growth factor type I receptor by a triple-helix strategy inhibits IGF-I transcription and tumorigenic potential of rat C6 glioblastoma cells. *Proc. Natl. Acad. Sci. U. S. A.* **94**, 5854–5859 (1997).

559. Quail, D. F. *et al.* The tumor microenvironment underlies acquired resistance to CSF-1R inhibition in gliomas. *Science* **352**, aad3018 (2016).

560. Abiega, O. *et al.* Neuronal Hyperactivity Disturbs ATP Microgradients, Impairs Microglial Motility, and Reduces Phagocytic Receptor Expression Triggering Apoptosis/Microglial Phagocytosis Uncoupling. *PLoS Biol.* **14**, e1002466 (2016).

561. Mildner, A. *et al.* Microglia in the adult brain arise from Ly-6ChiCCR2+ monocytes only under defined host conditions. *Nat. Neurosci.* **10**, 1544–1553 (2007).

562. Hong, L. T. A. *et al.* An injectable hydrogel enhances tissue repair after spinal cord injury by promoting extracellular matrix remodeling. *Nat. Commun.* **8**, 533 (2017).

563. Kigerl, K. a. *et al.* Toll-like receptor (TLR)-2 and TLR-4 regulate inflammation, gliosis, and myelin sparing after spinal cord injury. *J. Neurochem.* **102**, 37–50 (2007).